DESIGN, SYNTHESIS AND STUDY OF THE SELF-ASSEMBLING AND PHOTOCHEMICAL PROPERTIES OF SOME LIGHT-RESPONSIVE AMPHIPHILIC BLOCK COPOLYMERS

THESIS SUBMITTED TO
THE UNIVERSITY OF KERALA
FOR THE DEGREE OF
DOCTOR OF PHILOSOPHY
IN CHEMISTRY
UNDER THE FACULTY OF SCIENCE

By

SAJITH MENON

PHOTOSCIENCES AND PHOTONICS SECTION
CHEMICAL SCIENCES AND TECHNOLOGY DIVISION
NATIONAL INSTITUTE FOR INTERDISCIPLINARY
SCIENCE AND TECHNOLOGY (NIIST), CSIR,
TRIVANDRUM – 695 019
KERALA, INDIA

2011

Dedicated to

My Family

DECLARATION

I hereby declare that the Ph.D. thesis entitled: **"Design, Synthesis and Study of the Self-Assembling and Photochemical Properties of Some Light-Responsive Amphiphilic Block Copolymers"** is an independent work carried out by me at the Photosciences and Photonics Section, Chemical Sciences and Technology Division, National Institute for Interdisciplinary Science and Technology (NIIST), CSIR, Trivandrum, under the supervision of Dr. Suresh Das and it has not been submitted anywhere else for any other degree, diploma or title.

In keeping with the general practice of reporting the schematic observations, due acknowledgement has been made wherever the work described is based on the findings of other investigators.

Sajith Menon

राष्ट्रीय अंतर्विषयी विज्ञान तथा प्रौद्योगिकी संस्थान

वैज्ञानिक तथा औद्योगिक अनुसंधान परिषद्

इंडस्ट्रियल इस्टेट - पी. ओ, पाप्पनंकोड, तिरुवनंतपुरम, भारत - 695 019

NATIONAL INSTITUTE FOR INTERDISCIPLINARY SCIENCE & TECHNOLOGY

Council of Scientific & Industrial Research
Industrial Estate P. O., Pappanamcode, Thiruvananthapuram India - 695 019

डॉ. सुरेष दास, एफ ए एस सी
निदेशक
Dr. Suresh Das FASc
Director

December 15, 2011

CERTIFICATE

This is to certify that the work embodied in the thesis entitled: **"Design, Synthesis and Study of the Self-Assembling and Photochemical Properties of Some Light-Responsive Amphiphilic Block Copolymers"** has been carried out by Mr. Sajith Menon under my supervision and guidance at the Photosciences and Photonics Section, Chemical Sciences and Technology Division, National Institute for Interdisciplinary Science and Technology (NIIST), CSIR, Trivandrum and the same has not been submitted elsewhere for a degree.

Suresh Das
(Thesis Supervisor)

आई एस ओ 9001 प्रमाणित संस्थान (ISO 9001 Certified Institute)
Tel: 91 471 2490324 (O), 2493599 (D) Fax: 91 471 2491712 E-mail: sureshdas@niist.res.in, director@niist.res.in Website: http//www.niist.res.in

ii

ACKNOWLEDGEMENTS

Sajith Menon

CONTENTS

List of Figures

change in fluorescence emission spectra

aggregates (1 mg/mL) (a) before degradation of the PCL core and (b) crosslinking after degradation of the PCL core

various conditions

List of Schemes

List of Abbreviations

1) AFM   Atomic force microscopy

2) AIBN   Azobisisobutyronitrile

3) ATRP   Atom transfer radical polymerization

4) BC   Block copolymer

5) BPO   Benzoyl peroxide

6) C_{60} Buckminsterfullerene

7) $CDCl_3$ Chloroform-d

8) CRP   Controlled/living radical polymerization

9) CuBr   Cuprous bromide

10) DCC   Dicyclohexylcarbodiimide

11) DCM   Dichloromethane

12) DLS   Dynamic light scattering

13) DMAP   4-Dimethylaminopyridine

14) DMF   N, N-dimethylformamide

15) DMSO   Dimethylsulfoxide

16) DOX   Doxorubicin

17) DP_n Degree of polymerization

18) DT   Degenerative transfer

19) EPR   Enhanced permeability and retention

20) FAB MS   Fast atom bombardment mass spectrometry

21) FDA   Food and Drug Administration

22) FRET   Fluorescence resonance energy transfer

23)	GPC	Gel permeation chromatography
24)	HRTEM	High-resolution transmission electron microscopy
25)	LCST	Lower critical solution temperature
26)	LED	Light-emitting diode
27)	LFRP	Living free radical polymerization
28)	LRBC	Light -responsive block copolymer
29)	MC	Merocyanine
30)	M_n	Number average molecular weight
31)	M_w	Weight average molecular weight
32)	MWD	Molecular weight distribution
33)	MWNT	Multiwalled carbon nanotube
34)	NAC	Nitro aromatic compound
35)	NBS	N-bromosuccinimide
36)	NIR	Near-infrared
37)	NLO	Non-liner optics
38)	NMP	Nitroxide-mediated polymerization
39)	NMR	Nuclear magnetic resonance
40)	NR	Nile Red
41)	PAA	Polyacrylic acid
42)	PDI	Polydispersity index
43)	PEO	Polyethylene oxide
44)	PFS	Poly(ferrocenyldimethylsilane)
45)	PI	Polyisoprene

46) PMDETA   N,N,N′,N′,N″-Pentamethyldiethylenetriamine

47) PMMA   Polymethyl methacrylate

48) PNIPAM   Poly(N-isopropylacrylamide)

49) PSt   Polystyrene

50) RAFT   Reversible addition-fragmentation chain transfer

51) RP   Radical polymerization

52) SEM   Scanning electron microscopy

53) SP   Spiropyran

54) TEM   Transmission electron microscopy

55) TEMPO   2,2,6,6-tetramethyl- 1-piperidinyloxy free radical

56) THF   Tetrahydrofuran

57) TMS   Tetramethylsilane

58) TNT   Trinitrotoluene

59) TTF   Tetrathiafulvalene

60) UV   Ultraviolet

61) Vis.   Visible

PREFACE

Stimuli-responsive water soluble and amphiphilic (co)polymers represent a rapidly growing area with enormous technological and commercial potential. Impetus for innovation has come from the need for environmentally safe, yet "smart" materials which can be dispersed, and delivered in aqueous media. In recent years much interest has been focused on (co)polymer systems that undergo a conformational change or phase transition in response to an external stimulus. Classical chemical stimuli such as pH changes, hydrolysis, oxidation or reduction reaction, have been used to trigger a change in the hydrophilic-hydrophobic balance of the amphiphilic copolymers that in turn destabilises the nano or micro assemblies such as polymer vesicles, polymer micelles, nanotubes and nanofibers. Such (co)polymers are of great scientific and technological importance. They serve as important additives in fields as diverse as water treatment, enhanced oil recovery, controlled drug release, the formulation of water-borne coatings and personal care products. In this thesis we will examine specific examples of water-soluble light-responsive block copolymer systems. Photochromic compounds undergo a conformational change, such as isomerization or dimerization or a phase transition in response to exposure to light of an appropriate wavelength. These transitions can further induce changes in the optical, mechanical and chemical properties of the system containing the chromophore. The existence of two such states, which may be reversibly switched by means of an external light stimulus, can form the basis of molecular switches and/or optical storage data for example. The incorporation of photochromic molecules in (co)polymers yields photoactive materials of improved processibility and stability. The property changes of the chromophores that

occur after irradiation have been utilized to induce conformational changes in the (co)polymers to which they have been bound.

Chapter 1 provides a review of the various methods used for synthesizing block copolymers, self-assembly of amphiphilic block copolymers and the recent works on the synthesis and study of stimuli-responsive block copolymers.

Chapter 2 describes the synthesis, aggregation and photophysical properties of two stilbene based block copolymers, PDACS-b-PEO and PTFS-b-PSt-b-PEO constituting polyethylene oxide (PEO) as the common hydrophilic block. These polymers were synthesized by making use of the conventional atom transfer radical polymerization (ATRP). Addition of water to a THF solution of these polymers resulted in the formation of colloidal aggregates of the polymers brought about by the association of the hydrophobic blocks. When these colloidal solutions was exposed to UV light, spherical micelles formed by the diblock copolymer PDACS-b-PEO were completely destroyed whereas the vesicular aggregates formed by the triblock copolymer PTFS-b-PSt-b-PEO rearranged to rod shaped micelles. These morphological changes were brought about as a result of the isomerisation of less polar trans-stilbene to its more polar cis-form resulting in a substantial increase in the overall hydrophilicity of the polymer. Capability of these polymer aggregates to entrap hydrophobic dyes and to release them during UV irradiation was also analysed.

Chapter 3 deals with the morphological and spectral changes accompanying when two types of amphiphilic block copolymers containing pyreneylmethyl esters as pendent groups were exposed to UV light. These polymers, abbreviated as PPy-b-PSt-b-PEO and PPy-b-PBG, form vesicular aggregates in aqueous solutions. Irradiation with UV light resulted in the detachment of 1-pyrene methanol from the polymer structure resulting in the conversion of an ester group to a carboxylic acid group. As a result polymers become

predominantly hydrophilic resulting in complete destruction of the vesicular structures. Aqueous solutions of these polymers showed strong pyrene excimer emission which provided additional evidence for aggregation. Entrapment of Nile Red molecules within the hydrophobic domains of these aggregates resulted in fluorescence resonance energy transfer (FRET) from pyrene excimer to Nile Red indicating close association between these molecular species. Dissociation of polymer aggregates brought about by UV light resulted in the controlled release of Nile Red from the supramolecular aggregates.

The mechanistic details of UV light induced dissociation and visible light induced reformation of aggregates formed by a spiropyran (PSP-b-PBG) and an azobenzene (PMAzo-b-PBG) containing diblock glycopoymers in water were investigated and the results are described in Chapter 4. These processes were studied by carrying out light scattering, microscopic analysis of aggregates and photophysical properties of aqueous solutions of the individual polymers before and after being exposed to UV and visible light irradiation. The results indicated that dissociation of the vesicular aggregates of PSP-b-PBG was brought about by the isomerization of hydrophobic spiropyran units to hydrophilic zwitterionic merocyanine forms while irradiation with visible light produced a mixture of micelles and vesicles due to reverse isomerzation. Similarly dissociation of the spherical micellar aggregates of PMAzo-b-PBG resulted from the shift in the hydrophobic/hydrophilic balance brought about by trans-cis isomerisation of azobenzene units. The loading/reloading of hydrophobic dyes in the hydrophobic cavities of the block copolymer vesicular and micellar aggregates could be controlled by means of an external light source.

Stimuli Responsive Block Copolymers: an Overview

1.1. Abstract

Smart or stimuli responsive polymers represent a rapidly growing area with enormous technological and commercial importance. A responsive or smart polymer is one that responds to an external stimulus in a controlled and reproducible manner. This external stimulus may be optical, electrical, mechanical, or environmental such as a change in temperature or pH. The promise of smart polymeric materials stems from their flexibility and relative ease with which structural changes can be incorporated into a polymer to create a desired functionality. Moreover polymers possess the processability that facilitates their incorporation into a variety of device configurations. In the past decade there has been a dramatic increase in the amount of research dedicated to the synthesis of novel responsive polymers. Biomimetic approaches have been employed in the design, synthesis and engineering of stimuli-responsive polymeric systems, which undergo abrupt phase transitions upon variation of a variable around a critical point and their use in a plethora of applications, including sensors, logic operations, synthetic muscles, ''smart'' optical or micro-electromechanical systems, membranes, electronics and self-cleaning surfaces has been explored. Other technological concepts such as optical computing, transmitting for stealth systems, synthetic enzymes, and targeted drug delivery have been theorized, but the materials for making them are yet to be optimized. The enormous and exciting potential of stimuli responsive polymers in the development of emerging technologies have been highlighted in the paragraphs below.

1.2. Introduction

Amphiphiles (from the Greek αμφις, amphis: both and φιλία, philia: love, friendship) are molecules which have an affinity for two different kinds of environments. This dual attachment is built into the molecule by the covalent joining of parts of different chemical character and solution properties. Given the opportunity, the two (or more) different parts strive to minimize their contact, and can thus drive the amphiphilic molecules to attain a preferential orientation. As a result, amphiphilic molecules self-organize at interfaces and in solution and, in doing so, modify to great extent interfacial properties and enhance dramatically compatibility or partitioning [Alexandridis *et al.* 2000]. Surfactants (surface-active agents) and (polar) lipids are representative examples of low molecular weight amphiphiles with distinctive hydrophilic (water-loving) and hydrophobic (water-hating) parts.

Due to the amphiphilic nature of a surfactant or lipid, the two parts of the same molecule interact very differently with either a polar solvent or surface or a non-polar solvent or surface. There are two different ways to render favourable intermolecular contacts possible in surfactants while eliminating unfavourable ones: self-assembly in solution and adsorption at a surface or an interface. The self-assemblies can involve only the amphiphilic molecules, or there can be a mixed aggregate formed together with a low molecular weight cosolute or a macromolecule [Jönsson *et al.* 1998].

Self-assembly involves the formation of domains of hydrophobic groups (in contact with a nonpolar solvent) and domains of hydrophilic groups (in contact with a polar solvent). This leads to frequently complex phase behaviour [Laughlin 1994; Larsson 1994]. A general observation is that the phase behaviour becomes richer as the size of the surfactant molecule increases. Both technical applications and biological functions may be enhanced by increasing the size of the amphiphilic molecule. Firstly, a

stronger amphiphile has a low monomeric solubility, and thus has a stronger tendency to go to any interface. It is then more surface-active, and acts as a better detergent, a better stabilizer for dispersions or modifier of surfaces, and a better membrane-forming agent. Secondly, the richer self-assembly polymorphism gives a final control over macroscopic and microscopic properties. Another point relates to the dynamic nature of the self-assemblies. Surfactant micelles and other aggregates are highly dynamic, with low residence time of surfactant molecules [Evans *et al*. 1994]. The residence time increases very strongly with increasing surfactant molecule size. An important incentive for increasing the molecular size is to decrease the lability of aggregates and making technical systems and biological structures more stable and less sensitive to perturbations.

In this context, polymers are likely to play a key role not just for the ease of synthesis and processing, low cost, variability of chemical functionality and physical properties, that have made them successful materials so far, but also because of their intrinsic dimensions (typically in the tens of nanometers) and even more importantly the peculiar mesophase segregation in the case of block copolymers (BCs) [Lazzari *et al.* 2006; Hamley 1998]. BCs are a particular class of polymers that belong to a wider family known as soft materials [Hamley 2000] that, independent of the procedure of synthesis, can simply be considered as being formed by two or more chemically homogeneous polymer fragments (blocks) joined together by covalent bonds. The simplest and most studied architecture is the linear AB diblock, consisting of a long sequence of type A monomers covalently bonded to a chain of type B monomers. ABA triblocks and $(AB)_n$ multiblocks are formed by coupling additional A and B blocks. Use of three or more monomer types during polymer synthesis leads to the formation of ABC or other multicomponent molecular architectures. Various chemical coupling strategies permit the polymer chemist to configure two, three or more polymer molecules into branched

architectures as illustrated in Figure 1.1. Subtle variations in the molecular topology —

for example ABC versus ACB, or star-ABC (where blocks are not linear but are joined in

the center) — can lead to pronounced changes in morphology, as well as material

properties.
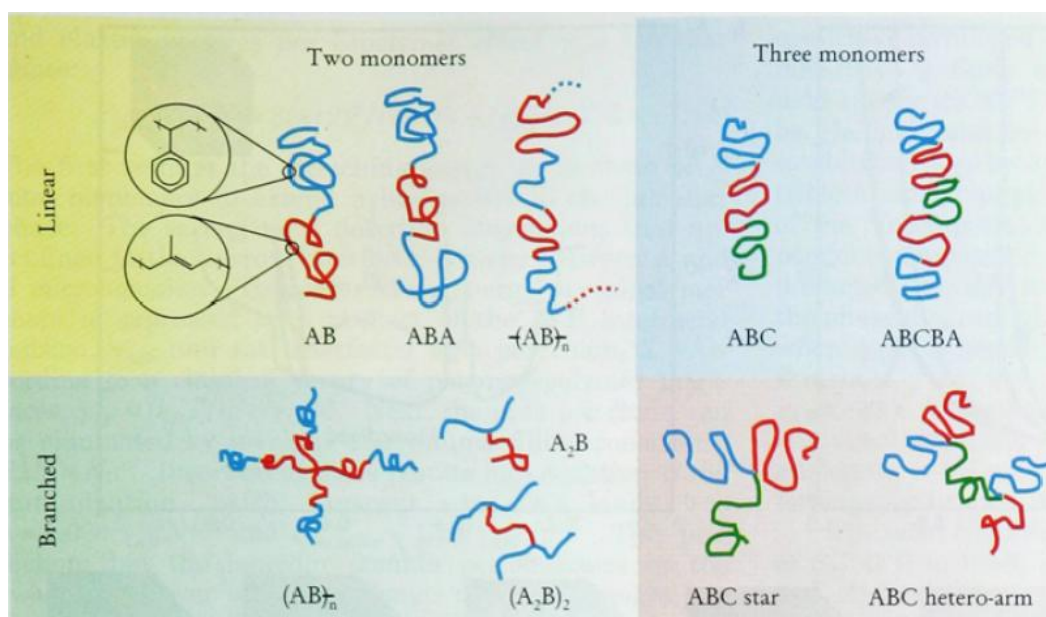
Figure 1.1. Pictorial representation of various classes of block copolymers. [Adapted from Blanazs *et al.* 2009].

BCs comprised of two flexible chemically incompatible and dissimilar blocks (e.g.,

poly(styrene)-b-poly(isoprene)) can microphase separate into a variety of morphologies.

The phase behaviour of such diblock copolymers has been the subject of numerous

theoretical and experimental studies over the past decades, and is today relatively well

understood [Leibler 1980; Bates 1991; Fredrickson *et al.* 1996; Klok *et al.* 2001]. This

self-assembly process is driven by an unfavourable mixing enthalpy and a small mixing

entropy, while the covalent bond connecting the blocks prevents macroscopic phase

separation. The microphase separation of coil-coil diblock copolymers depends on the

total degree of polymerization N (= $N_A + N_B$), the Flory-Huggins χ-parameter (which is a

measure for the incompatibility between the two blocks) and the volume fractions of the

constituent blocks (f_A and f_B, $f_A = 1 \pm f_B$). The segregation product χN determines the degree of microphase separation. Depending on χN, three different regimes are distinguished; i) the weak-segregation limit (WSL) for $\chi N \leq 10$; ii) the intermediate segregation region (ISR) for $10 < \chi N \leq 50$; and iii) the strong segregation limit (SSL) for $\chi N \rightarrow \infty$.

In bulk, the minority block is segregated from the majority block forming regularly shaped and uniformly-spaced nanodomains [Klok *et al.* 2001]. The shape of the segregated domains in a diblock is governed by the volume fraction of the minority block, *f* and block incompatibility. Figure 1.2 shows the equilibrium morphologies documented for diblock copolymers. At a volume fraction of ≈ 20%, the minority block forms a body-centred cubic spherical space in the matrix of the majority block. It changes to hexagonally packed cylinders at a volume fraction ≈ 38%, the minority block forms gyroid or perforated layers at moderate and high incompatibility, respectively [Khandpur *et al.* 1995]. Furthermore, the smallest dimension of a segregated domain, e.g. the diameter of a cylinder, is proportional to the two-thirds power of the molar mass of the minority block and can typically be tuned from ≈5 to ≈100 nm by changing the molar mass of the block [Bates *et al.* 1999].
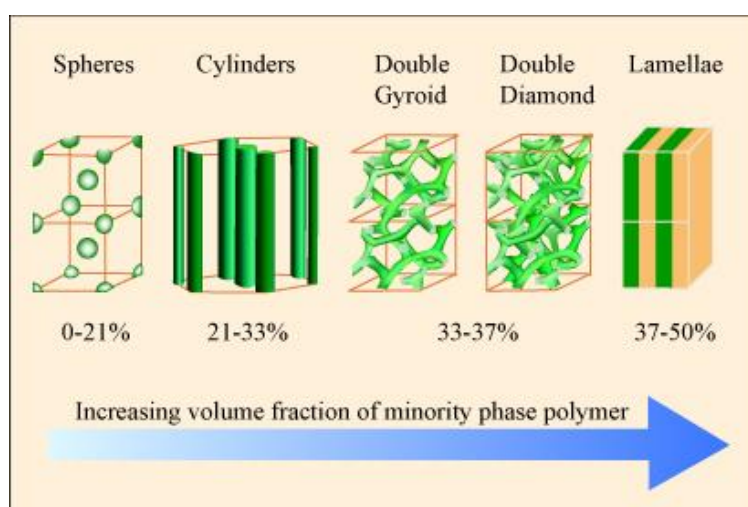
Figure 1.2. Schematic representations of the morphologies obtained for diblock copolymer melts.

In analogy to their bulk behaviour, diblock copolymers also self-assemble in block-selective solvents, which solubilise one and not the other block, forming micelles of various shapes [Blanazs *et al.* 2009; Choucair *et al.* 2003]. Self-assembly occurs in order to minimize energetically unfavourable insoluble block-solvent interaction. If the solubilising block is predominant, the insoluble block aggregates to produce spherical micelles. As the length of the solubilising block is decreased relative to the insoluble block, cylindrical micelles or vesicles are formed. For a given diblock, unusual micelles with shapes different from spheres can sometimes be induced by the use of increasingly poor solvent for the insoluble block [Bang *et al.* 2006]. The various reported morphologies are primarily a result of the inherent molecular curvature and how this influences the packing of the copolymer chains: specific self-assembled nanostructures can be targeted according to a dimensionless 'packing parameter', P, which is defined as $P = v / (a_o l_c)$ where v is the volume of the hydrophobic chains, a_o is the optimal area of the head group, and l_c is the length of the hydrophobic tail. Therefore, the packing parameter of a given molecule usually dictates its most likely self-assembled morphology. As a general rule [Blanazs *et al.* 2009, Shimizu *et al.* 2005], spherical micelles are favoured when $P \leq \frac{1}{3}$, cylindrical micelles when $\frac{1}{3} \leq P \leq \frac{1}{2}$, and enclosed membrane structures (vesicles, also known as polymersomes) when $\frac{1}{2} \leq P \leq 1$; if $P = 1$, planar bilayers will be favoured; and if $P < 1$, micellar aggregates with a reverse curvature will be formed. (Figure 1.3).

ABC triblock copolymers also undergo self-assembly in bulk or block-selective solvents. Triblocks have more block segregation patterns than diblocks and some of the patterns are aesthetically appealing [Zheng *et al.* 1995, Kim *et al.* 2010]. Figure 1.4 depicts some of the triblock bulk segregation patterns. Block copolymer complexity increases further for tetra- and pentablocks, thus making the list almost infinite.
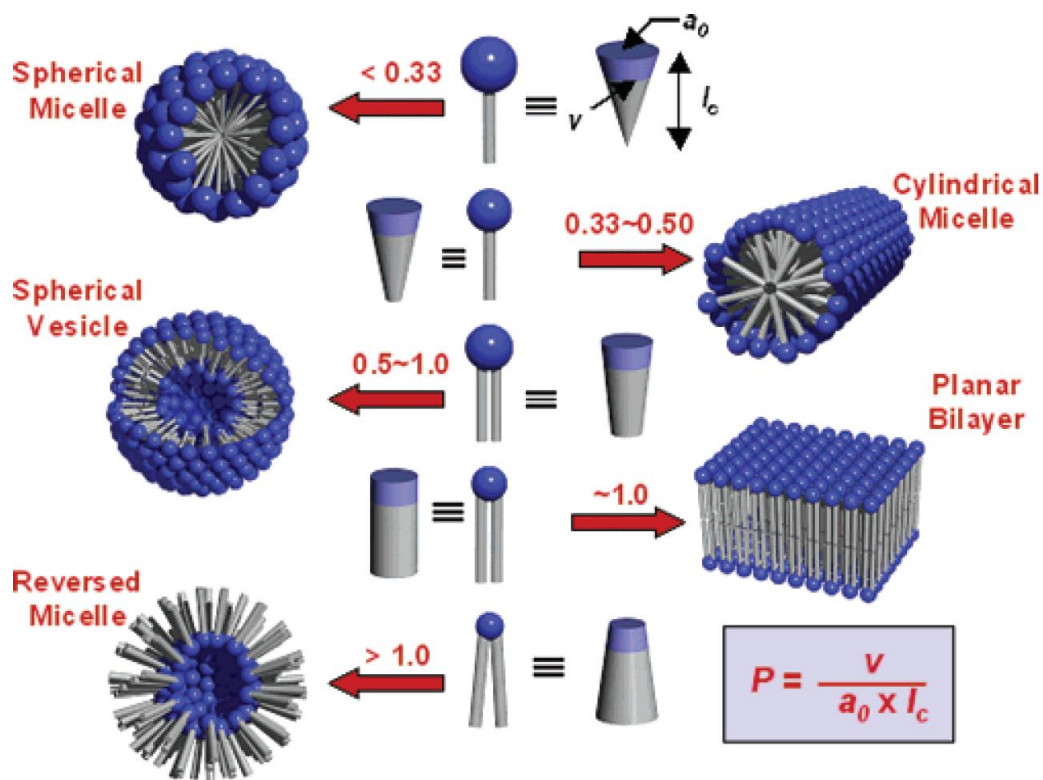
Figure 1.3. Various self-assembled structures formed by amphiphilic diblock copolymers in a block selective solvent. [Adapted from Shimizu *et al.* 2005].
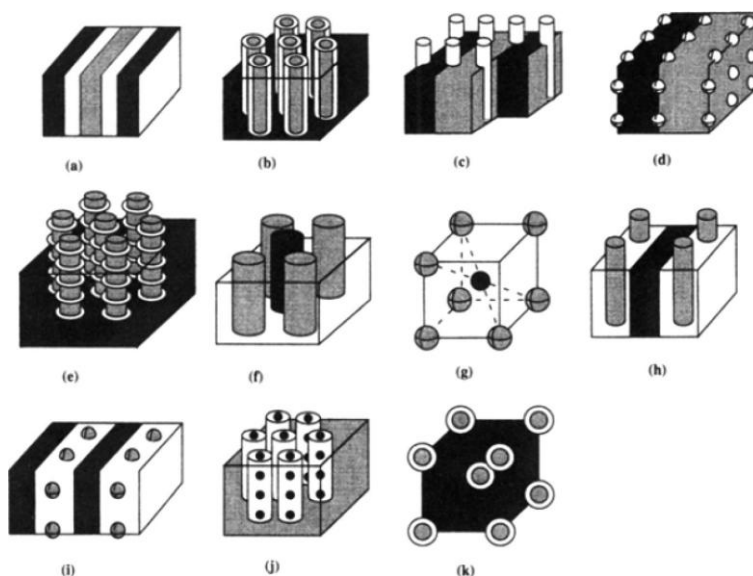
Figure 1.4. Schematic representation of the phases of ABC triblock copolymers. Dark, A; white, B; gray, C. (a) Lamellar phase; (b) coaxial cylinder phases; (c) lamella-cylinder phase; (d) lamella-sphere phase; (e) cylinder-ring phase; (f) cylindrical domains in a square lattice structure; (g) spherical domains in the CsCl-type structure; (h) lamella-cylinder-II; (i) lamella-sphere-II; (j) cylinder-sphere; (k) concentric spherical domain in the bcc structure. [Adapted from Kim *et al.* 2010].

Block copolymer micelles differ from micelles formed by small amphiphiles in terms of size (polymeric micelles being larger) and degree of segregation between the blocks that form the micelle core and these that form the shell or corona (the surfactant tail and head are strongly segregated), but most functional properties are common in micelles formed by both large and small amphiphilic molecules.

1.3. Guidelines for Synthesizing Block Copolymers

Macromolecular engineering of block copolymers is a vast multidisciplinary field which not only involves the concepts of molecular and macromolecular chemistry but also the physics and physic-chemistry of polymeric materials. In most cases the objective is to design and manipulate macromolecular objects that are capable of selective responses to an external stimulus such as pH, temperature, ionic strength, light, electric field, or any combination of these parameters [Lazzari *et al.* 2006; Riess 2003].

The discovery of living anionic polymerization by Michael Szwarc had a tremendous effect on polymer science [Szwarc 1956; Szwarc *et al.* 1956]. Living polymerization was defined by Szwarc as a chain growth process without chain breaking reactions (transfer and termination) [Matyjaszewski 1998]. Such a polymerization provides end-group control and enables the synthesis of block copolymers by sequential monomer addition. However, it does not necessarily provide for molecular weight control and narrow molecular weight distributions (MWD). Additional prerequisites to achieve these goals are that the initiator should be consumed at early stages of polymerization and that exchange between species of various reactivities is fast in comparison with propagation. If these additional criteria are met, a controlled polymerization results. Polymerization can also be defined as controlled, if side reactions occur, but only to an extent which does not considerably disturb the control of the molecular structure of the polymer chain. Provided that initiation is complete and exchange between species of

various reactivities is fast, one can adjust the final average molecular weight of the polymer by varying the initial monomer-to-initiator ratio ($DP_n = \Delta[M]/[I]_0$) while maintaining a narrow molecular weight distribution ($1.0 < M_w/M_n < 1.5$). Also, one has control over the chemistry and structure of the initiator and active end group, so polymers can be end-functionalized and block copolymerized with other monomers. Thus, using only a few monomers and a living polymerization, one can create many new materials with vastly differing properties simply by varying the topology of the polymer (i.e., comb, star, dendritic, etc.), the composition of the polymer (i.e., random, periodic, graft, etc.), or the functional groups at various sites on the polymer (i.e., end, center, side, etc.) [Patten *et al.* 1998] (Figure 1.5).
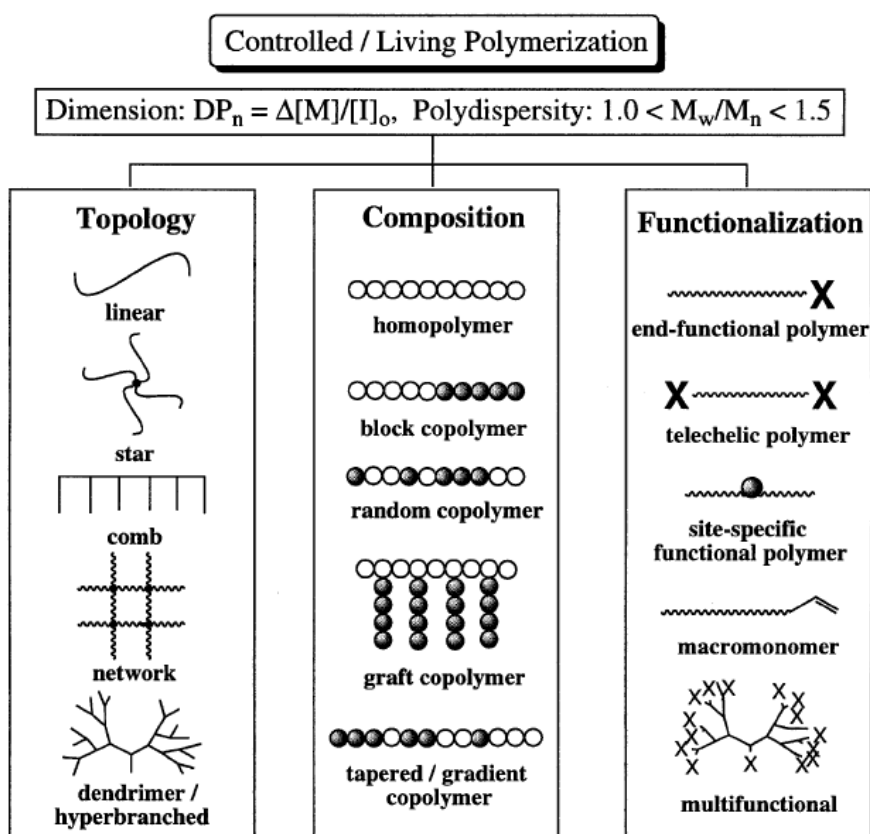
Figure 1.5. A schematic representation of how new polymers and materials can be prepared from a few monomers using controlled/living polymerizations. [Adapted from Patten *et al.* 1998].

1.4. Typical Features of Radical Polymerization

The active species in radical polymerization (RP) are organic (free) radicals. They are typically sp^2 hybridized intermediates and therefore show poor stereoselectivity. However, polymers formed by RP do show good regio- and chemoselectivity, as evidenced by the high degree of head-to-tail structures in the chain and the formation of high molecular weight polymers, respectively. Radicals can be stabilized by resonance and to a lesser degree by polar effects. They can be electrophilic or nucleophilic and in some instances possess a moderate tendency to alternate during copolymerization [Braunecker *et al.* 2007].

RP, like any chain polymerization, is comprised of four elementary reactions: initiation, propagation, transfer, and termination. Under steady state conditions, the initiation rate is the same as the rate of termination (i.e., ~1000 times slower than the propagation rate, k_p). Such a slow initiation can be accomplished by using radical initiators with appropriately long half lifetimes such as ~10 h. At the end of a polymerization, unreacted initiator is often left in the reaction mixture. The chain building reaction of propagation occurs by radical addition to the less substituted carbon atom in a monomer (resulting in head-to-tail polymers) with rate constants $k_p \sim 10^3 \, M^{-1} \, s^{-1}$ (k_p for acrylates $> 10^4 \, M^{-1} \, s^{-1}$ and for butadiene $< 10^2 \, M^{-1} \, s^{-1}$). In contrast to carbocationic polymerization, transfer is not the main chain breaking reaction in RP, and high molecular weight polymers can be formed from most monomers. Transfer has higher activation energy than propagation and becomes more important at higher temperatures. The bimolecular radical coupling/disproportionation termination reactions are very fast, essentially diffusion controlled ($k_t > 10^8 \, M^{-1} \, s^{-1}$), in contrast to ionic polymerization where electrostatic repulsion prevents a reaction between two cations or two anions. In order to grow long chains in RP, the termination rate (not rate constant) must be much

slower than propagation. Since termination is a 2nd-order reaction with respect to radical concentration while propagation is 1st-order, the rate of termination becomes slower than that of propagation at very low radical concentrations. Consequently, the radical concentration must be in the range of ppm or even ppb.

Because the average life of a propagating chain is ~1 s, which constitutes ~1000 acts of propagation with a frequency ~1 ms, the life of a propagating chain is too short for any synthetic manipulation, end functionalization, or addition of a second monomer to make a block copolymer. The overall kinetics can be described by Eq. (1), where the rate of polymerization is a function of the efficiency of initiation (f) and the rate constants of radical initiator decomposition (k_d), propagation (k_p) and termination (k_t) according to

$$R_p = k_p\,[M](f\,k_d[I]_o/k_t)^{1/2} \qquad \textbf{(1)}$$

The propagation rate scales with a square root of the radical initiator concentration and its efficiency of initiation (typically in the range of 50–80%). Molecular weights depend on the termination (= initiation) rate as well as the rate of transfer. When the contribution of transfer can be neglected, the degree of polymerization (DP_n) depends reciprocally on the square root of radical initiator concentration, as shown below.

$$DP_n = k_p\,[M](f\,k_d[I]_o/k_t)^{-1/2} \qquad \textbf{(2)}$$

Conventional RP can be carried out in bulk monomer, in solution, and also in dispersed media (suspension, emulsion, miniemulsion, microemulsion and inverse emulsion). Solvents should not contain easily abstractable atoms or groups, unless low MW polymers are desired. The range of reaction temperatures is quite large (-100 to >200 °C). Monomers are sufficiently reactive when the generated radicals are stabilized by resonance or polar effects (styrenes, (meth)acrylates, (meth)acrylamides, acrylonitrile, vinyl acetate, vinyl chloride and other halogenated alkenes). Due to its lower reactivity, ethylene polymerization requires high temperatures. However, it is accompanied by transfer under these conditions that leads to (hyper)branched polymers. Initiators are

typically peroxides, diazenes, redox systems and high-energy sources which slowly produce initiating radicals ($k_d \sim 10^{-5}$ s^{-1}).

The industrial significance of conventional RP is evident in the fact that it accounts for the production of ~50% of all commercial polymers. Low density polyethylene, poly(vinyl chloride), polystyrene and its copolymers (with acrylonitrile, butadiene, etc.), polyacrylates, polyacrylamides, poly(vinyl acetate), poly(vinyl alcohol) and fluorinated polymers comprise the most important of these materials. However, no pure block copolymers and essentially no polymers with controlled architecture can be produced by conventional RP.

Living free radical polymerizations (LFRP), although only about fifteen years old, have attained a tremendous following in polymer chemistry. The development of this process has been a long-standing goal because of the desire to combine the undemanding and industrial friendly nature of radical polymerizations with the power to control polydispersities, architectures, and molecular weights that living processes afford. A great deal of effort has been made to develop and understand different LFRP methods [Matyjaszewski 2000]. The methods at the forefront fall into one of three categories: atom transfer radical polymerization (ATRP) [Matyjaszewski *et al.* 2001], nitroxide mediated polymerization (NMP) [Hawker *et al.* 2001], and reversible addition-fragmentation chain transfer (RAFT) [Boyer *et al.* 2009].

1.5. Controlled/Living Radical Polymerization

Living polymerization is defined as a polymerization that neither undergoes termination or transfer [Entezami *et al.* 2006]. A plot of molecular weight vs. conversion is therefore linear, and the polymer chains all grow at the same rate, decreasing the polydispersity. The propagating centre at 100% conversion still exists and can be further reacted, which can allow novel block, graft, star, or hyperbranched copolymers to be

synthesized. Living polymerizations have been realized in anionic processes where transfer and termination are easy to suppress. Due to the favourable coupling of two radical propagating centres and various radical chain transfer reactions, the design and control of living radical processes are inherently a much more challenging task. The living process of radical polymerization involves the equilibration of growing free radicals and various types of dormant species. By tying up a great deal of the reactive centres as dormant species, the concentration of free radicals decreases substantially and therefore suppresses the transfer and termination steps. These reactions are also denoted as controlled/living polymerizations rather than as true living polymerizations because transfer and termination are decreased but not eliminated. Three processes, NMP, ATRP, and RAFT will now be introduced.

There are two caveats for living radical polymerizations. The first is that irreversible termination is only minimized in these polymerizations and not excluded from the   mechanism. Therefore, these polymerizations do not meet the strict definition of a living polymerization and are more properly termed controlled/living radical polymerizations (CRP) to reflect the uncertainty regarding the contribution of unavoidable irreversible termination. Second, above some molecular weight value specific to the polymerization of each monomer, all controlled/living radical polymerizations can no longer be considered controlled, because slower termination, transfer, and other side reactions become significant.

All of the known controlled/living radical polymerizations can be categorized into three subgroups based upon the general mechanism of radical generation. The first such mechanism involves the reversible capture of the polymeric radical by some species to form a stable, persistent radical (Eq. 3). This mechanism was proposed in the aluminum/ TEMPO-mediated (where TEMPO is the 2,2,6,6-tetramethyl- 1-piperidinyloxy free

radical) as well as the phosphite-mediated polymerization of vinyl acetate and in the "aged" chromium-acetate-mediated polymerization of methacrylates [Patten *et al.* 1998].

$$PX^{\bullet} \;\rightleftharpoons\; P^{\bullet} + X \qquad (3)$$
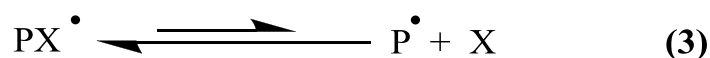
The second mechanism involves the rapid degenerative transfer of a functional group between dormant and active polymer chain ends (Eq. 4). An example of controlled/ living radical polymerizations that function via this mechanism is the iodine-atom-mediated radical polymerization of acrylates and styrene.

$$PX + P'^{\bullet} \;\rightleftharpoons\; P^{\bullet} + P'X \qquad (4)$$

The third mechanism involves the reversible homolytic cleavage of a dormant chain end adduct into the corresponding polymeric radical and a stable, persistent radical which cannot undergo addition to the monomer (Eq. 5). This mechanism is the most commonly occurring of the three, and the radical-forming equilibrium can be established via either the application of thermal energy or the addition of a catalyst.

$$PX \;\underset{\text{Catalyst}}{\overset{\Delta \text{ or}}{\rightleftharpoons}}\; P^{\bullet} + X^{\bullet} \qquad (5)$$
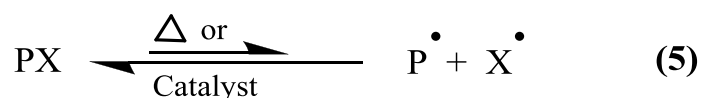
Examples of controlled/living radical polymerizations that function via an uncatalyzed homolytic cleavage mechanism include the diarylalkyl- or triarylalkyl-mediated polymerization of methacrylates [Braun *et al.* 1996], the dithiocarbamate-mediated polymerization of acrylates, methacrylates, and styrene, the TEMPO-mediated polymerization of styrenes, and the cobalt-macrocycle-mediated polymerization of acrylates.

Fast exchange among active and dormant species is required for good control over molecular weight, polydispersity and chain architecture in all CRP systems. A growing species should ideally react only with a few monomer units (within a few milliseconds) before it is deactivated to the dormant state (where it remains for several seconds). The

lifetime of a chain in the active state in a CRP process is comparable to the lifetime of a propagating chain in conventional RP. However, because the whole propagation process may take ≈ 1 day in CRP, there exists the opportunity to carry out various synthetic procedures, including chain-end functionalization or chain extension [Matyjaszewski, *Macromolecules* 1999].

1.5.1. Similarities and Differences between RP and CRP

CRP and RP proceed via the same radical mechanism, exhibit similar chemo-, regio- and stereo-selectivities, and can polymerize a similar range of monomers. However, several important differences between CRP and RP exist as summarized below [Braunecker *et al.* 2007].

1. The lifetime of growing chains is extended from ~1 s in RP to more than 1 h in CRP through the participation of dormant species and intermittent reversible activation.

2. Initiation is slow and free radical initiator is often left unconsumed at the end of a conventional RP. In most CRP systems, initiation is very fast and near instantaneous growth of all chains can be achieved, which ultimately enables control over chain architecture.

3. Nearly all chains are dead in RP, whereas in CRP the proportion of dead chains is usually < 10%.

4. Polymerization in CRP is often slower than in RP. However, the rates may be comparable in certain cases (e.g., when the targeted molecular weight in CRP is relatively low).

5. A steady state radical concentration is established in RP with similar rates of initiation and termination, whereas in CRP systems based on the persistent radical effect (PRE), a steady radical concentration is reached by balancing the rates of activation and deactivation.

6. Termination usually occurs between long chains and constantly generated new chains in RP. In CRP systems based on the PRE, all chains are short at the early stages of the reaction and become progressively longer; thus, the termination rate significantly decreases with time. In degenerative transfer (DT) processes, new chains are constantly generated by a small amount of conventional initiator, and therefore termination is more likely throughout the reaction.

1.5.2. Nitroxide-Mediated Polymerization (NMP)

Initial attempts producing a "living" system based on free radical chemistry involved the "iniferter" concept, which takes advantage of sulfur-centered radicals [Otsu *et al.* 1982]. These sulphur centered free radicals react reversibly with the growing polymer chain ends, thereby controlling the radical concentration; however, they also initiate new polymer chains, which leads to uncontrolled growth. As a result, the macromolecules obtained from such a system were found to have polydispersities similar to traditional free radical processes. While this leads to facile block copolymer formation, these systems cannot be considered to be truly "living" in nature and do not permit control of macromolecular architecture [Hawker *et al.* 1996].

To overcome these deficiencies, a nitroxide-mediated free radical polymerization having the characteristics of a living polymerization was developed. Although this process may not strictly obey the definition of a living polymerization, it does satisfy many of the requirements, hence the use of "living", or pseudo living. The success of this approach can be related to the ability of stable nitroxide free radicals, such as TEMPO, to react at near diffusion controlled rates with the carbon-centered free radical of the growing polymer chain end in a thermally reversible process. This dramatically lowers the concentration of free radicals in the polymerization system and, coupled with the inability of the nitroxide free radicals to initiate new chain growth, leads to controlled

polymerization. These features have been exploited in the preparation of star and graft polymers, hyperbranched systems, and low polydispersity random and block copolymers [Hawker *et al.* 2001; Hawker *et al.* 1996]. The living nature of this process also permits the molecular weight and chain ends of the macromolecules to be accurately controlled.

In this type of process, the propagating species ($P_n^{\bullet}$) reacts with a stable radical ($X^{\bullet}$) as seen in Scheme 1.1. The resulting dormant species (P_n-X) can then reversibly cleave to regenerate the free radicals once again. Once ($P_n^{\bullet}$) forms it can then react with a monomer, M, and propagate further. The most commonly used stable radicals have been nitroxides, especially TEMPO. Initiating systems in NMP can be divided into two classes, unimolecular initiators in which alkylated TEMPO (2,2,6,6-tetramethylpiperidinyloxy) derivatives dissociate to provide both the initiating radical and the stable radical (Scheme 1.2), and bimolecular systems in which a traditional free radical initiator, such as BPO or AIBN, is used in conjunction with TEMPO (Scheme1.3). For the unimolecular initiators it was found that an α-methyl group is essential for "living" character, while a variety of substituents could be placed on the phenyl ring or the *β*-carbon atom without affecting the efficiency of the unimolecular initiator. It was also found that the rate of polymerization is approximately the same for both the unimolecular and corresponding bimolecular systems; however, the unimolecular initiators afforded better control over molecular weight and polydispersity.

Although NMP is one of the simplest methods of LFRP, it has many disadvantages. Many monomers will not polymerize because of the stability of the dormant alkoxyamine that forms. Also, since the reaction is kinetically slow, high temperatures and bulk solutions are often required. Also, the alkoxyamine end groups are difficult to transform and require radical chemistry.
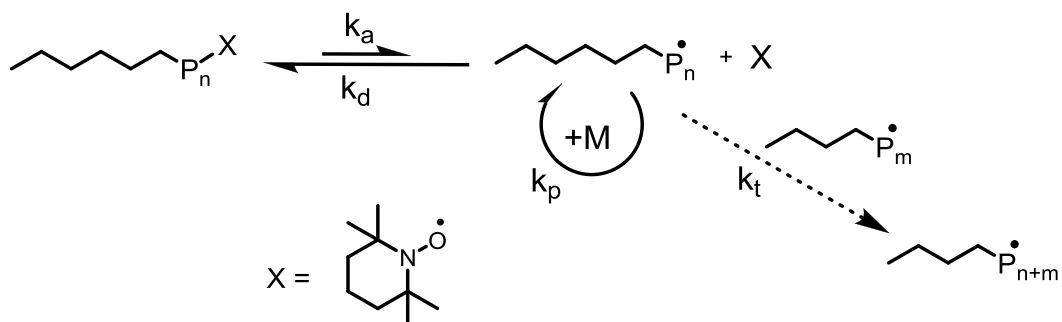
Scheme 1.1. Mechanism of NMP.
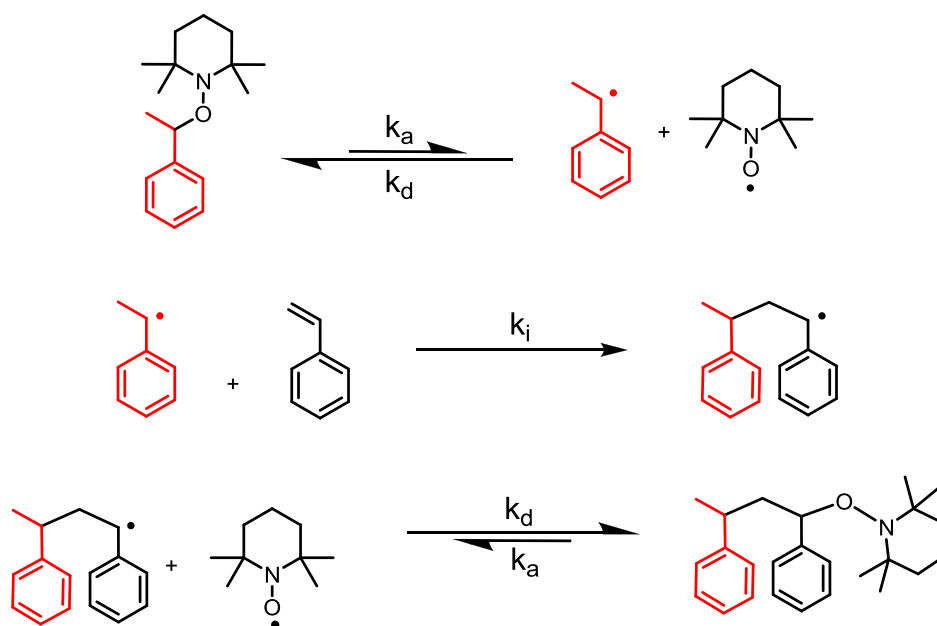
Scheme 1.2. Mechanism of unimolecular NMP.
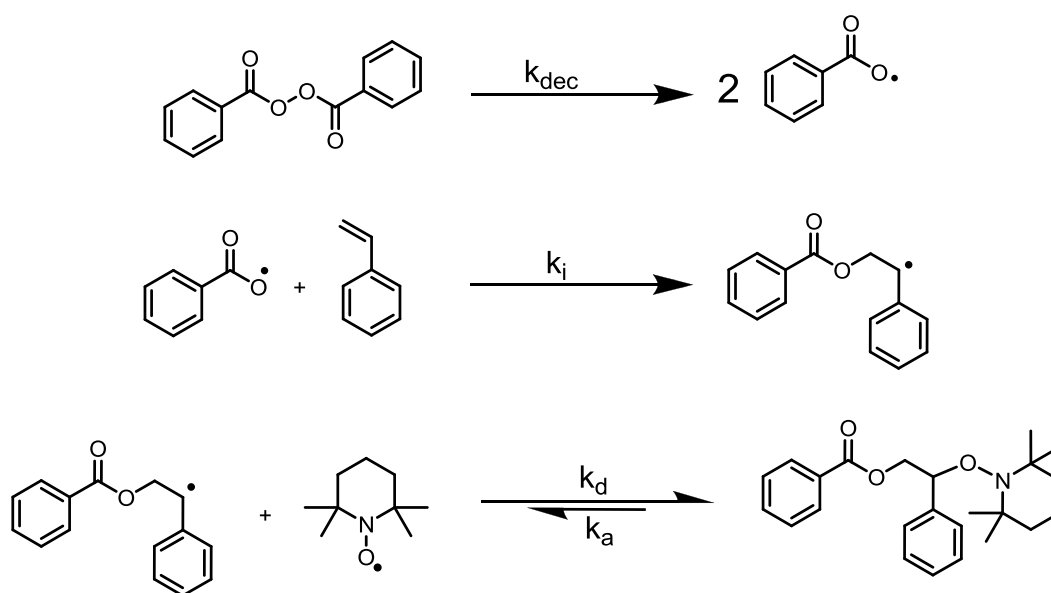
Scheme 1.3. Mechanism of bimolecular NMP.

1.5.3. Atom Transfer Radical Polymerization (ATRP)

ATRP is based on the reversible transfer of an atom or group from a dormant polymer chain (R-X) to a transition metal (M_t^n / Ligand) to form a radical ($R^\bullet$), which can initiate the polymerization, and a metal-halide, whose oxidation state has been increased by one (X- M_t^n / Ligand); the transferred atom or group is covalently bound to the transition metal. A catalytic system employing copper (I) halides complexed with substituted 2, 2'-bipyridines (bpy) has proven to be quite robust, successful polymerizing styrenes, various (meth)acrylates, acrylonitrile and various other monomers [Matyjaszewski 2003; Wang, J.-S. *et al., J. Am. Chem. Soc.* 1995; Wang, J.-S. *et al., Macromolecules* 1995]. Other metal centres have been used, such as ruthenium, nickel and iron based systems [Matyjaszewski 2002, Kamigaito *et al.* 2001]. Copper atoms with various anions and polydentate complexing ligands were used, such as substituted bpys, pyridines, and linear polyamines. The rate constants of the exchange process, propagation and termination shown in Scheme 1.4 below refer to bulk styrene polymerization at 110 °C.

An ATRP system consists of an initiator, a metal halide complexed with some ligand(s), and the monomer. Thus far, the copper-based ATRP system has been adapted successfully for the controlled/living polymerization of styrenes, acrylates, methacrylates, acrylonitrile, and other monomers. The ruthenium/aluminum alkoxide based ATRP system has been demonstrated to work with methacrylates, acrylates and styrene. The iron-based ATRP system has been demonstrated to work with styrenes and methacrylates, while the nickel-based ATRP systems have been shown to work for methacrylates. The choice of monomer to be polymerized dictates the types of other components that can be used. The initiator usually, but not always, should have a structure homologous to the corresponding polymer end group. Also, the halogen atom in

the initiator and metal complex should correspond with one other, but again, in some cases this is not necessary. For copper-based ATRP, typically two equivalents of a bidentate ligand is added per copper center [Patten *et al.* 1998]. The most effective ligands are derivatives of 2,2'-bipyridine other π-accepting, chelating nitrogen-based ligands such as 2-iminopyridines, and some aliphatic polyamines. As complexes of 2,2'-bipyridine with copper(I) halides are largely insoluble in the non-polar media of bulk polymerizations, long alkyl chain substituents at the 4,4'-positions of the bipyridine ligand serve to increase the solubility of the resulting copper complex.
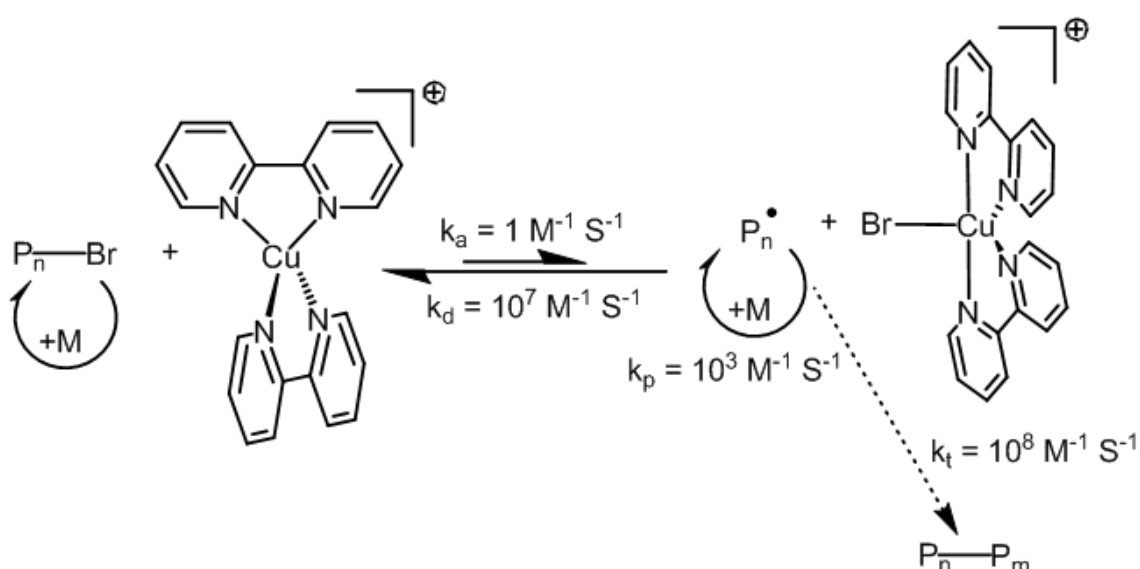
Scheme 1.4. ATRP equilibrium with a copper halide complex that contains two bipyridine ligands.

The mechanism of ATRP is shown in Scheme 1.5. The mechanism consists of initiation and propagation processes that are phenomenologically related. ATRP involves first a reduction of the initiator by a transition metal complex forming a radical initiating species and a metal halide complex. The reactive centre can then initiate the monomer, which can then propagate with additional monomer or abstract the halide from the metal complex forming a dormant alkyl halide species. The alkyl halide species is then activated by the metal complex and propagates once more.

Initiation

$$R\text{-}X \;+\; L_nM_t^{+z} \quad \underset{}{\overset{K'_{eq}}{\rightleftharpoons}} \quad R^{\bullet} \;+\; L_nM_t^{+(z+1)}X$$

$$[\, X = Cl,\ Br \,]$$

$$R^{\bullet} \;+\; {=\!\!\!\diagdown}_R \quad \xrightarrow{\;k_{p'}\;} \quad P_1^{\bullet}$$

Propagation

$$P_n\text{-}X \;+\; L_nM_t^{+z} \quad \underset{}{\overset{K'_{eq}}{\rightleftharpoons}} \quad P_n^{\bullet} \;+\; L_nM_t^{+(z+1)}X$$

$$P_n^{\bullet} \;+\; {=\!\!\!\diagdown}_R \quad \xrightarrow{\;k_{p}'\;} \quad P_{n+1}^{\bullet}$$

Termination

$$P_n^{\bullet} \;+\; P_m^{\bullet} \quad \xrightarrow{\;k_t\;} \quad P_{n+m}^{\bullet} \;+\; \left(P_n^{=} \;+\; P_m^{H} \right)$$
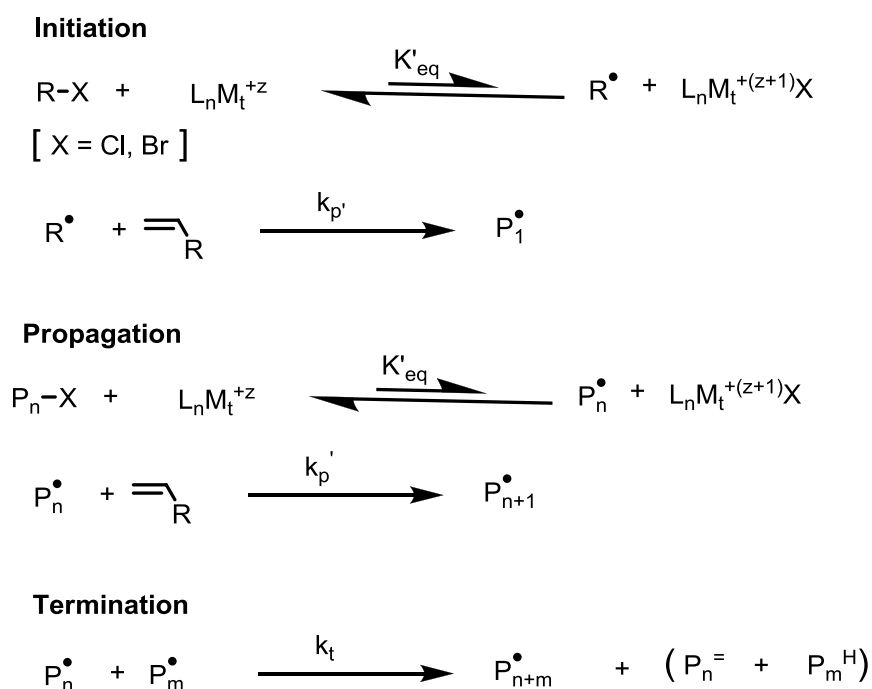
Scheme 1.5. General mechanism of ATRP.

The rate of ATRP is internally first order in monomer, externally first order with respect to initiator and activator, Cu(I), and negative first order with respect to the deactivator, XCu(II). The kinetics depends on many factors including the solubility of activator and deactivator, their possible interactions, and variations of their structures and reactivities with concentrations and composition of the reaction medium [Patten *et al.* 1997].

One of the most important parameters in ATRP is the dynamics of exchange, and especially the relative rates of deactivation. If the deactivation rate is slow in comparison with propagation, then a classical redox initiation process operates, leading to conventional, and not controlled, radical polymerization. Polydispersities in ATRP decrease with conversion, with the rate constant of deactivation, k_d, and also with the concentration of the deactivator, [XCu(II)]. They, however, increase the propagation rate constant, k_p, and the concentration of initiator $[RX]_0$. This means that more uniform polymers are obtained at higher conversions, when the concentration of deactivator in

solution is high and the concentration of initiator is low [Matyjaszewski, *Chem. Eur. J.* 1999; Patten *et al.* 1996]. Also, more uniform polymers are formed when deactivator is very reactive (e.g. copper(II) complexed by 2, 2'-bipyridine or PMDETA rather than by water) and monomer propagates slowly (styrene rather than acrylate).

The most important component of ATRP is the catalyst. It is the key to ATRP since it determines the position of the atom transfer equilibrium and the dynamics of exchange between the dormant and active species. There are several prerequisites for an efficient transition metal catalyst. First, the metal center must have at least two readily accessible oxidation states separated by one electron. Second, the metal center should have reasonable affinity toward a halogen. Third, the coordination sphere around the metal should be expandable upon oxidation to selectively accommodate a (pseudo)-halogen. Fourth, the ligand should complex the metal relatively strongly. Eventually, the position and dynamics of the ATRP equilibrium should be appropriate for the particular system [Patten *et al.* 1998; Ouchi *et al.* 2009]. From these requirements, most likely, late transition metals of group 8-11 have been employed for the metal-catalyzed living radical polymerization; most typically, these metals include iron, nickel, ruthenium, and copper.

The main role of the ligand in ATRP is to solubilise the transition-metal salt in the organic media and to adjust the redox potential of the metal center for appropriate reactivity and dynamics for the atom transfer [Boffa *et al.* 2000]. There are several guidelines for an efficient ATRP catalyst. First, fast and quantitative initiation ensures that all the polymer chains start to grow simultaneously. Second, the equilibrium between the alkyl halide and the transition metal is strongly shifted toward the dormant species side. This equilibrium position will render most of the growing polymer chains dormant and produce a low radical concentration. As a result, the contribution of radical termination reactions to the overall polymerization is minimized. Third, fast deactivation of the active radicals by halogen transfer ensures that all polymer chains are growing at

approximately the same rate, leading to a narrow molecular weight distribution. Fourth, relatively fast activation of the dormant polymer chains provides a reasonable polymerization rate. Fifth, there should be no side reactions such as β-H abstraction or reduction/oxidation of the radicals. Examples of nitrogen-based ligands used successfully in Cu-based ATRP are shown in Scheme 1.6.

ATRP can be used on a large number of monomers and requires ambient reaction conditions. The reaction is unaffected by the presence of O_2 and other inhibitors. Also, the alkyl halide end groups can be easily transformed by SN_1, SN_2, or radical chemistry. The major drawback to ATRP is that a transition metal catalyst must be used which after polymerization must be removed and possibly recycled. Future work in this field includes the removal and recycling of the catalyst as well as the design of catalysts that react with a larger range of monomers [Shen *et al.* 2004; Tsarevsky *et al.* 2007].
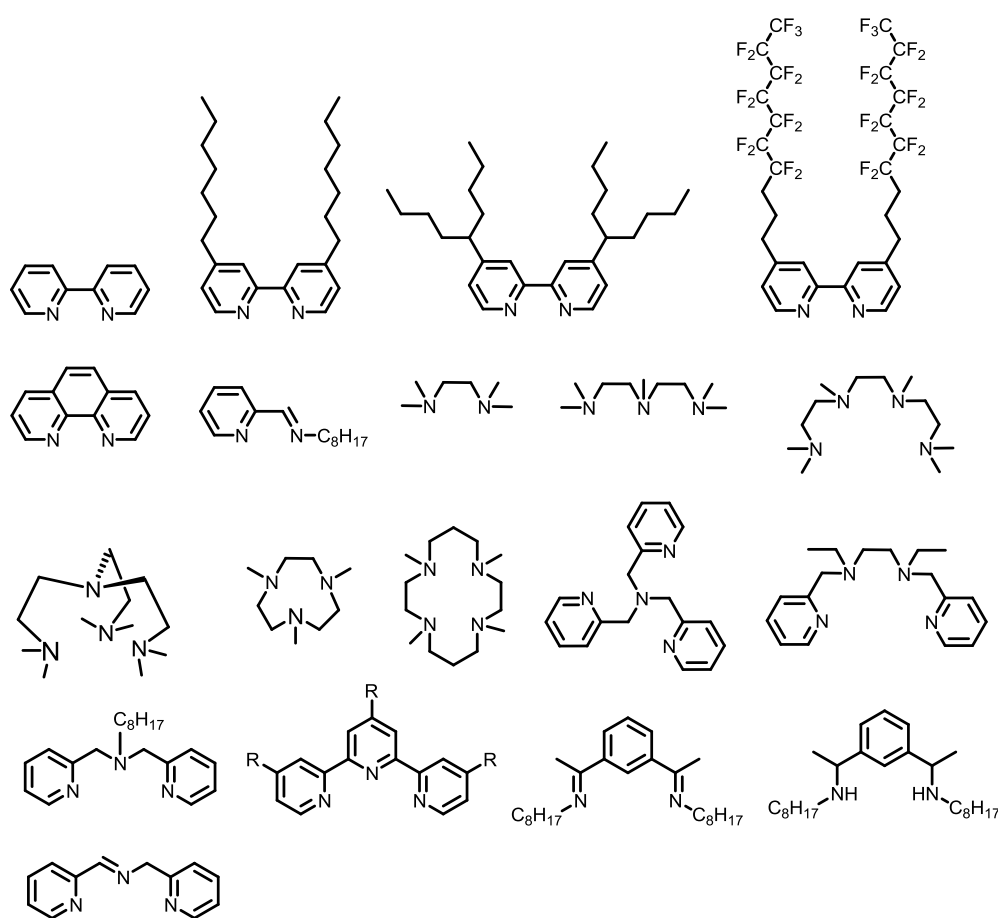
Scheme 1.6. Examples of ligands used in copper-mediated ATRP.

1.5.4. Radical Addition-Fragmentation Chain Transfer (RAFT)

RAFT agents are organic compounds possessing a thiocarbonylthio moiety. The generic structures of RAFT agents employed in RAFT are shown below (Scheme 1.7). The R group initiates the growth of polymeric chains, while the Z group activates the thiocarbonyl bond toward radical addition and then stabilizes the resultant adduct radical [Boyer *et al.* 2009].
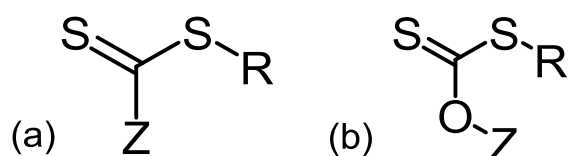
Scheme 1.7. Generic structures of RAFT chain transfer agents.

The generally accepted mechanism for a RAFT polymerization is shown in Scheme 1.8. The first step of polymerization is the initiation step, where a radical is created (step 1). Many different sources of initiation have been reported for a RAFT polymerization, such as the thermal autoinitiation of monomers such as styrene, direct photochemical stimulation of the chain transfer agent by ultraviolet light, γ-radiation, and pulsed laser irradiation. The thermal decomposition of radical initiators is, however, the most widely adopted method of initiation, due to the commercial availability of such compounds.

The oligomeric radicals produced in the initiation step react with the RAFT agent (**1**) in a step of initialization (step 2). There is compelling evidence in the literature that the entire RAFT agents (if appropriately selected) are consumed in this step before any propagation commences. This is due to the highly reactive C=S bond of the RAFT agent, which means that radical addition is favoured over the addition to any of the double bonds that are present on the monomer. The radical intermediate (**2**) can fragment back to the original RAFT agent (**1**) and an oligomeric radical or fragment to yield an oligomeric RAFT agent (**3**) and a reinitiating R radical. The structure of R should be such that it is a

good reinitiating group. It should fragment at least as quickly as the initiator or polymer chains from the stabilized radical intermediate (**2**). Following initialization, polymer chains grow by adding monomer (step 3), and they rapidly exchange between existing growing radicals (as in the propagation step) and the thiocarbonylthio group capped species (step 4, **4**). The rapid interchange in the chain transfer step ensures that the concentration of growing radical chains is kept lower than that of the stabilized radical intermediates (**4**), therefore limiting termination reactions. Although limited, termination reactions still occur *via* combination or disproportionation mechanisms (step 5).
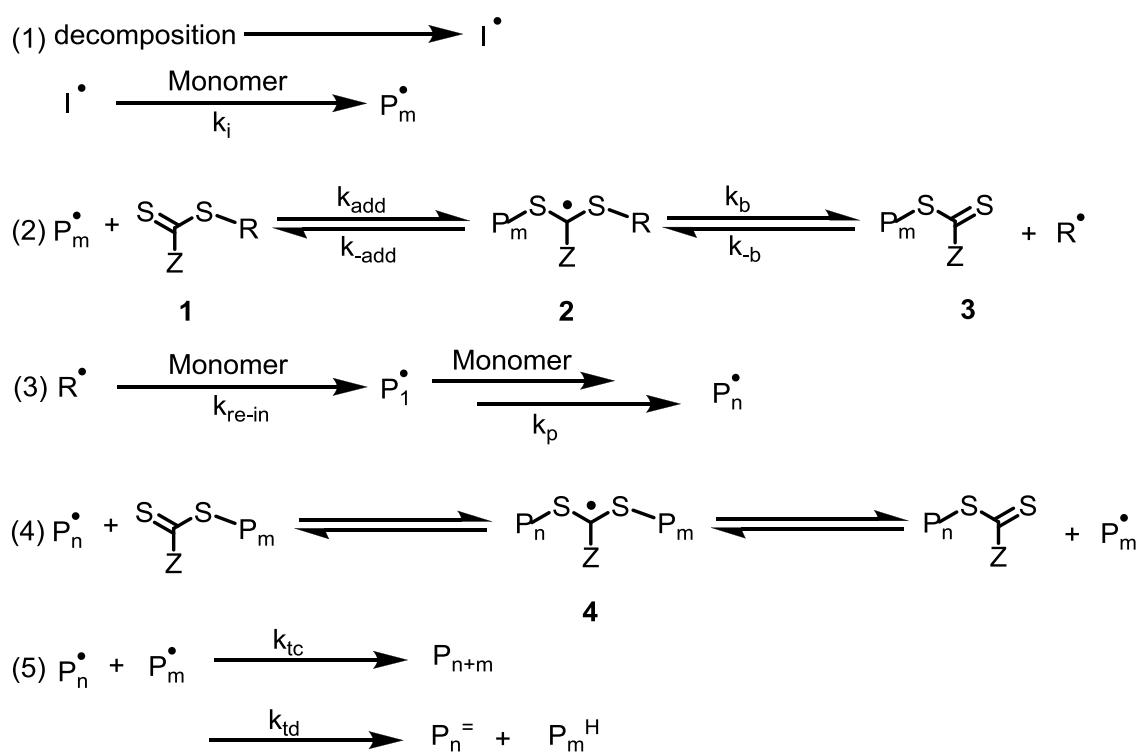
Scheme 1.8. General accepted mechanism for a RAFT polymerization.

The greatest advantage to RAFT is the incredible range of polymerizable monomers. As long as the monomer can undergo radical polymerization, the process will most likely be compatible with RAFT [Chong *et al.* 1999; Chiefari *et al.* 1998]. However, there are many major drawbacks that arise when using this process. The dithio end groups left on the polymer give rise to toxicity, colour, and odour and their removal

or displacement requires radical chemistry. Also, the RAFT agents are expensive and not commercially available. Another drawback is that the process requires an initiator, which can cause undesired end groups and produce too many new chains which can lead to increased termination rates [Lowe *et al.* 2007].

1.6. Self-Assembly of Amphiphilic Block Copolymers

The ability of amphiphilic block copolymers to self-assemble in selective solvents forming colloidal size aggregates or micelles has attracted considerable attention over the past few years [Zhang *et al.* 1995; Froster *et al.* 1998; Massey *et al.* 1998; Yu, K. *et al.* 1998; Discher *et al.* 2002]. Self-assembly, or the organized association of block copolymers dissolved in a solvent selective for one of the blocks, occurs in order to minimize contact between the insoluble block and the solvent system. If, for example, the formed structures are micelles, they consist of a compact core of the insoluble block surrounded by a flexible corona of the soluble block. Block copolymer micelles can be divided into two types, regular and reverse. In a polar solvent, such as water, regular micelles are formed, which have a hydrophobic core and a hydrophilic corona [Xu *et al.* 1991; Astafieva *et al.* 1993; Khougaz *et al.* 1995]. In an apolar (or low polarity) solvent, the locations of the blocks are reversed, i.e. the hydrophilic segments form the core which is surrounded by a hydrophobic corona shell. In this case, the micelles are referred to as reverse [Desjardins *et al.* 1991; Desjardins *et al.* 1992; Gao *et al.* 1992]. Depending on the composition of the block copolymers, each of the micelle types can be further divided into star and crew-cut micelles. Two types of micelles can be distinguished based on the relative block length of the copolymer: star micelles, which have a relatively small core and a long corona, and crew-cut micelles, which are characterized by a large core and a relatively shorter corona [Choucair *et al.* 2003; Zhang *et al.* 1998].

There are two major differences between the star and crew-cut micelles, the process of the micelle formation and their morphogenesis. Generally, star-type micelles [Tuzar *et al.* 1993] can be prepared directly by dissolving a highly asymmetric block copolymer in a solvent which is selective (good) for the long block. During the dissolution of the block copolymers, the insoluble (short) blocks form the core while the long blocks form the corona of the micelles. Usually, the method of direct dissolution is not suitable for the preparation of crew-cut aggregates because of the very high fraction and the large relative size of the insoluble block. To prepare stable solutions of crew-cut aggregates, highly asymmetric diblock copolymers are first dissolved in a common solvent for both blocks. Subsequently, a precipitant for the long block, but a good solvent for the short block, of the copolymers is added to induce the aggregation of the long blocks. Because a variation of the solvent quality is involved, the system of crew-cut micelles is more complicated than that of star micelles, where a one- component solvent or a solvent mixture with a fixed composition is usually used [Cameron *et al.* 1999].

Crew-cut micelle-like aggregates of highly asymmetric copolymers of polystyrene-b-poly(acrylic acid) diblock copolymers (PSt-b-PAA), which in aqueous solution form anionic micelles, have been extensively studied by Eisenberg et al. Since 1995 [Riegel *et al.* 2003], a vast array of structures was identified [Zhang *et al., J. Am. Chem. Soc.* 1996; Shen *et al.* 1999] and detailed investigations have begun on the thermodynamic and kinetic aspects that induce morphogenesis [Zhang *et al.* 1999; Burke *et al.*, *Langmuir* 17 (**2001**) 6705]. Many factors were found to influence the resulting morphologies, as for example, the copolymer composition and concentration [Shen *et al.* 2000], the nature of the common solvent [Yu, Y. *et al.* 1998], the type and concentration of added ions [Zhang *et al., Science* 1996], among other factors [Burke *et al.*, *Langmuir* 17 (**2001**) 8341].

Battaglia *et al.* in 2005 reported the self-assembly of a block copolymer $E_{115}B_{103}$ (where E is used to denote an oxyethylene unit, $-OCH_2CH_2-$, B is used to denote an oxybutylene unit, $-OCH_2CH(CH_2CH_3)-$, and the subscripts are the number-average degree of polymerization) in water at different concentrations. The samples were prepared by mixing the copolymer with water and leaving it to equilibrate for several weeks before analysis. In Figure 1.6 all of the results are summarized in a phase diagram. Four different transitions have been identified on dilution: lamellae → interconnected sponge → hexagonal-packed vesicles → isotropic vesicles. At room temperature the pure (slightly hydrated) copolymer has a lamellar architecture as a result of the phase separation between the blocks. When more water is added, it will dissolve into the hydrophilic layers, generating a swollen lamellar phase. At a certain concentration, the lamellar layers start separating from each other and the edges drive the lamellae to assemble into a sequence of different phases. The unbinding does not seem to occur homogeneously, owing to inherent defects in the lamellar structure, and the result will be the formation of holes in the lamellar sheets and, at the microscale, biphasic regions that scatter light and cause turbidity. The interconnected structure is known as the sponge phase; in this specific case most of the structure is random and retains the form birefringence of the parent membranes. At around 10% w/w the copolymer–water system transforms from a gel to a liquid, water is no longer absorbed into the copolymer and the block copolymer now forms discrete aggregates in a continuous water matrix. The excess of water forces the lyotropic phases to break up into microclusters that seem to retain their long-range order. This order has been observed to be retained even at concentrations below 1% amphiphile. Only at very low concentrations below 0.5% w/w do vesicles detach from each other and dissolve as discrete entities in water.
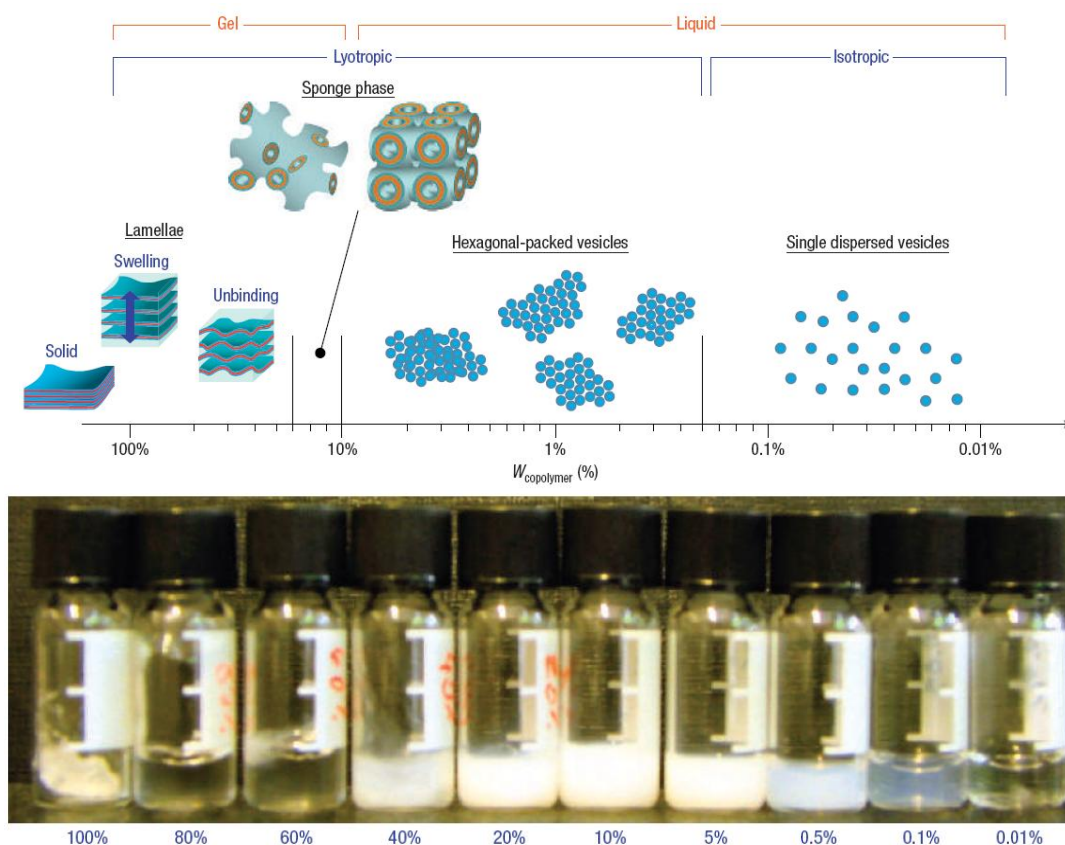
Figure 1.6. The phase diagram of $E_{115}B_{103}$ in water. [Adapted from Battaglia *et al.* 2005].

By using a combination of ATRP and [3 + 2] cycloaddition reaction between reactive azide residue and C_{60} Liu and co-workers synthesized an amphiphilic block copolymer $PEO_{45}(-C_{60})$-b-PSt_{380} incorporating a single C_{60} moiety at the diblock junction point [Wang, X. *et al.* 2008]. Fullerene containing hybrid vesicles were then fabricated for the first time via the supramolecular self-assembly of $PEO_{45}(-C_{60})$-b-PSt_{380} in aqueous solution using 1,4-dioxane as the cosolvent. Figure 1.7 shows the structure of $PEO_{45}(-C_{60})$-b-PSt_{380} and HRTEM images of the vesicles obtained from its aqueous solution.

PEO₄₅(-C₆₀)-b-PSt₃₈₀
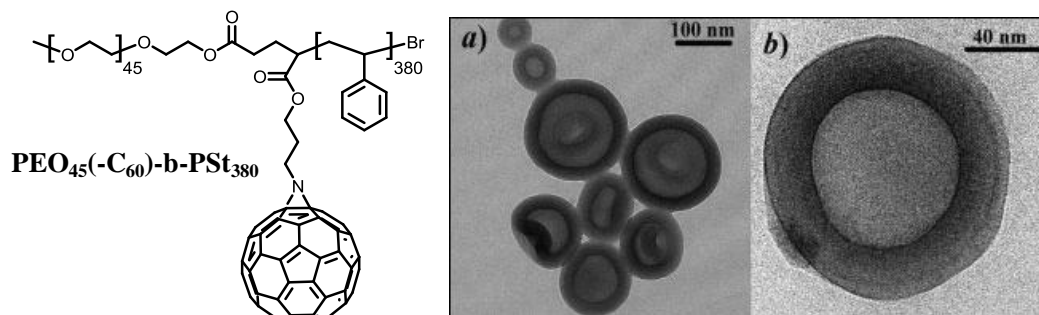
Figure 1.7. HRTEM images of fullerene-containing hybrid vesicles self-assembled from in aqueous solution using 1,4-dioxane as the cosolvent. [Adapted from Wang *et al.* 2008].

Interesting organic/inorganic hybrid vesicles based on a reactive block copolymer poly(ethylene oxide)-*block*-poly(3-(trimethoxysilyl) propyl methacrylate) (PEO-*b*-PTMSPMA), were prepared by Chen *et al.* [Du *et al.* 2003]. Vesicle solution were prepared by adding water into a methanol solution of the block copolymer. TEM images of the resultant solution revealed a vesicular morphology, and the diameter of vesicle was nearly 100 nm. Addition of triethylamine (TPA) into the vesicle solution hydrolyzed R-Si(OCH₃)₃ groups into -Si(OH)₃, which are subsequently transferred into cross-linked polysilsesquioxane by polycondensation. TEM image (Figure 1.8a) of this sample showed vesicular morphology with an average outer radius of 45 nm. SEM image (Figure 1.8b) of this sample shows mainly donut shaped particles, which are believed to be collapsed vesicles due to very high vacuum applied during preparation of sample for SEM analysis. It also demonstrates there are solvent pools included inside vesicles.
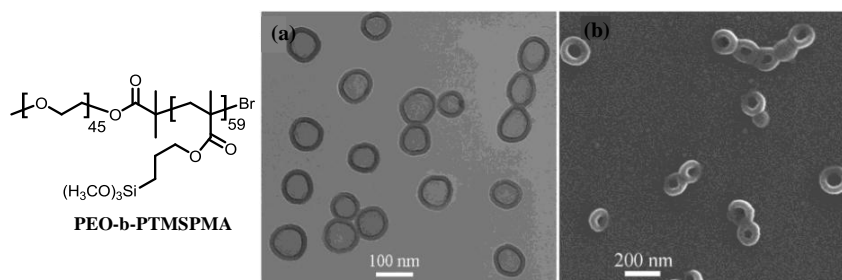
PEO-b-PTMSPMA

Figure 1.8. (a) TEM image of PEO-b-PTMSPMA vesicles after the addition of TPA in methanol/water 45:55 (w/w) at a polymer concentration of 0.45 g/L and (b) SEM image of the vesicles. [Adapted from Du *et al.* 2003].

Pochan and coworkers combined synthetic block copolymer molecular design with solution conditions that favour self-attraction of charged semi-flexible biopolymers to produce toroidal, or ring-shaped, micelles with a high degree of control and uniformity [Pochan *et al.* 2004]. The toroidal micelles are stable reproducible structures that are formed by the collapse of negatively charged cylindrical micelles, driven by interaction with a divalent organic cation. The assemblies are formed by a mixture of poly(acrylic acid–b–methyl acrylate–b-styrene) (PAA_{99}-PMA_{73}-PSt_{66}) triblock copolymer amphiphile, water, tetrahydrofuran (THF), and 2,2'-(ethylenedioxy)diethylamine (EDDA). All four components are critical for toroid formation. Under optimized conditions, the toroidal phase is the predominant structure of the amphiphilic triblock copolymer, as seen from the low magnification transmission electron microscopy (TEM) micrograph of Figure 1.9a. Figure 1.9b illustrates the expected morphology that is generated in solutions composed predominantly of water; the hydrophobic PS and PMA are packaged within the core domain and are partially solvated by THF, and the hydrophilic PAA and hydrophilic but oppositely charged EDDA comprise the micelle corona.
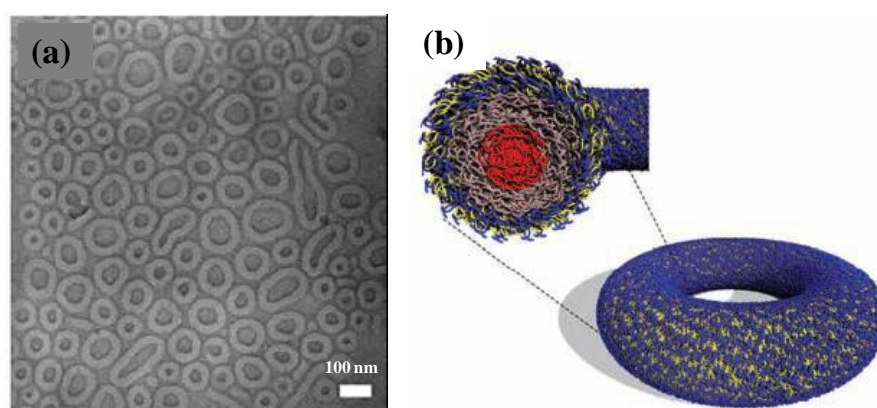
Figure 1.9. (a) TEM image of toroidal micelle structure and (b) cartoon schematic of toroidal micelle with cross section showing hydrophobic PSt (red) and PMA (brown) core and hydrophilic PAA (yellow) corona with closely associated EDDA (blue). [Adapted from Pochan *et al.* 2004].

Winnik, Manners and co-workers have shown that block copolymers consisting of a soluble poly(isoprene) (PI) block and a short, highly crystalline poly(ferrocenyldimethylsilane) (PFS) block (for example, PI_{342}-b-PFS_{57}), form cylindrical micelles (Figure. 1.10) on account of the crystallization of the PFS core [Massey *et al.* 2000]. They also showed that the growth of these micelles can occur in a controlled 'living-like' manner [Wang, X. *et al.* 2007]. That is to say, as is the case for the living covalent polymerizations of monomers [Szwarc 1998], the size of the growing chain (cylindrical micelle, in this case) is controlled by the amount of monomer (block copolymer) present, and that chain ends of the polymer (cylindrical micelle) are still active, or alive, even after all the monomer (block copolymer) has been consumed. In living covalent polymerizations this persistent active site has allowed access to block copolymers and more complex polymer architectures, which is how most of the block copolymers used in the self-assembly of micelles are synthesized [Wang, X. *et al.* 2007; Rowan 2009].
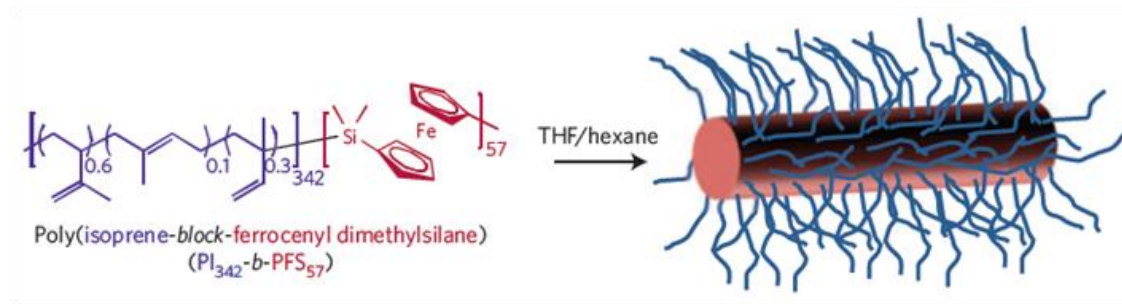
Figure 1.10. Chemical structure of PI_{342}-b-PFS_{57} and a schematic of its cylindrical micelle. [Adapted from Rowan 2009].

Recently Winnik, Manners and co-workers [Gädt *et al.* 2009] have probed the potential of this interesting crystallization driven polymerization concept to access much more complex micelle-like architectures. For example, assembly of the block copolymer PI_{76}-b-PFS_{76}, in which the ratio of the soluble block to the crystallizable block is greatly reduced relative to the cylindrical-micelle-forming PI_{342}-b-PFS_{57}, yields platelet micelles.

Using these tape-like architectures, it is shown that simple addition of PI_{342}-b-PFS_{57} results in the epitaxial growth of a number of cylindrical 'tassels' from the ends of the platelet yielding what is called 'scarf-shaped' co-micelles (Figure 1.11a, b). The researchers also show that by depositing the crystalline homopolymer PFS onto a surface, and exposing the crystalline surface to the cylindrical-micelle-forming PI_{342}-b-PFS_{57}, brushes of the cylindrical micelle grow from the step edges on the surface (Figure 1.11c, d). This seems to be analogous to the process used for the growth of polymer brushes [Edmondson *et al.* 2004] from a surface using living covalent polymerizations. In addition, there is some flexibility in the nature of the crystalline block used as it is demonstrated that tri- and penta-block co-micelles can be accessed by using a heteroepitaxial growth process and growing a related crystalline block copolymer derived from poly(ferrocenyldimethylgermane) (PFG) off a micelle containing the PFS block.
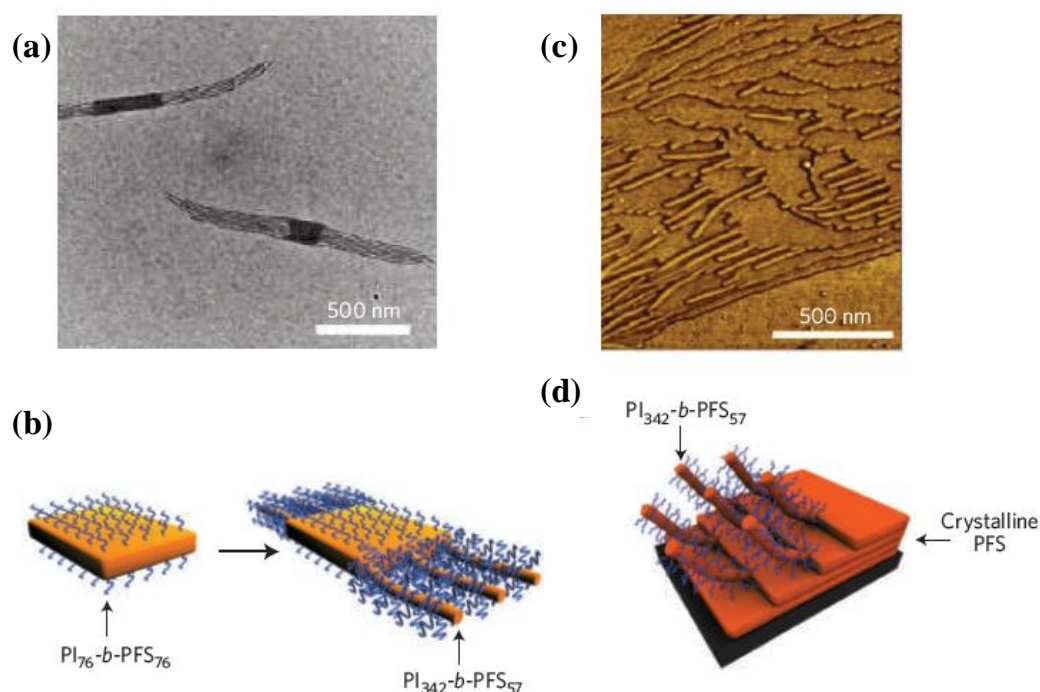
Figure 1.11. (a) A TEM micrograph of a scarf-shaped micelles and (b) a schematic of their assembly. (c) An AFM image of PI_{342}-b-PFS_{57} cylinders grown from a poly(ferrocenyldimethylsilane) coated silicon wafer and (d) a schematic of their assembly. [Adapted from Rowan 2009].

Winnik, Manners and co-workers have nicely demonstrated that epitaxial crystallization-driven assembly of micellar structures is not only a living process but, like its covalent counterpart, it allows access to a range of new architectures. The controllability of this approach that allows one to not only easily tailor the length but also the nature of self-assembled nanostructures may well revolutionize approaches to controlled nano-assemblies in the same way the development of living covalent polymerization conditions dramatically impacted the accessibility of complex covalent polymer architectures.

1.7. Block Copolymer Micelles for Drug Delivery

Since liposomes were first described in the 1960s and proposed as carriers of proteins and drugs for disease treatment, nanotechnology has made a significant impact on the development of drug delivery systems. A variety of organic/inorganic nanomaterials and devices have been used as delivery vehicles to develop effective therapeutic modalities (Figure 1.12). So far, there are over two dozen nanotechnology-based therapeutic products approved by Food and Drug Administration (FDA) for clinical use, and more are in clinical trials [Wagner *et al.* 2006; Zhang *et al.* 2008; Davis *et al.* 2008]. Of these products, the majority are composed of a non-targeted delivery system (e.g., liposomes and polymers) and a drug, and are therefore considered first generation nanotherapeutics [Riehemann *et al.* 2009].

Compared to conventional drug delivery, first generation nanosystems provide a number of advantages. In particular, they can enhance the therapeutic activity by prolonging drug half-life, improving solubility of hydrophobic drugs, reducing potential immunogenicity, and/or releasing drugs in a sustained or stimuli-triggered fashion. Thus, the toxic side effects of drugs can be reduced, as well as the administration frequency. In addition, nanoscale particles can passively accumulate in specific tissues (e.g., tumors)

through the enhanced permeability and retention (EPR) effect [Matsumura *et al.* 1986]. Beyond these clinically efficacious nanosystems, nanotechnology has been utilized to enable new therapies and to develop next generation nanosystems for "smart" drug delivery [Shi *et al.* 2010].
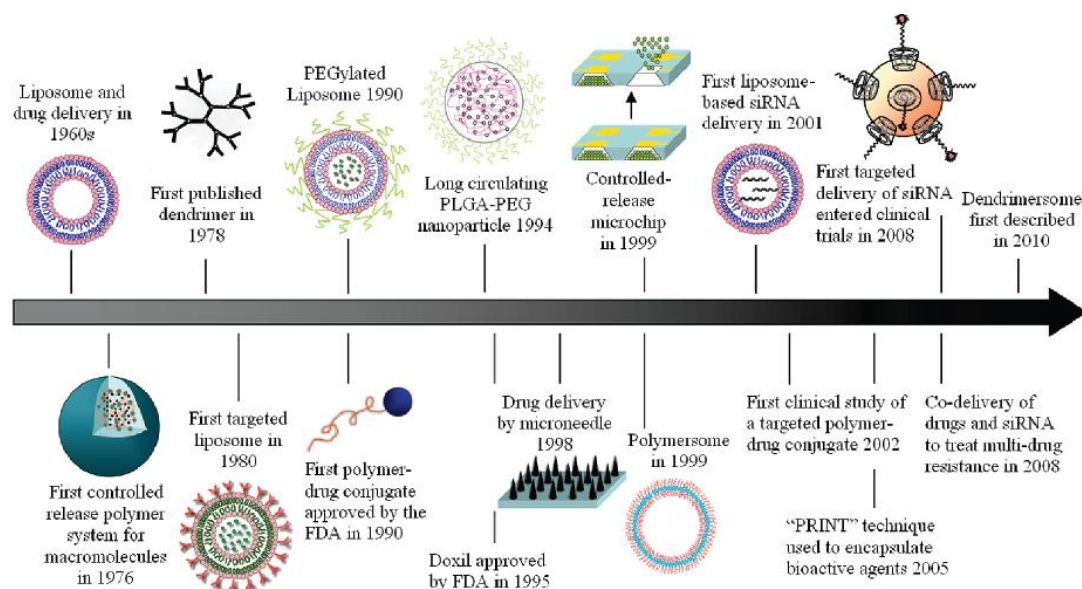
Figure 1.12. Timeline of nanotechnology-based drug delivery. [Adapted from Shi *et al.* 2010].

Ideally, a drug delivery system should respond to physiological requirements, sense the changes and alter the drug-release profile accordingly [Gupta *et al.* 2002]. This encompasses the two concepts of (1) temporal modulation and (2) site-specific drug targeting [Qiu *et al.* 2001]. The symptoms of most disease states follow a rhythmic pattern, e.g. angina pectoris, diabetes mellitus, etc, and require drug delivery as per the rhythms. More importantly, if the drug possesses side effects, drug release when not required poses an extra burden on the body's metabolic system [Gupta et al. 2002]. A more appropriate and effective approach of managing some of these conditions is by chronotherapy. This approach allows for pulsed or self-regulated drug delivery which is adjusted to the staging of biological rhythms, since the onset of certain diseases exhibit strong circadian temporal dependence [Bawa *et al.* 2009].

Stimuli-responsive polymeric drug delivery is a more recent development in the field of controlled drug delivery. These systems closely follow the normal physiological process of the disease state where the amount of drug released is affected according to the physiological need [Kost *et al.* 2001]. Biopolymers such as proteins, carbohydrates and nucleic acid are all basic components of living organic systems that are responsible for the construction and operation of the cells' complicated machinery [Galaev *et al.* 1999; Kumar *et al.* 2007].

These 'natural' polymers have led to the development of numerous synthetic polymers that have been designed to mimic these biopolymers. Based on their chemical and physical properties, these synthetic polymers have been named as 'stimuli-responsive' polymers, 'smart' polymers, 'environmental-sensitive' polymers or 'intelligent' polymers. The distinguishing characteristic of these stimuli-responsive polymers is their ability to undergo rapid changes in their microstructure from a hydrophilic to a hydrophobic state which is triggered by small changes in the environment. The macroscopic changes that occur are reversible; therefore the system is capable of returning to its initial state when the trigger is removed.

Many synthetic polymers that exhibit environmentally responsive behaviour can thus be considered as biomimetic and their development is central to emerging 'smart' applications in biology and medicine [Galaev *et al.* 1999]. Of special interest are synthetic or modified biological materials that can undergo conformational or phase changes in response to variations in temperature and/or pH. Polymers of this type are being developed for uses in fields as diverse as bulk engineering and microscale medicine, while specific examples range from microfluidic devices [Barker *et al.* 2000], pulsatile drug release systems [Kikuchi *et al.* 2002; Li *et al.* 2001], bioadhesion mediators [Yamanto *et al.* 2002] and motors/actuators [Ohm *et al.* 2010; Kim *et al.*

2003]. Responsive polymers are also a major focus in emerging nanoscale technologies [Raula *et al.* 2003; Schild 1992].

In all these cases the key parameter defining the responsive or 'smart' behaviour of the polymers is a non-linear response to an external signal. Although there are many responsive elements that can be incorporated in synthetic materials or engineered/modified biopolymers, much of the research to date has involved pH, temperature or light as the stimulus. As in nature, the bulk response of the polymer is usually due to multiple co-operative interactions such as progressive ionisation or loss of H-bonding, that, although individually small, ultimately evoke a large structural change in the material when summed over the whole polymer. This behaviour intrinsically lends itself to biomedical applications making them potential materials for therapeutic use [Alarcón *et al.* 2005].

1.8. Thermally Responsive Polymers

Many of the triggerable devices described below function by inducing a thermally induced phase change in a polymer. These have been reviewed extensively elsewhere [Gil *et al.* 2004; Jeong *et al.* 2002]. Poly(N-isopropylacrylamide) (PNIPAM) is one such polymer that abruptly changes from hydrophilic to hydrophobic material at a lower critical solution temperature (LCST) of 32 ^{o}C [Schild *et al.* 1992]. PNIPAM has been copolymerized with monomers designed to introduce steric hindrance or add additional hydrophilic content, in order to alter the LCST or to adjust the deswelling ratio of the polymer [Keerl *et al.* 2008; Wang, Q. *et al.* 2007]. Other synthetic techniques have been utilized to produce PNIPAM nano- or microgels [Das *et al.* 2006]. It is worth mentioning that although PNIPAM has been used in many temperature-sensitive drug delivery systems, it appears that photothermal heating of the polymer itself is not the mechanism by which near-infrared (NIR) irradiation induces collapse. Rather, this is caused by

pressure phenomena [Juodkazis *et al.* 2000], and effective laser-induced thermal collapse of the polymer requires a form of NIR sensitization [Timko *et al.* 2010].

Studies on thermal-sensitive polymersomes (polymer vesicles) are so far mainly directed to their formation as well as the temperature-induced release of incorporated compounds. An elegant example of temperature-induced self-assembly of polymersomes from amphiphilic block copolymers in water was reported [Li *et al.* 2006]. These polymersomes were prepared from poly[*N*-(3-aminopropyl)-methacrylamide hydrochloride]-*b*-poly(*N*-isopropylacrylamide) (PAMPA-b-PNIPAM). The polymer exists as unimers in aqueous solution at room temperature and self-assembled into vesicles when the solution temperature was raised above the LCST of the PNIPAM chain (Figure 1.13). The transition was reversible and occurred in a narrow temperature range (2-3 °C), between 30 to 40 °C, depending on the composition of the polymer. The vesicles were further "locked" by ionic crosslinking of PAMPA block with an oppositely charged polyelectrolyte poly(sodium 2-acrylamido-2-methylpropanesulfonate) (PAMPS). Thermal-sensitive polymersomes based on PLA-b-PNIPAM [Hales *et al.* 2004] and poly(2-cinnamoylethyl methacrylate)-*b*- PNIPAM [Chen *et al.* 2006] were also reported.
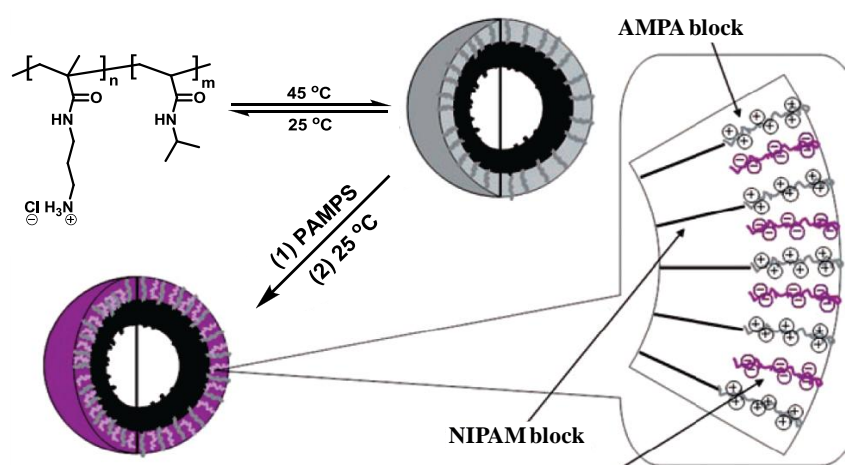
Figure 1.13. Schematic illustration of the formation of vesicles from diblock copolymers PAMPA-b-PNIPAM and their subsequent ionic cross-linking. [Adapted from Li *et al.* 2006].

1.9. pH Responsive Polymers

Systems which respond to pH have attracted great attention and are one of the most studied stimuli-sensitive systems because of the presence of pH variations within the body. For example, along the GI tract the pH changes from acidic in the stomach (pH = 2) to more basic in the intestine (pH = 5-8) [Schmaljohann *et al.* 2006], which is an important point to be considered for oral drug delivery. The pH differences within different tissues and cellular compartments are more subtle. For instance, cancerous tissue is slightly acidic extracellularly (pH = 6.5-7.2) [Rofstad *et al.* 2006; Watson *et al.* 2005]. In cytosol, like in normal tissue and blood, the pH is about 7.4, in endosome the pH is about 5.0-6.5, and lysosome has an even lower pH of 4.5-5.0 [Meng *et al.* 2009]. This intrinsic characteristic of the body has been used to direct the response to a certain tissue (e.g., tumor tissue) or cellular compartment.

Multifunctional micelles for cancer cell targeting, distribution imaging, and anticancer drug delivery were prepared from an environmentally-sensitive graft copolymer, poly(*N*-isopropyl acrylamide-*co*-methacryl acid)-*g*-poly(D,L-lactide) (P(NIPAAm-*co*- MAAc)-*g*-PLA), a diblock copolymer, methoxy poly(ethylene glycol)-*b*-poly(D,L-lactide) (mPEG-PLA) and two functionalized diblock copolymers, galactosamine-PEG-PLA (Gal-PEG-PLA) and fluorescein isothiocyanate-PEG-PLA (FITC-PEG-PLA) [Huang *et al.* 2007]. Anticancer drug, free base doxorubicin (Dox) was incorporated into the inner core of multifunctional micelles by dialysis. From the drug release study, a change in pH (from pH 7.4 to 5.0) deformed the structure of the inner core from that of aggregated P(NIPAAm-*co*-MAAc), causing the release of a significant quantity of doxorubicin (DOX) from multifunctional micelles. Multifunctional micelles target specific tumors by an asialoglycoprotein (HepG2 cells)-Gal (multifunctional micelle) receptor-mediated tumor targeting mechanism. This

mechanism then causes intracellular pH changes which induce DOX release from multifunctional micelles and that micelles have strong effects on the viability of HepG2 cells and are abolished by galactose (Figure 1.14).
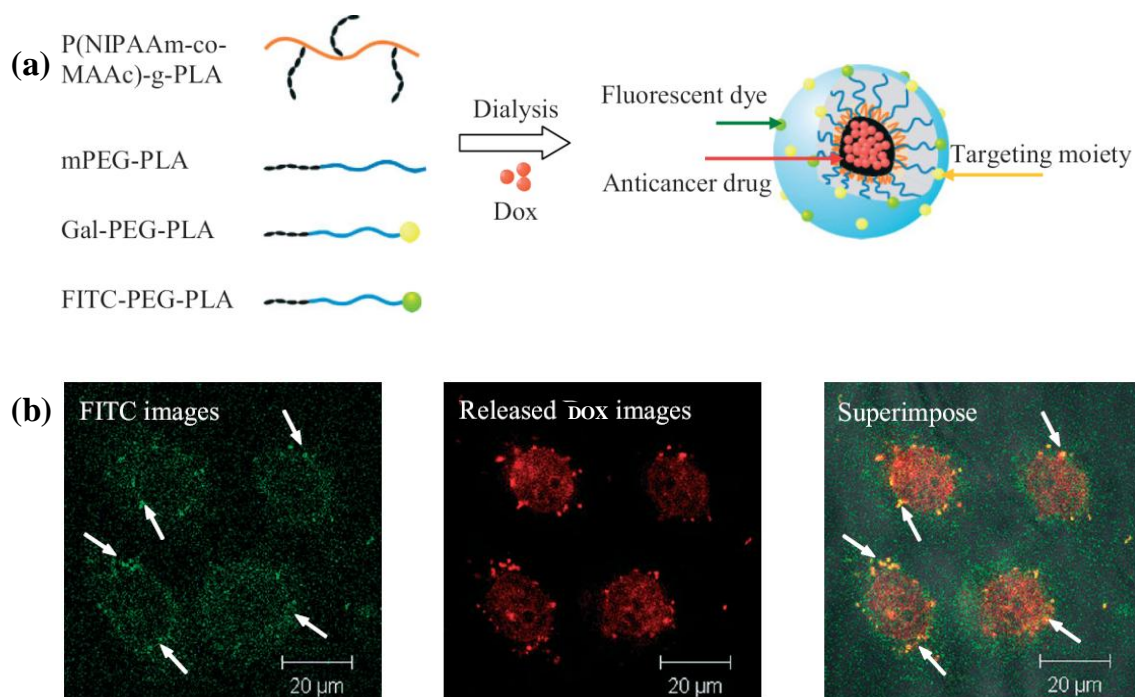
Figure 1.14. (a) Schematic representation of multifunctional micelle structure made of a graft copolymer, a diblock copolymer and two functionalized diblock copolymers and (b) Confocal images of HeLa cells incubated with multifunctional micelles (50 μg mL^{-1}) showing the particulate distribution and localization of released DOX after 6 h internalization. Green fluorescence represents FITC-labeled multifunctional micelles, and red fluorescence represents released DOX. Arrows indicate multifunctional micelle accumulation. [Adapted from Huang *et al.* 2007].

Self-assembly of thermo- and pH-responsive poly(acrylic acid)-b-poly(N-isopropylacrylamide) (PAA-b-PNIPAM) micelles for entrapment and release of DOX was reported by Ma *et al.* [Li et al. 2008]. Block copolymer PAA-b-PNIPAM associated into core-shell micelles in aqueous solution with collapsed PNIPAM block or protonated PAA block as the core on changing temperature or pH. Complex micelles incorporated with DOX exhibited pH-responsive and thermoresponsive drug release profile. The release of DOX from micelles was suppressed at pH 7.2 and accelerated at pH 4.0 due to

the protonation of carboxyl groups. Furthermore, the cumulative release of DOX from complex micelles was enhanced around LCST ascribed to the structure deformation of the micelles. The schematic illustration of DOX induced complexation from PAA-b-PNIPAM and release of DOX from complexes is shown in Figure 1.15.
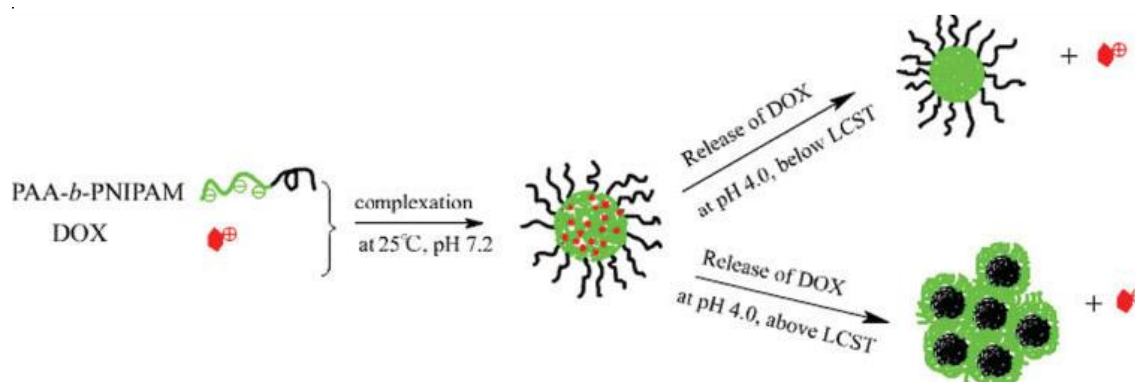
Figure 1.15. Schematic representation of the complexation and release of DOX from PAA-b-PNIPAM in water. [Adapted from Li *et al.* 2008].

1.10. Redox-Potential Sensitive Polymers

Naturally occurring redox potentials within the body can be utilized as a stimulus to trigger the release of encapsulated molecules from nanocarrier systems. Both oxidative conditions existing physiologically in extracellular fluids and pathophysiologically in, for instance, inflamed or tumor tissues, as well as reductive environments within the cell, can be exploited to destabilize carrier systems [Meng *et al.* 2009]. Thayumanavan and co-workers developed highly stable polymeric nanogels, in which the kinetics of guest molecule release can be fine-tuned by control over cross-linking density [Ryu *et al.* 2010]. The polymer nanogel precursor was based on a random copolymer that contains oligoethyleneglycol (OEG) and pyridyldisulfide (PDS) units as side-chain functionalities. Significant control over nanogel size was achieved by introducing variations into the precursor polymer, such as molecular weight and the relative percentages of hydrophilic OEG units and hydrophobic PDS functionalities. Hydrophobic molecules could be noncovalently encapsulated inside the nanogel and the guest molecules can be released in

response to a redox trigger, glutathione (GSH). Stability of dye encapsulation inside the nanogels and tunability in the release of guest molecules was demonstrated through in vitro fluorescence resonance energy transfer (FRET) experiments. Additionally, they have utilized these polymeric nanoparticles to sequester hydrophobic chemotherapeutic drug molecules and release them intracellularly to achieve drug-induced cytotoxicity (Figure 1.16).

(a)

1) x:y = 5:5 Mₙ = 6K 2) x:y = 5:5 Mₙ = 12K
3) x:y = 3:7 Mₙ = 14K 4) x:y = 3:7 Mₙ = 24K

(b)

Random copolymer forms a nano aggregate

The lipophilic interior of the Aggregate can sequester lipophilic molecules in water

Crosslinking reactions forms the nanogel, where lipophilic molecules are locked in
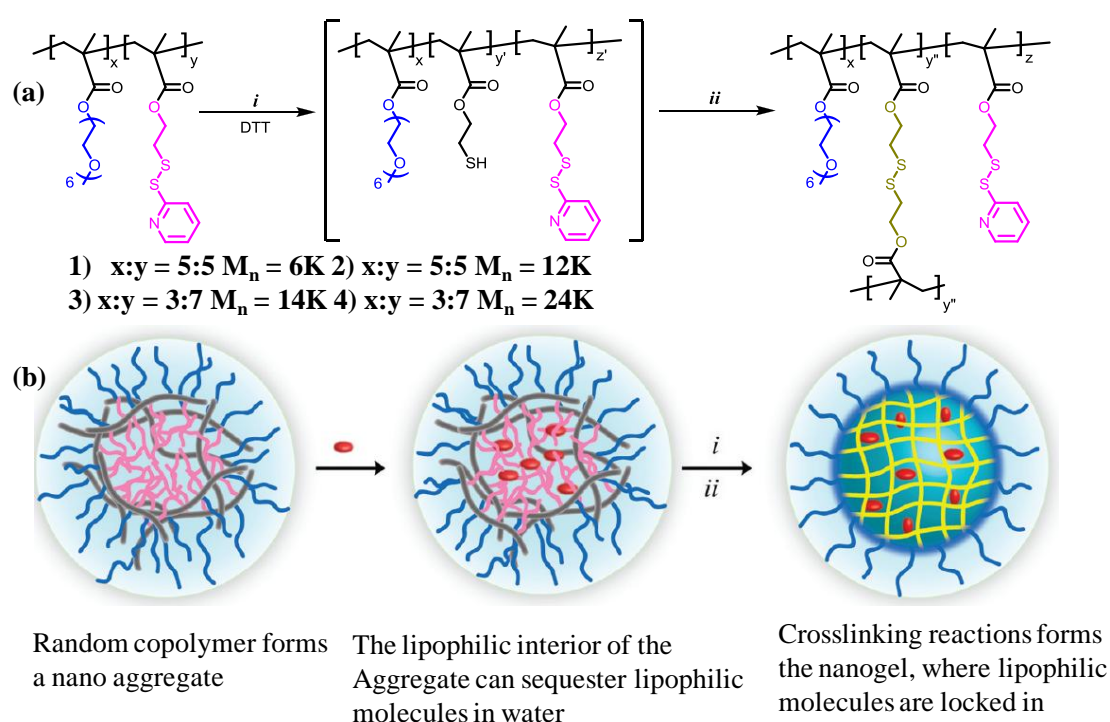
Figure 1.16. (a) Structure of the polymer precursors and nanogels: (i) cleavage of specific amount of PDS group by dithiothreitol (DTT), and (ii) nanogel formation by inter/intrachain cross-linking. (b) Schematic representation of the preparation of the biodegradable nanogels. [Adapted from Ryu *et al.* 2010].

A dual responsive amphiphilic polymer featuring a redox active TTF hydrophobic unit and a temperature-sensitive hydrophilic poly(NIPAM) abbreviated as **1** shell was synthesized by Woisel *et al.* in 2010 [Bigot *et al.* 2010]. As shown in Figure 1.17 this amphiphilic polymer self-associates to form micelles in aqueous media and is able to encapsulate the hydrophobic guest Nile Red (NR). Increasing temperature above the LCST causes the micelles to form large aggregates due to the coil-globule transition of

the poly(NIPAM) chains. It was shown that micelles can be disassembled following the chemical oxidation of the TTF moiety to a more hydrophilic dicationic state, thereby inducing the partial released of NR. In addition, hydrophilic macrocycle CBPQT4+ has the ability to complex with the TTF moiety of **1** leading to a near-complete disruption of the micelle and the efficient release of NR. This methodology paves the way for the formation of a new class of responsive micelles with advanced materials and drug delivery applications.
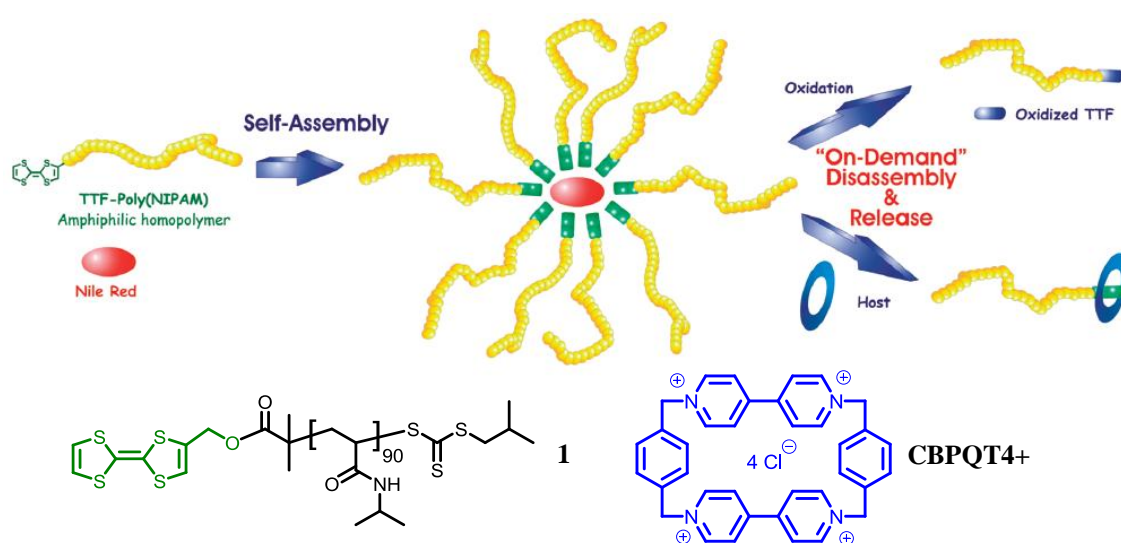
Figure 1.17. Schematic representation of the formation of micelles from polymer **1** and their subsequent disassembly. [Adapted from Bigot *et al.* 2010].

A multi-stimuli sensitive amphiphilic BC assembly that responds to changes in temperature, pH and redox potential was reported by Thayumanavan and co-workers [Klaikherd *et al.* 2009]. The block copolymer design constitutes an acid sensitive tetrahydropyran (THP)-protected 2-hydroxyethyl methacrylate (HEMA) as the hydrophobic part and a temperature-sensitive PNIPAM as the hydrophilic part with an intervening disulfide bond (Figure 1.18). Amphiphilic BC was shown to self-assemble into micellar structure in aqueous solution and is capable of encapsulating hydrophobic guest molecules, such as Nile red. The stimuli-sensitive degradation of the assembly can be achieved under the following conditions: (i) above the LCST, the hydrophilic thermo-

responsive block is converted to a hydrophobic one, rendering the polymer insoluble in water and hence no assembly; (ii) lowering the pH has transformed the acid sensitive hydrophobic block to a hydrophilic one, resulting in the dissolution of the assembly; and (iii) a reducing environment affords the scission of the amphiphilic BC into individual homopolymers and hence disruption of the assembly. Responsiveness to combination of stimuli not only allows for fine-tuning the guest molecule release kinetics, but also provides the possibility of achieving location-specific delivery.
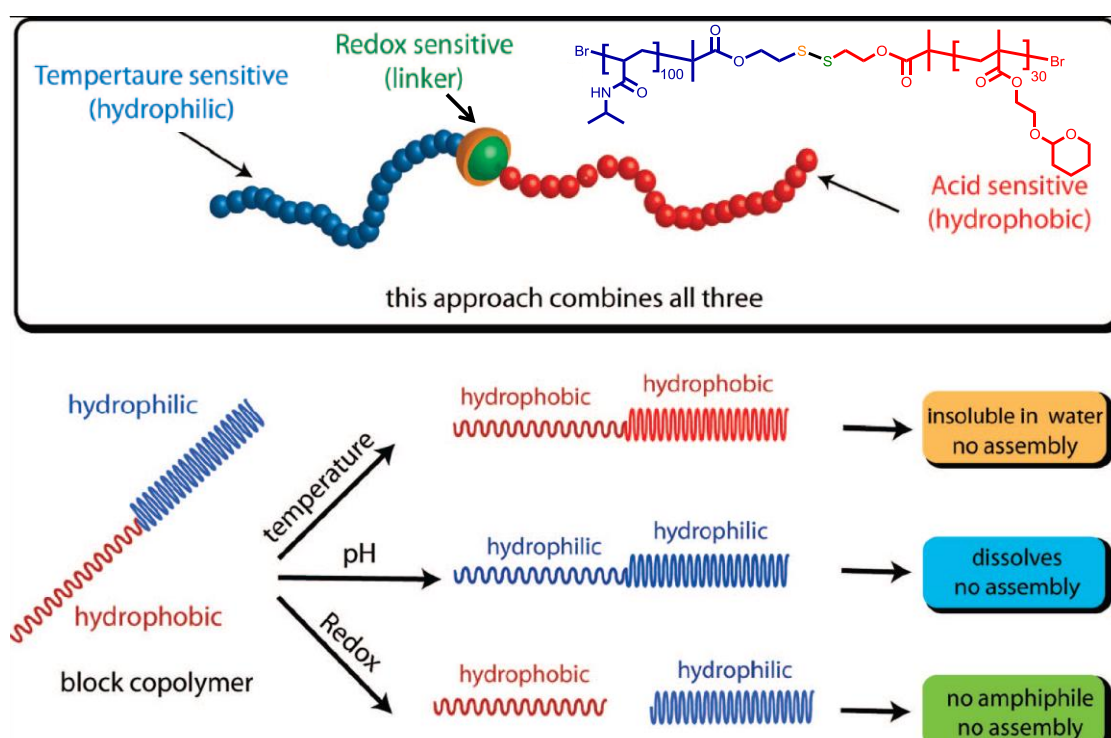
Figure 1.18. Structure and schematic representation of the amphiphilic block copolymer which can respond to three stimuli: temperature, pH and redox. [Adapted from Klaikherd *et al.* 2009].

1.11. Light-Responsive Polymers

Stable, light-responsive block copolymers (LRBCs) are attractive because the release of entrapped species can be rapidly induced at a specific time and location via exposure to light. While pH, oxidation and reduction-responsive systems can also respond quickly, they require that the chemical environment be modified by the addition

of acids or bases or other reagents. These environment changes may not necessarily be compatible with the drug targeting sites (in the case of applications in drug delivery) or with other applications such as controlled chemical reactions in microfluidics. In contrast, light is a remote stimulus that does not require any chemical environmental change [Li *et al.* 2009]. As compared to other stimuli, the use of light to trigger a desired reaction of polymer micelles enables more temporal and positional control [Zhao *et al., J. Mater. Chem.* 2009].

The general strategy for light-induced release is, firstly, the incorporation of small molecules in the core of block copolymer micelles. Upon irradiation, a change in the nature of the core-forming block occurs which further leads to the disruption of the micelles and the subsequent release of the trapped compounds (Figure 1.19). In the case of amphiphilic block copolymer micelles, upon illumination, the photoreaction of the chromophore shifts the hydrophilic/hydrophobic balance toward the dissociation of the micellar aggregates. Two types of photoreactions can lead to this result. In one, the photoreaction of the chromophore increases significantly the polarity of the hydrophobic polymer so that it is no longer hydrophobic enough to hold the micellar association. In the other case, the photoreaction of the dye causes such a structural change that the hydrophobic polymer is simply converted into a hydrophilic one. In the latter case, the basic condition for block copolymer micelle formation is gone, and their micelles should be dissociated by light. In all these cases, disruption can be either irreversible or reversible depending on the kind of used photo-sensitive moiety. The common feature of all the LRBCs encountered for this application is their structure which consists of one water-soluble linear block linked to an insoluble block bearing the chromophores as side groups [Schumers *et al.* 2010; Zhao 2007].
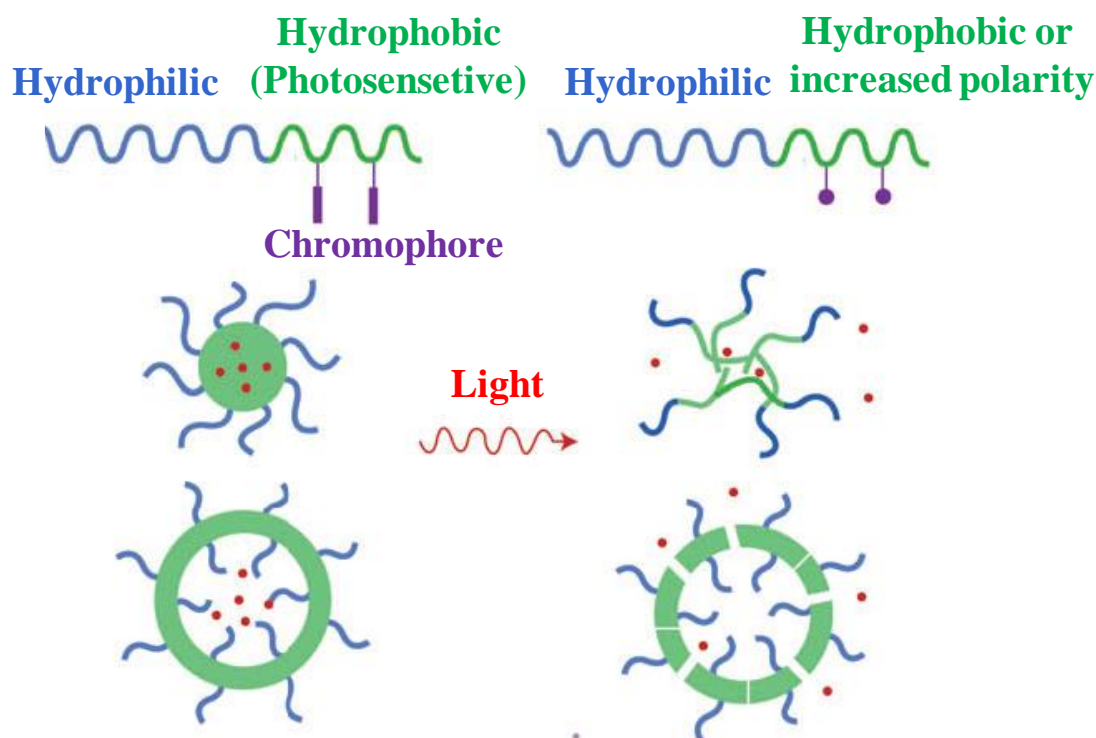
Figure 1.19. Schematic illustration of the rational design of light-dissociable block copolymer core-shell micelles or vesicles. The photoreaction of the chromophore on the hydrophobic polymer either increases its polarity or converts it into a hydrophilic polymer; in both cases, the hydrophilic/hydrophobic balance can be shifted toward the destabilization of the micellar association. [Adapted from Zhao *et al.* 2007].

1.11.1. Polymer Micelles with Reversible Light-Controlled Dissociation and Formation

Azobenzene moieties have been recognized early as candidates of choice for reversible light-induced micellization processes [Wang, G. *et al.* 2004]. Indeed, these molecules are one of the most studied photo-responsive systems in polymer science since the mid 20th century [Kumar *et al.* 1989; Ichimura 2000; Natansohn *et al.* 2002; Zhao *et al., Soft Matter 2009*]. Their great attractiveness is due to the easily reversible trans–cis photo-isomerization of their nitrogen–nitrogen double bond (N=N). In this process, the trans isomer can be converted to the cis one upon UV light irradiation and the back isomerization can be triggered by visible light.

As the photoisomerization is a reversible process, Zhao and coworkers designed a micellar system which can disintegrate upon UV irradiation and reform itself when

irradiated with visible light [Wang *et al.* 2004; Tong *et al.* 2005]. They synthesized by ATRP a block copolymer containing one random poly(t-butyl acrylate-co-acrylic acid) sequence connected to a poly-(methacrylate) bearing azobenzene chromophores as side chains, P(tBA$_{46}$-co-AA$_{22}$)-b-PMAz$_{74}$. Core–shell micelles and/or vesicles could be obtained from this polymer in a dioxane/water mixture depending on the water percentage added to form those objects. For both morphologies, it was possible to disrupt the aggregates upon UV irradiation and reform them after exposure to visible light as shown in Figure 1.20. This disruption–reformation process was explained by the change in the hydrophilic–hydrophobic balance of the block copolymer induced by the photoisomerization of the azobenzenes side groups. Indeed, the azobenzene trans form is relatively apolar (dipole moment ≈0 D) while the cis form is on the other hand more polar (dipole moment ≈4.4 D) which accounted for the reversible dissociation–association of azobenzene containing micelles. Although a significant increase in the polarity of azobenzene moieties in the initially hydrophobic block happened after UV-irradiation, it may not be sufficient to dissociate micellar aggregates in all cases. Actually, a similar block copolymer but with a different composition [P(tBA$_{19}$-co-AA$_{33}$)-b-PMAz$_{31}$] displayed limited response to UV and visible light irradiations certainly due to a too short azobenzene-containing sequence [Tong *et al.* 2005].

In order to enhance the efficiency of reversible photoinduced micellar dissociation–association process, Matyjaszewski and coworkers proposed the use of photosensitive spiropyran moieties [Lee *et al.* 2007]. They synthesized by ATRP a PEO-block-poly(methacrylate) whose methacrylate block bears spyropyran (SP) side-chains (PEO-b-PMSP) (Figure 1.21). The hydrophobic spiropyran moieties undergo photoisomerization into their hydrophilic zwitterionic merocyanine counterparts under UV irradiation and the reverse process is triggered by visible light (620 nm). This process is accompanied by a deep change in the hydrophobic to hydrophilic balance in the LRBC, which causes

micellar disruption. Moreover, this system can be successfully used for the encapsulation and release of molecules of interest. In this respect, coumarin 102 was demonstrated to be encapsulated in micelles made of the PEO-b-PMSP and then released upon excitation at 365 nm. Moreover, the authors described the partial reincorporation of the fluorescent dyes triggered by visible light (up to almost 50% of the initially released coumarin 102).
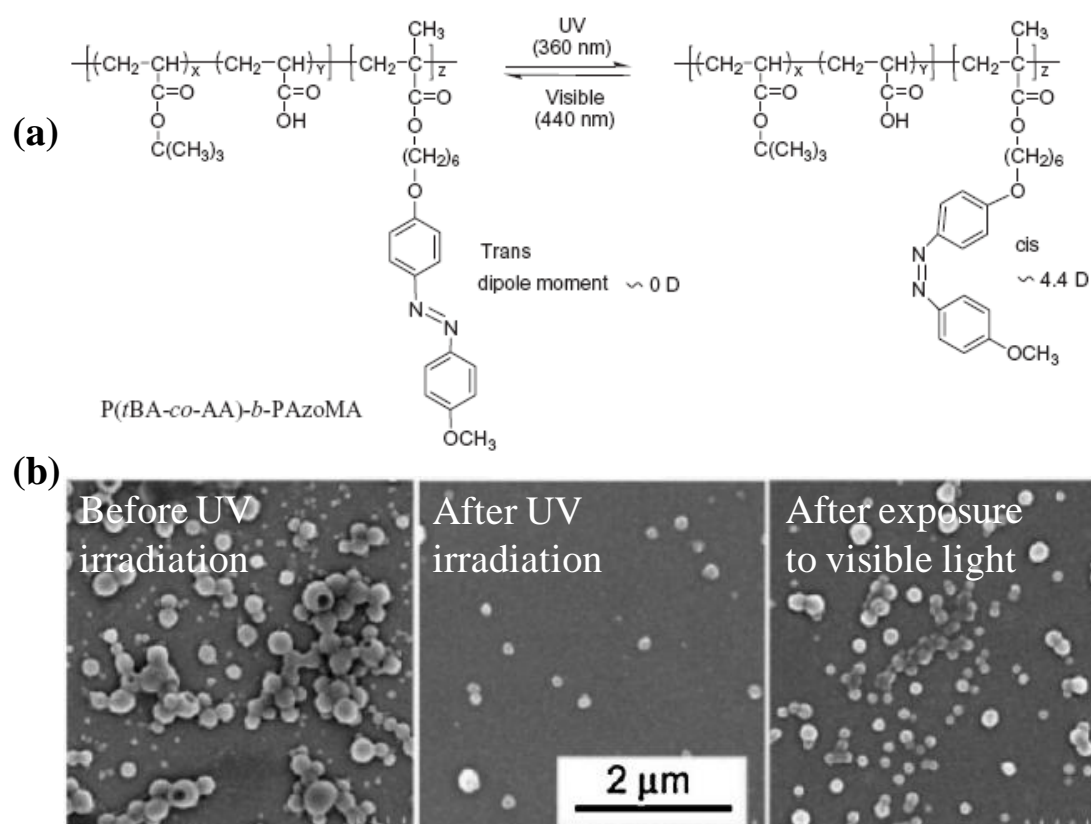
Figure 1.20. (a) Reversible change in the polarity of P(tBA-co-AA)-b-PMAz copolymer induced by photoisomerization of azobenzene moeities. (b) SEM images show the vesicles prior to UV illumination, their dissociation under UV, and their reformation under visible light exposure. [Adapted from Tong *et al.* 2005].
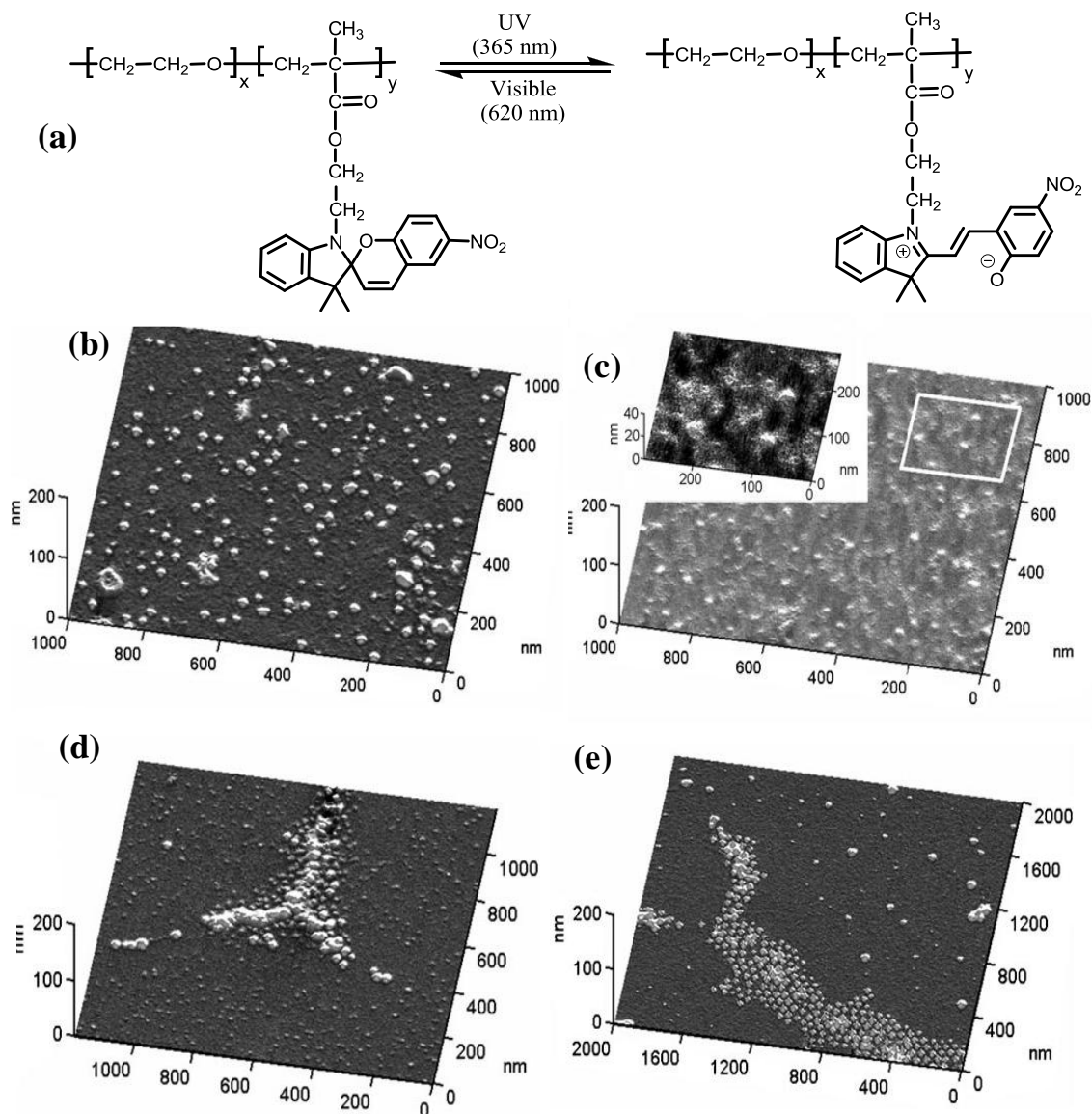
Figure 1.21. (a) Chemical structure and the photoreaction of a spiropyrancontaining amphiphilic diblock copolymer. AFM height images of PEO-b-SP solutions spin-coated on mica under various conditions: (b) PEO-b-SP micelles; (c) PEO-b-SP micelles after 365 nm UV exposure for 30 min; (d) PEO-b-SP micelles after 365-nm UV exposure for 30 min followed by 620 nm visible-light exposure for 30 min; (e) PEO-b-SP micelles after 365 nm UV exposure for 30 min followed by 620 nm visible-light exposure for 120 min. [Adapted from Lee *et al.* 2007].

Zhao *et al.* recently reported a novel coumarin-containing amphiphilic diblock copolymer, whose micelles can be reversibly cross-linked and de-cross-linked using light at two different wavelengths [Jiang *et al.* 2007]. The designed amphiphilic BC has the chemical structure shown in Figure 1.22, with PEO as the hydrophilic block and a poly(coumarin methacrylate) (PCMA), or a random copolymer of CMA and methyl

methacrylate (P(CMA-co-MMA)), as the hydrophobic block. Upon absorption of photons of $\lambda > 310$ nm, coumarin moieties can dimerize through a cycloaddition reaction, giving rise to micelle cross-linking; while upon absorption at $\lambda < 260$ nm, photoinduced cleavage of cyclobutane bridges can occur leading to micelle de-cross-linking. The de-cross-linking reaction (cleavage of cyclobutane ring) appears to be less efficient than the cross-linking reaction (coumarin dimerization), suggesting a photostationary state with equilibrated populations of the two isomeric forms of the chromophore. The effect of micelle core cross-linking and de-cross-linking on the release rate of entrapped NR into a THF/water (2/3, v/v) solution was investigated by monitoring NR's fluorescence emission. The results revealed that micelle core cross-linking could slow the release rate while subsequent micelle core de-cross-linking could recover the release rate partly, showing the potential of this photocontrol concept: using light to afford both the stabilization of encapsulation and the destabilization of micelles for controlled release at the required time and location.
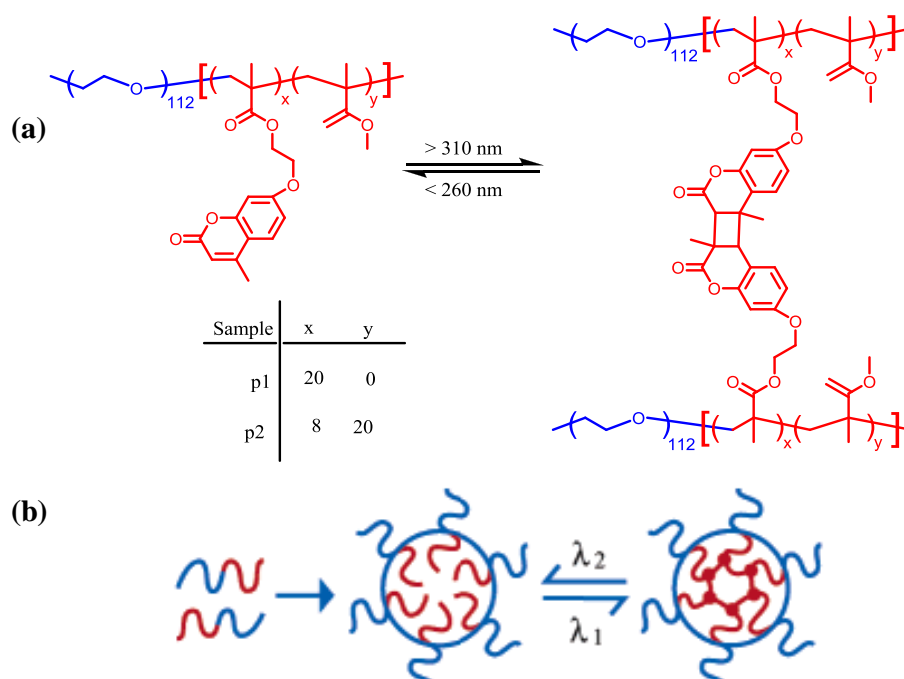
Figure 1. 22. (a) Chemical structure of the diblock copolymer and the photodimerization and photocleavage of coumarin side groups. (b) Schematic illustration of the reversible cross-linking of micelles. [Adapted from Jiang *et al.* 2007].

1.11.2. Polymer Micelles with Irreversible Light-Induced Dissociation

On the basis of the same principal of using light to shift the hydrophilic-hydrophobic balance towards the micellar dissociation, probably more photochromic molecules can be used to design amphiphilic BCs whose micelles dissociate irreversibly as a result of the photoreaction. The reversibility of micellar dissociation and formation using bistable photoswitches is interesting but unnecessary for controlled delivery applications. To achieve irreversible photocontrolled dissociation of amphiphilic BC micelles, the photoreaction of the used chromophore should result in a permanent structural change for the hydrophobic block that triggers the process. This can be accomplished through a photoinduced cleavage reaction of pendant photochromic groups that transforms the hydrophobic block into a hydrophilic one. It is easy to understand the dissociation of micelles when the initially amphiphilic amphiphilic BC becomes a double-hydrophilic amphiphilic BC.

The required photoinduced cleavage reaction is possible by linking a number of chromophores to a polymer chain backbone via a methyl ester group [Pincock 1997]. Zhao and coworkers have described three amphiphilic LRBCs based on the same strategy [Jiang *et al.* 2005; Jiang *et al.* 2006; Babin *et al.* 2009]. They synthesized polymers containing one hydrophilic poly(ethylene oxide) (PEO) sequence linked to a hydrophophic polymethacrylate (PMA) block bearing photolabile side groups (Figure 1.23). The block copolymers were prepared by the ATRP of the photosensitive monomers initiated by a PEO macroinitiator. Light illumination induced the cleavage of the side chromophores, unmasking the protected acrylic acid (AA) functions. As the resulting PEO-b-PMAA was fully hydrophilic, the block copolymer became soluble in water. For micelles built from those photocleavable polymers in aqueous media, light stimulation resulted in the disruption of the micelles and in the subsequent release of the

previously encapsulated molecules. Esters of pyrenylmethyl (Py) were firstly proposed as photocleavable moieties to validate the concept of light-induced drug delivery (Figure 1.23) [Jiang *et al.* 2005]. Nile Red fluorescent dyes were incorporated into micelles made of PEO-b-PPy. Upon UV irradiation, the photo-solvolysis of the pyrenyl groups caused the disruption of the micelles while releasing the encapsulated Nile Red. Afterward, the authors showed the possibility to control the release of encapsulated molecules by changing the intensity of the illumination. This behaviour was demonstrated for block copolymers containing o-nitrobenzyl esters as side groups (Figure 1.23) [Jiang *et al.* 2006]. Such chromophores cleave themselves upon light excitation and, as the photocleavage proceed via a Norrish II type intra-molecular rearrangement, no molecule of solvent is needed to enable the process. Furthermore, o-nitrobenzyl esters are very interesting because they also undergo photocleavage upon the absorption of two near-infrared (NIR) photons. For biomedical drug release applications, this point is very important because NIR radiations (vs. UV) penetrate deeper through water and cell tissues, and they are less harmful for healthy cells. Even if the photo-dissociation of o-nitrobenzyl containing micelles at 700nm (NIR) was demonstrated, the process efficiency was lower than for UV irradiation (much longer irradiation time was needed in case of NIR) due to a much smaller absorption cross-section for the two NIR photons [Jiang *et al.* 2006]. In order to address this problem, the chromophores were changed to esters of (diethylamino)methylcoumarinyl which display a larger two-photon absorption cross-section and whose photosolvolysis occurs at 794nm (Figure 1.23) [Babin *et al.* 2009].
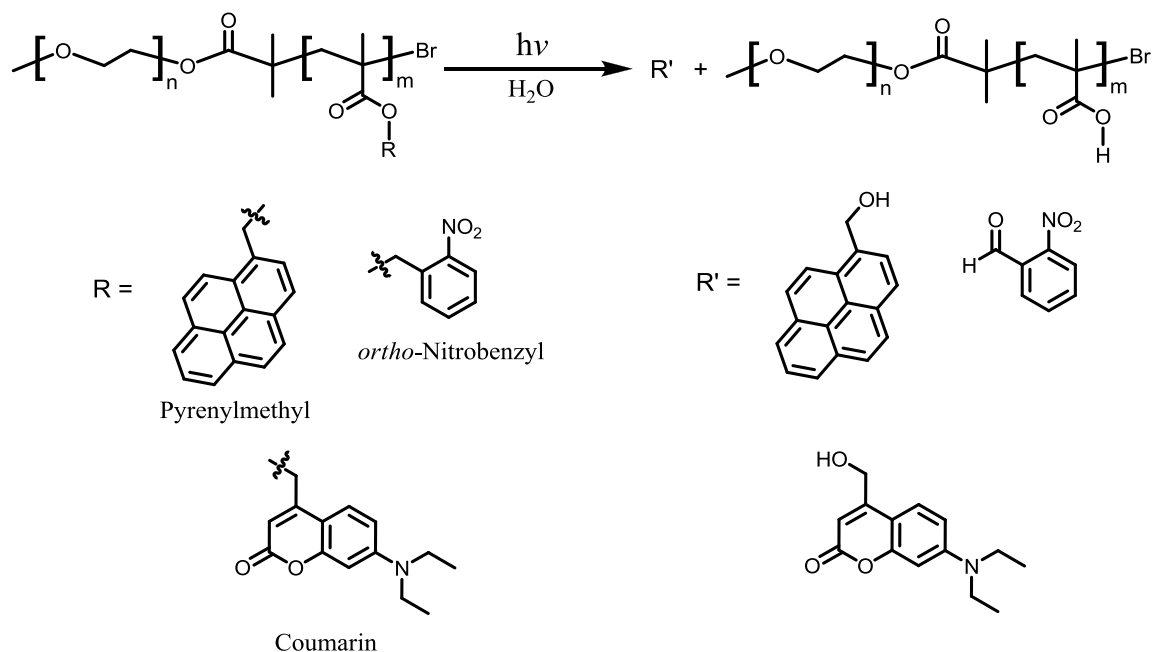
Figure 1.23. Changing the hydrophilic-hydrophobic balance of block copolymers by illumination. [Adapted from Schumers *et al.* 2010].

Recently Zhao's group demonstrated a new amphiphilic BC design strategy for the preparation of fast light-breakable micelles [Han *et al.* 2011]. It consists in positioning a photocleavable unit repeatedly on the main chain of the hydrophobic block. Figure 1.24a shows the structure of the amphiphilic ABA triblock copolymer of which the end block A is water-soluble poly(ethylene oxide) (PEO) and the middle block B is a hydrophobic polyurethane containing photodegradable nitrobenzyl groups (PEO-b-PUNB-b-PEO). This approach differs from those based on either light-changeable hydrophilic-hydrophobic balance or the use of a single photocleavable junction linking the constituting hydrophilic and hydrophobic blocks. As confirmed by atomic force microscope (AFM) studies irradiation of the amphiphilic BC micellar solution with 300 nm UV light leads to fast degradation of the micelles due to randomly occurring photocleavage reaction on the main chain of PUNB (Figure 1.24b). The authors showed that with this type of amphiphilic BC micelles undergoing fast photoinduced disintegration of micelle core, light-triggered burst release of loaded hydrophobic guest

molecules such as NR in aqueous solution could be achieved. This progress is of fundamental interest because the approach is general and can easily be applied to design amphiphilic BCs with photocleavable groups other than *o*-nitrobenzyl.

The recent significant progress in the synthesis of well-defined macromolecular architectures and the polymerization of highly functional building blocks using precisely controlled polymerization methods has led to the construction of numerous examples of stimuli responsive polymers. While most reports are related to systems that respond to the effect of temperature, pH and redox, materials being sensitive to other physical or (bio-) chemical stimuli such as light irradiation are very limited. Understanding the materials' physico-chemical properties and complex function is an ambiguous goal and a lot of work is required before their implementation in useful applications is possible.
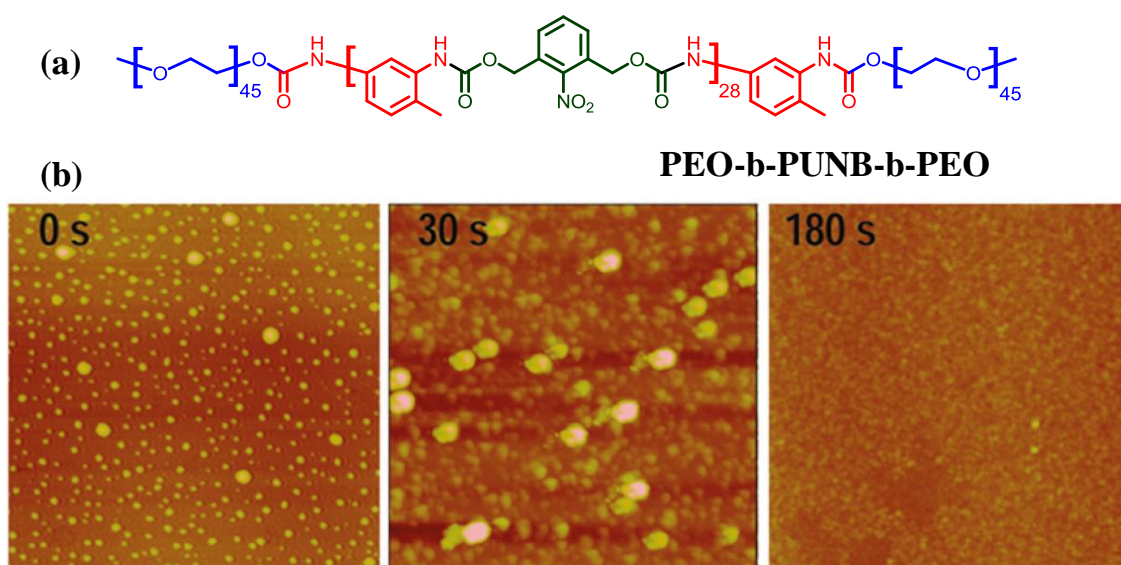
Figure 1.24. (a) Chemical structure of the ABA triblock copolymer (b) AFM height images of the micelle solution cast on mica before and after UV irradiation (30 and 180 s) (image area: 2 μm X 2 μm). [Adapted from Han *et al.* 2011].

1.12. Objectives of the Present Work

The major objective of the present thesis is to synthesize and investigate the aggregation properties of a few photoresponsive amphiphilic BCs and to monitor the changes in their photophysical properties upon self-assembly. The main rationale behind

the design of the BCs was to investigate the possibility of optically controlling the solubility of their hydrophobic photoresponsive block in water thereby achieving a more photocontrol on the polymer properties. Another objective was to find out the effect of structure on the self-assembling and photophysical properties of the BCs. These BC aggregates were also utilised to encapsulate various types of hydrophobic dyes in water. We have also investigated the ability of these hydrophobic dyes to modulate the fluorescence of some of the BCs by interparticle energy transfer.

Photoresponsive Soft Materials: Synthesis and Photophysical Studies of Stilbene-Based Block Copolymers

2.1. Abstract

*ATRP was utilized to synthesize two types of stilbene based amphiphilic block copolymers poly(dialkoxycyanostilbene methacrylate)-block-poly(ethylene oxide) (**PDACS-b-PEO**) and poly(trifluorostilbene methacrylate)-block-polystyrene-block-poly(ethylene oxide) (**PTFS-b-PSt-b-PEO**). Amphiphilic nature of the block copolymers caused them to self-assemble in water and the nature of the aggregates was found to depend upon the hydrophobic-hydrophilic ratio of the block copolymers. **PDACS-b-PEO** forms spherical micellar aggregates while **PTFS-b-PSt-b-PEO** formed vesicular aggregates in water. UV irradiation resulted in the structural transformation of the self-assembled superstructures which could be attributed both to change in shape of the stilbene chromophore from the linear trans isomer to the bent cis isomer which would alter the self-assembly of the molecules and the higher dipole moment of the cis isomer leading to a reduction of the hydrophobic nature of the stilbene containing block. Complete disruption of the micellar aggregates was observed in the case of **PDACS-b-PEO** whereas in the case of **PTFS-b-PSt-b-PEO** a transformation from vesicular to rod like morphology was observed. Morphological transition of the aggregates was studied using DLS, AFM, SEM, TEM, UV-vis and fluorescence spectroscopy. Moreover it was found that the polymeric aggregates have the ability of trapping organic dyes inside their hydrophobic cavity thereby making them water soluble. Subsequently the encapsulated dye can be released upon UV irradiation.*

2.2. Introduction

Stilbenes are certainly one of the most thoroughly studied classes of compounds from the standpoint of mechanistic and preparative photochemistry. The stilbene chromophore is a very useful building block for many applications in photochemistry since E/Z isomerization, cyclization, $[\pi^2s+ \pi^2s]$ cyclodimerization, and statistical C-C bond formations (polymerization, crosslinking) offer various reaction possibilities in synthetic chemistry as well as in materials science [Weldeck 1991; Meier 1992]. A fast and efficient C-C bond formation of stilbenoid compounds can be applied as basic process for imaging and photoresist techniques. The connection between stilbenoid compounds and light is a field that has implications for many potential applications. More particularly, stilbenoid compounds exhibit interesting photochemical and photophysical properties and are suitable for various applications in material science [Meier 1992]. Apart from their commercial use as optical brighteners and laser dyes, their applications in light-emitting diodes (LEDs), photoresists, photoconductive devices, imaging and optical switching techniques, and materials for nonlinear optics (NLO) are being investigated on this molecular basis [Martin *et al.* 1999; Spiliopoulos *et al.* 2002].

Self-assembly of stilbene and its derivatives has been extensively investigated in-order to gain insights on the properties of molecules in their aggregated state. The aggregation of several amphiphilic *trans*-stilbene fatty acid, phospholipid and cholesterol derivatives in micellar media have been extensively investigated by Whitten and co-workers [Whitten *et al.* 1998; Song *et al.* 1998; Song *et al.* 1997]. These amphiphiles form organized assemblies when the fatty acids are spread as monolayers at the air-water interface or when the phospholipids are dispersed in aqueous solutions. Cholesterol tethered *trans*-stilbene derivatives act as efficient gelators towards a variety of solvents which includes benzene, dioxan, pyridine, acetonitrile and several alcohols.

Enhancement in fluorescence and negligible isomerisation quantum yield was observed when the stilbene chromophore was embedded in the lipid layer at low temperature or in gel phase.

Sol-gel phase transition process of a cholesterol derivative of trans-stilbene was reported by Whitten and co-workers [Wang *et al.* 2000]. They found that gel formation is initiated by a change in the gelator-solvent interaction, resulting in dewetting of sol phase from a solid support. As gel formation commenced, the solution dewetted from the surface, forming circular and elongated droplets, leaving the exposed substrate. Upon further development, fine fibers became dominant at the expense of the sol-phase droplets, forming condensed islands (Figure 2.1). Further condensation allowed combination of neighbouring fine fibers into thicker ones.
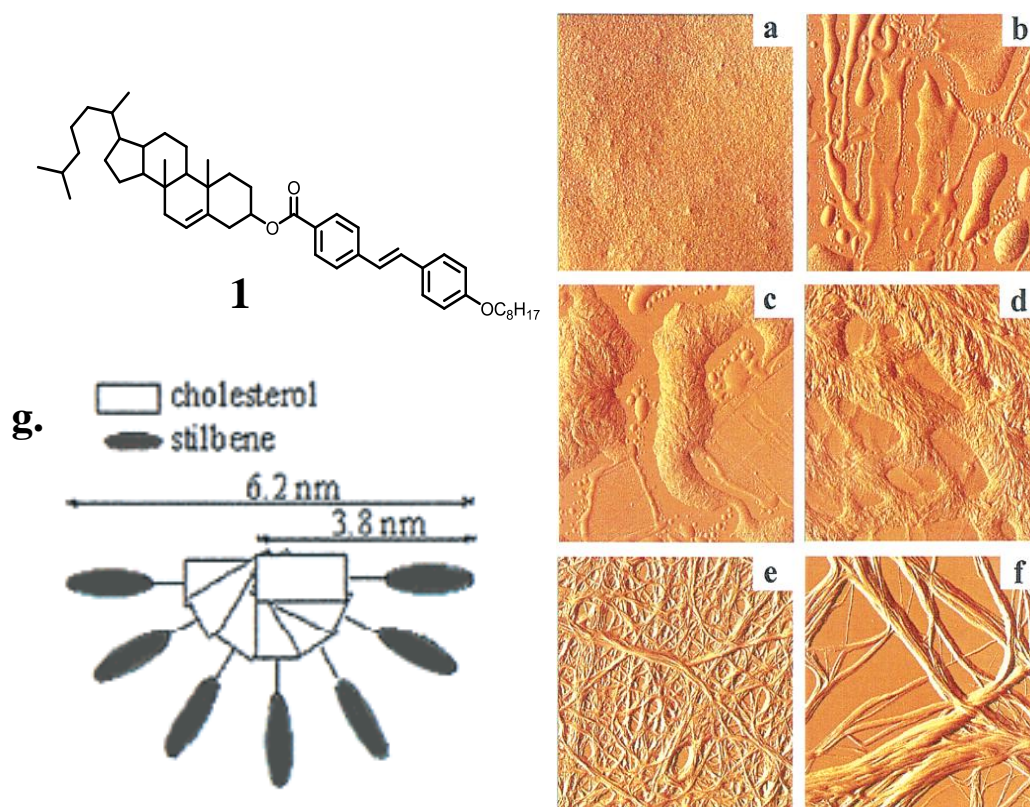
Figure 2.1. Time transient AFM images (in amplitude mode) of sol-gel phase transition. Images were acquired after the heated sol-phase solution (1.6%) was cooled to room temperature for (a) 0, (b) 10, (c) 15, (d) 18, (e) 21, and (f) 31 min. The scale of all the images is 12 X 12 μm. g) Possible helical stacking model of the molecules in a unit fiber. [Adapted from Wang *et al.* 2000].

The synthesis and study of the liquid crystalline, photophysical, and aggregation behavior of novel octupolar oxadiazole derivatives was reported by Das and co-workers [Varghese *et al.* 2009]. These molecules formed columnar mesophases at elevated temperatures which transformed into a glassy state at ambient temperatures wherein the columnar order was retained. Microscopic investigations provided clear evidence for the hierarchical self-assembly of these molecules in nonpolar solvents leading to gel formation. Hard spheres of nanometric dimensions were observed at lower concentrations which merged together to form nanoscopic fibers at higher concentrations resulting in an extended network of interlocked fibrils which immobilize the solvent to form the gel. Retention of the hexagonal columnar order was also observed in the fibrous aggregates. Concentration dependent luminescence spectral studies indicated that the change in morphology from spheres to fibrous aggregates was associated with a shift in chromophore packing from predominantly H-type to J-type aggregates. Figure 2.2 shows the crosslinked network of the gel phase and the schematic representation of the chromophore packing.
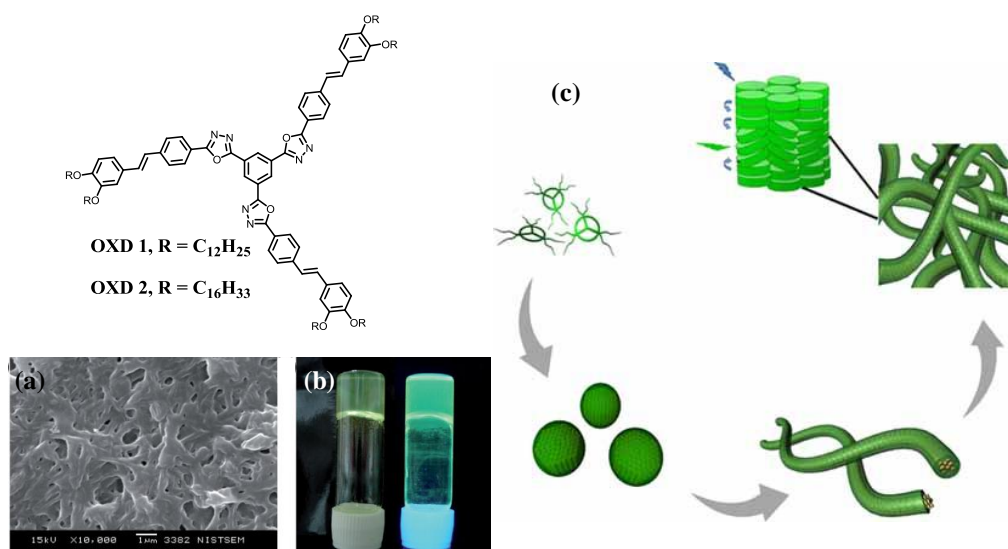
Figure 2.2. (a) SEM images of entangled fibrous aggregates of 1 in the xero-gel state derived from decane at its critical gelation concentration. (b) Photographs of decane gel under ordinary light and on 365 nm illumination. (c) Schematic representation of the hierarchical self-assembly of OXD 1. [Adapted from Varghese *et al.* 2009].

In this Chapter we describe our detailed investigations on the self-assembling and photophysical properties of two stilbene block copolymers **PDACS-b-PEO** and **PTFS-b-PSt-b-PEO**. Adding water to separate solutions of the block copolymers in THF caused them to self-assemble. Microscopic investigations of the self-assembled structures revealed that spherical micellar aggregates are formed in the case of the diblock copolymer **PDACS-b-PEO** whereas solvent filled vesicular aggregates are formed by the triblock copolymer **PTFS-b-PSt-b-PEO**. Effect of UV light on the self-assembled structures were studied which was found to bring upon morphological transformations in the self-assembled polymeric structures. The role played by these supramolecular aggregates in trapping hydrophobic dyes in water was also investigated.
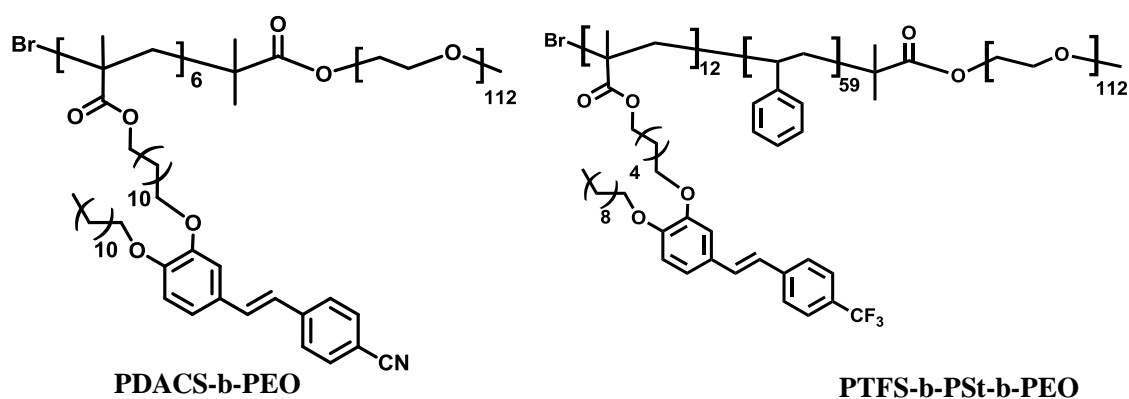
Chart 2.1.

2.3. Results and Discussion

2.3.1. Synthesis and Characterization

Using ATRP we have synthesized a well-defined stilbene based photoresponsive block copolymer, **PDACS-b-PEO**. **PDACS-b-PEO** was prepared as shown in Scheme 2.1. First the hydroxyl terminated poly(ethylene oxide)monomethyl ether (**1**) was esterified with 2-bromo-2-methylpropionic acid to get the corresponding bromo-terminated poly(ethylene oxide) (PEO-Br). Using PEO-Br as the macroinitiator, the

dialkoxy substituted cyanostilbene monomer (**9**) was polymerized in 1,4 dioxan using

PMDETA as the catalyst at 85 ^{0}C for 24 hours.
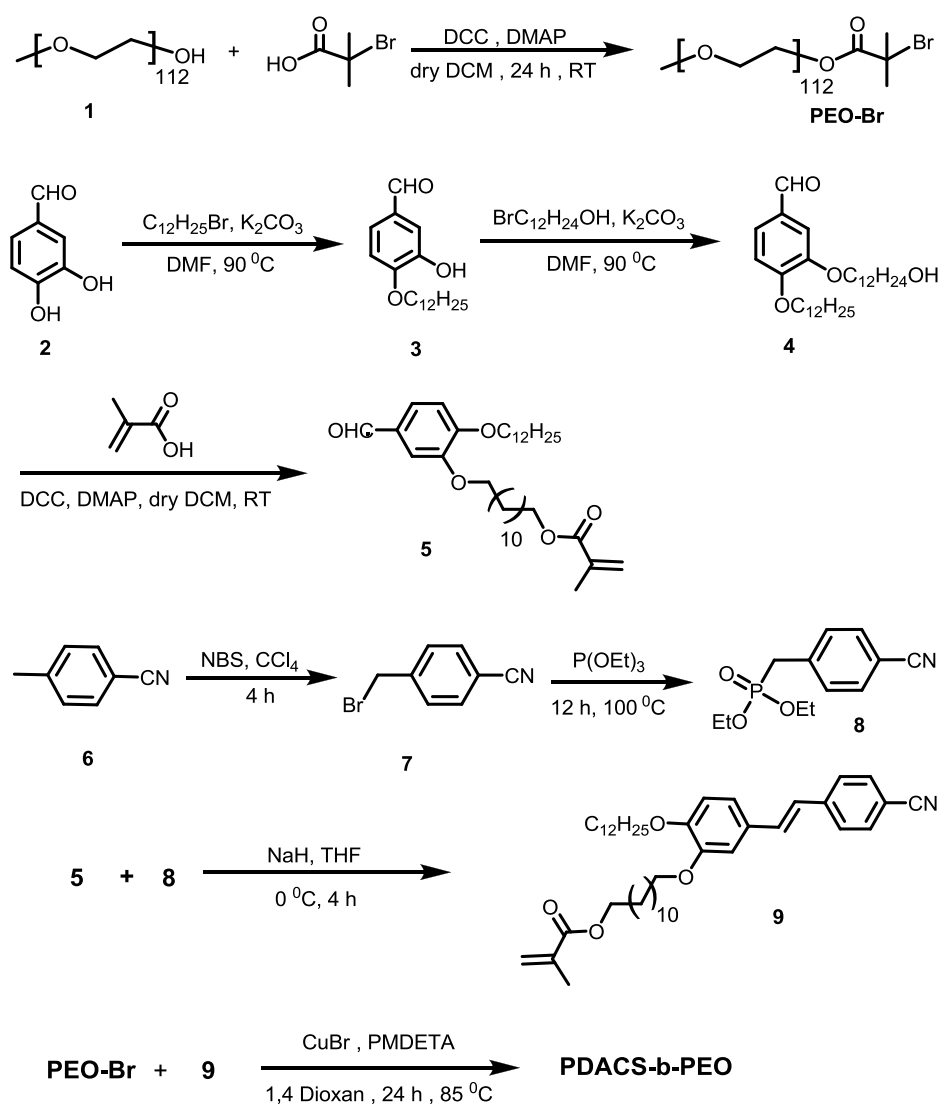
Scheme 2.1. Synthesis of **PDACS-b-PEO**.

Figure 2.3 shows the combined NMR spectra of the bromo-terminated

poly(ethylene oxide) (PEO-Br) with that of **PDACS-b-PEO** in CDCl$_3$. Comparison of

the integrals of the ether methyl group (3.38 ppm) and the methyl group(s) from the acid

moiety (1.95 ppm in the case of the 2-bromo-2-methylpropionate) indicates that the

esterification reaction is very efficient; i.e., no significant amount of non-functionalized

polymeric alcohol remained after esterification. After the synthesis of **PDACS-b-PEO**

new peaks were observed in the region 6.8-7.8 ppm corresponding to the aromatic protons of stilbene. GPC analysis was carried out to determine the molecular weight and polydispersity of the diblock copolymer. Figure 2.4 shows the GPC trace of **PDACS-b-PEO** diblock copolymer together with that of the macroinitiator (PEO-Br). Poly(ethylene oxide) initiator had a molecular weight of 5,078 and a polydispersity (PDI) of 1.12. After the synthesis of **PDACS-b-PEO** the molecular weight and PDI value increase to 9,166 and 1.36 respectively. The final diblock copolymer was purified four times by precipitation from THF into hexane. The resulting **PDACS-b-PEO** was composed of 6 units of stilbene and 112 units of ethylene oxide.
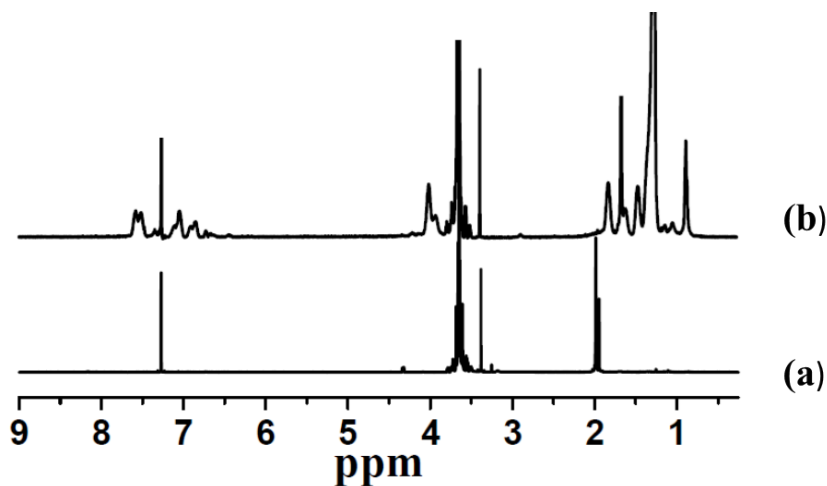
Figure 2.3. ^{1}H NMR spectra of the homopolymer and copolymer in CDCl$_3$ (a) PEO-Br (b) **PDACS-b-PEO**.
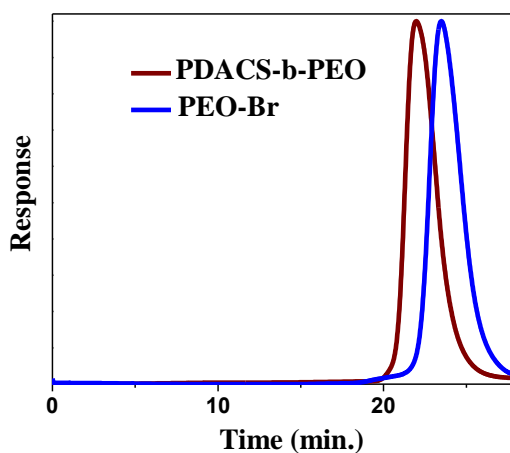
Figure 2.4. GPC curves of **PDACS-b-PEO** and the corresponding precursor PEO-Br.

Synthesis of the triblock copolymer **PTFS-b-PSt-b-PEO** is outlined in Scheme 2.2. **PTFS-b-PSt-b-PEO** was synthesized by first polymerizing styrene in bulk with PEO-Br to get the diblock copolymer PSt-b-PEO. PSt-b-PEO which was then used as the macroinitiator to polymerize the dialkoxy substituted trifluorostilbene monomer (**16**) in THF at 60 ^{0}C for 24 hours yielding **PTFS-b-PSt-b-PEO**. All these compounds were characterized based on analytical and spectral data. Detailed synthetic methods and the characterization data are provided in the experimental section.
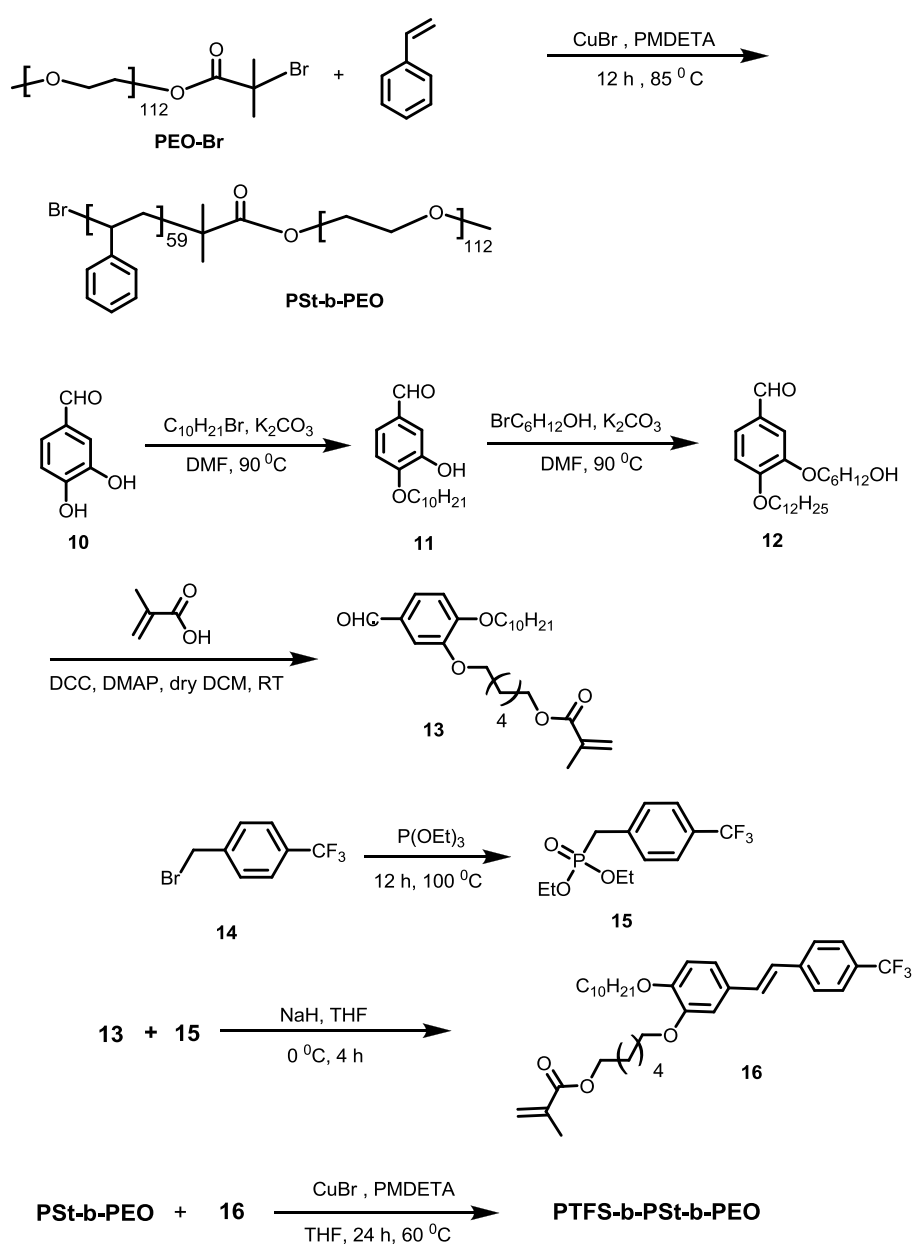
Scheme 2.2. Synthesis of **PTFS-b-PSt-b-PEO**.

Figure 2.5 shows the combined NMR spectra of the bromo-terminated poly(ethylene oxide) (PEO-Br), PSt-b-PEO and **PTFS-b-PSt-b-PEO** in $CDCl_3$. PEO-Br was then used to polymerize styrene in bulk to produce the diblock copolymer PSt-b-PEO. PSt-b-PEO block copolymer was then used to polymerize **16** in THF at 60 ^{0}C to produce fluorescent **PTFS-b-PSt-b-PEO** triblock copolymer. The characteristic resonance peaks at 3.65 ppm arising from the ethylene oxide chains, 6.46 and 7.06 ppm corresponding to the styrene block and 7.47 ppm corresponding to aromatic protons of stilbene provided strong evidence for the presence of PEO, PSt and PTFS segments in the final polymer. Figure 2.6 shows the GPC trace of **PTFS-b-PSt-b-PEO** triblock copolymer together with that of the diblock copolymer PSt-b-PEO and the homopolymer PEO-Br. It can be seen that the molecular weight of **PTFS-b-PSt-PEO** shifts towards the high molecular weight region without any trace of the low molecular weight macroinitiators. This shows that PSt-b-PEO is an efficient macroinitiator for the polymerization of stilbene while maintaining low polydispersity. The polydispersity however increases slightly during each polymerization stage. The final triblock copolymer **PTFS-b-PSt-b-PEO** was purified four times by precipitation from THF into hexane. The resulting copolymer was composed of 12 units of stilbene, 59 units of styrene and 112 units of ethylene oxide and had a M_n value of 18,354 with a PDI of 1.48.
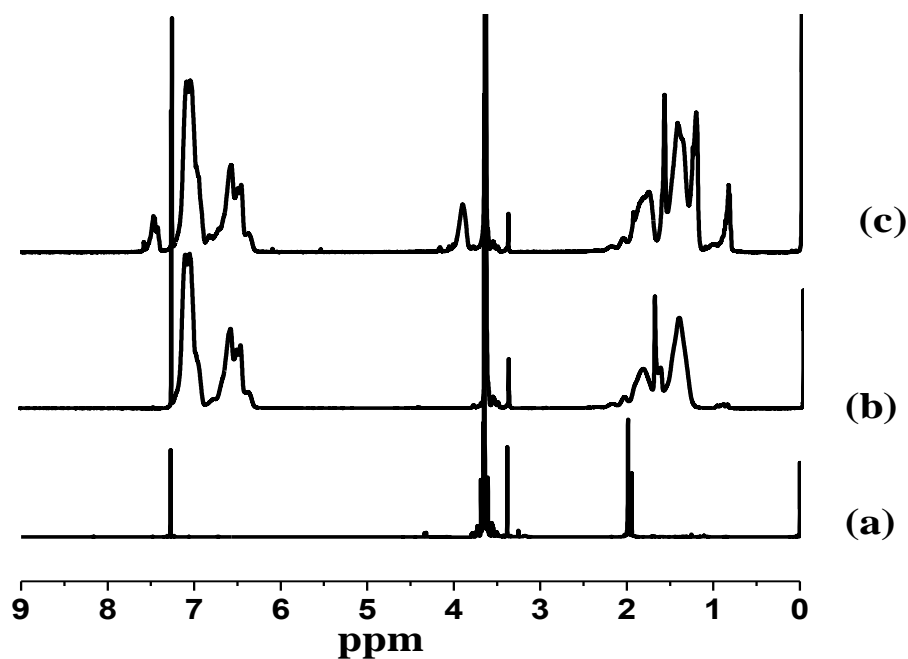
Figure 2.5. ^{1}H NMR spectra of the homopolymer and copolymers in CDCl$_3$ (a) PEO-Br (b) PSt-b-PEO (c) **PTFS-b-PSt-b-PEO**.
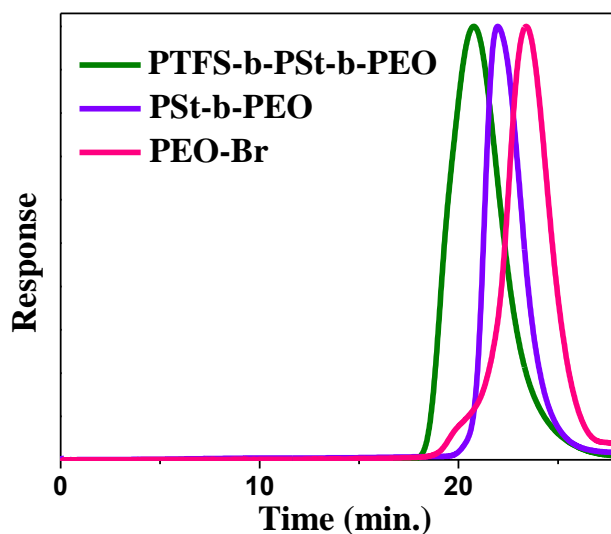
Figure 2.6. GPC curves of **PTFS-b-PSt-b-PEO** and the corresponding precursors PSt-b-PEO and PEO-Br.

2.3.2. Aggregation Studies of PDACS-b-PEO

Due to the amphiphilic nature of **PDACS-b-PEO** it was expected that it could form supramolecular aggregates in water. In order to confirm this we carried out DLS measurements on aqueous solutions of the polymer. For this measurement aggregates of **PDACS-b-PEO** in water was prepared using the following procedure. One mg

PDACS-b-PEO was dissolved in 1 mL THF, to which 1 mL of deionized water was added at a rate of 500 µL/h to induce aggregation. The solution progressively became turbid during water addition indicating aggregation. This is because when water is gradually added to a homogeneous solution of the polymer in THF, the solvent becomes progressively worse for the hydrophobic blocks; and after a critical amount of water has been added, the hydrophobic portion starts to self-assemble resulting in the formation of aggregates. Following this, 9 mL water was added quickly into this solution to quench the aggregates and THF was removed by evaporation at room temperature. The solution were filtered through a 0.45 µm filter (Millipore Millex-HV) before use. Figure 2.7 shows the DLS measurement of the block copolymer in water. DLS studies for the aqueous solution of **PDACS-b-PEO** showed that the particles were almost uniform in size with an average diameter of 160 nm with a PDI value of 0.116.
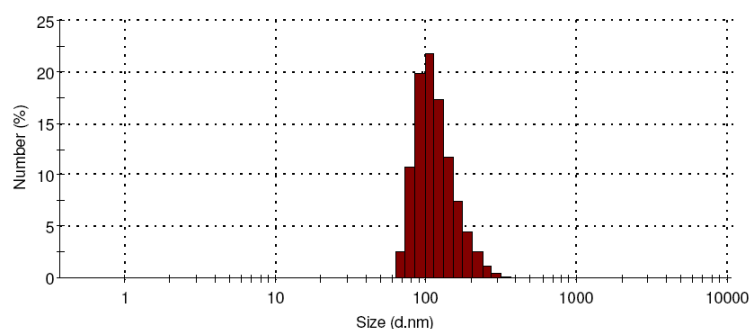
Figure 2.7. Size distribution of the colloidal aggregates of **PDACS-b-PEO** using DLS.

Microscopic studies were carried out to further characterize the morphology of the aggregates. The same solution used for DLS measurements was used for microscopic measurements. For AFM and SEM measurements a part of the colloidal solution of **PDACS-b-PEO** were cast on different glass slides and dried. Another part of the solution, was exposed to UV light (355 nm) in a quartz cuvette for 1, 2 and 3 hours and each of these solutions was cast and dried on glass slides for AFM observation. Figure 2.8 shows the AFM images obtained from the four solutions. AFM images of these

micelles before irradiation showed a high density of spheres. The concentration of these spherical micelles decreased upon continued UV irradiation and practically no micelles were observed in the solution exposed to UV light for 3 hours. DLS analysis confirmed the above observation which showed that that the solution after 3 hour UV irradiation contained only polydisperse particles with an average size of 16 nm. The gradual disappearance of the micellar aggregates upon UV irradiation can be explained as follows. Photoisomerization of *trans*-stilbene results in the formation of *cis*-stilbene which as a result of its higher dipole moment is less hydrophobic than the *trans*-form. Consequently UV irradiation increases the overall hydrophilicity of the polymer and due to the relatively short length of the DACS block. This increase is sufficient enough to break the colloidal aggregates upon irradiation. Figure 2.9 shows the SEM obtained by solution before UV irradiation. TEM was further used to characterize the micellar morphology. TEM images confirmed that the aggregates have micellar morphology since there was no sharp contrast difference between the periphery and core of the aggregates (Figure 2.10). Thus microscopic investigation conclusively revealed that the amphiphilic polymer forms well-defined spherical micellar aggregates in water which can be almost entirely dissociated with the help of UV light. The particle size measured using AFM, SEM and TEM for the diblock copolymer was much larger (~500 nm) when compared with the DLS measurement which indicated particles with an average diameter of 160 nm. A possible explanation for this is that DLS measurements are done in the solution state whereas AFM and TEM measurements are done in the dried state, during which the smaller particles present in water, can combine to form larger spheres during solvent evaporation process.
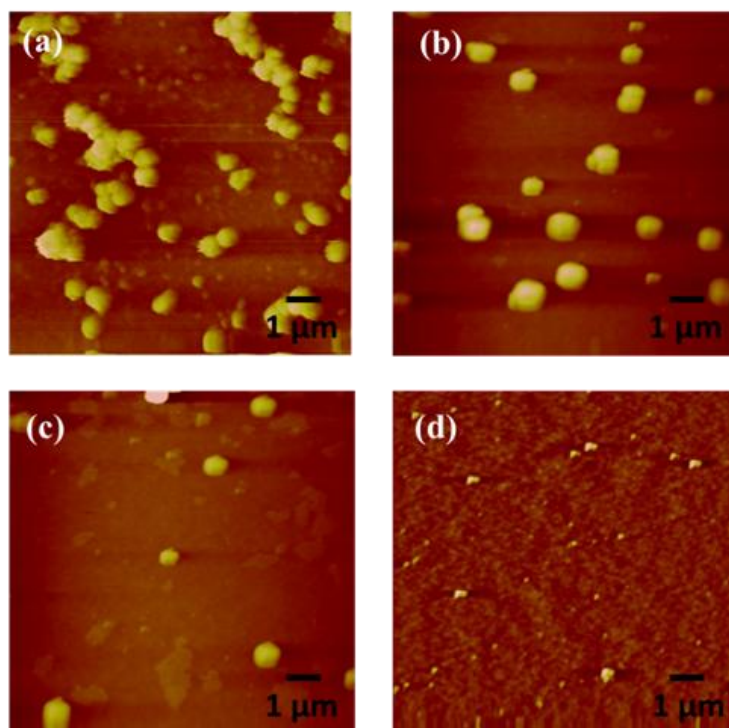
Figure 2.8. AFM images of air-dried aggregates formed by **PDACS-b-PEO** in water: (a) before irradiation (b) after UV irradiation for 1 h (c) after UV irradiation for 2 h and (d) after UV irradiation for 3 h.
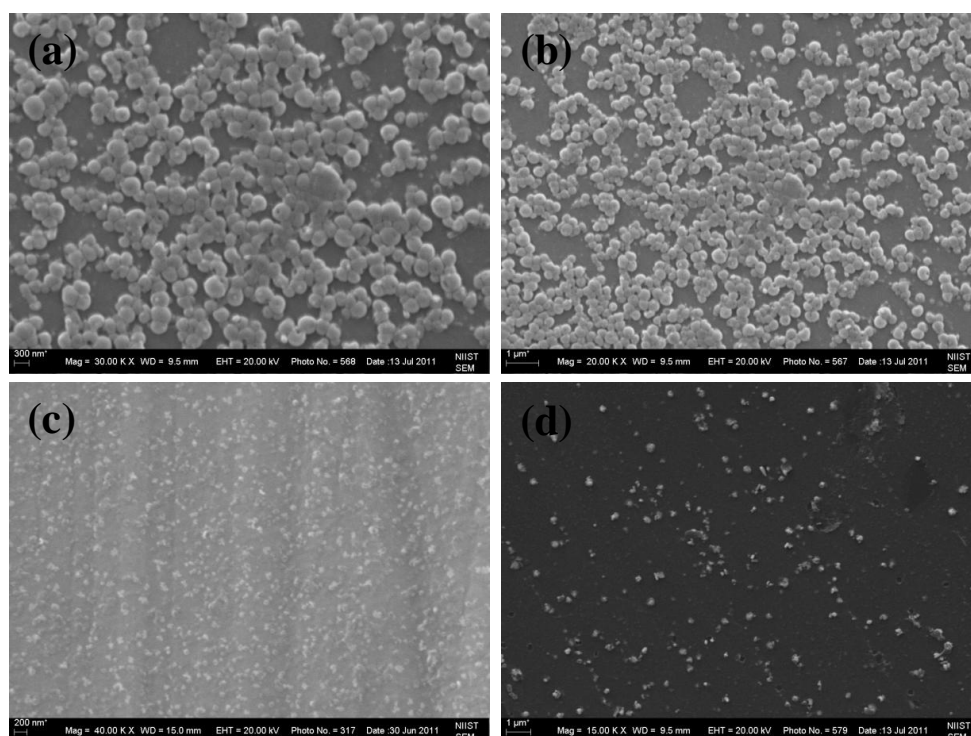
Figure 2.9. SEM images of air-dried aggregates formed by **PDACS-b-PEO** in water: (a, b) before irradiation (c, d) after UV irradiation for 3 h.
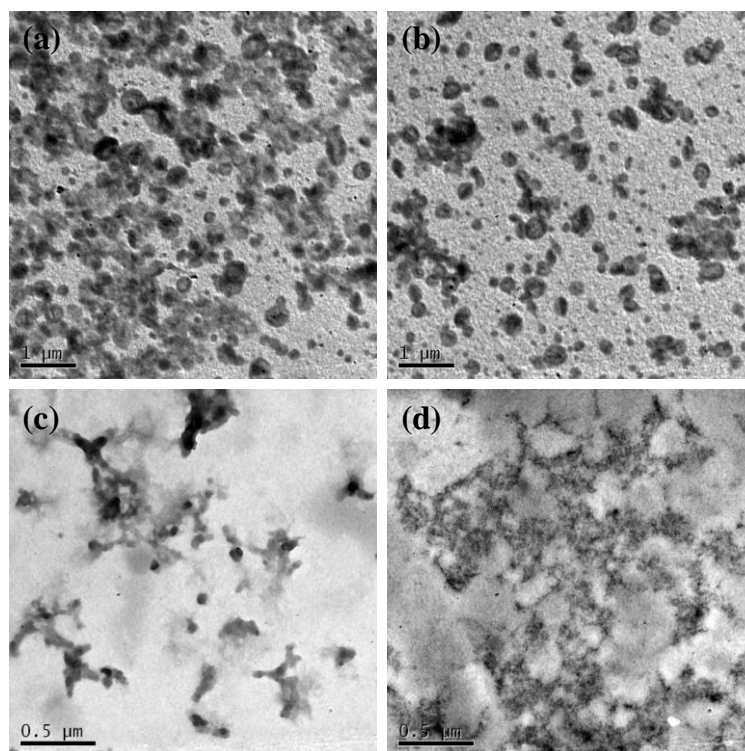
Figure 2.10. TEM images of air-dried aggregates formed by **PDACS-b-PEO** in water: (a) before irradiation (b) after UV irradiation for 1 h (c) after UV irradiation for 2 h and (d) after UV irradiation for 3 h.

2.3.3. Photophysical Studies of PDACS-b-PEO

Photoisomerization of the block copolymers upon UV irradiation was further investigated using UV-vis and fluorescence spectroscopy. Figure 2.11a shows the changes in the UV-vis absorption spectra of the polymer in THF upon continuous UV irradiation. In pure THF, **PDACS-b-PEO** exhibited a typical stilbene absorption spectrum with an intense band at 348 nm corresponding to the *trans*-isomer and a weak band at 238 nm. On photolysis with 355 nm light, a decrease in intensity in the 355 nm region and a small increase in intensity in the 238 nm region due to the formation of *cis*-isomer [Meier 1992; Seydack *et al.* 2000; Soomro *et al.* 2006] was observed. The linear *trans*-isomer exhibits a sharp emission at 434 nm but the bent *cis* form is non-fluorescent [Soomro *et al.* 2006]. Irradiation with 355 nm light resulted in a gradual decrease in the emission at 355 nm corresponding to the formation of the *cis*-isomer (Figure 2.11b).
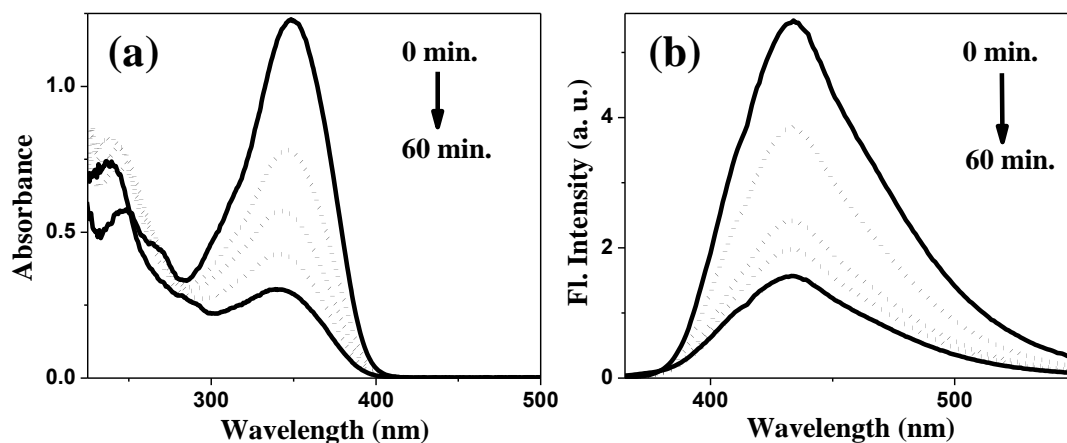
Figure 2.11. (a) Change in absorption spectra on photoirradiation of **PDACS-b-PEO** in THF with 355 nm light. (b) Corresponding change in fluorescence emission spectra.

Figure 2.12a and 2.12b show respectively the absorption and emission spectra of the diblock copolymer in water. The spectra are similar to that in THF except that it is slightly broader in water compared to than in THF. The isomerization process is schematically depicted in Figure 2.13. In order to find out whether the isomerization was thermally reversible the irradiated solution was kept in the dark at 60 ^{0}C for 2 hours. The absorption spectra and emission spectra did not show any significant change which indicated that the *cis*-form was stable and did not revert back to the *trans*-form.
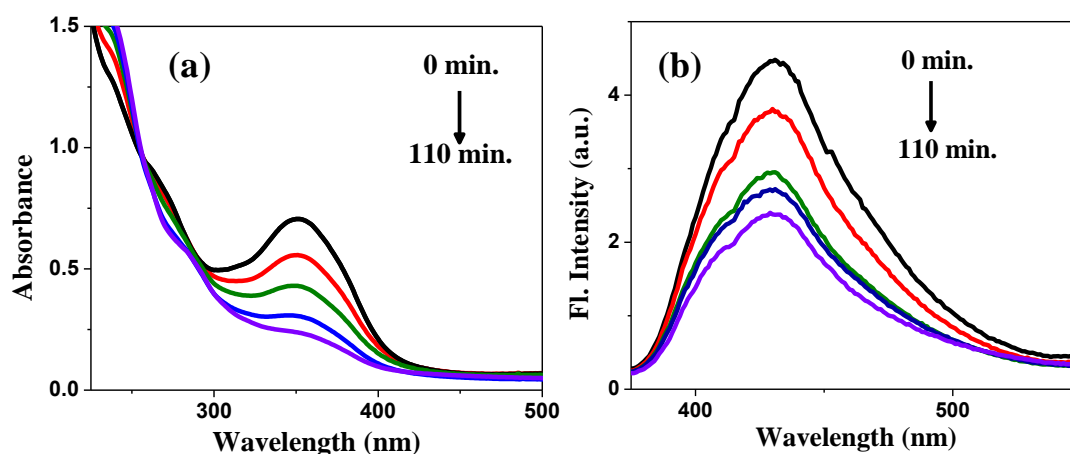
Figure 2.12. (a) Change in absorption spectra on photoirradiation of **PDACS-b-PEO** in water with 355 nm light. (b) Corresponding change in fluorescence emission spectra.

Trans-stilbene   *Cis*-stilbene
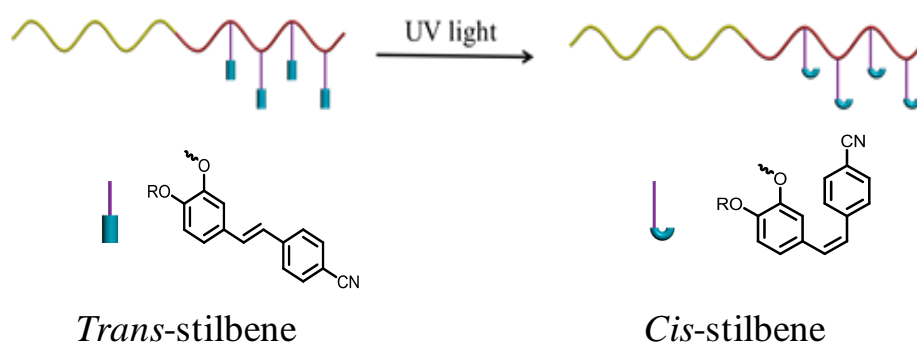
Figure 2.13. Schematic illustration of the photoisomerization of stilbene units present in the polymer chain.

2.3.3.1. Encapsulation and Photo-Controlled Release of Curcumin from Supramolecular Aggregates of PDACS-b-PEO

Curcumin is the principal curcuminoid of the popular Indian curry spice turmeric, which has been used historically as a component of Indian ayurvedic medicine. In vitro and animal studies have suggested that curcumin has anti-tumor, antioxidant, anti-arthritic, anti-amyloid, anti-ischemic and anti-inflammatory properties [Aggarwal *et al.* 2006]. In addition it may be effective in treating malaria, prevention of cervical cancer, and may interfere with the replication of HIV virus [Vemula *et al.* 2006]. There is also circumstantial evidence that curcumin improves mental functions. Due to its limited solubility and instability in the gut very little of curcumin which is ingested is absorbed by the body. In 2007, a polymer nanoparticle encapsulated formulation of curcumin ("nanocurcumin") [Bisht *et al.* 2007] has been synthesized which has the potential to bypass many of the shortcomings associated with free curcumin, such as poor solubility and poor systemic bioavailability.

Curcumin could be solubilized in water using the supramolecular aggregates of **PDACS-b-PEO**. Figure 2.14a shows the absorption spectra of **PDACS-b-PEO** and curcumin in THF. The emission spectrum of curcumin in THF is shown in Figure 2.14b. As can be seen from the Figure 2.14a curcumin has negligible absorption in the range of 340-360 nm, its maximum absorption is centered at ~423 nm.
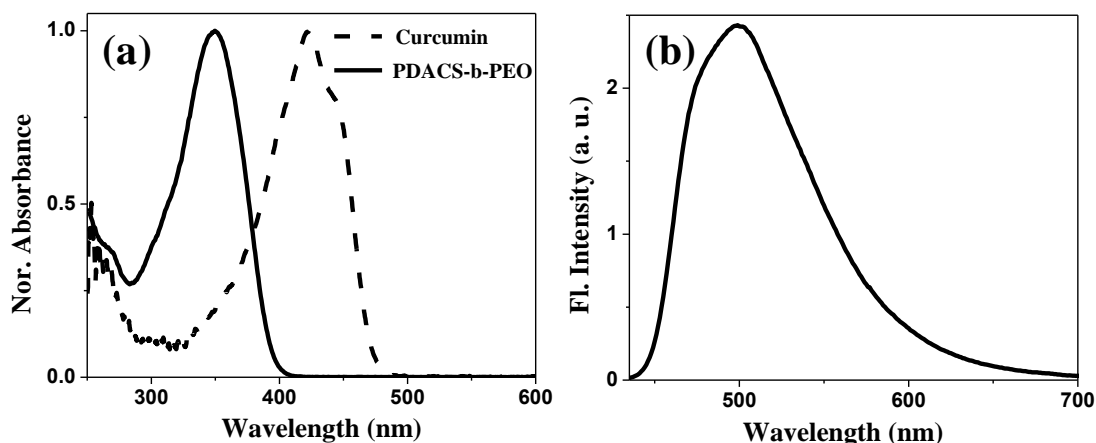
Figure 2.14. (a) UV/Vis spectra of **PDACS-b-PEO** and curcumin THF. (b) Fluorescence emission spectra (λ_{ex} = 423 nm) of curcumin in THF.

To incorporate curcumin into the core of the micelles 1.0 mg of the polymer and 0.06 mg of curcumin were dissolved in 1 mL THF. To this 1 mL of water was added drop wise. After dilution with 9 mL of water and complete evaporation of THF the resultant solution was filtered through a 0.45 μm filter. Curcumin exhibits very low absorbance and emission in pure water owing to its very low solubility in water; however, as the dye was incorporated into the micelles, the dispersion exhibited a strong fluorescent emission at 499 nm. In addition, the emission maximum displayed a blue-shift for the dye in the aggregate system compared with that in pure THF, indicating that curcumin molecules reside in a more hydrophobic environment (compared with that of THF) inside the micelles. Figure 2.15a and 2.15b show the absorption and emission spectra of curcumin encapsulated in polymer aggregates in water.

On excitation of the curcumin/micellar dispersion with UV light (353 nm), it was observed that the characteristic fluorescence emission for stilbene at 437 nm was reduced to small hump and an emission band at 491 nm corresponding to that of curcumin was observed, suggesting fluorescence resonance energy transfer (FRET) from stilbene to curcumin.
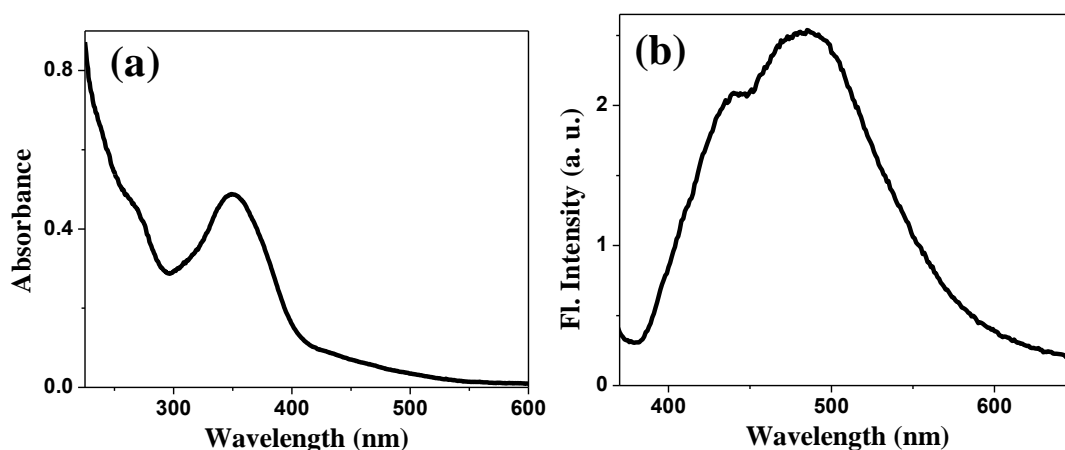
Figure 2.15. (a) UV/Vis spectra and (b) Fluorescence emission spectra ($\lambda_{ex} = 353$ nm) of copolymer aggregates containing curcumin in water.

The photochemically controlled release of curcumin was confirmed by monitoring the changes in the absorption and emission spectra as a function of irradiation time (Figure 2.16). Emission spectra in Figure 2.16b provide evidence for the encapsulation and release of curcumin following UV irradiation of the aqueous polymer solution. On irradiation with 355 nm light, the emission intensity of curcumin decreases with time of irradiation. On the other hand the emission band of stilbene at 437 nm first decreases and then starts to increase upon continued UV irradiation. The decrease in curcumin emission upon UV irradiation is due to its control release from the polymer aggregates into water due to the formation of the comparatively more polar *cis*-stilbene which ensures a decrease in hydrophobicity of the polymer resulting in the dissociation of the polymer aggregates.

Figure 2.17a shows the fluorescence emission spectra of the polymer solution with encapsulated curcumin before and after UV light exposure (excitation wavelength, 353 nm); in comparison, the emission spectrum of the polymer solution without curcumin, prepared under the same conditions, is also shown. Figure 2.17b shows that the encapsulation of curcumin by micelles made the micellar solution appear yellow.
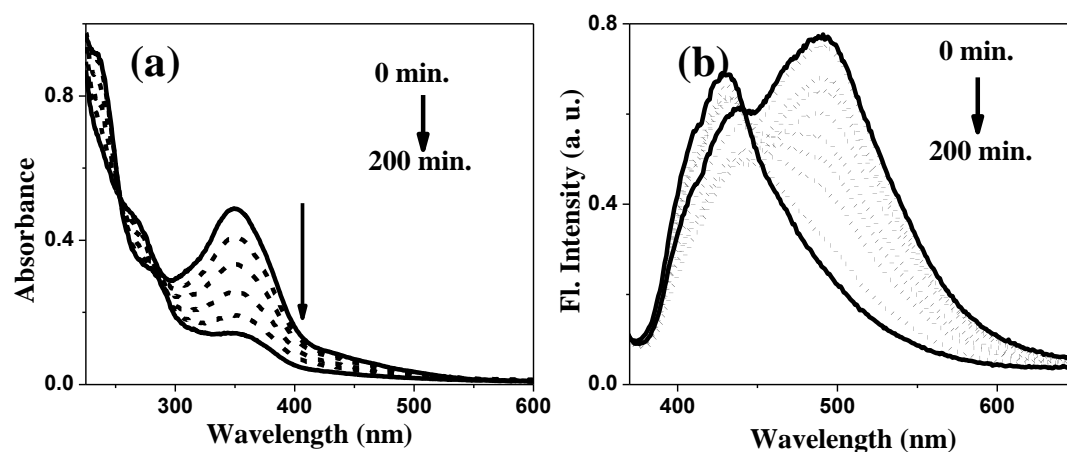
Figure. 2.16. (a) Changes in UV/Vis spectra and (b) Fluorescence emission spectra (λ_{ex} = 353 nm) of polymer aggregates in water containing curcumin on UV irradiation.
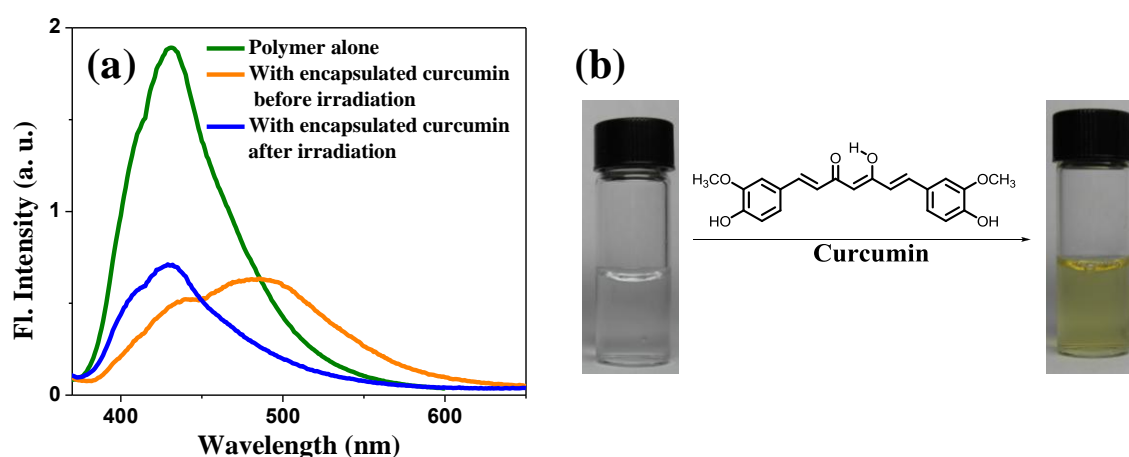
Figure 2.17. (a) Fluorescence emission spectra (λ_{ex} = 353 nm) of polymer micelles in water containing curcumin before and after UV irradiation compared to that of the non-irradiated micellar solution without curcumin. (b) Photograph of an aqueous solution of **PDACS-b-PEO**; without curcumin, (left) with encapsulated curcumin (right).

For the polymer solution without curcumin, only emission of stilbene at 437 nm is observed while for the polymer aqueous solution containing curcumin, excitation at 353 nm, where curcumin has negligible absorption, resulted in the fluorescence emission of curcumin centered at 491 nm. This can be attributed to FRET between the polymer and the dye, which indicates that the chromophores are closely packed. This supports the view that curcumin is encapsulated within the hydrophobic core of the self-assembled polymer. Figure 2.18a shows the excitation spectra of the curcumin encapsulated solution when the emission is collected at 491 nm. Excitation spectra confirm that the emission

from curcumin is maximum when the dye encapsulated solution is excited at the absorption maxima of stilbene chromophore. The photoisomerization of stilbene and release of curcumin were revealed by the decrease in the fluorescence emission after UV irradiation, since released curcumin molecules are water insoluble. Scheme 2.3 illustrates this mechanism. The slight enhancement of stilbene emission upon continued UV irradiation can be attributed to the fact that when more and more curcumin molecules are released from the polymer micelles energy transfer process becomes less efficient which results in the slight enhancement in stilbene emission. Here it can be argued that the decrease in curcumin emission is not due to the release of encapsulated curcumin but due to the formation of non-fluorescent *cis*-stilbene which inhibits FRET. In order to prove that this argument is invalid we took the ratio of the absorbance at 353 nm of the curcumin encapsulated aggregates before and after irradiation and multiplied that factor to the emission spectra of the curcumin encapsulated solution obtained after UV irradiation. The corrected spectra exactly superimposes with the emission spectra of the non-irradiated polymer solution without curcumin. The corrected emission spectra clearly proved that the curcumin is in fact getting released from the polymer aggregates upon UV irradiation. Also direct excitation of the curcumin encapsulated solution at the absorption maxima of curcumin (423 nm) before and after UV irradiation where **PDACS-b-PEO** has no absorption revealed that curcumin emission is mostly quenched after UV irradiation (Figure 2.18b). Thus we have succeeded in controlling the solubilization of curcumin in water by utilizing the *cis–trans* isomerization of stilbene chromophores. This is achieved through UV irradiation which causes an increase in solubility of the resultant polymer in water sufficient enough for the dissociation of the micellar aggregates.
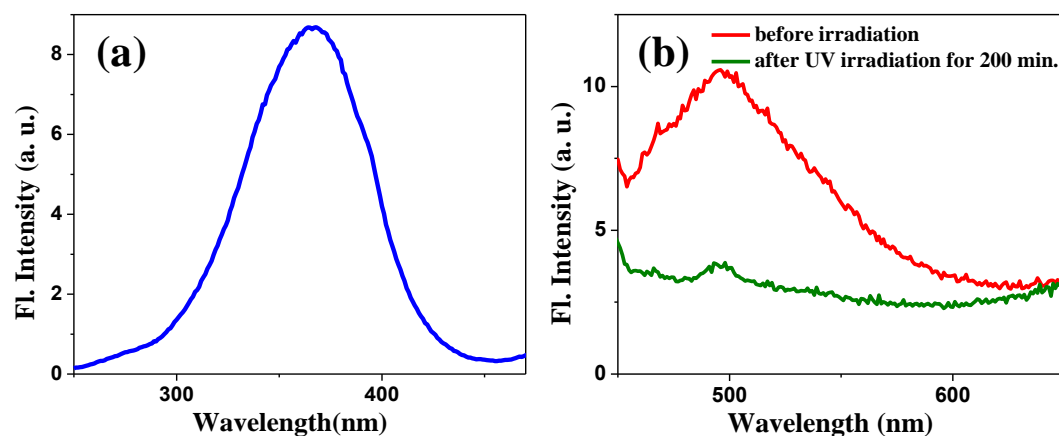
Figure 2.18. (a) Fluorescence excitation spectra of polymer aggregates in water containing encapsulated curcumin (Emission collected at 491 nm). (b) Emission spectra of curcumin obtained upon excitation of curcumin encapsulated polymer aggregates in water at 423 nm before and after UV irradiation.
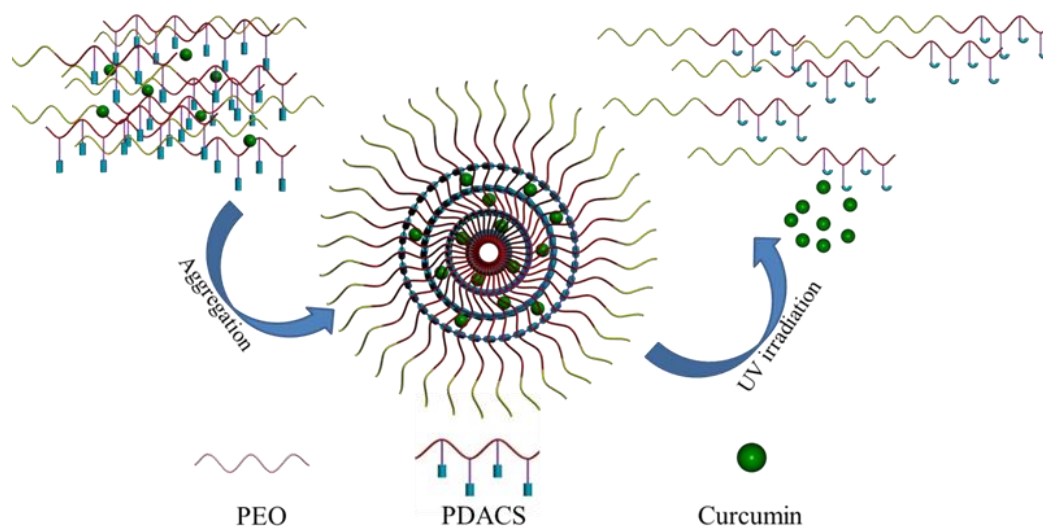
Scheme 2.3. Schematic representation of the encapsulation of curcumin within the hydrophobic core of the polymer aggregates and its release upon disruption of the polymer aggregates by UV light.

2.3.4. Aggregation Studies of PTFS-b-PSt-b-PEO

Aggregates of the triblock copolymer in water were prepared in a manner similar to that of **PDACS-b-PEO**. In the case of the colloidal aqueous solution of **PTFS-b-PSt-b-PEO**, DLS studies revealed that the presence of particles with average diameter 195 nm. The polydispersity of the aggregates were found to be 0.089 (Figure 2.19).
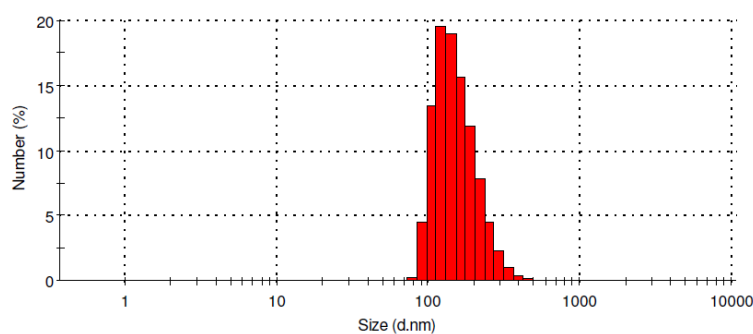
Figure 2.19. Size distribution of the colloidal aggregates of **PTFS-b-PSt-b-PEO** using DLS.

AFM, SEM and TEM were used to further characterize the morphology of **PTFS-b-PSt-b-PEO** aggregates. For AFM and SEM studies the aqueous colloidal solution of the polymer prepared above was drop-cast onto a freshly cleaved mica sheet and dried at room temperature. Figure 2.20 and Figure 2.21 show respectively the AFM and SEM images of the aggregates obtained after solvent evaporation. Both AFM and SEM indicate the presence of uniform colloidal spheres. The AFM height profile of the aggregates is shown in Figure 2.20d. As seen from the figure the height from the top of the spheres to the mica substrate is about 90 nm whereas the horizontal diameters of the spheres is about 400 nm which indicate that the colloidal aggregates are somewhat soft and undergo shrinkage during solvent evaporation. This indicates that these colloidal spheres are vesicles which are bilayer liquid filled blisters rather than micelles which are single layered hard spheres. This was confirmed from the TEM image. In order to get the TEM image two drops of the polymer aqueous solution was drop-cast onto a formvar coated copper grid under ambient conditions and the solvent was allowed to evaporate. Figure 2.22 show the TEM images the polymer aggregates. From the TEM image it is clear that there is a clear contrast difference between the core and periphery of the spherical aggregates which means that they are hollow thereby confirming that the polymer aggregates are in fact vesicles. The average wall thickness of these vesicles as obtained from the TEM images was 42 nm.
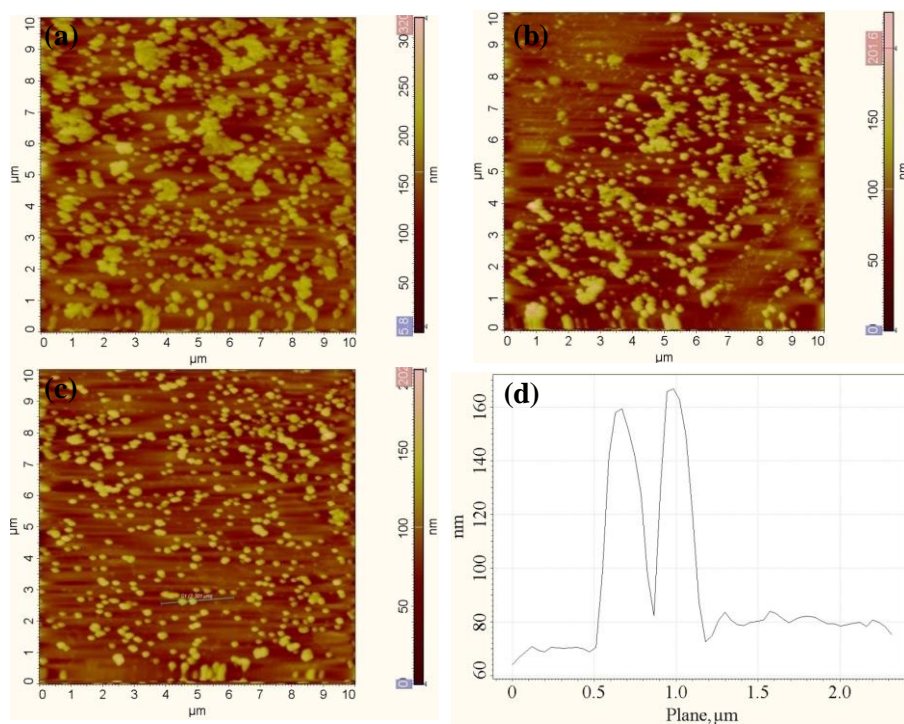
Figure 2.20. (a, b, c) AFM images of air-dried aggregates formed by **PTFS-b-PSt-b-PEO** in water and (d) height profile of the aggregates.
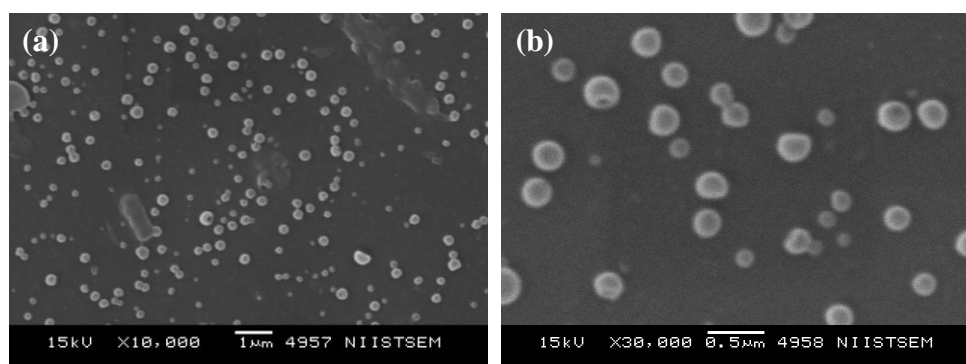
Figure 2.21. (a, b) SEM images of air-dried aggregates formed by **PTFS-b-PSt-b-PEO** in water.
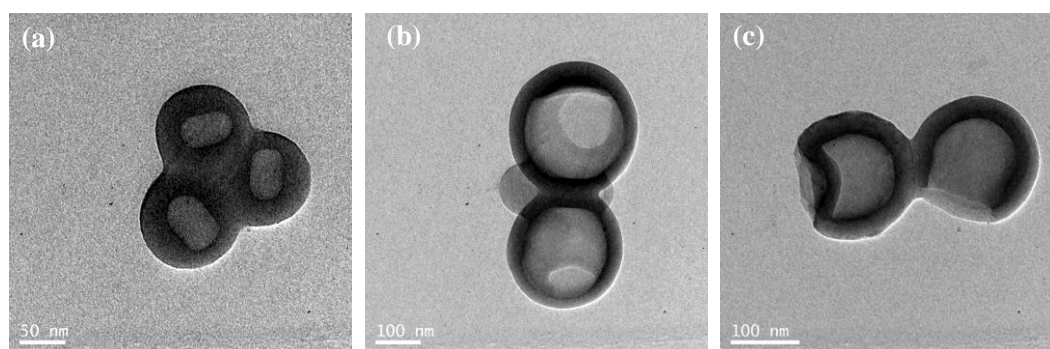
Figure 2.22. (a, b, c) TEM images of air-dried aggregates formed by **PTFS-b-PSt-b-PEO** in water.

Since **PTFS-b-PSt-b-PEO** contains photoresponsive stilbene moieties which can undergo *trans-cis* isomerization upon UV irradiation it was anticipated that the structural and polarity change associated with the isomerization process will bring about a change in the morphology of the spherical aggregates. In order to investigate this aspect the colloidal solution of the polymer was taken in a quartz cuvette and was irradiated with 350 nm UV light for 30 minutes. Microscopic analysis of the resultant solution was then carried out. Figure 2.23 shows the AFM images of the UV irradiated solution obtained after solvent evaporation. From the Figure it is clear that that the spherical aggregates transferred to rod shaped aggregates following UV irradiation. Figure 2.23d shows the height profile of the corresponding rod shaped aggregates. From the height profile it was observed that the surface of the rods were somewhat rough. The rods had a length of about 1.5 μm, breadth of 400 nm and a height of 30 nm. Morphological transition from vesicles to rods was also confirmed through SEM and TEM images as shown in Figure 2.24.
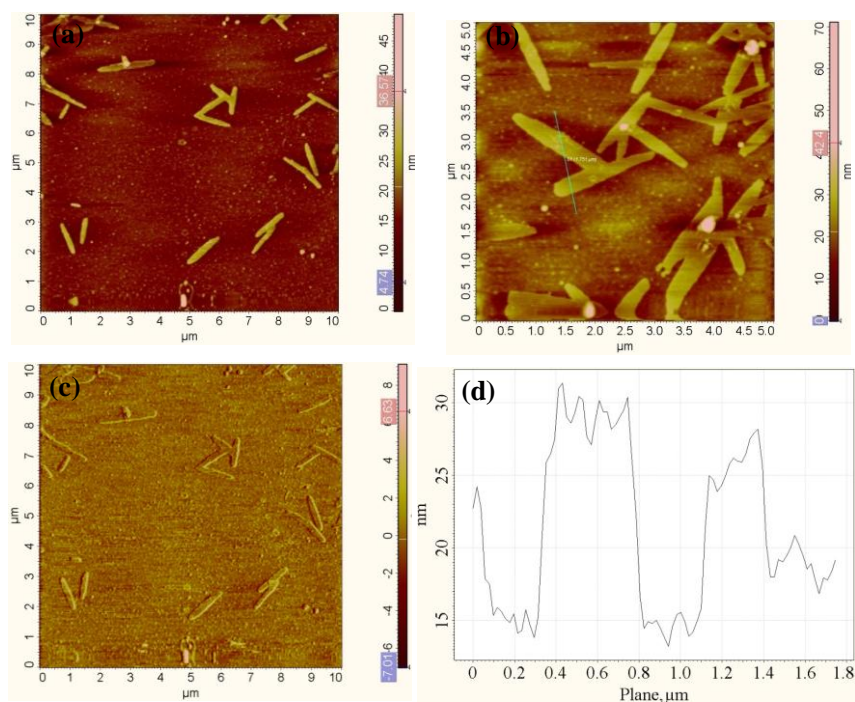
Figure 2.23. (a, b) AFM height images of air-dried aggregates formed after the UV irradiation of **PTFS-b-PSt-b-PEO** in water (c) phase image of the aggregates (d) height profile of the aggregates.

The sphere to rod transition of the aggregates is expected to be formed as a result of the formation of the bent *cis*-stilbene units from the linear *trans*-configuration. This change in structure makes the polymer difficult to associate in a spherical fashion thereby causing the vesicular aggregates to transform into a rod like morphology which may be the thermodynamically more favored morphology for the amphiphilic triblock copolymer containing *cis*-stilbene units. Morphological transformation of the polymer aggregates occurs not only from the conformational change of stilbene, but also from the polarity change accompanying isomerization resulting in a decrease in the packing parameter, *p*. Before UV irradiation **PTFS-b-PSt-b-PEO** has a large hydrophobic domain due the presence of PSt and *trans*-PTFS blocks. As a result the value of *p* of the block copolymer lies between ½ and 1 giving rise to spherical vesicles in water. But UV irradiation transforms the *trans*-PTFS block to *cis*-PTFS block which has a higher polarity than the *trans*-PTFS block. This increase in polarity or the decrease in hydrophobicity reduces the value of *p* so that its new value probably falls between ⅓ and ½ in which case rod like micelles are the most thermodynamically favored morphology. Thus the conformational change along with decrease in value of *p* associated with polarity change are suspected to be the two main factors which drives the formation of rod like aggregates from the initial soft micelles or vesicles. To the best of our knowledge this is the first time such a sphere-to-rod transformation of the block copolymer aggregates has been observed solely by the application of light and not by a change of the block length.
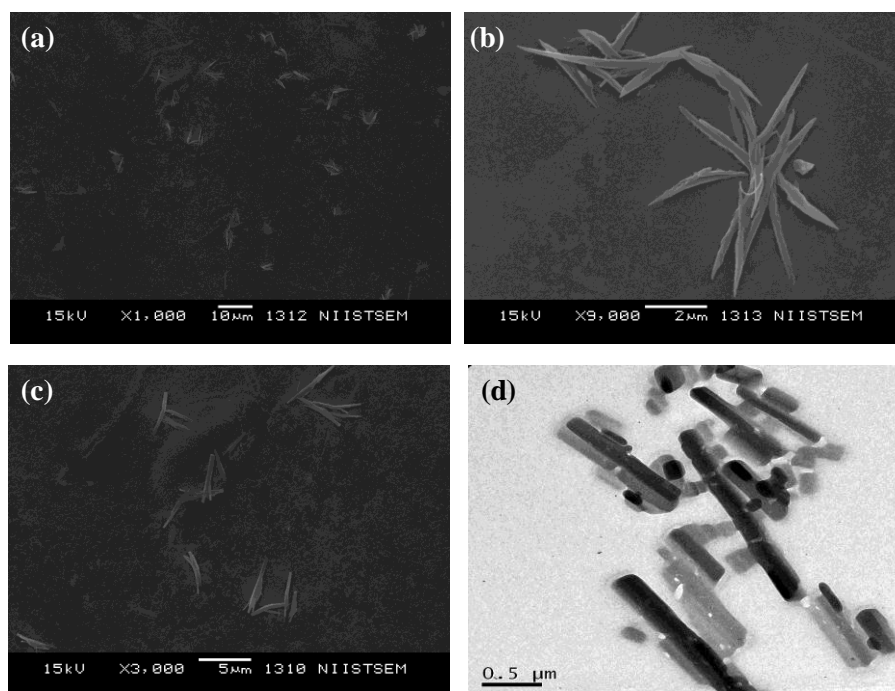
Figure 2.24. (a, b, c) SEM images of air-dried aggregates formed after the UV irradiation of **PTFS-b-PSt-b-PEO** in water (d) TEM image of the aggregates.

In order to find out the mechanism of transformation of the aggregates from vesicles to rods, the colloidal aqueous solution of **PTFS-b-PSt-b-PEO** was irradiated with UV light for different lengths of time and each time a drop of the irradiated solution was drop-cast on a freshly cleaved mice sheet, dried and analyzed using AFM. Figure 2.25 shows the AFM images obtained from each of these solutions. Fusion of the vesicular aggregates was observed after 5 minutes of UV irradiation thereby completely destroying the spherical morphology of the aggregates. AFM image of the dried film obtained after 10 minutes of UV irradiated solution showed that the vesicular aggregates transformed into a lamellar morphology with an average height of 30 nm. Further irradiation caused the lamellar structure to break and rod like particles began to separate out of it. After 30 minutes of UV irradiation it was observed that the lamellar structure had completely transformed into rod like aggregates. Height profiles of the AFM images of the lamellar structure and final rod like micelles showed that both of them had an

average height of 30 nm which confirmed that these structures are formed during the dissociation stage of the vesicular aggregates.
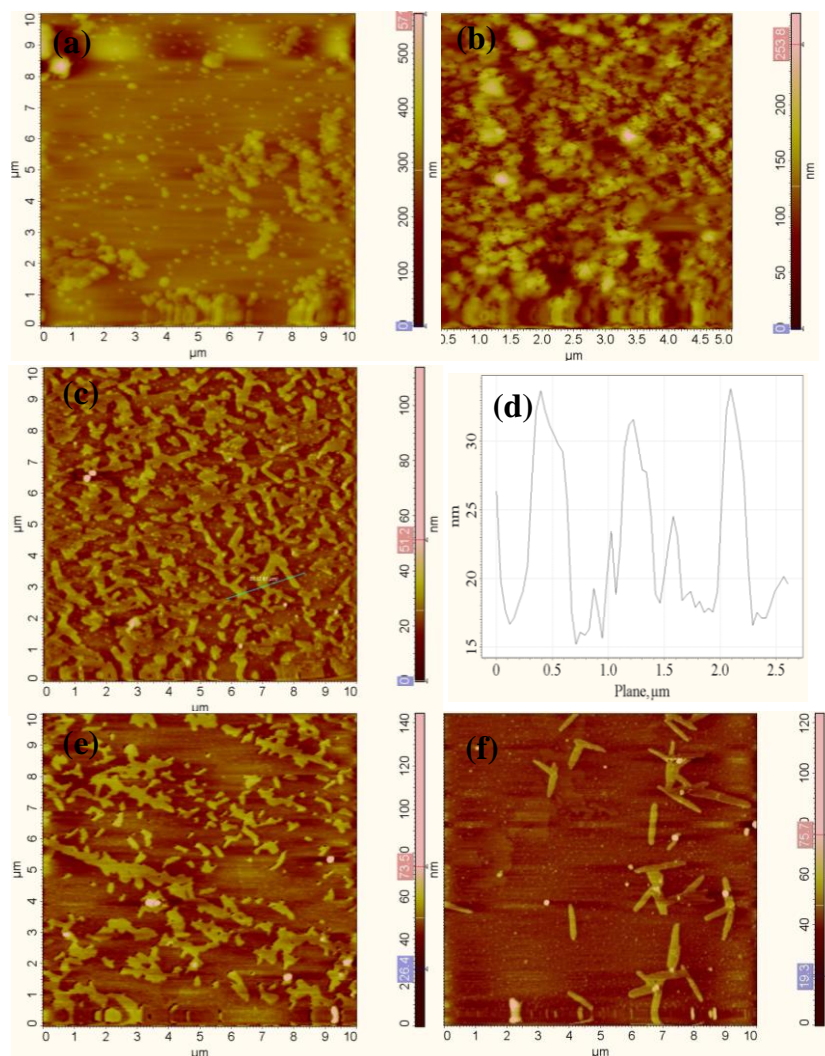
Figure 2.25. AFM images of air-dried **PTFS-b-PSt-b-PEO** aggregates obtained during various stages of UV irradiation (a) 0 minutes (b) 5 minutes (c) 10 minutes (d) height profile of Fig. c (e) 20 minutes (f) 30 minutes.

2.3.5. *Photophysical Studies of PTFS-b-PSt-b-PEO*

2.26a shows the changes in the UV-vis absorption spectra of the **PTFS-b-PSt-b-PEO** in THF upon continuous UV irradiation. In THF the polymer shows absorption maxima at 335 nm corresponding to that of the *trans*-stilbene units in the polymer. Upon 350 nm UV irradiation the peak at 335 nm decreases continuously with concomitant gradual increase in the absorption at 240 nm which corresponds to the *cis*-

isomer. Thus the absorption spectra indicate photoisomerization of stilbene units in the polymer. The photoisomerization was complete after 20 minutes of irradiation after which no further decrease in emission intensity was observed. Figure 2.26b shows the decrease in the fluorescence of the polymer solution in THF following UV irradiation supporting the fact that fluorescent *trans*-stilbene units in the polymer is getting converted to *cis*-stilbene units upon UV irradiation. A comparison of the emission intensities before and after irradiation shows that the relative percentage of the *cis*-isomer in the photostationary state is ~50% assuming complete absence of the *cis*-isomer before irradiation. In order to check whether the isomerization was reversible under thermal conditions the UV irradiated solution was kept in the dark at 60 ^{0}C for 1 hour. Even after 1 hour there was no detectable change in the absorption or emission spectra of the solution indicating that the isomerization is thermally irreversible.
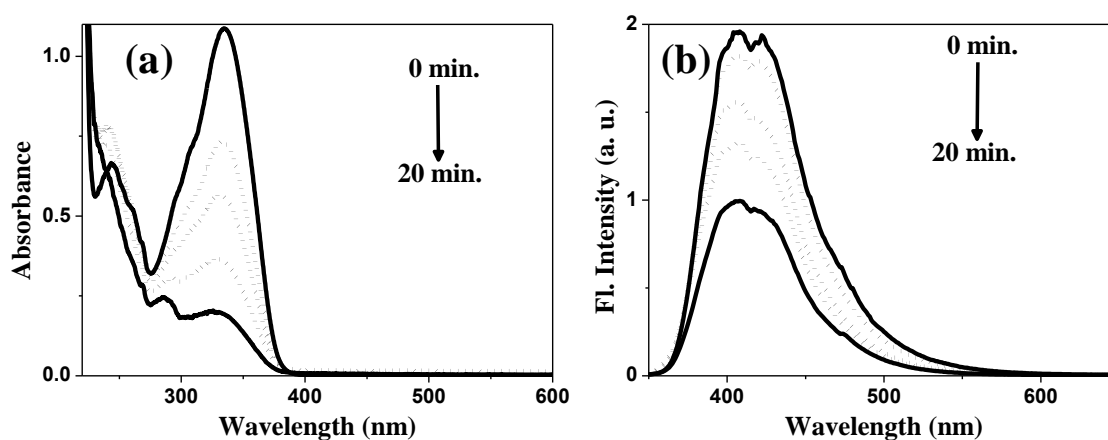
Figure 2.26. (a) Change in absorption spectra on photoirradiation of **PTFS-b-PSt-b-PEO** in THF with 355 nm light. (b) Corresponding change in fluorescence emission spectra.

Next we checked the changes in the absorption and emission of **PTFS-b-PSt-b-PEO** aggregates in water following UV irradiation. The same polymeric aqueous solution used for DLS and microscopic analysis was used for spectroscopic studies. Figure 2.27 shows the absorption spectra and emission spectra of the polymer aggregates. The rate of isomerization was much more pronounced in water than in THF

and the amount of the *cis*-isomer after 30 minute irradiation was calculated to be ~79%. Clearly after 30 minute UV irradiation the amount of *cis*-isomer formed is much greater in water than in THF. This is to be expected because water has a higher dielectric constant than THF and so it can stabilize the more polar *cis*-stilbene to a greater extent than THF.
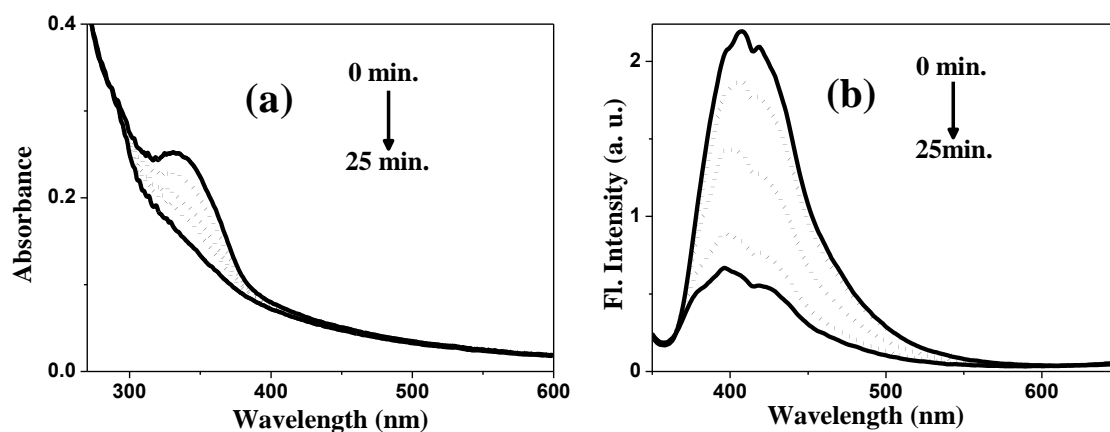
Figure 2.27. (a) Change in absorption spectra on photoirradiation of **PTFS-b-PSt-b-PEO** in water with 355 nm light. (b) Corresponding change in fluorescence emission spectra.

2.3.5.1. *Encapsulation and Photo-Controlled Release of Coumarin 102 from Supramolecular Aggregates of PTFS-b-PSt-b-PEO.*

In order to test the ability of the vesicular aggregates to encapsulate hydrophobic molecules in water we took coumarin 102 dye as the hydrophobic dye. Coumarin 102 is a fluorescent dye which is practically insoluble in water. In THF its absorption is centered at 378 nm and emission at 430 nm. In order to prepare dye encapsulated **PTFS-b-PSt-b-PEO** aggregates, 1 mg of the polymer and 0.1 mg of coumarin 102 dye was dissolved in 1 mL HPLC grade THF. To this 1 mL deionized water was added with gentle stirring at a rate of 500 µL/h. Since water is a good solvent for PEO and bad solvent for PSt and PTFS blocks, association of the polymer takes place. After the addition of 1 mL water 9 mL more water was added quickly into the turbid solution to quench the aggregates. THF was then allowed to evaporate by keeping the solution

exposed to air at room temperature for one week. Finally the solution was filtered through a 0.45 μm filter before use. DLS analysis of the dye encapsulated solution indicated the presence of spherical particles with an average diameter of 225 nm (PDI = 0.162) which was slightly larger than that obtained in the absence of the dye (Figure 2.28). Microscopic investigation of the dye encapsulated aggregates showed that the vesicular nature of the aggregates is preserved even after dye encapsulation. When this dye encapsulated solution was excited at 380 nm where the polymer has no absorption the solution showed a strong emission at 433 nm which corresponds to the emission of coumarin 102 trapped inside the polymer aggregates. To check the photocontrolled release of the dye the aqueous solution was irradiated with 350 nm UV light for 60 minutes. It was observed that continued UV irradiation resulted in a gradual decrease in the emission intensity of coumarin 102. Figure 2.29a shows changes in the absorption spectra upon UV irradiation of aqueous solution of **PTFS-b-PSt-b-PEO** containing encapsulated coumarin dye and Figure 2.29b shows the changes in the emission intensity of the dye during irradiation. Decrease in the emission intensity at 433 nm confirmed the slow release of coumarin 102 from the polymer aggregates. But complete release of the dye from **PTFS-b-PSt-b-PEO** aggregates was not observed even after 60 minutes of UV irradiation. The release of the dye is expected to occur during the rearrangement of the vesicular aggregates into rod like micelles upon UV irradiation. As confirmed from the microscopic studies of the polymer aggregates before and after irradiation the shift in the hydrophobic-hydrophilic balance in the amphiphilic polymer after irradiation is not sufficient enough to solubilize the polymer completely in water and breakup the aggregates. Instead there is only a transformation in the morphology of the aggregates from spherical vesicles to rod-like structure. Due to the presence of the long styrene block, **PTFS-b-PSt-b-PEO** retains sufficient hydrophobicity which prevents aggregate dissociation even after formation of *cis*-stilbene there by resulting in a morphology

transformation. Due to the non-destruction of the aggregates some of the coumarin dye remains trapped inside the polymer aggregates even after UV irradiation. This shows that although **PTFS-b-PSt-b-PEO** aggregates can be effectively used for encapsulating and solubilising hydrophobic molecules in water the trapped dye can be only partially released during UV irradiation.
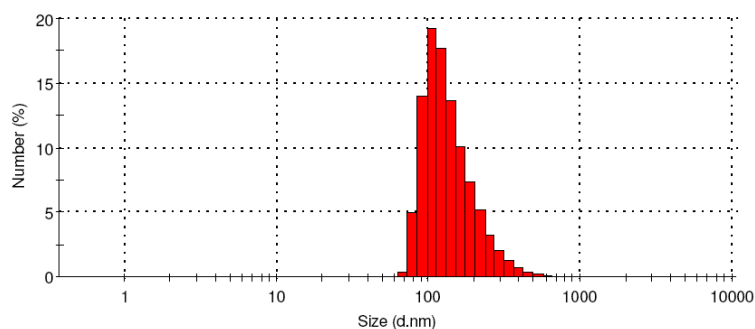
Figure 2.28. Size distribution of coumarin 102 loaded **PTFS-b-PSt-b-PEO** aggregates.
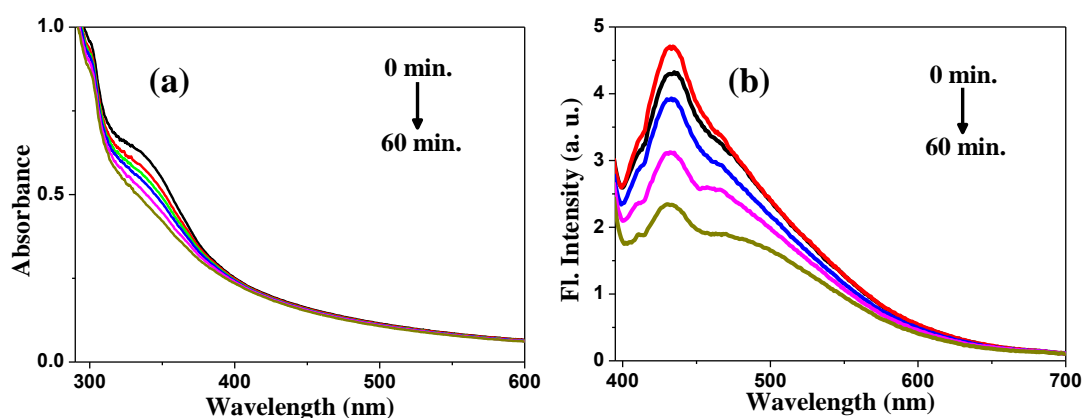
Figure. 2.29 (a) Changes in the absorption spectra of coumarin 102 encapsulated **PTFS-b-PSt-b-PEO** aggregates in water during UV irradiation (b) Changes in the emission intensity of coumarin 102 during UV irradiation.

Morphological characterization of the dye encapsulated **PTFS-b-PSt-b-PEO** was carried out using AFM, SEM and TEM. Microscopic studies showed that the vesicular morphology is retained even after dye encapsulation. Figure 2.30 and Figure 2.31 shows respectively the SEM and AFM images of coumarin 102 loaded vesicular aggregates of **PTFS-b-PSt-b-PEO** and Figure 2.32 shows its TEM image.
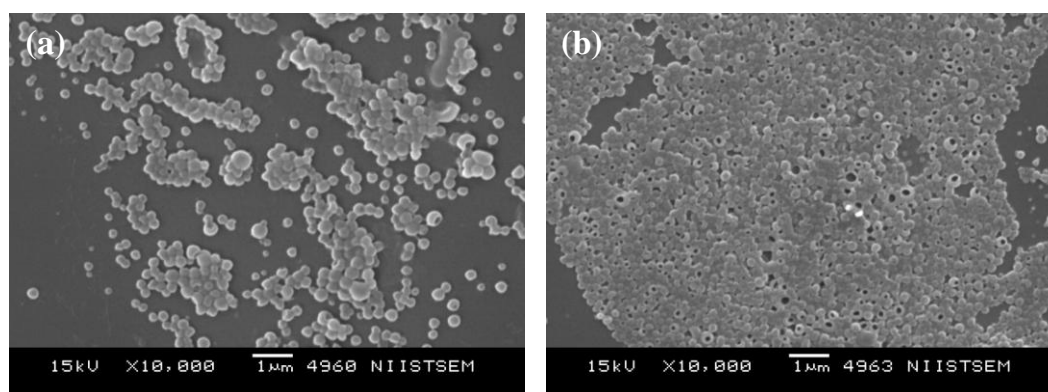
Figure 2.30. (a, b) SEM images of air-dried coumarin 102 loaded vesicular aggregates of **PTFS-b-PSt-b-PEO**.
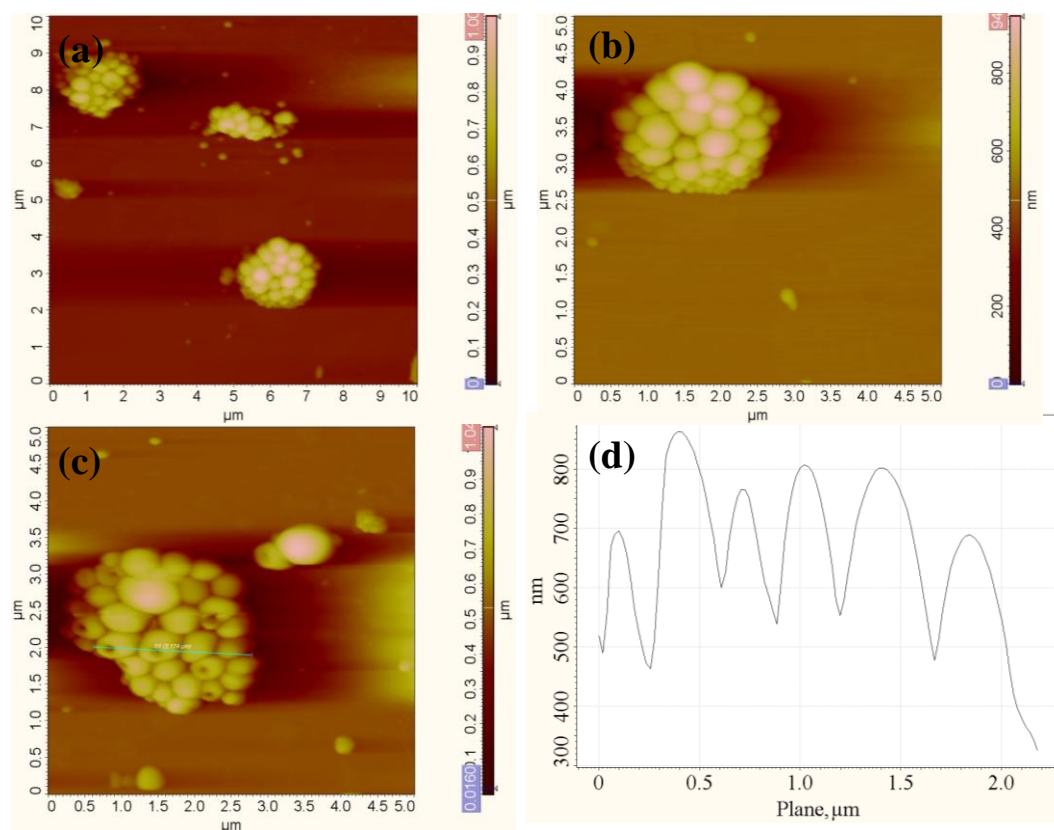
Figure 2.31. (a, b, c) AFM height images of air-dried coumarin 102 loaded **PTFS-b-PSt-b-PEO** vesicles (d) height profile of the aggregates.
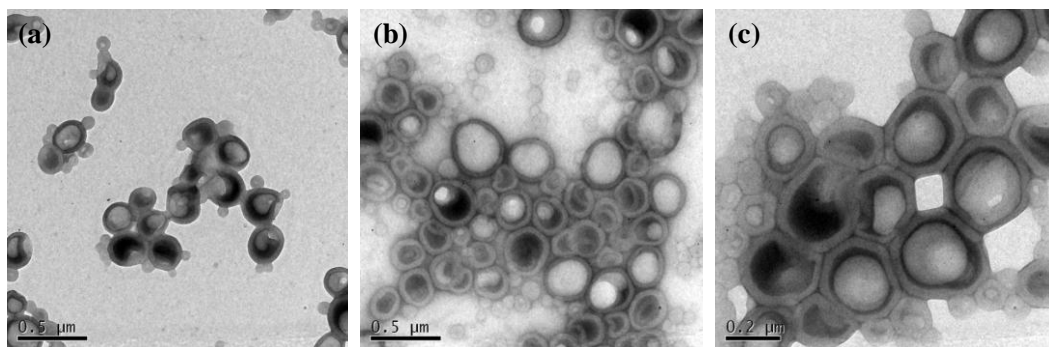
Figure 2.32. (a, b, c) TEM images of air-dried coumarin 102 loaded vesicular aggregates of **PTFS-b-PSt-b-PEO**.

2.4. Conclusions

Photoresponsive aggregates from stilbene block copolymers are obtained by the gradual hydrophobic aggregation of the polymer chains upon slow addition of water to the solution of the polymers in THF. The spherical morphology of the aggregates was confirmed by DLS, AFM, SEM and TEM. When the aqueous solution containing colloidal aggregates of these polymers was irradiated with 350 nm UV light, aggregates underwent morphological transition. This transition is brought about due to the shift in the hydrophobic-hydrophilic balance of the photoresponsive amphiphilic block copolymer resulting from the formation of the more polar *cis*-stilbenes. This increase in hydrophilicity caused by the isomerization of the polymer brings about a change in the packing mode of the hydrophobic chain in the polymer thereby resulting in the formation of rod like aggregates. It was also found that these polymer aggregates have the property of encapsulating hydrophobic dyes in water and hence these aggregates can be used as a carrier of such dye molecules. UV irradiation brings about release of the dye from the polymeric aggregates. It is expected that such photoresponsive polymers which change their aggregation pattern in water by just UV illumination will have immense applications in the coming future.

2.5. Synthesis and Experimental Section

2.5.1. Materials

N,N,N',N',N''-Pentamethyldiethylenetriamine (PMDETA), ethyl-2-bromoisobutyrate, poly(ethylene oxide)monomethyl ether, 3,4-dihydroxy benzaldehyde, dodecyl bromide, 4-methylbenzonitrile, N-bromosuccinimide (NBS), methacrylic acid, 2-bromo-2-methylpropionic acid, trifluoromethyl benzyl bromide, triethyl phosphate, 6-bromo-1-hexanol, dicyclohexylcarbodiimide (DCC), 4-(N,N-dimethylamino)pyridine (DMAP), curcumin and coumarin102 were purchased from Aldrich and used without further purification. CuBr (98%, Aldrich) was stirred in glacial acetic acid overnight, filtered, and then it was washed with ethanol and dried under vacuum overnight. Styrene purchased from Aldrich was washed with 5% NaOH solution and water successively for three times, dried over anhydrous Na_2SO_4, and then distilled under reduced pressure at 40 ^{0}C. Solvents and other chemicals were purchased locally and purified using standard procedures before use.

2.5.2. Analysis and Measurements

^{1}H and ^{13}C NMR spectra were recorded on Bruker DPX 500 MHz Spectrometer using tetramethylsilane (TMS) as the internal standard and chloroform-d (CDCl$_3$) as solvent. FT-IR spectra were recorded on a Shimadzu IR Prestige-21 Fourier Transform Infrared Spectrophotometer. The molecular weights of the polymers were determined by gel permeation chromatography (GPC) in tetrahydrofuran (THF) using polystyrene standards for the calibration. The GPC was calibrated with different polystyrene standards having molecular weights ranging from 2950 to 177,000 g/mol (Polymer Standards Service).Waters 515 pump connected through three series of Styragel HR columns (HR-3, HR-4E, and HR-5E) and Waters Model 2487 Dual wavelength UV-Vis

Detector and a Waters 2414 Differential Refractometer were used for analyzing the samples. The flow rate of the THF was maintained as 1 mL/min throughout the experiments, and the sample solutions at very dilute concentration were filtered and injected for recording the GPC chromatograms at 30 ^{0}C. Mass spectral analyses were carried out using a JEOL JMS600 instrument in FAB ionization mode. Melting points are uncorrected and were determined on a Mel-Temp II melting point apparatus. Absorption spectra were recorded on a Shimadzu UV-3101PC UV-Vis-NIR spectrophotometer. The excitation and emission spectra were recorded on a SPEX Fluorolog F112X spectrofluorimeter. Steady-state photolysis was carried out using the output from a 200 W high-pressure mercury lamp filtered through a 350 nm Oriel band-pass filter. Dynamic light scattering (DLS) measurements were done by using a Nano ZS Malvern instrument employing a 4-mW He-Ne laser (λ = 632.8 nm) and equipped with a thermo stated sample chamber. Samples for scanning electron microscopy (SEM) were provided with a thin gold coating using JEOL JFC-1200 fine-coater. SEM images were recorded using a JEOL JSM-5600 LV instrument. Atomic force microscopy (AFM) images were recorded under ambient conditions using NTEGRA Prima - NT-MDT, Russia Scanning probe microscope operated in tapping mode. Micro-fabricated silicon cantilever tips (NSG 20) with a resonance frequency of 260-630 kHz and a force constant of 20-80 Nm^{-1} were used. The tip curvature radius was 10 nm. The scan rate was 1 Hz. To prepare samples for SEM and AFM measurements, a drop of the polymer colloidal solution was placed on a freshly cleaved mica sheet and the solution was allowed to evaporate at room temperature in air. Transmission electron microscopy (TEM) images were recorded using a JEOL JEM 1011 instrument with an accelerating voltage of 100 kV. Samples were prepared by drop-casting aqueous solutions of the polymers on carbon coated copper grids under ambient conditions. The solvent was allowed to evaporate at room temperature. TEM images were obtained without staining.

2.5.3. Synthesis and Characterization Details

2.5.3.1. Synthesis of PEO-Br.

Poly(ethylene glycol)monomethyl ether (**1**) (M_n = 5000 g/mol, 20 g, 4 mmol) was reacted with 2-bromo-2-methylpropionic acid (750 mg, 4.4 mmol) in the presence of 1,3-dicyclohexyl carbodiimide (1.1 g, 5.3 mmol) and a catalytic amount of dimethylaminopyridine (80 mg, 0.62 mmol) in dichloromethane (130 mL). Precipitated dicyclohexyl urea was filtered off and washed with dichloromethane. The macroinitiator was purified by dissolving it in THF, filtering the solution, concentrated and finally precipitated in diethyl ether to get **PEO-Br**.
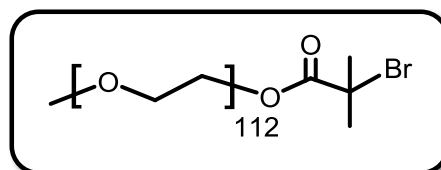
Yield = 17.18 g (86%); ^{1}H NMR (500 MHz, CDCl$_3$, Me$_4$Si): δ (ppm) = 4.33 (2H, dd, -OCOC**H$_2$**-), 3.65 (4H, m, -OC**H$_2$**C**H$_2$**-), 3.38 (3H, s, -OC**H$_3$**) and 1.94 (6H, s, -OCOC(C**H$_3$**)$_2$Br); GPC (THF): M_n = 5,078, M_w/M_n = 1.12.

2.5.3.2. Synthesis of 4-(dodecyloxy)-3-hydroxybenzaldehyde (3).

3,4-Dihydroxybenzaldehyde (**2**) (10 g, 72 mmol), dodecylbromide (18.02 g, 72.46 mmol) and K$_2$CO$_3$ (20.0 g, 145 mmol) were suspended in 10 mL DMF and heated at 90 ^{0}C for 12 hours. The reaction mixture was then poured into ice cold water, precipitated compound was filtered and redissolved in DCM, washed with water and separated. Trace amount of water was removed by adding sodium sulphate and the excess solvent was distilled off. The product was purified by column chromatography using hexane as eluent and (100-200) mesh silica as stationary phase to give **3**.
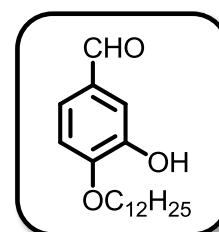
Yield = 15.4 g (67%); FAB MS : m/z = 308.39 [M+H]$^+$; IR ν$_{max}$ (in KBr)/cm^{-1}: 3439, 2920, 2848, 1683, 1512, 1276 and 1002; ^{1}H NMR (500 MHz, CDCl$_3$, Me$_4$Si): δ (ppm) = 9.83 (1H, s, -C**HO**), 7.44 (1H, d, aromatic), 7.41 (1H, s, aromatic), 6.95 (1H, d,

aromatic), 5.85 (1H, s, -O**H**), 4.14 (2H, t, -OC**H₂**-) and 0.89 (3H, t, -C**H₃**); ^{13}C NMR (125 MHz, CDCl₃, Me₄Si): δ (ppm) = 191.07, 151.36, 146.21, 130.4, 124.54, 114.03, 110.88, 69.3, 31.9, 29.52, 25.91, 22.68 and 14.11.

2.5.3.3. Synthesis of 4-(dodecyloxy)-3-(12-hydroxydodecyloxy) benzaldehyde (4).

Compound **3** (5 g,16 mmol), 12-bromododecane-1-ol (8.67 g, 32.7 mmol) and K₂CO₃ (6.76 g, 49.0 mmol) were suspended in 10 mL DMF and heated at 90 ^{0}C for 12 hours .The reaction mixture was then poured into ice cold water, precipitated compound was filtered and redissolved in DCM, washed with water and separated. Trace amount of water was removed by adding sodium sulphate and the excess solvent was distilled off. The product was purified by column chromatography using hexane as eluent and (100-200) mesh silica as stationary phase to give **4**.
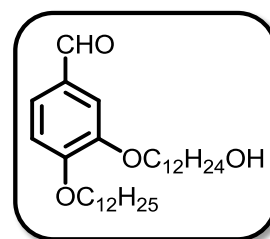
Yield = 5.6 g (70%); FAB MS : *m/z* = 492.81 [M+H]$^+$; IR ν$_{max}$ (in KBr)/cm^{-1} : 3334, 3080, 2918, 2848,1678, 1273, 1130, 1064, 1238 and 806; ^{1}H NMR (500 MHz, CDCl₃, Me₄Si): δ (ppm) = 9.83 (1H, s, -C**H**O), 7.42 (1H, d, aromatic), 7.39 (1H, s, aromatic), 6.96 (1H, d, aromatic), 4.09 (4H, t, -OC**H₂**-), 3.63 (2H, t, -C**H₂**-OH) and 0.90 (3H, s, -C**H₃**); ^{13}C NMR (125 MHz, CDCl₃, Me₄Si): δ (ppm) = 191.07, 154.68, 149.41, 129.66, 111.73, 110.91, 69.12,63.08,32.81, 31.92, 29.44, 25.94, 22.69 and 14.12.

2.5.3.4. Synthesis of 12-(2-(dodecyloxy)-5-formylphenoxy)dodecyl methacrylate (5).

Compound **4** (5 g, 10 mmol), methacrylic acid (1.7 mL, 20.4 mmol), dimethyl amino pyridine (1speck) were suspended in 40 mL dry DCM and stirred at 0 ^{0}C and 1,3-dicyclohexyl carbodiimide (3.16 g, 15.3 mmol) was added under argon atmosphere. The reaction mixture was then stirred at room temperature for 24 hours. It was filtered and the precipitate of dicyclohexyl urea was washed several times with
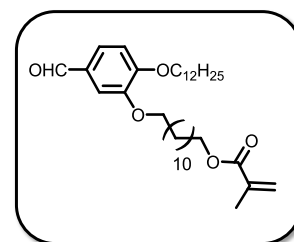
DCM. The solvent was removed under reduced pressure and crude product was purified by column chromatography using hexane as eluent and (100-200) mesh silica as stationary phase to give **5**.

Yield = 4.0 g (71%); FAB MS : m/z = 559.98 [M+H]$^+$; IR ν_{max} (in KBr)/cm^{-1} : 2918, 2848, 1724, 1687, 1585, 1510, 1274, 1165, 1132 and 806; ^{1}H NMR (500 MHz, CDCl$_3$, Me$_4$Si): δ (ppm) = 9.83 (1H, s, -**CHO**), 7.42 (1H, d, aromatic), 7.26 (1H, s, aromatic), 6.96 (1H, d, aromatic), 6.10 (1H, s, =**CH$_2$**), 5.55 (1H, s, =**CH$_2$**), 4.10 (6H, t, -**OCH$_2$**-) and 0.89 (3H, t, -**CH$_3$**); ^{13}C NMR (125 MHz, CDCl$_3$, Me$_4$Si): δ (ppm) = 191.04, 167.57, 154.67, 149.42, 136.56, 129.85, 126.64, 125.13, 111.74, 110.91, 69.12, 64.85, 31.92, 29.05, 25.98, 22.69, 18.34 and 14.12.

2.5.3.5. Synthesis of 4-cyanobenzylbromide (7).

4-methylbenzonitrile (**6**) (10 g, 85 mmol) and N-bromosuccinimide (19.0 g, 103 mmol) were dissolved in 40 mL of dry CCl$_4$, added a speck of azobisisobutyronitrile and heated
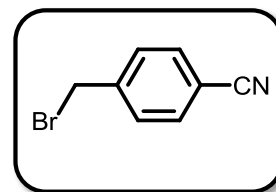
to 80 ^{0}C. After 12 hours the solution was concentrated and kept for crystallization to give **7**.

Yield = 8 g (48%); ^{1}H NMR (500 MHz, CDCl$_3$, Me$_4$Si): δ (ppm) = 7.65 (2H, d, aromatic), 7.51 (2H, d, aromatic) and 4.48 (2H, s, -**CH$_2$**Br); ^{13}C NMR (125 MHz, CDCl$_3$, Me$_4$Si): δ (ppm) = 142.83, 132.60, 129.73, 118.37, 112.21 and 31.48.

2.5.3.6. Synthesis of Diethyl-4-cyanobenzylphosphonate (8).

Compound **7** (14.98 g, 76.8 mmol) and triethylphosphate (15.3 mL, 92.2 mmol) were added to a 250 mL RB and heated to 100 ^{0}C for 12 hours. After 12 hours
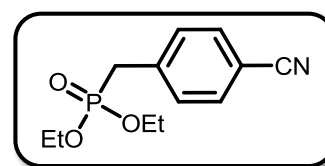
temperature was raised to 130 ^{0}C and excess triethylphosphate was removed by purging argon. The product was purified by column chromatography using hexane as eluent and

(100-200) mesh silica as stationary phase to give **8**.

Yield = 11.7 g (60%); ^{1}H NMR (500 MHz, CDCl$_3$, Me$_4$Si): δ (ppm) = 7.62 (2H, d, aromatic), 7.43 (2H, d, aromatic), 4.04 (4H, q, P(OC**H$_2$**CH$_3$)$_2$), 3.23 (2H, d, -C**H$_2$**PO) and 1.27 (6H, t, P(OCH$_2$C**H$_3$**)$_2$); ^{13}C NMR (125 MHz, CDCl$_3$, Me$_4$Si): δ (ppm) =137.59, 132.26, 130.57, 118.68, 110.88, 62.44, 34.65 and 16.36.

2.5.3.7. Synthesis of 12-(5-(4-cyanostyryl)-2-(dodecyloxy)phenoxy)dodecyl methacrylate (9).

To a solution of compound **8** (2.16 g, 7.53 mmol) in THF, NaH (752 mg, 31.4 mmol) was added at ice temperature. After stirring the reaction mixture for 10 minutes compound **5** (3.5 g, 6.3 mmol) was added drop wise and the resulting mixture was stirred for 4 hours in argon atmosphere. Excess NaH was filtered off. The product was purified by column chromatography by using silica as stationary phase and 5% EtOAc/hexane as eluent to give product **9**.
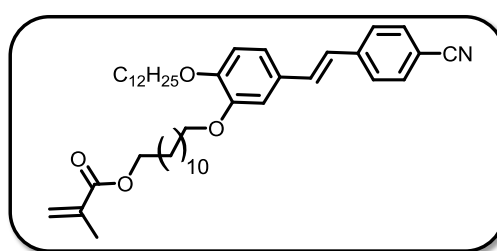
Yield = 2.4 g (68.5%); m.p. = 56 [0]C; FAB MS : *m/z* = 658.39 [M+H]$^+$; IR ν$_{max}$ (in KBr)/cm^{-1} : 2916, 2848, 2223, 1714, 1516, 1174 and 1136; ^{1}H NMR (500 MHz, CDCl$_3$, Me$_4$Si): δ (ppm) = 7.64 (2H, d, aromatic), 7.57 (2H, d, aromatic), 7.17 (1H, d, aromatic), 7.09 (2H, d, aromatic), 6.95 (1H, d, aromatic), 6.89 (1H, d, aromatic), 6.11 (1H, s, =C**H$_2$**), 5.56 (1H, s, =C**H$_2$**), 4.16 (2H, t, -OCOC**H$_2$**), 4.07 (4H, d, Ar-OC**H$_2$**) and 0.89 (3H, t, -C**H$_3$**); ^{13}C NMR (125 MHz, CDCl$_3$, Me$_4$Si): δ (ppm) = 167.58, 149.28, 142.22, 136.55, 132.46, 129.6, 126.73, 125.5, 121.96, 119.16, 111.75, 110.01, 69.19, 64.84, 31.92, 29.7, 26.02, 22.69, 18.34 and 14.12.

2.5.3.8. Synthesis of PDACS-b-PEO.

CuBr (15 mg, 0.11 mmol) was added to a 10 mL RB flask containing compound **9** (500 mg, 0.76mmol), **PEO-Br** (500 mg, 0.10 mmol) and PMDETA (17.43 mg, 0. 10 mmol) in 1,4-Dioxan (3 mL). As soon as CuBr was added the color changed to pale green indicating the start of polymerization. The flask was then sealed with a rubber septum and was purged with argon for 20 minutes. The flask was placed in a preheated oil bath at 85 ^{0}C for 24 hours. The viscous liquid was dissolved in THF and was passed through neutral alumina column to remove the catalyst and was then concentrated and precipitated in hexane to get **PDACS-b-PEO**. The obtained polymer were purified by repeated precipitation from THF into hexane and dried.
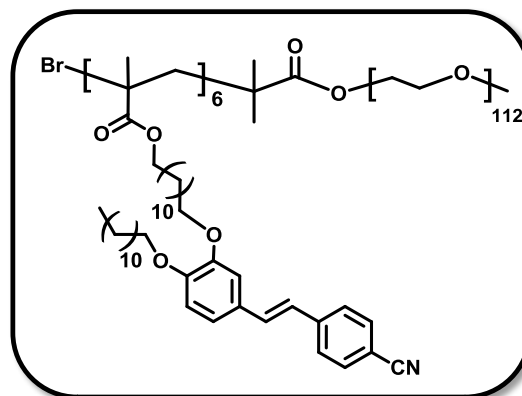
Yield = 650 mg (65%); ^{1}H NMR (500 MHz, CDCl$_3$, Me$_4$Si): δ (ppm) = 7.57 (4H, m, aromatic), 7.10 (3H, m, aromatic), 6.85 (2H, m, aromatic), 4.00 (6H, m, -OCOC**H$_2$**-, 2 X -OC**H$_2$**-), 3.65 (4H, m, -OC**H$_2$CH$_2$**-), 3.38 (3H, s, -OC**H$_3$**), 1.24-1.48 (45H, m, 2 X -OCH$_2$(C**H$_2$**)$_{10}$-, -C(CH$_3$)C**H$_2$**-, -CH$_2$C**H$_3$**) and 0.86 (3H, m, C**H$_3$**CCH$_2$-); GPC (THF): M$_n$ = 9,166, M$_w$/M$_n$ = 1.39.

2.5.3.9. Synthesis of PSt-b-PEO.

CuBr (75 mg, 0.52 mmol) was added to a 25 mL RB flask containing styrene (5 g, 48 mmol), **PEO-Br** (2.5 g, 0.50 mmol) and PMDETA (87.2 mg, 0.50 mmol). The flask was sealed with rubber septum and was purged with argon for 20 minutes before adding the catalyst. The flask was placed in a preheated oil bath at 85 ^{0}C for 24 hours. The viscous liquid was dissolved
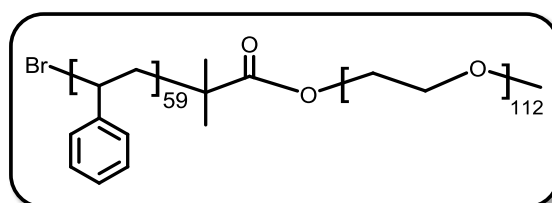
in THF and was passed through a neutral alumina column to remove the catalyst and was then concentrated and precipitated in methanol twice to get **PSt-b-PEO**.

Yield = 5.50 g (73.33%); ^{1}H-NMR (500 MHz, CDCl$_3$, Me$_4$Si): δ (ppm) = 7.07 (m, 3H, styrene aromatic), 6.57 (m, 2H, styrene aromatic), 3.65 (m, 4H, -OC**H$_2$CH$_2$**-), 3.38 (s, 3H, -OC**H$_3$**), 1.42-1.84 (m, 3H, -**CH$_2$CH**-),0.86-0.98 (m, 9H, -C(C**H$_3$**)$_2$-, C**H$_3$**CH$_2$O-); GPC (THF): M$_n$ = 11,126, M$_w$/M$_n$ = 1.19.

2.5.3.10. Synthesis of 4-(decyloxy)-3-hydroxybenzaldehyde (11).

Yield = 8.93 g (44.28%); FAB MS : *m/z* = 279.77 [M+H]$^+$; ^{1}H-NMR (500 MHz, CDCl$_3$, Me$_4$Si): δ (ppm) = 9.84 (s, 1H, -C**H**O), 7.44 (m, 2H, aromatic), 6.96 (d, 1H, aromatic), 5.77 (s, 1H, -O**H**), 4.14 (t, 2H, -OC**H$_2$**), 1.88 (m, 2H, -OCH$_2$-C**H$_2$**-), 1.34-1.47 (m, 14H, -CH$_2$-(C**H$_2$**)$_7$-CH$_3$), 0.89 (t, 3H, -C**H$_3$**); ^{13}C-NMR (125 MHz, CDCl$_3$, Me$_4$Si): δ (ppm) = 191.07, 151.36, 146.21, 130.4, 124.54, 114.03, 110.88, 69.3, 31.9, 29.52, 25.91, 22.68, 14.11.
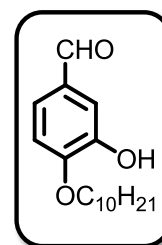
2.5.3.11. Synthesis of 4-(decyloxy)-3-(6-hydroxyhexyloxy) benzaldehyde (12).

Yield = 3.05 g (86.52%); FAB MS : *m/z* = 379.69 [M+H]$^+$; ^{1}H-NMR (500 MHz, CDCl$_3$, Me$_4$Si): δ (ppm) = 9.84 (s, 1H, -C**H**O), 7.44 (m, 2H, aromatic), 6.96 (d, 1H, aromatic), 4.15 (m, 4H, -OC**H$_2$-**), 3.73 (t, 2H, -C**H$_2$**-OH), 1.93 (m, 4H, -OCH$_2$-C**H$_2$**-), 1.32-1.71 (m, 20H, -CH$_2$-(C**H$_2$**)$_7$-CH$_3$, -CH$_2$-(C**H$_2$**)$_4$-CH$_2$-OH), 0.89 (t, 3H, -C**H$_3$**); ^{13}C-NMR (125 MHz, CDCl$_3$, Me$_4$Si): δ (ppm) = 191.07, 154.64, 149.32, 129.82, 126.75, 111.70, 110.85, 69.11, 62.88, 32.67, 31.90, 29.55, 25.92, 22.68, 14.11.
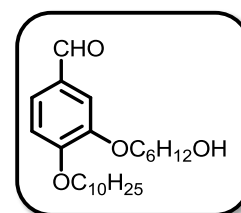
2.5.3.12. Synthesis of 6-(2-(decyloxy)-5-formylphenoxy)hexyl methacrylate (13).

Yield = 2.9 g (84.77%); FAB MS : m/z = 447.74 [M+H]$^+$; ^{1}H-NMR (500 MHz, CDCl$_3$, Me$_4$Si): δ (ppm) = 9.83 (s, 1H, -C**H**O), 7.42 (m, 2H, aromatic), 6.9 6 (d, 1H, ar omatic), 6.10 (s, 1H, -OCO-C(CH$_3$)=C**H$_2$**), 5.55 (s, 1H, -OCO-C(CH$_3$)=C**H$_2$**), 4.15 (m, 2H, -OC**H$_2$**-), 4.07 (m, 4H, -OC**H$_2$**-, -C**H$_2$**-OCO-), 3.73 (t, 2H, -C**H$_2$**-OH), 1.94-1.25 (m, 24H, alkyl), 0.89 (t, 3H, -C**H$_3$**); ^{13}C-NMR (125 MHz, CDCl$_3$, Me$_4$Si): δ (ppm) = 191.07, 167.51, 154.64, 149.28, 136.46, 129.79, 126.75, 125.25, 111.66, 110.81, 69.11, 64.63, 31.90, 29.55, 25.92, 22.68, 18.34, 14.11
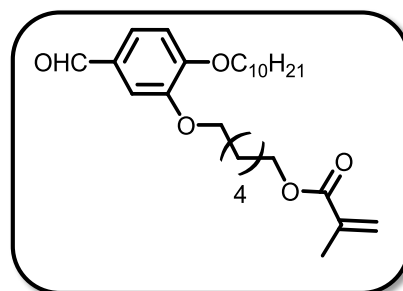
2.5.3.13. Synthesis of diethyl-4-(trifluoromethyl)benzylphosphonate (15).

Yield = 11.9 g (94.4%); FAB MS : m/z = 297.41 [M+H]$^+$; ^{1}H-NMR (500 MHz, CDCl$_3$, Me$_4$Si): δ (ppm) = 7.58 (d, 2H, aromatic), 7.43 (d, 2H, aromatic), 4.04 (m, 4H, P(OC**H$_2$**CH$_3$)$_2$), 3.23 (d, 2H, -C**H$_2$**PO), 1.27 (t, 6H, P(OCH$_2$C**H$_3$**)$_2$); ^{13}C-NMR (125 MHz, CDCl$_3$, Me$_4$Si): δ (ppm) = 135.95, 129.58, 127.37, 125.41, 123.04, 62.31, 34.27, 16.34.
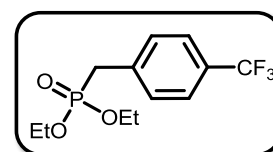
2.5.3.14. Synthesis of 6-(5-(4-trifluoromethyl)-2-(decyloxy)styryl phenoxy)hexyl methacrylate (16).

Yield = 1.94 g (56.53 %); m.p. = 55 ^{0}C; FAB MS : m/z = 588.83 [M]$^+$; ^{1}H-NMR (500 MHz, CDCl$_3$, Me$_4$Si): δ (ppm) = 7.58 (m, 4H, aromatic), 7.26 (m, 3H, aromatic), 7.08 (d, 1H, aromatic), 6.87 (d, 1H, aromatic), 6.10 (s, 1H, -OCO-C(CH$_3$)=C**H$_2$**), 5.55 (s, 1H, -OCO-C(CH$_3$)=C**H$_2$**), 4.18 (t, 2H, -OCOC**H$_2$**), 4.07 (m, 4H, Ar-OC**H$_2$**), 1.94-1.25 (m, 24H, alkyl), 0.89 (t, 3H, -C**H$_3$**); ^{13}C-NMR (125 MHz, CDCl$_3$, Me$_4$Si): δ (ppm) = 167.58, 149.28, 149.16, 141.12,
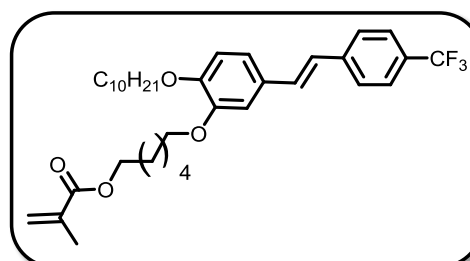
136.50, 131.06, 129.67, 126.26, 125.57, 120.62, 113.47, 111.73, , 69.17, 64.65, 31.91, 29.7, 26.02, 22.69, 18.34, 14.13.

2.5.3.15. Synthesis of PTFS-b-PSt-b-PEO.

CuBr (7 mg, 0.05 mmol) was added to a 10 mL RB flask containing **PSt-b-PEO** (588 mg, 1.0 mmol), **16** (556 mg, 0.05 mmol) and PMDETA (8.30 mg, 0.05 mmol) in 5 mL THF. The flask was sealed with rubber septum and was purged with argon for 20 minutes before adding the catalyst. The flask was placed in a preheated oil bath at 60 ^{0}C for 24 hours. The viscous liquid was dissolved in THF and was passed through a neutral alumina column to remove the catalyst and was then concentrated and precipitated in hexane four times.
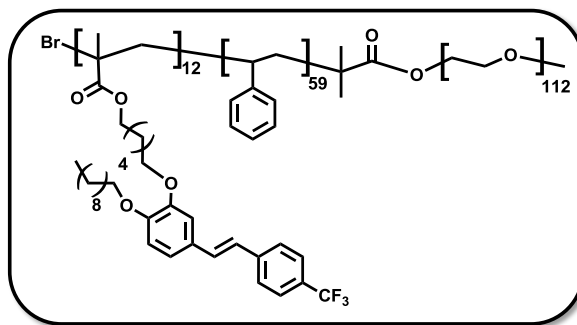
Yield = 561 mg (49.03%); ^{1}H-NMR (500 MHz, CDCl$_3$, Me$_4$Si): δ (ppm) = 7.47 (m, 4H, aromatic), 7.08 (m, 7H, aromatic), 6.50 (m, 3H, aromatic), 3.90 (m, 6H, Ar-OC**H$_2$**, -OCOC**H$_2$**-), 3.65 (m, 4H, -OC**H$_2$CH$_2$**-), 3.38 (s, 3H, -OC**H$_3$**), 1.58-1.94 (m, alkyl), 1.42-1.84 (m, 3H, -C**H$_2$CH**-), 0.86-0.98 (m, 9H, -C(C**H$_3$**)$_2$-, C**H$_3$**CH$_2$O-); GPC (THF): M$_n$ = 18,354, M$_w$/M$_n$ = 1.48.

Photoresponsive Self-Assembling Structures from Pyrene-Based Block Copolymers

3.1. Abstract

Two new photoresponsive amphiphilic block copolymers, poly(pyrenylmethyl methacrylate)-block-polystyrene-block-poly(ethylene oxide) **(PPy-b-PSt-b-PEO)** *and poly(pyrenylmethylmethacrylate)-b-poly(3-O-4-vinylbenzoyl-D-glucopyranose)* **(PPy-b-PBG)** *were synthesized using atom transfer radical polymerization (ATRP). Formation of colloidal aggregates of these macromolecules was observed in solutions under controlled conditions due to the amphiphilic nature of the polymers. Irradiation of the polymeric aggregates using UV light resulted in the photodissociation of 1-pyrenemethanol units from the polymer back-bone resulting in break-up of the aggregates due to the mainly hydrophilic nature of the residual polymer. A hydrophobic fluorescent dye Nile Red was introduced into these aggregates to form Nile Red loaded polymeric aggregates in water. The polymeric aggregates not only enhances the solubility and fluorescence of the hydrophobic dye in water by accommodating the dye in the hydrophobic interior of the aggregates but also modulate the fluorescence of the dye through fluorescence resonance energy transfer (FRET).*

3.2. Introduction

Polymers containing appropriate fluorescent or phosphorescent group such as anthracene [Liu *et al.* 2001; Tong *et al.* 2000; Zhang *et al.* 2002] and pyrene [Slomkowski *et al.* 1989; Strukelj *et al.* 1991] have been prepared and investigated by many authors. The interest in these polymers is mainly due to the expectations to create fluorescent probes and photoresponsive materials using the photosensitivity of anthracene and pyrene.

Traditionally, fluorescence has been the technique of choice to study long-range polymer chain dynamics [Duhamel 2006]. A direct correlation of self-organization in solution and morphology of solvent-cast films of the polymer sample could be obtained by introducing fluorescent probes into the polymer design [Deepak *et al.* 2009]. Fluorophores have been well-recognized as probes to study conformational changes and molecular motions in polymers, since they open up a broad range of pathways through which one can trace the system behavior at the molecular level in addition to their typical photophysical as well as photochemical properties. Special attention must be paid to the choice of a chromophore since it is essential that its lifetime match the time window over which chain dynamics occur. Pyrene is one of the most widely used fluorophores for this purpose. The reason for choosing pyrene resides in its relatively large extinction coefficients, its long lifetime (200-300 ns), which enables the study of the long time scales associated with the large scale motions of polymer chains, and its strong excimer emission at around 480 nm, a wavelength that is more than 50 nm longer than that of monomer emission [Winnik 1999]. The excimer formation in pyrene follows the classic Birk's scheme in which an excited pyrene can either emit a photon with its own lifetime or encounter a ground-state pyrene via diffusion and form a complex called an excimer. By monitoring the process of excimer formation between two pyrene groups, information

about the nature of polymer association can be retrieved. Since the pyrene moieties are attached onto the polymer, excimer formation indicates that two units of the polymer have encountered. By analyzing the process of excimer formation, information on the behavior of the polymer in solution can be retrieved [Duhamel 2006].

Burattini *et al.* synthesized a novel, pyrene-functionalised copolymer in a single step via imidisation of poly(maleic anhydride-alt-1-octadecene) with 1-pyrenemethylamine, and investigated its potential for the detection of volatile nitro aromatic compounds (NACs) [Burattini *et al.* 2009]. The new copolymer forms complexes in solution with NACs such as 2, 5-dinitrobenzonitrile. Moreover, thin films of this copolymer, cast from THF solution, undergo almost instantaneous fluorescence quenching when exposed to the vapor of 2, 5-dinitrobenzonitrile (a model for TNT) at ambient temperatures and pressures (Figure 3.1).
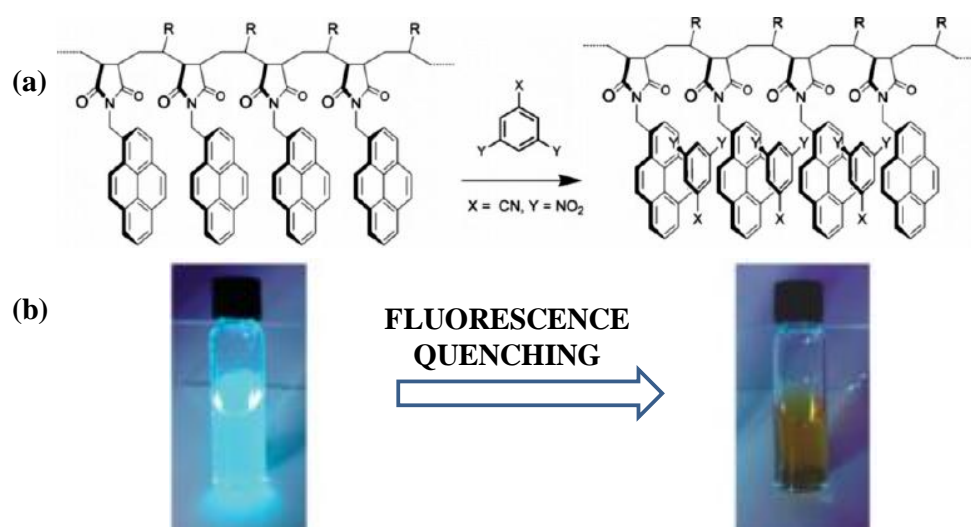
Figure 3.1. (a) Schematic representation of the complex formed between the polymer and NAC and (b) Photos showing a THF solution of the polymer before (left) and after addition of 2, 5-dinitrobenzonitrile. [Adapted from Burattini *et al.* 2009].

A pyrene end-labeled amphiphilic block copolymer, poly(ε-caprolactone)-block-poly[6-O-(4-vinylbenzyl)- D-galactose] (Py-PCL$_{32}$-b-PVBG$_{10}$), was reported by Lu and co-workers in 2005 [Lu *et al.* 2005]. The aggregation behavior of the diblock copolymer in solution was studied by monitoring the fluorescence of pyrene. TEM measurements

revealed that the aggregates obtained by first dissolving the copolymer in N,N-dimethylformamide (DMF), followed by the addition of water were primarily spheres with the PCL blocks in the core (Figure 3.2a). The PVBG corona was then crosslinked with glutaraldehyde. Final removal of the PCL core was accomplished by degradation under basic conditions, which resulted in the formation of hollow glycopolymer nanospheres (Figure 3.2b).
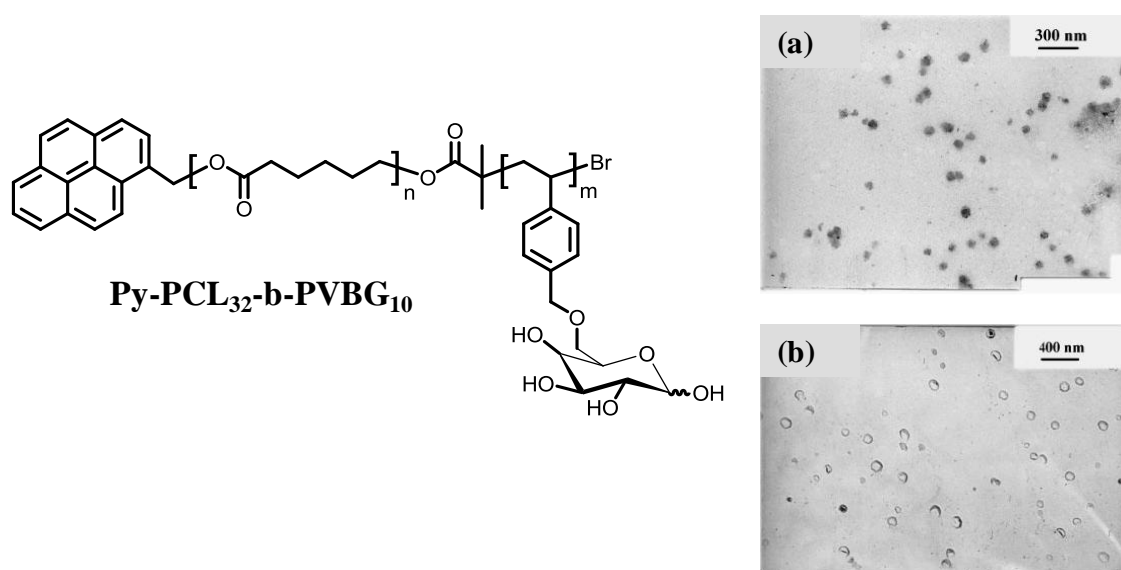
Figure 3.2. (a) TEM micrographs of Py-PCL$_{32}$-b-PVBG$_{10}$ aggregates (1 mg/mL) (a) before degradation of the PCL core and (b) crosslinking after degradation of the PCL core. [Adapted from Lu *et al.* 2005].

Jérôme and co-workers synthesized two pyrene containing polymers, including (1-pyrene)methyl 2-methyl-2-propenoate (PyMMP) copolymerized with methyl methacrylate (MMA) and poly-(ethylene-*co*-butylene)-*b*-poly(MMA-*co*-PyMMP) which was used for the functionalization of multiwalled carbon nanotubes (MWNTs).[Lou *et al.* 2004]. The surface of MWNTs, produced by both the catalytic carbon vapor deposition (CCVD) and arc discharge methods, was modified by these copolymers for making them dispersible in a variety of organic solvents. These copolymers were strongly adsorbed onto MWNTs, even after extensive washing by good solvents. Figure 3.3 shows typical TEM images of MWNTs modified by poly(MMA-*co*-PyMMP). Very well separated

nanotubes are observed in contrast to densely entangled nanotubes that persist with PMMA. This indicates that the poly(MMA-*co*-PyMMP) chains immobilized at the surface of the MWNTs form an effective steric barrier against agglomeration. Microscopic analysis revealed that the grafted polymer layer was homogeneously deposited along the nanotube.

PEB-b-poly(MMA-*co*-PyMMP)
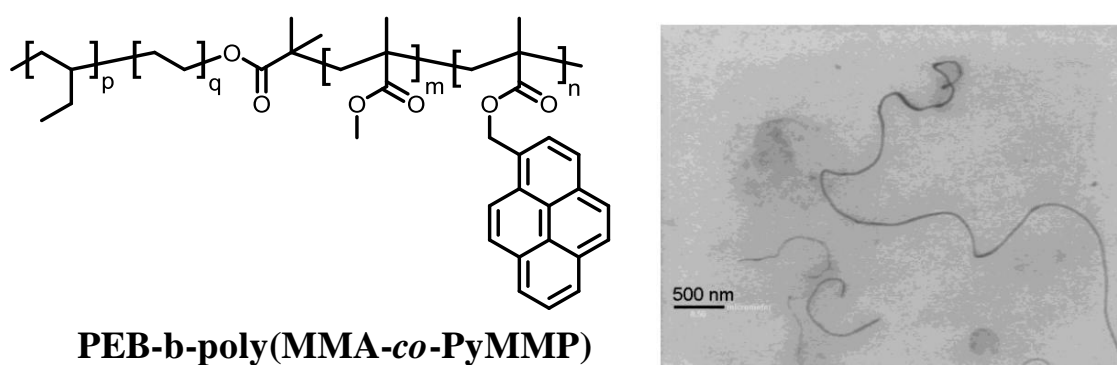
Figure 3.3. TEM micrographs of nanocyl MWNTs after dispersion in a THF solution of PEB-b-poly(MMA-*co*-PyMMP). [Adapted from Lou *et al.* 2004].

Zhao and coworkers have recently communicated that UV irradiation of a diblock copolymer containing pyrenyl esters could be effectively used for developing controlled release systems [Jiang *et al.* 2005]. In view of the potential interest in developing such controlled release systems we have conducted a detailed study on the synthesis and photoresponsive behavior of two pyrene based amphiphilic block copolymers **PPy-b-PSt-b-PEO** and **PPy-b-PBG**. It was expected that introduction of PSt units in **PPy-b-PSt-b-PEO** could increase the hydrophobicity of the polymer resulting in an increased hydrophobic volume during aggregation. **PPy-b-PSt-b-PEO** formed highly monodisperse microsized aggregates in water and in water/THF mixtures, and the presence of monomer emission of pyrene along with its excimer emission in the aggregates was indicative of the larger hydrophobic domain available for the pyrene linked unit. **PPy-b-PBG** on the other hand formed vesicular aggregates in water showing a very strong excimer emission with negligible monomer emission. In aqueous solutions,

the photosolvolysis of pyrenylmethyl esters under UV light irradiation resulted in the cleavage of 1- pyrenemethanol, resulting in conversion of the ester groups to carboxylic acid groups and the hydrophobic PPy to hydrophilic poly(methacrylic acid) (PMA) (Scheme 1). These aspects, as well as the encapsulation of the hydrophobic dye Nile Red within the polymer aggregates and its photocontrolled release are described.
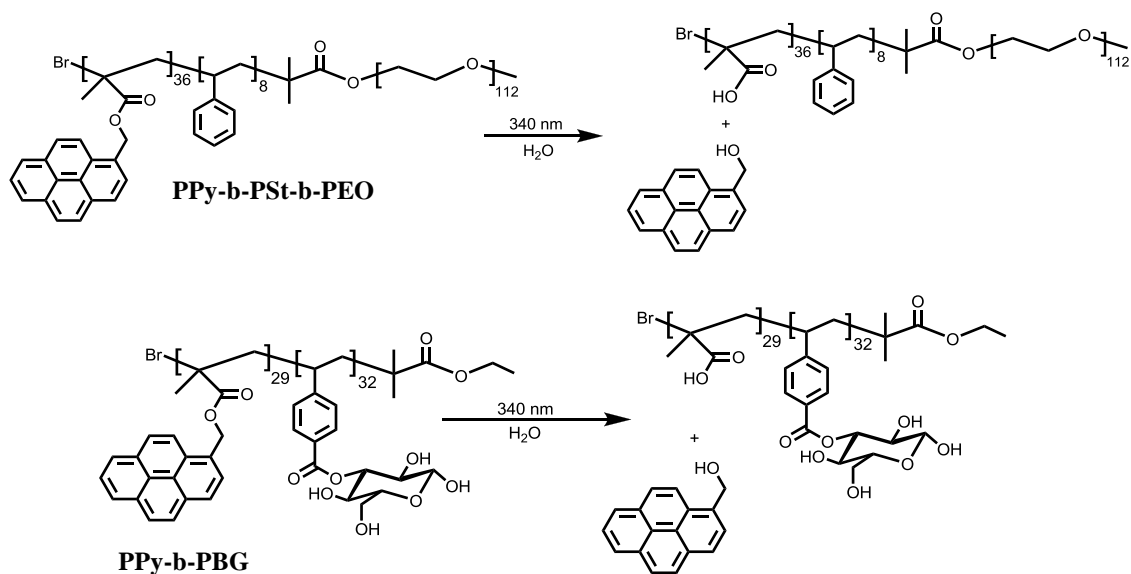
Scheme 3.1. Scheme depicting photosolvolysis of the block copolymer under UV irradiation.

3.3. Results and Discussion

3.3.1. Synthesis and Characterization

The synthesis of the triblock copolymer **PPy-b-PSt-b-PEO** is outlined in Scheme 3.2. Details of the synthesis and characterization are provided in Section 3.5.3. In our work the bromo-terminated PEO macroinitiator (PEO-Br) was prepared by the esterification reaction of poly(ethylene oxide) monomethyl ether using 2-bromo-2-methylpropionic acid. After the esterification, a new peak at 1.95 ppm was observed in the ^{1}H NMR spectra of PEO-Br corresponding to the two methyl groups in 2-bromo-2-methylpropionic ester. The macroinitiator thus obtained was dissolved in styrene. The

ATRP reaction between the macroinitiator and styrene was initiated using CuBr as the catalyst and N,N,N',N',N''-Pentamethyldiethylenetriamine (PMDETA) as the ligand at 80 ^{0}C to obtain PSt-b-PEO. The resultant diblock copolymer was then reacted with (1-pyrene)methylmethacrylate (PyM) in THF at 60 ^{0}C to produce the fluorescent **PPy-b-PSt-b-PEO** triblock copolymer. Figure 3.4 shows the ^{1}H NMR spectrum of PEO-Br, PSt-b-PEO and **PPy-b-PSt-b-PEO** in CDCl$_3$. The characteristic resonance peaks at 3.65 ppm arising from the ethylene oxide chains, 6.46 and 7.06 ppm corresponding to the styrene block and 7.45 ppm corresponding to aromatic protons of pyrene provided strong evidence for the presence of PEO, PSt and PPy segments in the final polymer.
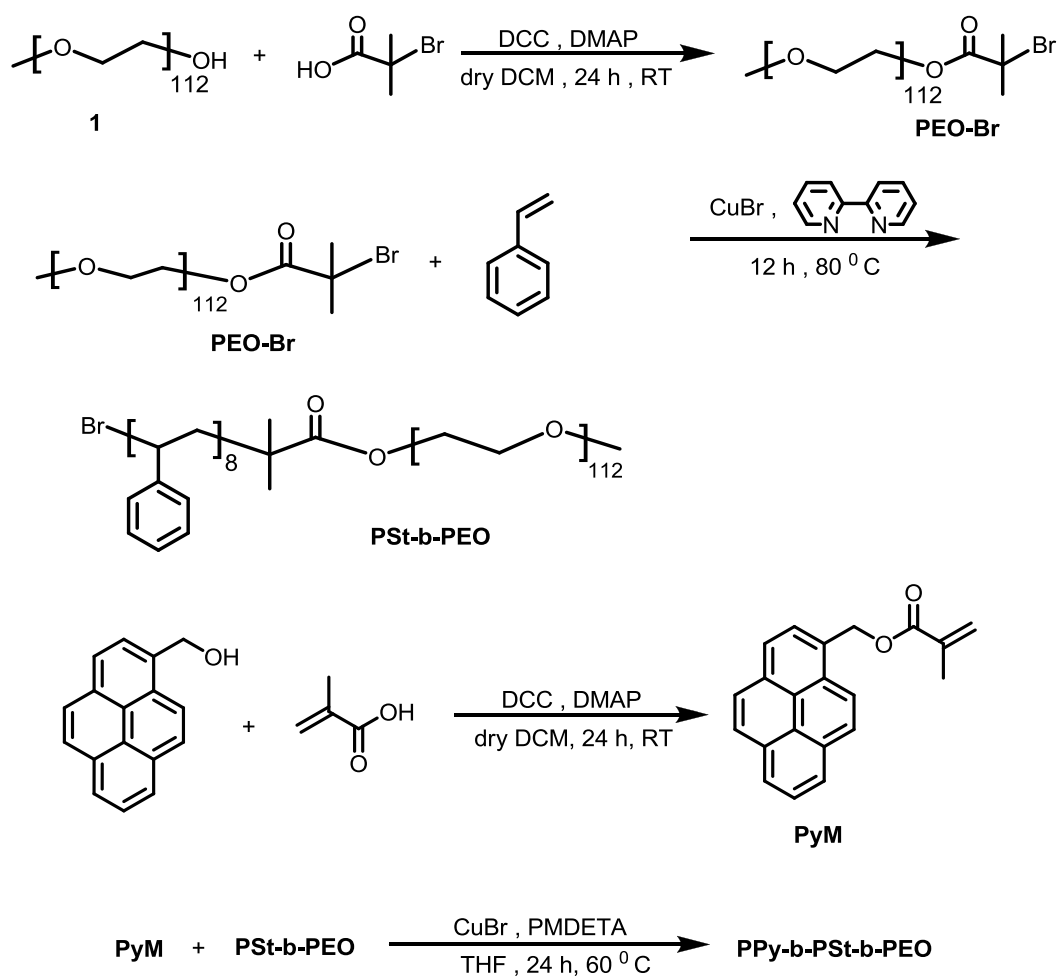
Scheme 3.2. Synthesis of **PPy-b-PSt-b-PEO**.

Figure 3.4d shows the GPC trace of **PPy-b-PSt-b-PEO** triblock copolymer together with that of the diblock copolymer PSt-b-PEO and the homopolymer PEO-Br. It can be seen that the molecular weight of **PPy-b-PSt-PEO** shifts towards the high molecular weight region without any trace of the low molecular weight macroinitiators. This shows that PSt-b-PEO is an efficient macroinitiator for the polymerization of PyM while maintaining low polydispersity. The polydispersity however increased slightly during each polymerization stage. The polydispersity of PEO-Br was 1.12 which increased to 1.31 during the synthesis of PSt-b-PEO and finally increased to 1.48 after the attachment of the pyrene block. The final triblock copolymer **PPy-b-PSt-b-PEO** was purified five times by precipitation from THF into methanol. The resulting polymer had a number average molecular weight (M_n) of 16,679 consisting of 36 units of PyM, 8 units of St and 112 units of EO.
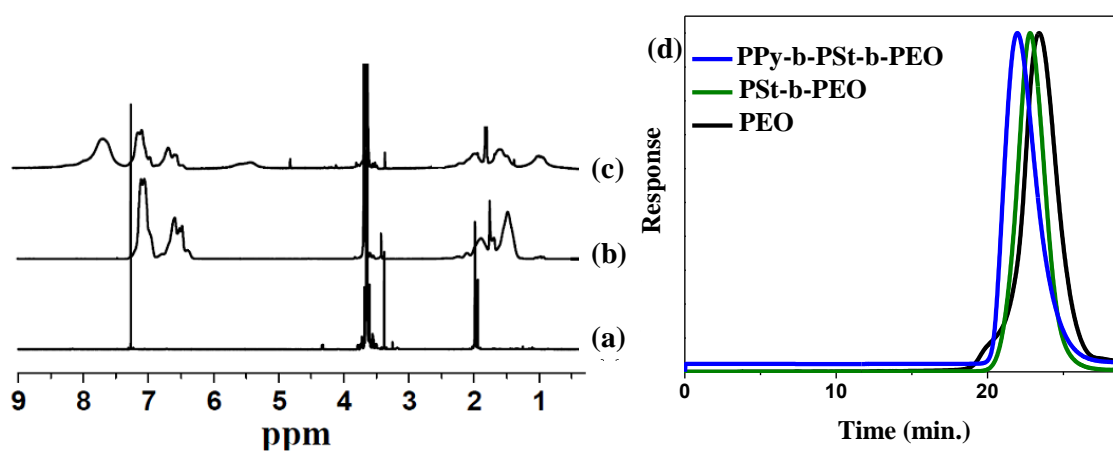
Figure 3.4. ^{1}H NMR spectra of the homopolymer and copolymers in CDCl$_3$ (a) PEO-Br (b) PSt-b-PEO (c) **PPy-b-PSt-b-PEO** (d) GPC curves of **PPy-b-PSt-b-PEO** and the corresponding precursors PSt-b-PEO and PEO-Br.

Scheme 3.3 outlines the synthesis of **PPy-b-PBG**. BipG was first polymerized under ATRP conditions using CuBr/PMDETA with ethyl 2-bromoisobutyrate at 60 ^{0}C in THF for 24 hours. The number-average molecular weight of PBipG as determined by conventional GPC was 12,297 which correspond to 32 BipG units and the polydispersity

index (PDI) was 1.19. Copolymerization of PyM was conducted using CuBr/PMDETA with PBipG as the macroinitiator at 60 ^{0}C in THF for 24 hours. The resultant polymer PPy-b-PBipG had a number-average molecular weight of 21,194 and a PDI value of 1.46.
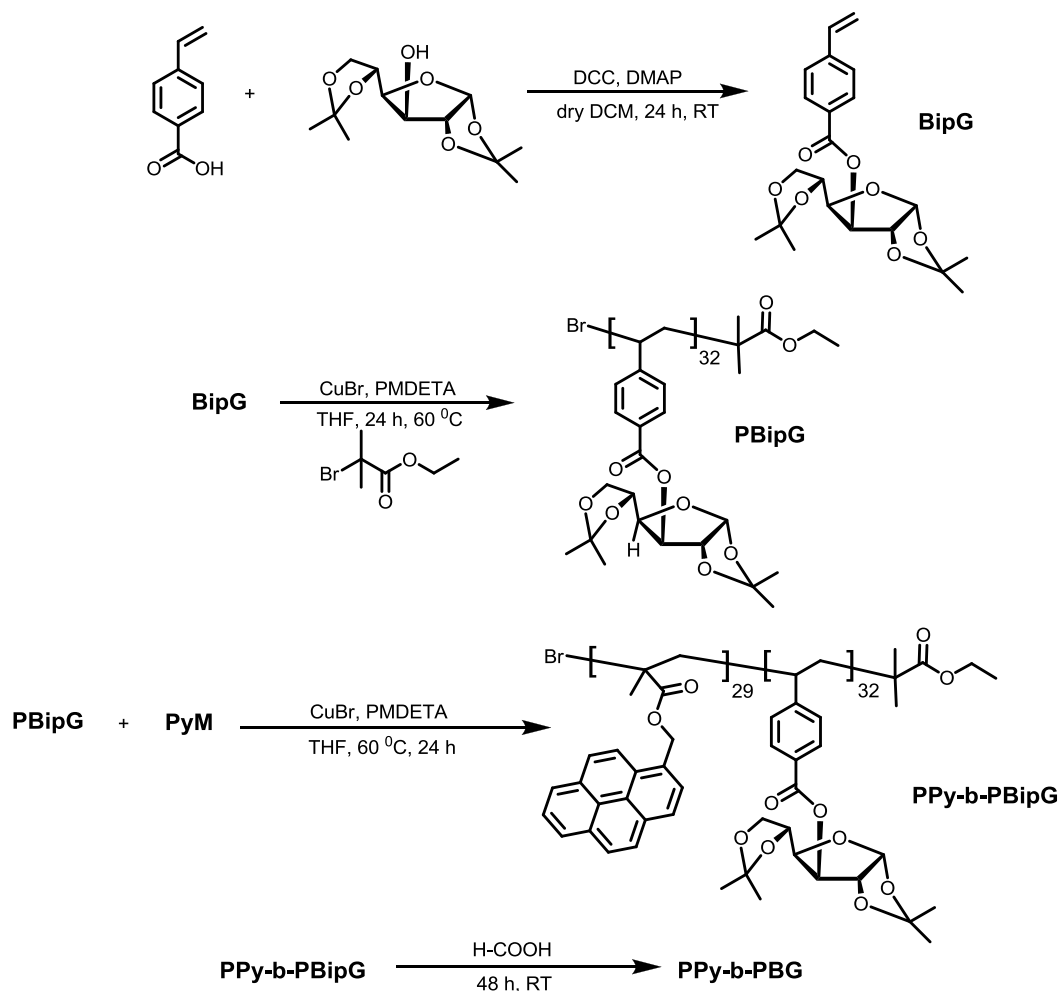
Scheme 3.3. Synthesis of **PPy-b-PBG**.

Figure 3.5 shows the GPC trace of PPy-b-PBipG together with that of the homopolymer PBipG. It can be seen that the molecular weight of PPy-b-PBipG shifts towards the high molecular weight region without any trace of the low molecular weight macroinitiator. The diblock copolymer PPy-b-PBipG was purified by reprecipitating it three times from THF into methanol. The resulting polymer PPy-b-PBipG was composed of 29 units of Py and 32 units of BipG.
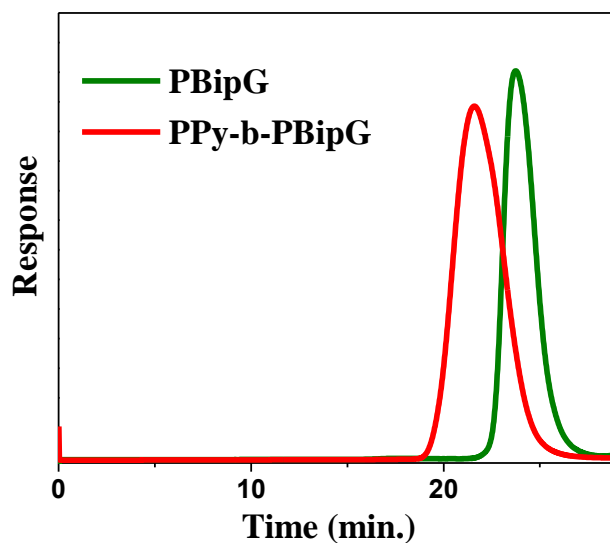
Figure 3.5. GPC curves of **PPy-b-PSt-b-PEO** and the corresponding precursors PSt-b-PEO and PEO-Br.

Hydrolysis of the isopropylidene groups in PPy-b-PBipG was performed by treating the samples with formic acid [Ohno *et al.* 1999]. The final product **PPy-b-PBG** was obtained by freeze-drying following dialysis of the deprotected polymer against water. The structure of the polymers PBipG, PPy-b-PBipG and **PPy-b-PBG** was confirmed by ^{1}H NMR. Figure 3.6 shows the ^{1}H NMR spectra of the respective polymers. The characteristic peaks at 1.2-1.4 (isopropylidene protons), 6.3-6.5 (aromatic protons), 7.4-7.7 ppm (aromatic protons) are clearly seen in PBipG. In the case of the copolymer PPy-b-PBipG, besides the signals of the PBipG segment, the PPy signals appear at 5.1-5.3 attributable to methylene protons and at 7.2-7.6 ppm corresponding to the pyrene aromatic protons. This confirmed the presence of both PPy and PBipG block in the resultant copolymer. The structure of the deprotected polymer could be determined by ^{1}H NMR in DMSO-d_6. Figure 3.6c reveals that the signals of the isopropylidene protons (1.2-1.4 ppm) completely disappear after the hydrolysis of PPy-b-PBipG and a broad signal corresponding to the anomeric hydroxyl groups of the sugar moieties (6.5-7.0 ppm) appears. This indicates the quantitative deprotection of the isopropylidene protecting groups. PPy block could not be clearly observed in the ^{1}H NMR spectrum of

PPy-b-PBG in DMSO-d$_6$ which indicate that the PPy block do not dissolve on a molecular level in DMSO-d$_6$.
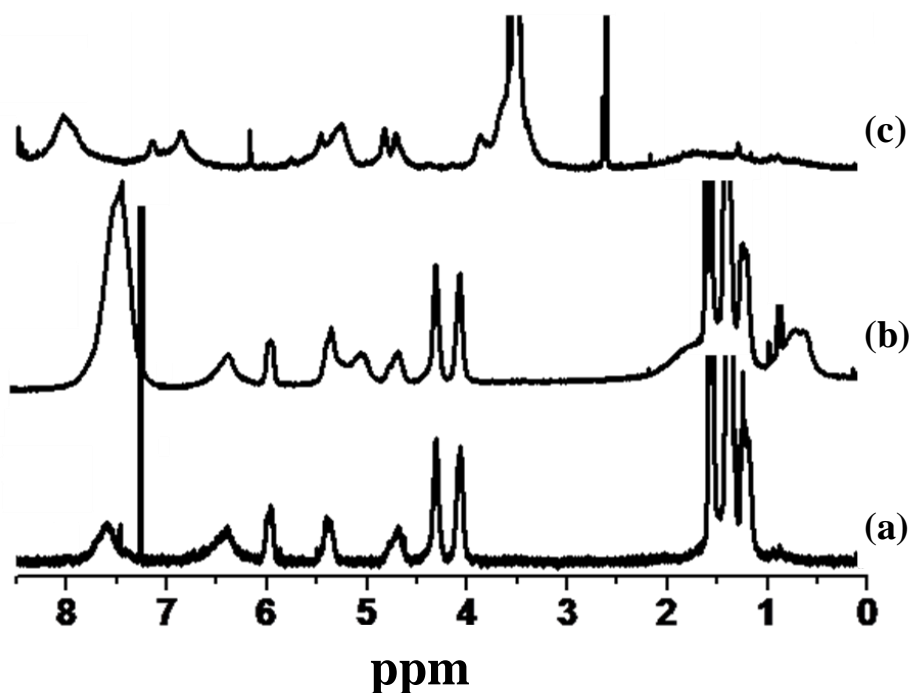
Figure 3.6. ^{1}H NMR spectra of (a) PBipG in CDCl$_3$ (b) PPy-b-PBipG in CDCl$_3$ and (c) **PPy-b-PBG** in DMSO-d$_6$ at room temperature.

3.3.2. Morphological Investigation of PPy-b-PSt-b-PEO Aggregates

In the amphiphilic triblock copolymer **PPy-b-PSt-b-PEO**, PEO forms the hydrophilic block, and the PSt and PPy form the hydrophobic block. In order to study the aggregation behavior the polymer a 0.5 mg/mL solution of the polymer in THF was prepared. Distilled water was added into this solution at a rate of 500 µL/h until the amount of water in the solvent mixture reached 15%. The initial clear solution gradually became turbid during water addition indicating the formation of colloidal particles. Dynamic light scattering (DLS) was employed to characterize the size, size distribution and aggregation number of the polymer aggregates. Figure 3.7 shows the DLS measurement of **PPy-b-PSt-b-PEO** in 15% water-THF mixture with an initial polymer concentration of 0.5 mg/mL. DLS data showed that the polymer aggregates have almost uniform shape with an average size of 1.54 µm with a polydispersity of 0.074.
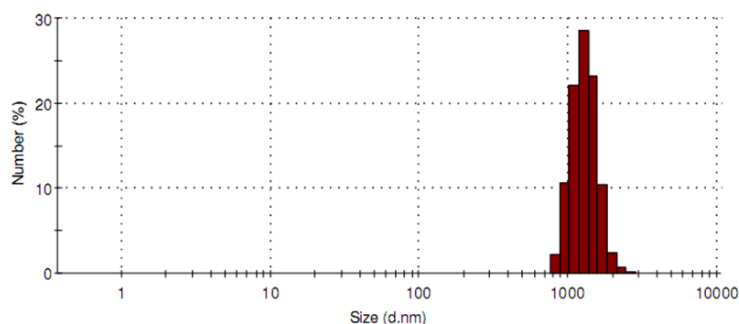
Figure 3.7. Size distributions of the aggregates of **PPy-b-PSt-b-PEO** (0.5 mg/mL) in 15% water-THF mixture.

The nature of the aggregates formed in 15% water-THF mixture was investigated using scanning electron microscopy (SEM), atomic force microscopy (AFM) and transmission electron microscope (TEM). The samples for microscopic studies were prepared from solutions with the same concentration as those employed for DLS. For microscopic studies a part of this solution was drop-cast on a glass slide and dried. SEM images of the sample deposited after aggregation showed the presence of uniform biconcave shaped or tip centered aggregates (Figure 3.8). AFM images of the colloidal solution also showed the presence of biconcave shaped aggregates (Figure 3.9). Such aggregates are probably formed as a result of the compression of large vesicles after solvent evaporation. Samples for TEM were prepared by drop-casting a drop of the colloidal on a formvar coated copper grid and the solvent was removed at room temperature. Figure 3.10 shows the TEM image of the **PPy-b-PSt-b-PEO** aggregates.
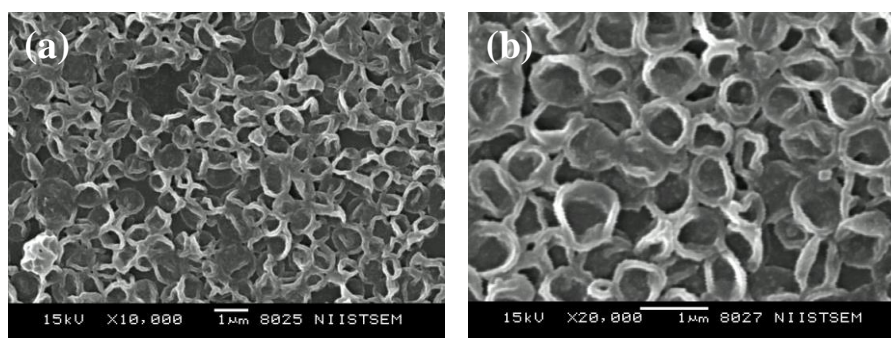
Figure 3.8. (a, b) SEM images showing air-dried aggregates formed by **PPy-b-PSt-b-PEO** in 15% water-THF mixture.
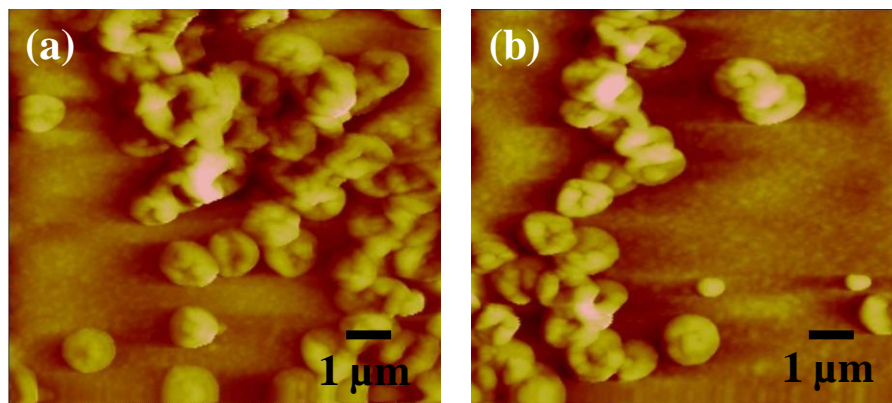
Figure 3.9. (a, b) AFM images showing air-dried aggregates formed by **PPy-b-PSt-b-PEO** in 15% water-THF mixture drop-cast and dried on mica sheet.
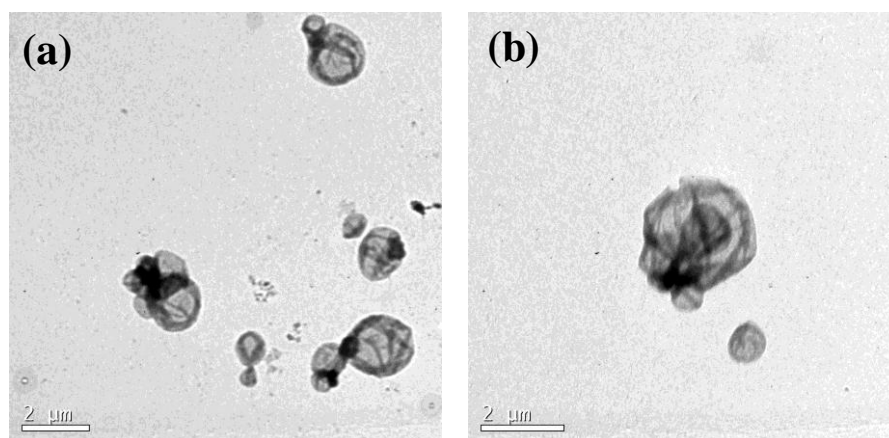
Figure 3.10. (a, b) TEM images of air-dried aggregates formed by **PPy-b-PSt-b-PEO** in 15% water-THF mixture.

In order to observe the effect of UV light on the morphology of the aggregates, a part of the solution used for DLS and microscopic studies was taken in a quartz cuvette and exposed to 340 nm UV light for 5 hours. The white turbid solution slowly became clear on continued UV irradiation which is a direct indication of aggregate dissociation. DLS analysis of the irradiated solution showed only the presence of some irregular particles with diameter of approximately 1 nm confirming complete dissociation of the polymer aggregates. This solution was then drop-cast on a clean glass plate and the morphology was investigated using SEM and AFM. SEM and AFM images obtained from solutions drop-cast after exposure to UV light for 5 hours indicated that the well defined biconcave shape aggregates were replaced by some ill-defined ones. Figure 3.11

shows the SEM (Figure 3.11a) and AFM images (Figure 3.11b) obtained from the UV irradiated solution. Aggregate dissociation occurs as a result of cleavage of 1-pyrenemethanol from the polymer main chain thereby converting **PPy-b-PSt-b-PEO** polymer to PMA-b-PSt-b-PEO. As a result both the end blocks of the polymer become hydrophilic there by increasing the hydrophilic nature of the triblock copolymer. This shift in hydrophilicity is sufficient to break the aggregates as revealed by SEM and AFM images.
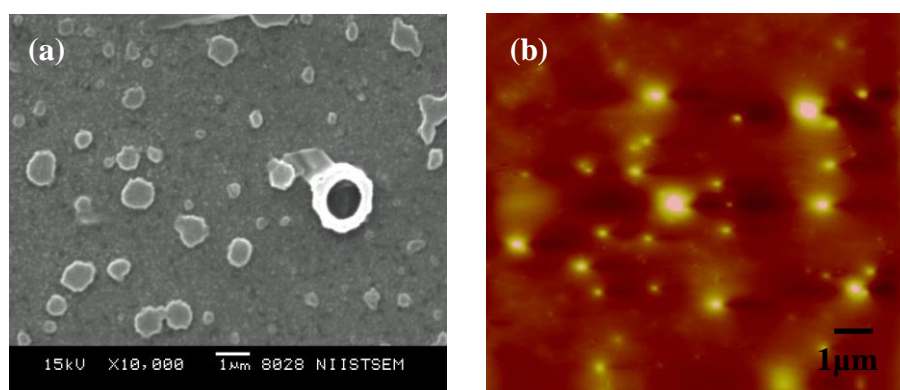
Figure 3.11. (a) SEM image obtained on air-drying a solution of **PPy-b-PSt-b-PEO** in 15% water-THF mixture after 5 h UV irradiation and (b) its corresponding AFM image.

The morphology of the aggregates formed by **PPy-b-PSt-b-PEO** in pure water was also investigated by SEM and AFM. In order to prepare aggregates of the polymer in pure water 0.5 mg of the polymer was dissolved in 1 mL THF. To this 1 mL water was added slowly with stirring. When water addition was complete 10 mL water was further added quickly to kinetically freeze the aggregates. THF was then allowed to evaporate slowly at room temperature. After complete evaporation of THF about 3 mL of the aqueous solution was taken in a cuvette and DLS studies was carried out. Figure 3.12 shows the DLS data obtained from the solution. DLS measurements showed that the particles have a narrow size distribution (PDI = 0.110) and their size was much smaller and well separated from each other than that observed in water-THF mixtures indicating good order during aggregation in water. The average size of the aggregates was about 86

nm. SEM and AFM investigations were carried out in order to observe the morphology of these polymer aggregates. Figure 3.13 shows the SEM and AFM images of the dried films cast from the same solution as that used for DLS study. AFM images of the dried films obtained from this solution showed the presence of well dispersed spherical aggregates with an average height of around 35 nm.
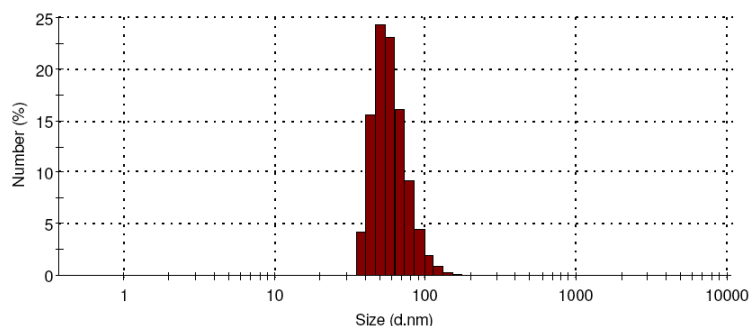
Figure 3.12. Size distribution of **PPy-b-PSt-b-PEO** aggregates formed in water.

A part of the aqueous solution used for DLS and microscopic investigations was then exposed to 340 nm UV light for 3 hours. DLS studies of this solution showed the presence of non-uniform particles with a broad size distribution and with an average size of 417 nm. These particles are probably formed as a result of the precipitation of 1-pyrenemethanol upon irradiation. Figure 3.14 shows the SEM and AFM images of the resultant film obtained after solvent evaporation. As seen from the Figure, after UV irradiation the number of spherical aggregates reduced dramatically indicating almost complete dissolution of the irradiated polymer.
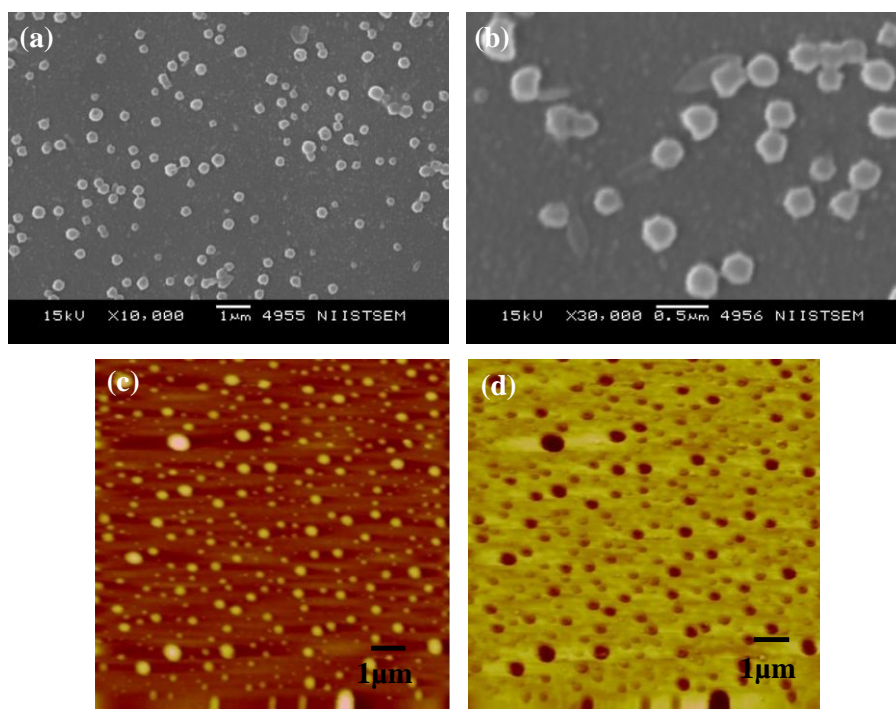
Figure 3.13. (a, b) SEM images showing air-dried aggregates formed by **PPy-b-PSt-b-PEO** in water (c) AFM height and (d) AFM phase image.
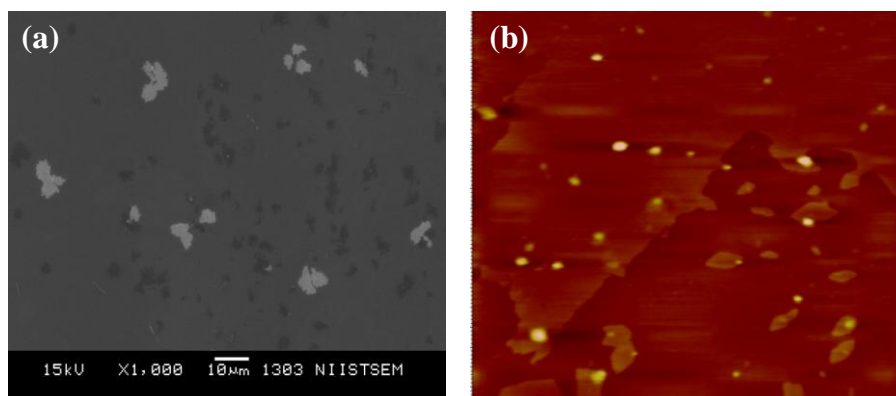
Figure 3.14. (a) SEM image obtained on air-drying a solution of **PPy-b-PSt-b-PEO** in water after 3 h UV irradiation and (b) its corresponding AFM image.

3.3.3. *Photophysical Studies of PPy-b-PSt-b-PEO Aggregates*

In order to get further insight about the aggregation behavior of **PPy-b-PSt-b-PEO**, photophysical studies were carried out on solution prepared in 15% water-THF mixture as well as in pure water. The polymer solutions used for the photophysical studies were prepared in the same manner as that used for the DLS and microscopic studies. Upon excitation at 340 nm, the colloidal solution in the water-THF

mixture showed a strong excimer emission peak at about 478 nm, with a weak monomer emission around 380-410 nm. The presence of strong excimer peak indicates that the pyrene moieties are in close proximity, supporting the formation of aggregates observed in the microscopic studies. This solution was then exposed to UV light (340 nm) and its emission spectra was recorded at different time intervals of irradiation. Figure 3.15a shows fluorescence emission spectra of the resultant solution obtained during UV irradiation. On UV irradiation, the monomer emission intensity increased at the expense of the excimer emission. These results clearly confirm the photo-solvolysis of pendant pyrene groups from the PPy block leading to formation of 1-pyrenemethanol and **PMA-b-PSt-b-PEO** in the solution. Since cleaved pyrenemethanol molecules are soluble in 15% water-THF mixture the monomer emission could be observed.

^{1}H NMR studies confirmed the detachment of 1-pyrenemethanol from the polymer back-bone. For this purpose 10 mg of the polymer was dissolved in 0.5 mL deuterated THF. To this 50 μL D_2O was added to induce aggregation. As shown in Figure 3.15b, UV irradiation caused the formation of a new peak at 5.33 ppm whose emergence can be assigned to the methylene protons of 1-pyrenemethanol. The intensity of this peak increased with increasing irradiation time.
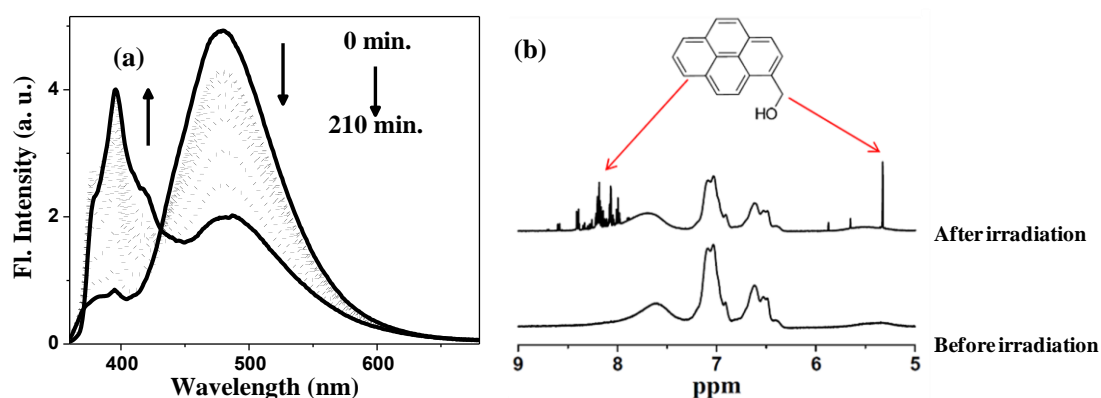
Figure 3.15. (a) Fluorescence emission spectra (λ_{ex} = 345 nm) of polymer aggregates in 15% water-THF before and after UV irradiation and (b) Changes in ^{1}H NMR spectra of a micellar solution of **PPy-b-PSt-b-PEO** on UV irradiation for 3 hours.

The same experiment was carried out for **PPy-b-PSt-b-PEO** aggregates formed in pure aqueous solution. The solution of the block copolymer in water exhibited excimer as well as monomer emission with the monomer emission being slightly more intense than the excimer emission. It is expected that this is due to the presence of hydrophobic styrene block. The more closely packed aggregation of styrene in water provides the pyrene units a strong hydrophobic domain wherein the pyrene units are more protected from each other, which could account for the much stronger monomer emission of **PPy-b-PSt-b-PEO** in water compared to that in water-THF mixture. Irradiation of the aqueous solution with UV light resulted in a dramatic decrease in the excimer and monomer emission since the detached pyrenemethanol is insoluble in water and gets precipitated (Figure 3.16).
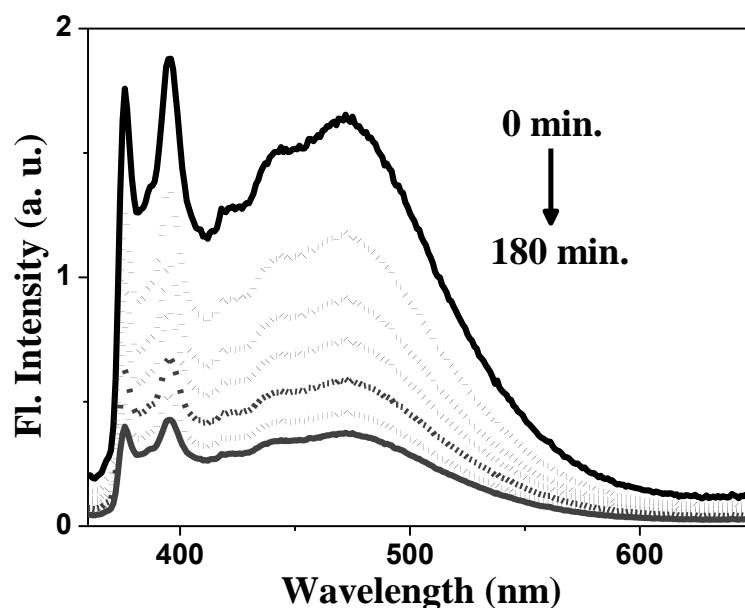
Figure 3.16. Fluorescence emission spectra ($\lambda_{ex} = 345$ nm) of polymer aggregates in water before and after UV irradiation.

The ability of **PPy-b-PSt-b-PEO** aggregates to trap organic molecules in water, can make them useful for encapsulating and in control release such molecules. This aspect was investigated using the organic dye Nile Red (Strukelj *et al.* 2000). Figure 3.17a shows UV-Vis spectra of **PPy-b-PSt-b-PEO** and Nile Red in THF. Nile Red is a

hydrophobic fluorescent dye which is practically insoluble in water, with negligible absorption in the range 340-400 nm and its maximum absorption is centered at around 530 nm. Since there is a clear overlap between the excimer emission band of pyrene and the absorption band of Nile Red there is a possibility of FRET between pyrene donor units and Nile Red acceptor moieties provided that the distance between the donor and the acceptor is within the Forster distance which is typically in the range of $15 - 60$ A^0 [Lakowicz 2006; Chen *et al.* 2008] In this experiment, Nile Red was first dissolved in a THF solution of **PPy-b-PSt-b-PEO** (polymer concentration, 1 mg mL^{-1}; 6 wt % of Nile Red with respect to the amount of polymer); water was then added drop wise to induce aggregation, following which 10-fold volume of water was added to quench the aggregates and THF was removed by evaporation at room temperature. Figure 3.17b shows changes in the emission spectra of Nile red encapsulated aqueous polymer solution during UV irradiation. Figure 3.18a shows the fluorescence emission spectra of the colloidal solution with encapsulated Nile Red before and after UV light exposure (excitation wavelength, 345 nm); for comparison, the emission spectrum of the colloidal solution without Nile Red, prepared under the same conditions, is also shown in the Figure. Without the added Nile Red, there is only the monomer and excimer emission of pyrene, while for the colloidal solution containing Nile Red, excitation at 345 nm where Nile Red has negligible absorption, resulted in strong fluorescence emission of Nile Red centered at 620 nm, with the excimer emission of pyrene being reduced drastically. Thus the emission spectra of the polymer aggregates before and after Nile Red encapsulation clearly suggests the occurrence of FRET between the two dyes, which indicates the close proximity between them as a result of the encapsulation of Nile Red in the core of the hydrophobic PPy block. The release of Nile Red and the cleavage of 1-pyrenemethanol were revealed by dramatic decrease in their fluorescence emission following UV irradiation. UV irradiation resulted in the cleavage of 1-pyrenemethanol from the

polymer main frame resulting in rupture of the aggregates simultaneously followed by the release of Nile Red into water. Since cleaved pyrene moieties and released Nile Red molecules are water insoluble they are precipitated in water. Hence emission from both these species decreases after UV irradiation. The excitation spectra of the Nile Red encapsulated polymer aggregates in Figure 3.18b provide additional evidence for the presence of Nile Red inside the polymer aggregates. From the excitation spectra it is clear that the emission of Nile Red at 620 nm is strongest when the colloidal solution is excited at the absorption maxima of pyrene which confirms that the distance between pyrene and Nile Red is less than 60 A^0. Thus the emission spectra and the excitation spectra prove beyond any doubt that Nile Red is trapped inside the polymer aggregates. The entire process is depicted schematically in Scheme 3.4.
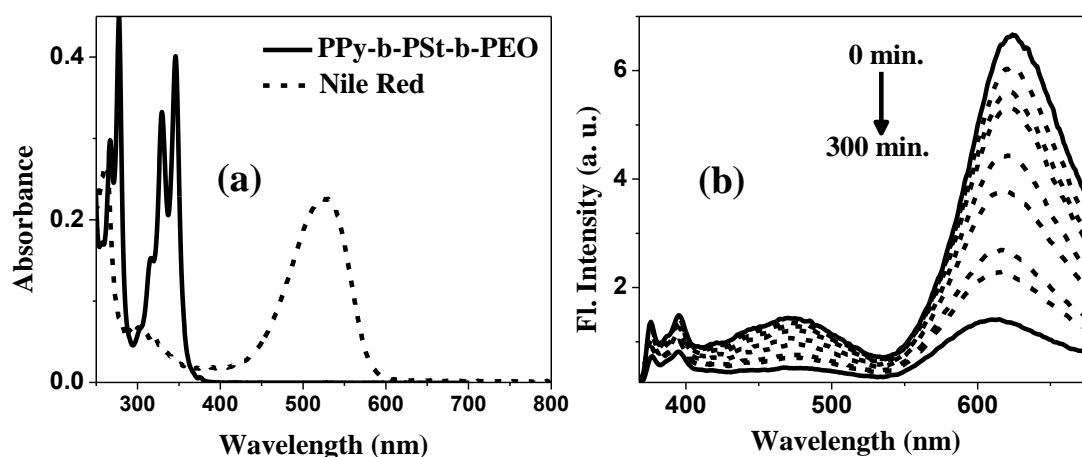
Figure 3.17. (a) UV-Vis spectra of **PPy-b-PSt-b-PEO** and Nile Red in THF and (b) Changes in the fluorescence emission spectra (λ_{ex} = 345 nm) of Nile Red loaded polymer micelles in water on UV irradiation.
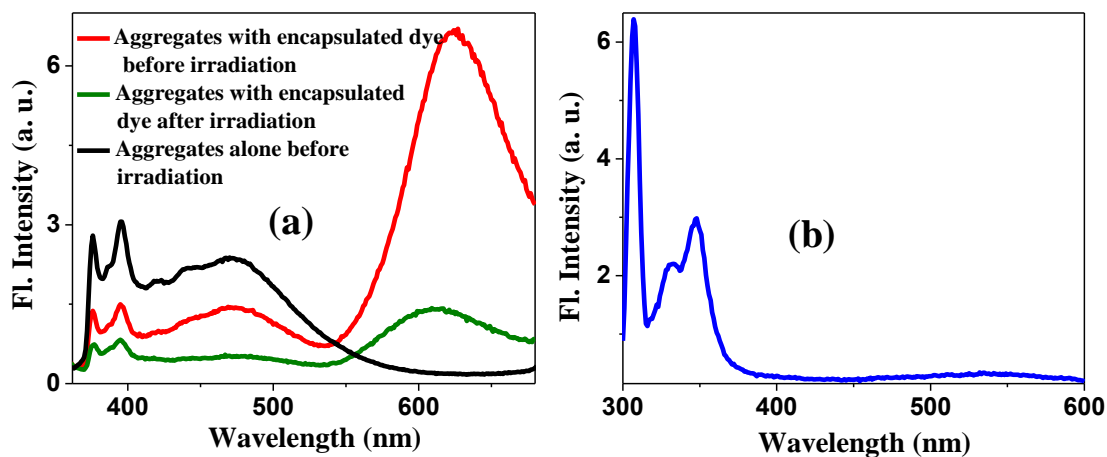
Figure 3.18. (a) Fluorescence emission spectra (λ_{ex} = 345 nm) of polymer micelles in water before and after UV irradiation compared to that of the non-irradiated micellar solution in the absence of Nile Red. (b) Fluorescence excitation spectra (excitation collected at 620 nm) of the polymer aggregates containing Nile Red.
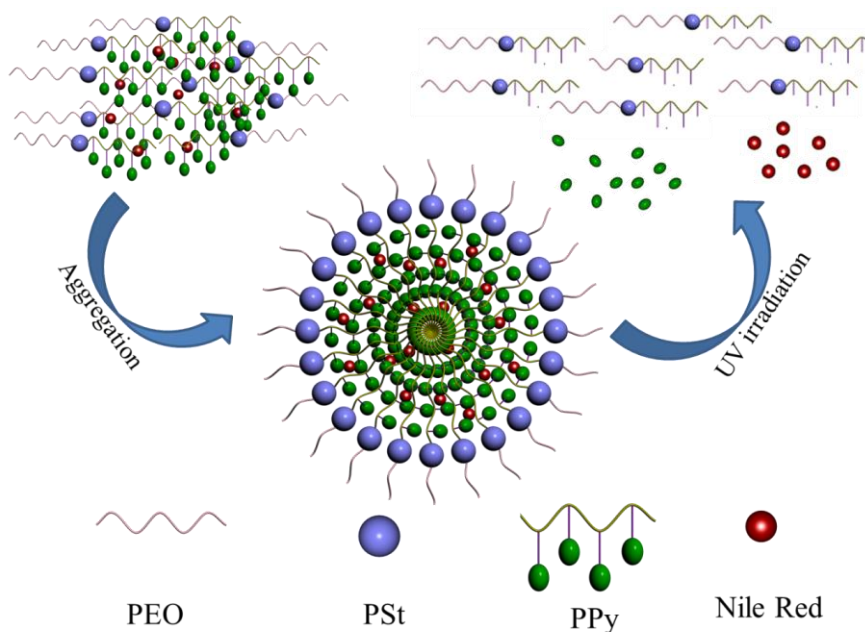
Scheme 3.4. Schematic representation of the encapsulation of Nile Red within the hydrophobic core of the polymer aggregates and its release upon disruption of the polymer aggregates by UV light.

3.3.4. Morphological Investigation of PPy-b-PBG Aggregates

To study the aggregation behavior of **PPy-b-PBG** block copolymer in water 1 mg of the dried block copolymer was dissolved in DMF. To this 1 mL deionized water was added into it at a rate of 500 µL/h with gentle stirring. When addition of water was complete 10 mL water was added quickly to quench the aggregates. The sample was then

put into dialysis bag (molecular weight cut: 3,500) and dialyzed against deionized water for 2 days to remove DMF. The solution was filtered through a 0.45 μm filter (Millipore Millex-HV) before use. DLS measurements of the resultant solution showed the presence of well-defined spherical particles with an average diameter of 473 nm with a PDI value of 0.094. Figure 3.19 shows the size distribution of **PPy-b-PBG** in water.
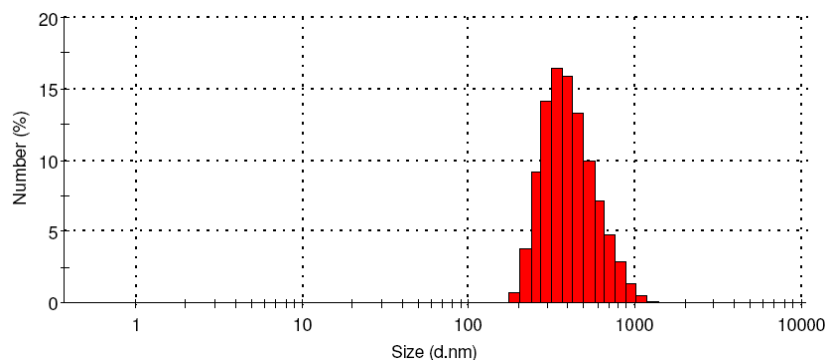
Figure 3.19. Size distribution of **PPy-b-PBG** aggregates in water.

Photoinduced formation and disruption of polymer aggregates was confirmed by AFM, SEM and TEM. For AFM measurements part of the micellar solution after dialysis was drop cast on a mica sheet and dried. Another part of the solution was exposed to UV light for 2 hours and then drop-cast and dried on a mica sheet. Figure 3.20 shows the AFM images obtained from the two solutions. Spherical aggregates with an average diameter of 500 nm were observed in the AFM images of the dried film obtained from the solution unexposed to UV light. In contrast no aggregates were observed in the dried film obtained from the solution which was exposed to UV light for 2 hours. SEM images indicated a vesicular nature for the spherical aggregates (Figure 3.21). In several cases, half-opened vesicular structure that probably resulted from wall collapse was observed which could be attributed to the high vacuum applied during SEM analysis. TEM images of the aggregates revealed that the aggregates are in fact vesicles as there was a clear contrast difference between the core and the periphery of the aggregates (Figure 3.22).
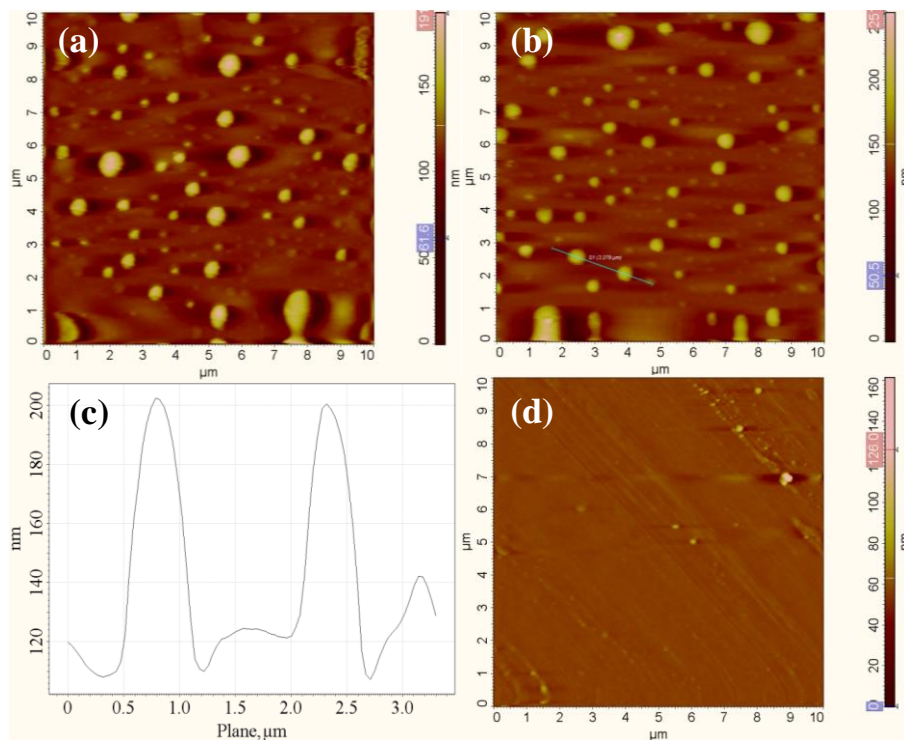
Figure 3.20. (a, b) AFM images showing air-dried aggregates of **PPy-b-PBG** obtained from aqueous suspension before UV irradiation (c) height profile of the aggregates (d) AFM image obtained after 2 h UV irradiation.
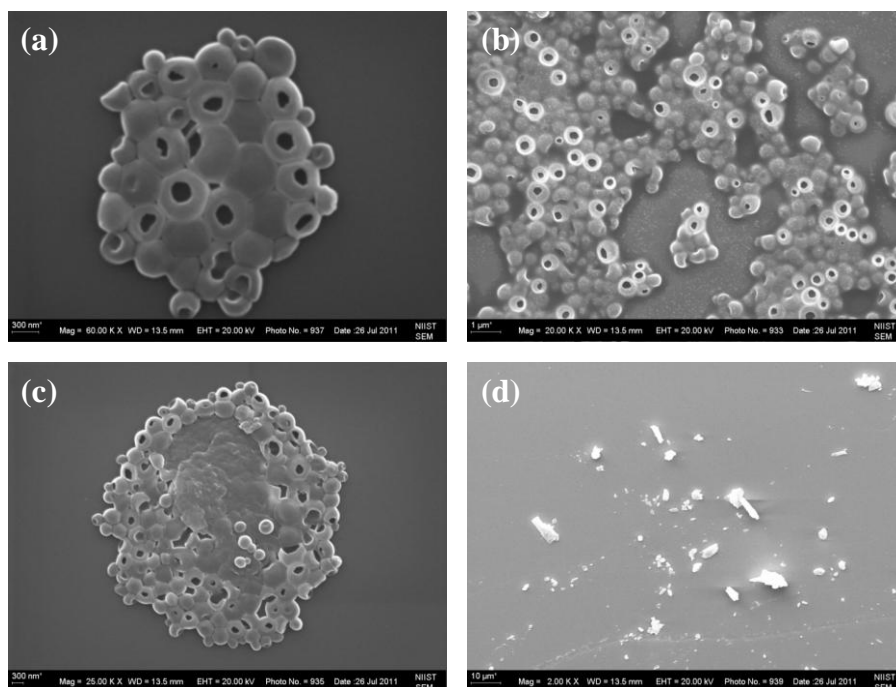
Figure 3.21. (a, b, c) SEM images showing air-dried aggregates of **PPy-b-PBG** aggregates obtained from aqueous suspension before UV irradiation (d) SEM image obtained after 2 h UV irradiation.
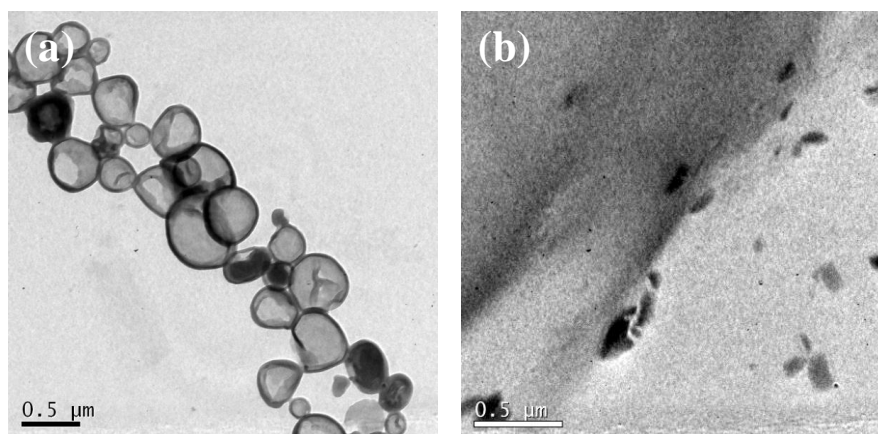
Figure 3.22. TEM images of air-dried aggregates of **PPy-b-PBG** obtained under various conditions (a) before exposure to UV light (b) after exposure to UV light for 2 hours.

3.3.5. *Photophysical Studies of PPy-b-PBG Aggregates*

Photochemical cleavage of pyrene entities from **PPy-b-PBG** was confirmed by fluorescence spectroscopy. Figure 3.23a shows the decrease in fluorescence of the colloidal solution of **PPy-b-PBG** in water following irradiation. Compared to **PPy-b-PSt-b-PEO** which showed monomer as well as excimer emission of almost equal intensities in water, aqueous solution of the diblock copolymer **PPy-b-PBG** showed a very strong excimer emission at about 486 nm with negligible monomer emission. This indicates that the pyrene units are more tightly held in the aggregated state of **PPy-b-PBG** than in the self-assembled state of the triblock copolymer. Foillowing UV irradiation however, there was a dramatic decrease in excimer emission with a slight increase in monomer emission around 380-410 nm. Since the byproduct of the photosolvolysis reaction ie. 1-pyrene methanol is sparingly soluble in water we observe only a slight increase in the pyrene monomer emission. These results clearly confirm the photosolvolysis reaction which results in the cleavage of pyrene moieties from the polymer main chain thereby disrupting the micellar structure.

The ability of **PPy-b-PBG** to encapsulate hydrophobic dyes and release them was also demonstrated using Nile Red. Figure 3.23b shows the extend of overlap between the

absorption spectra of Nile Red in THF and the emission spectra of **PPy-b-PBG** in water. Since **PPy-b-PBG** solution in water exhibits pure excimer emission it was felt that non-radiative energy transfer process between the **PPy-b-PBG** donor and Nile Red acceptor would be much more effective in the case of **PPy-b-PBG** than in the case of **PPy-b-PSt-b-PEO**.
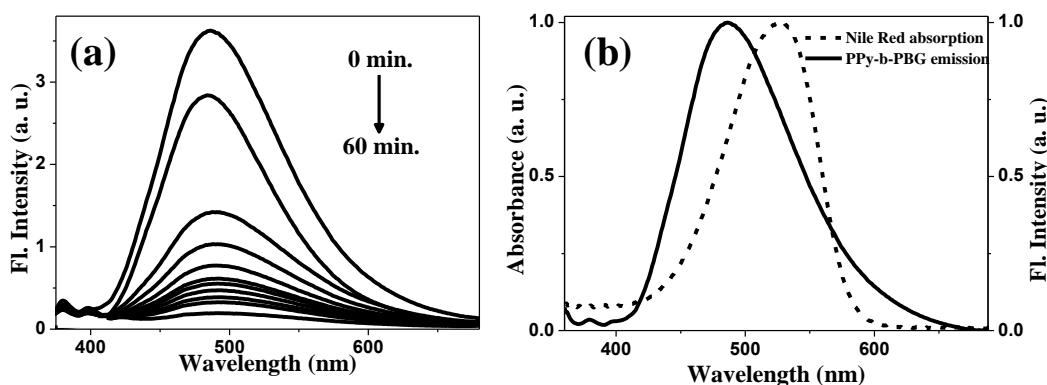
Figure. 3.23. (a) Change in fluorescence emission spectra of **PPy-b-PBG** in water, following UV irradiation and (b) Comparison of the absorption spectra of Nile Red in THF with the fluorescence spectra of **PPy-b-PBG** in water.

In order to encapsulate Nile Red inside **PPy-b-PBG** aggregates 1 mg of the copolymer and 0.1 mg of Nile Red were first dissolved in 1 mL DMF. The solution was gently stirred and 1 mL of deionised water was added into it at a rate of 500 µL/h. When addition of water was complete 10 mL water was added quickly to quench the aggregates. Then the sample was put into dialysis bag (molecular weight cut: 3,500) and dialyzed against deionised water for 2 days and filtered before use. When the Nile Red encapsulated solution was excited at 350 nm the solution showed a strong emission at 655 nm corresponding to that of Nile Red with drastic decrease in excimer emission of pyrene. Irradiation with UV light results in cleavage of 1-pyrenemethanol and simultaneous release of encapsulated Nile Red. Since both compounds are water insoluble dramatic decrease in the fluorescence emission occurs. Figure 3.24a indicates fall in the emission of Nile Red encapsulated colloidal solution of **PPy-b-PBG** during

UV irradiation. Figure 3.24b shows the fluorescence emission spectra of the colloidal solution with encapsulated Nile Red before and after UV light exposure (excitation wavelength, 345 nm); for comparison, the emission spectrum of the colloidal solution without Nile Red, prepared under the same conditions, is also shown in the Figure.
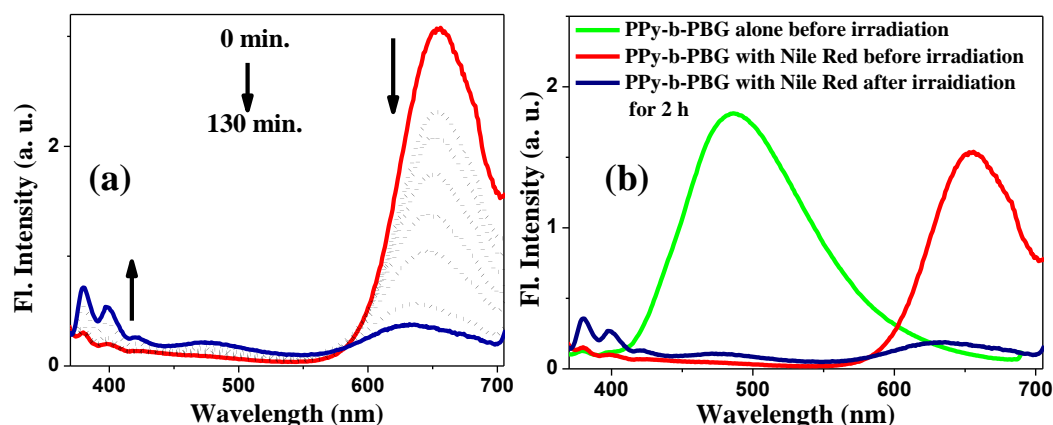
Figure 3.24. (a) Changes in the fluorescence emission spectra (λ_{ex} = 345 nm) of Nile Red loaded polymer aggregates in water upon UV irradiation and (b) Fluorescence emission of the Nile Red encapsulated aggregate solution compared with that of the non-encapsulated solution.

Emission of Nile Red from Nile Red loaded **PPy-b-PBG** aggregates could be also observed by directly exciting the dye at its absorption maxima. The absorption spectra of the dye encapsulated colloidal solution exhibited a peak at 561 nm which corresponds to the absorption of Nile Red trapped inside the polymer aggregates. Irradiation with UV light resulted in a fall in the absorption dye due to its release into water (Figure 3.25a). Similarly upon excitation at 561 nm, the dye encapsulated solution emitted at 647 nm which kept on decreasing upon continued UV irradiation with a concomitant release of dye into water (Figure 3.25b). The excitation spectra of the solution indicated that the Nile Red emission is maxima when the solution was excited at the absorption maxima of pyrene (Figure 3.26a). Figure 3.26b shows a photograph of an aqueous solution of **PPy-b-PBG** before and after Nile Red encapsulation.
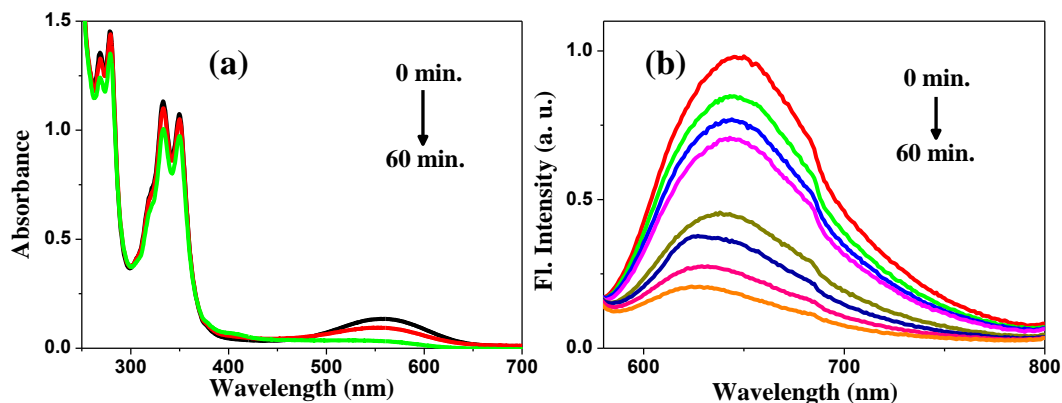
Figure 3.25. (a) Changes in the absorption spectra of Nile Red loaded polymer aggregates in water upon UV irradiation (b) Changes in the fluorescence emission spectra (λ_{ex} = 550 nm) of Nile Red upon UV irradiation of Nile Red loaded polymer aggregates in water.
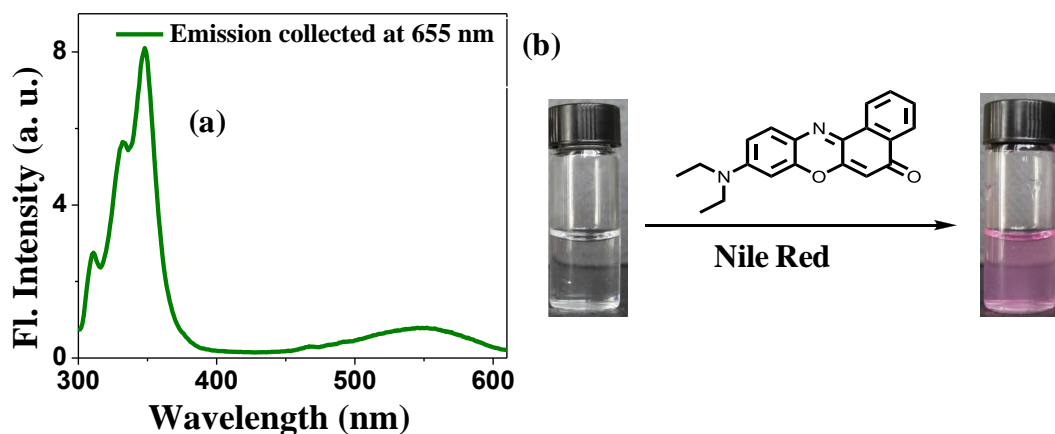
Figure 3.26. (a) Fluorescence excitation spectra (emission collected at 655 nm) of Nile Red loaded polymer aggregates in water (b) Photograph showing an aqueous solution of **PPy-b-PBG**; (left) without Nile Red and (right) in the presence of Nile Red.

3.4. Conclusions

In this chapter we report a synthetic method for the preparation of light-responsive amphiphilic block copolymers composed of a hydrophobic photolabile PPy block. The block copolymers were synthesized using the conventional ATRP method. These amphiphilic polymers aggregate in water as well as in water-THF mixtures. Emission spectra of the aqueous solution of the triblock copolymer **PPy-b-PSt-b-PEO** showed the presence of both monomeric and associated pyrene species. Presence of monomeric

pyrene emission clearly revealed the presence individual pyrene units even in water. This suggests that the pyrene units are trapped in a cage of PSt in which the pyrene molecules exist predominantly in their non-associated form. Thus the presence of PSt block not only increases the hydrophobicity of the overall polymer but also furnishes a suitable location in which the pyrene units reside. Consequently the short PSt block reduces to some extend the solvation effect on pyrene which accounts for its monomer emission in water and enhanced stability towards photosolvolysis. But only the excimer emission was observed in the case of the diblock copolymer **PPy-b-PBG**. The so formed polymer aggregates can respond to light by dissociation of 1-pyrenemethanol from the polymer backbone upon irradiation with UV light. As a result both the end blocks of the polymer now become hydrophilic thereby destroying the aggregates. It was also shown that these polymer aggregates can take-up hydrophobic dyes in water. Irradiation with UV light results in the destruction of the polymer aggregates which in turn results in controlled release of the encapsulated dye.

3.5. Synthesis and Experimental Section

3.5.1. Materials

2,2'bipyridine, N,N,N',N',N''-Pentamethyldiethylenetriamine (PMDETA), ethyl-2-bromoisobutyrate, poly(ethylene oxide)monomethyl ether, 1-pyrenemethanol, methacrylic acid, 2-bromo-2-methylpropionic acid, 1,2:5,6-Di-o-isopropylidene-α-D-glucofuranose dicyclohexylcarbodiimide (DCC), 4-(N,N-dimethylamino)pyridine (DMAP), 4-vinylbenzoic acid and Nile Red were purchased from Aldrich and used without further purification. CuBr (98%, Aldrich) was stirred in glacial acetic acid overnight, filtered, and then it was washed with ethanol and dried under vacuum overnight. Styrene purchased from Aldrich was washed with 5% NaOH solution and water successively for three times, dried over anhydrous Na_2SO_4, and then distilled under

reduced pressure at 40 ^{0}C. Solvents were purchased locally and purified using standard procedures before use.

3.5.2. Analysis and Measurements

^{1}H and ^{13}C NMR spectra were recorded on Bruker DPX 500 MHz Spectrometer using tetramethylsilane (TMS) as the internal standard and chloroform-d (CDCl$_{3}$) as solvent. The molecular weights of the polymers were determined by gel permeation chromatography (GPC) in tetrahydrofuran (THF) using polystyrene standards for the calibration. The GPC was calibrated with different polystyrene standards having molecular weights ranging from 2950 to 177,000 g/mol (Polymer Standards Service).Waters 515 pump connected through three series of Styragel HR columns (HR-3, HR-4E, and HR-5E) and Waters Model 2487 Dual wavelength UV-Vis Detector and a Waters 2414 Differential Refractometer were used for analyzing the samples. The flow rate of the THF was maintained as 1 mL/min throughout the experiments, and the sample solutions at very dilute concentration were filtered and injected for recording the GPC chromatograms at 30 ^{0}C. Mass spectral analyses were carried out using a JEOL JMS600 instrument in FAB ionization mode. Melting points are uncorrected and were determined on a Mel-Temp II melting point apparatus. Absorption spectra were recorded on a Shimadzu UV-3101PC UV-Vis-NIR spectrophotometer. The excitation and emission spectra were recorded on a SPEX Fluorolog F112X spectrofluorimeter. Steady-state photolysis was carried out using the output from a 200 W high-pressure mercury lamp filtered through a 350 nm Oriel band-pass filter. Dynamic light scattering (DLS) measurements were done by using a Nano ZS Malvern instrument employing a 4-mW He-Ne laser ($\lambda = 632.8$ nm) and equipped with a thermo stated sample chamber. Samples for scanning electron microscopy (SEM) were provided with a thin gold coating using JEOL JFC-1200 finecoater. SEM images were recorded using a JEOL JSM-5600 LV

instrument. Atomic force microscopy (AFM) images were recorded under ambient conditions using NTEGRA Prima - NT-MDT, Russia Scanning probe microscope operated in tapping mode. Micro-fabricated silicon cantilever tips (NSG 20) with a resonance frequency of 260-630 kHz and a force constant of 20-80 Nm^{-1} were used. The tip curvature radius was 10 nm. The scan rate was 1 Hz. To prepare samples for SEM and AFM measurements, a drop of the polymer colloidal solution was placed on a freshly cleaved mica sheet and the solution was allowed to evaporate at room temperature in air. Transmission electron microscopy (TEM) images were recorded using a JEOL JEM 1011 instrument with an accelerating voltage of 100 kV. Samples were prepared by drop-casting aqueous solutions of the polymers on a carbon coated copper grids under ambient conditions. The solvent was allowed to evaporate at room temperature. TEM images were obtained without staining.

3.5.3. Synthesis and Characterization Details

3.5.3.1. Synthesis of PEO-Br .

Poly(ethylene glycol)monomethyl ether (M_n = 5000 g/mol, 20 g, 4 mmol) was reacted with 2-bromo-2-methylpropionic acid   (750 mg, 4.4 m mol) in the

presence of 1,3-dicyclohexyl carbodiimide (1.1 g, 5.3 mmol) and a catalytic amount of dimethylaminopyridine (80 mg, 0.62 mmol) in dichloromethane (130 mL). Precipitated dicyclohexyl urea was filtered off and washed with dichloromethane. The macroinitiator was purified by dissolving it in THF, filtering the solution, concentrated and finally precipitated in diethyl ether to get **PEO-Br**.

Yield = 17.2 g (86%); ^{1}H NMR (500 MHz, CDCl$_3$, Me$_4$Si): δ (ppm) = 4.33 (2H, dd, -OCOC**H$_2$**-), 3.65 (4H, m, -OC**H$_2$CH$_2$**-), 3.38 (3H, s, -OC**H$_3$**) and 1.94 (6H, s, -OCOC(C**H$_3$**)$_2$Br); GPC (THF): M_n = 5,078, M_w/M_n = 1.12.

3.5.3.2. Synthesis of PSt-b-PEO.

CuBr (29 mg, 0.52 mmol) was added to a 25 mL RB flask containing styrene (2.0 g, 19 mmol), **PEO-Br** (1.0 g, 0.20 mmol) and 2,2'bipyridine (63 mg, 0.40 mmol). The flask was sealed with rubber septum and was purged with argon for 20 minutes before adding the catalyst. The flask was placed in a preheated oil bath at 80 ^{0}C for 12 hours. The viscous liquid was dissolved in THF and was passed through a neutral alumina column to remove the catalyst and was then concentrated and precipitated in methanol twice to get **PSt-b-PEO**.
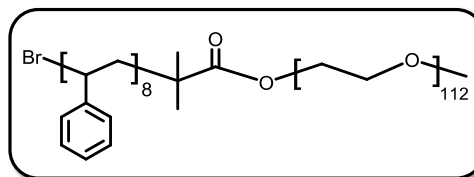
Yield = 300 g (10%); ^{1}H-NMR (500 MHz, CDCl$_3$, Me$_4$Si): δ (ppm) = 7.07 (m, 3H, styrene aromatic), 6.57 (m, 2H, styrene aromatic), 3.65 (m, 4H, -OC**H$_2$CH$_2$**-), 3.38 (s, 3H, -OC**H$_3$**), 1.42-1.84 (m, 3H, -C**H$_2$CH**-),0.86-0.98 (m, 9H, -C(C**H$_3$**)$_2$-, C**H$_3$**CH$_2$O-); GPC (THF): M$_n$ = 5,853, M$_w$/M$_n$ = 1.31.

3.5.3.3. Synthesis of PyM.

To a mixture of 1-pyrenemethanol (5.0 g, 21.5 mmol), methacrylic acid (2.15 g, 25.0 mmol) and 1,3-dicyclohexylcarbodiimide (5.16 g, 25.0 mmol) in dichloromethane (100 mL) was added dimethylaminopyridine (305 mg, 2.50 mmol), and stirred at room temperature for 24 hours. After the reaction the solid was filtered off, washed several times with dichloromethane and the filtrate was concentrated and finally purified by column chromatography (Silica gel, 3% EtOAc-hexane as eluent).

Yield = 5.6 g (86.6%); m.p. = 99 ^{0}C ; FAB MS : *m/z* = 301.40 [M+H]$^+$; ^{1}H-NMR (500 MHz, CDCl$_3$, Me$_4$Si): δ (ppm) = 7.98-8.31 (m, 9H, pyrene aromatic), 6.15 (s, 1H, C**H$_2$**=C), 5.89 (s, 2H, -C**H$_2$O**-), 5.55 (s, 1H, C**H$_2$**=C), 1.96 (s, 3H, -C**H$_3$**); ^{13}C-NMR (125

MHz, CDCl$_3$, Me$_4$Si): δ (ppm) = 167.65, 143.99, 136.60, 135.42, 134.58, 132.63, 132.03, 130.07, 128.61, 128.15, 127.99, 127.12, 126.87, 126.35, 126.04, 124.76, 124.10, 121.09, 120.56, 66.75, 17.20.

3.5.3.4. Synthesis of PyM-b-PSt-b- PEO.

CuBr (4 mg, 0.3 mmol) was added to a 10 mL round bottom flask containing PyM (300 mg, 0.10 mmol), PSt-b-PEO (285 mg, 0.02 mmol) and PMDETA (4.15 mg, 0.02 mmol) in 2 mL THF. The flask was sealed with rubber septum and was purged with argon for 20 minutes before adding the catalyst. The flask was placed in a preheated oil bath at 60 ^{0}C for 18 hours. The viscous liquid was dissolved in THF and was passed through a neutral alumina column to remove the catalyst and was then concentrated and precipitated in methanol four times.
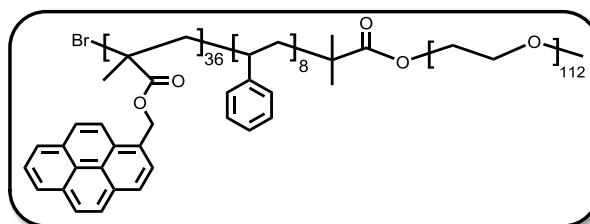
Yield = 450 mg (76.92%); ^{1}H-NMR (500 MHz, CDCl$_3$, Me$_4$Si): δ (ppm) = 7.45 (m, 9H, pyrene aromatic), 7.07 (m, 3H, styrene aromatic), 6.57 (m, 2H, styrene aromatic), 5.26 (m, 2H, -OCOC**H$_2$**-), 3.65 (m, 4H, -OC**H$_2$**C**H$_2$**-), 3.38 (s, 3H, -OC**H$_3$**), 1.42-1.84 (m, 3H, -C**H$_2$**C**H**-), 0.86-0.98 (m, 9H, -C(C**H$_3$**)$_2$-, C**H$_3$**CH$_2$O-); GPC (THF): M$_n$ = 16,679, M$_w$/M$_n$ = 1.48.

3.5.3.5. Synthesis of 3-O-4-vinylbenzoyl-1,2:5,6-di-O-isopropyliden-D-glucofuranose (BipG).

To a mixture of 4-vinylbenzoic acid (2.85 g, 19.3 mmol), 1,2:5,6-di-O-isopropyliden-D-glucofuranose (5.00 g, 19.2 mmol) and 1,3-dicyclohexylcarbodiimide (4.20 g, 20.4 mmol) in dichloromethane (100 mL) was added dimethylaminopyridine (250 mg, 2.05 mmol), and stirred at
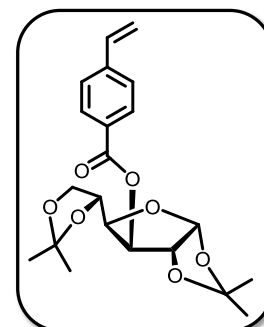
room temperature for 24 hours. After the reaction the solid was filtered off, washed several times with dichloromethane and the filtrate was concentrated and finally purified by column chromatography (Silica gel, 10% EtOAc-hexane as eluent).

Yield = 6.2 g (81.9%); FAB MS : m/z = 413.38 [M+Na]$^+$; ^{1}H-NMR (500 MHz, CDCl$_3$, Me$_4$Si): δ (ppm) = 7.99 (d, 2H, aromatic), 7.47 (d, 2H, aromatic), 6.75 (m, 1H, -**CH**=CH$_2$), 6.00 (dd, 1H, -CH=C**H$_2$**), 5.89 (dd, 1H, -O-C**H**(O)-CH-), 5.52 (dd, 1H, -CH=C**H$_2$**), 4.71 (m, 1H, -CH(COOAr)-C**H**(O)-CH-), 4.34 (m, 2H, -CH-C**H**(COOAr)-CH-, -CH-C**H**O-CH(COOAr)-), 4.10 (m, 1H, -CH$_2$(O)-C**H**(O)-CH-), 3.77 (m, 2H, -O-C**H$_2$**-CH(O)-), 1.32-1.42 (m, 12H, -O-C(C**H$_3$**)$_2$-O-) ; ^{13}C-NMR (125 MHz, CDCl$_3$, Me$_4$Si): δ (ppm) = 165, 142.50, 135.8, 130.29, 130.04, 126.26, 117, 112.50, 109.40, 105.50, 83.13, 76.81, 72.59, 68.27, 64.23, 26.82, 25.20.

3.5.3.6. Synthesis of poly(3-O-4-vinylbenzoyl-1,2:5,6-di-O-isopropyliden-D-glucofuranose) (PBipG).

CuBr (10.0 mg, 0.07 mmol) was added to a 10 mL round bottom flask containing BipG (1.0 g, 2.7 mmol), ethyl-2-bromoisobutyrate (11 mg, 0.06 mmol) and PMDETA (9.1 mg, 0.05 mmol) in THF (3.0 mL). The flask was sealed with rubber septum and was purged with argon for 20 minutes before adding the catalyst. The flask was placed in a preheated oil bath at 60 ^{0}C for 24 hours. The viscous liquid was dissolved in THF and was passed through a neutral alumina column to remove the catalyst and was then concentrated and precipitated in methanol twice.

Yield = 675 mg (67.5%); ^{1}H-NMR (500 MHz, CDCl$_3$, Me$_4$Si): δ (ppm) = 7.59 (m, 2H, aromatic), 6.40 (m, 2H, aromatic), 5.97 (m , 1H), 5.37 (m, 1H), 4.69 (m, 1H,), 4.31 (m, 2H), 4.06 (m, 2H), 1.55-1.60 (m, 3H, -C**H$_2$CH**-), 1.25-1.38 (m, 12H, -O-C(C**H$_3$**)$_2$-O-); GPC (THF): M$_n$ = 12,297, M$_w$/M$_n$ = 1.19.

3.5.3.7. Synthesis of poly(pyrenylmethyl methacrylate)-b-poly(3-O-4-vinylbenzoyl-1,2:5,6-di-O-isopropyliden-D-glucofuranose) (PPy-b-PBipG).

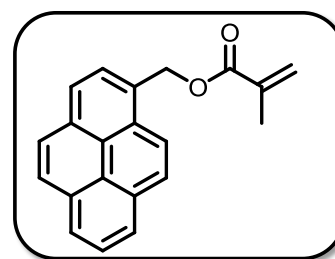CuBr (11 mg, 0.08 mmol) was added to a 10 mL round bottom flask containing PPy (500 mg, 1.67 mmol), PBipG (500 mg, 0.04 mmol) and PMDETA (12.50 mg, 0.07 mmol) in THF (3.0 mL). The flask was sealed with rubber septum and was purged with argon for 20 minutes before adding the catalyst. The flask was placed in a preheated oil bath at 60 ^{0}C for 24 hours. The viscous liquid was dissolved in THF and was passed through a neutral alumina column to remove the catalyst and was then concentrated and precipitated in methanol thrice.
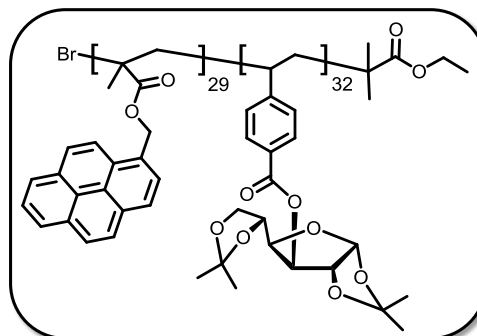
Yield = 550 mg (55%); ^{1}H-NMR (500 MHz, CDCl$_3$, Me$_4$Si): δ (ppm) = 7.49 (m, 11H, aromatic), 6.40 (m, 2H, aromatic), 5.97 (m , 1H), 5.37 (m, 1H), 5.27 (m, 2H, -OCOCH$_2$-Py), 4.69 (m, 1H), 4.31 (m, 2H), 4.06 (m, 2H), 1.55-1.60 (m, 3H, -CH$_2$CH-), 1.25-1.38 (m, 12H, -O-C(CH$_3$)$_2$-O-), 0.69-0.88 (m, 5H, -(CH$_3$)C(COOCH$_2$Py)CH$_2$-); GPC (THF): M$_n$ = 21,194, M$_w$/M$_n$ = 1.46.

3.5.3.8. Synthesis of poly(pyrenylmethyl methacrylate)-b-poly(3-O-4-vinylbenzoyl-D-glucopyranose) (PPy-b-PBG).

120 mg of the protected polymer PPy-b-PBipG was dissolved in 80% formic acid (12 mL) and stirred for 48 hours at room temperature. Additional 6 mL water was added and stirred for another 3 hours. The solution was dialyzed against distilled water for 2 days, concentrated in-vacuum and finally lyophilized to give **PPy-b-PBG** in quantitative yield.
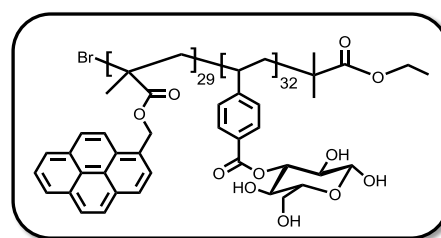
Photoinduced Reversible Formation of Supramolecular Glycopolymer Aggregates

4.1. Abstract

*Two different photoresponsive AB block copolymers of 3-O-4-vinylbenzoyl-1,2:5,6-di-O-isopropyliden-D-glucofuranose (BipG) with spiropyran (SP) or azobenzene (MAzo) have been synthesized by atom transfer radical polymerization (ATRP) using well-defined bromo-terminated Poly(3-O-4-vinylbenzoyl-1,2:5,6-di-O-isopropyliden-D-glucofuranose) (PBipG) as a macroinitiator. Deprotection of the isopropylidene protecting groups of the precursor copolymers afforded amphiphilic block copolymers, **PSP-b-PBG** and **PMAzo-b-PBG**, with well-defined glycopolymer segments and narrow molecular weight distributions (PDI < 1.5). The examination of the aqueous solution of these amphiphilic block copolymers revealed the formation of ordered aggregates. Under alternate UV or visible light illumination, reversible changes in the aggregate morphology, for both vesicles and core-shell micelles, took place as a result of the reversible SP to merocyanine (MC) photoisomerization of spiropyran units in **PSP-b-PBG** or the trans-cis photoisomerization of azobenzene mesogens in **PMAzo-b-PBG**. Hydrophobic fluorescent molecules could be trapped in the hydrophobic portion of the polymer aggregates and the ability to release and re-encapsulate these dyes during irradiation was investigated using fluorescence spectroscopy.*

4.2. Introduction

The traditional view of carbohydrate polymers as nature´s energy source (starch and glycogen) and structural materials has expanded. Glycopolymers, synthetic sugar-containing polymers, are increasingly attracting chemists due to their role as biomimetic analogues and their potential for commercial applications [Namazi *et al.* 2005; Okada 2001]. Different polymerization techniques have enabled the synthesis of glycopolymers featuring a wide range of controlled architectures and functionalities. Methodologies for the synthesis of glycopolymers can be roughly classified into two main categories: (1) polymerization of sugar-bearing monomers and (2) chemical modifications of preformed polymers with sugar-containing reagents. In general, the latter method frequently results in glycopolymers having less regular structures because of incomplete reactions due to steric hindrance. Therefore, it is often better to use polymerizations of sugar-carrying monomers for synthesizing linear glycopolymers of well-defined architectures [Okada 2001].

Synthetic carbohydrate polymers with biocompatible and biodegradable properties are used in tissue engineering and controlled drug release devices. Many of them are used also as surfactants [Klein *et al.* 1990] and biologically active polymers [Muthukrishnan *et al.* 2005]. These glycopolymers are widely investigated for pharmaceutical and medical applications in the treatment of infectious diseases [Petronio *et al.* 1997]. Glycopolymers generally include natural as well as synthetic carbohydrate-bearing polymers, while synthetic polymers containing sugar moieties as pendant groups can be referred in a narrower sense as glycopolymers [Ladmiral *et al.* 2004]. There are various types of synthetic sugar-carrying polymers. Linear polymers, comb-shaped polymers, dendrimers, and cross-linked hydrogels represent the four major classes [Wang *et al.* 2002]. Because of their biocompatibility and hydrophilicity, sugar-based hydrogels are used in biomedical engineering as super-absorbents, contact lenses, and matrices for drug delivery systems [Dordick *et al.* 1994; Chen *et al.* 1995].

Schlaad *et al.* reported an easy and efficient route to amphiphilic glycopolymers, which involves grafting of a 1-thioglucose derivative onto the double bonds of a 1,2-polybutadiene-*block*-polystyrene through photoaddition at room temperature [You et al. 2006]. A so prepared amphiphilic glycopolymer (17 wt % glucose) could be dispersed in organic and in aqueous media, leading to the formation of sugar-containing polymer vesicles or "glycosomes" (Figure 4.1).
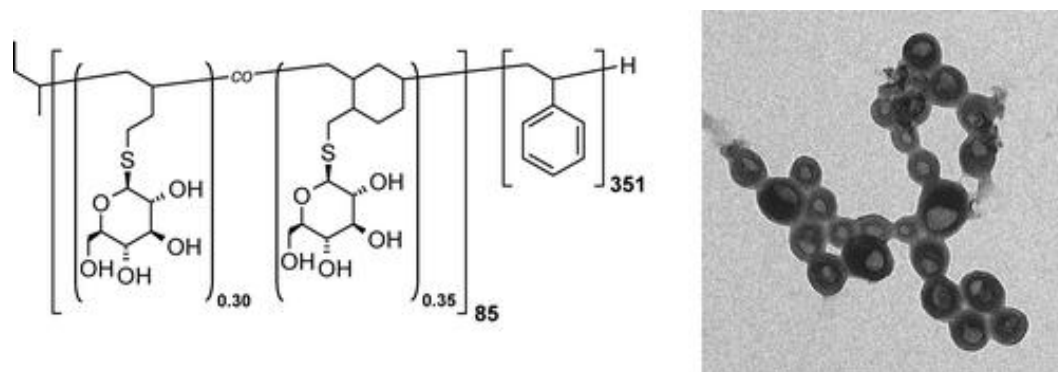
Figure 4.1. TEM image of the collapsed vesicles, prepared from 0.03 wt % solution of the glycopolymer in water. [Adapted from You *et al.* 2006].

Li, Liang and coworkers jointly reported the synthesis of polystyrene-block-poly[2-(β-D-glucosyloxy)ethyl acrylate] (PSt-b-PGEA) by ATRP using bromo-terminated PSt as the macroinitiator [Li *et al.* 2000; Li *et al.* 2002; Liang *et al.* 2000]. In aqueous media PSt-b-PGEA formed a variety of molecular assemblies when dissolved in water-soluble organic solvents, such as DMF and THF. The morphologies of these molecular assemblies were sensitive to the copolymer composition, nature of solvent and the initial copolymer concentration. PSt-b-PGEA yielded predominantly spheres in water when initially dissolved in DMF at a concentration of 0.1-0.2 wt %. A transformation of the morphology to bilayer structures upon addition of different amount of additives such as glucose, HCl, Concanavalin A, and $CaCl_2$ was observed. The morphological transitions were ascribed to the decrease of the repulsive interactions among corona-forming blocks. Figure 4.2 shows the PS-b-PGEA crew-cut aggregates prepared from DMF and THF.
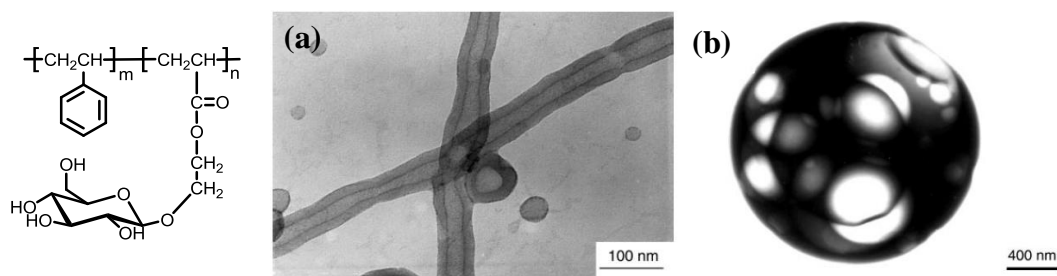
Figure 4.2. (a)Tubular morphology of PSt_{77}-b-$PGEA_6$ crew-cut aggregates made from DMF and (b) porous sphere of PSt_{88}-b-$PGEA_4$ crew-cut aggregates made from THF. [Adapted from Liang *et al.* 2000].

Pasparakis *et al.* utilised thermoresponsive glycopolymers (P1 and P2) with poly(N-isopropylacrylamide) as the central component for controlled and reversible aggregation of a specific bacterial strain as the first step toward robust and reusable cell-sensing materials [Pasparakis *et al.* 2007]. Furthermore, it was also shown that polymer activity in bacterial agglutination is achievable with rather simple sugar functionality, employing multiple glucose residues able to control cell aggregation through a combination of the cluster glycoside effect and polymer conformation. To probe the mechanism underlying the changed accessibility of the sugars below and above LCST the authors employed a three-component system comprising alizarin red S dye (AR), phenylboronic acid (PBA), and P1 or P2. AR is inherently non-fluorescent but fluoresces strongly when bound to PBA in alkaline conditions. The covalent, but reversible binding of PBA with the catechol diol groups induces emission at 578 nm. The introduction of glucose, which has high affinity to PBA, in the polymer results in competition for diol-binding sites on PBA between AR and polymer-bound glucose. Binding of glucose to PBA was thus monitored by variations in the AR-PBA complex fluorescence intensity as the concentration of glucose from the glycopolymer changed. The polymer-bound glucose reacted with PBA when the polymer was in a soluble phase (T < LCST) as shown by reduction in AR-PBA complex fluorescence intensity. By contrast, an increased fluorescence intensity of the AR-PBA complex was observed at T > LCST,

when the polymer was in a globular state and the glucose residues were not available for competitive binding with AR for PBA. The effect was apparent to the naked eye, with the color change of a vial containing all three components (AR, PBA, and P1 or P2) from burgundy to orange at low and high temperatures, respectively (Figure 4.3).
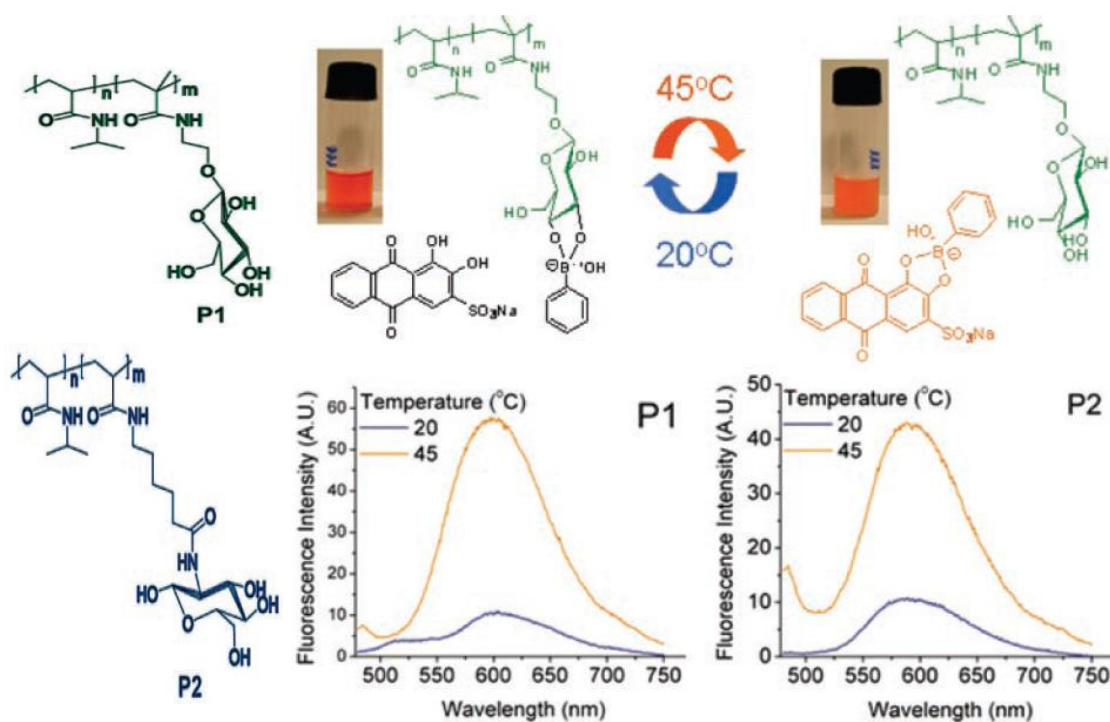
Figure 4.3. (Top) Visual inspection of diol binding and release at temperatures below (left) and above LCST (right) for polymer P1. (Bottom) Corresponding fluorescence spectra using AR and PBA in glycine buffer (0.1 M, pH 9.3). [Adapted from Pasparakis *et al.* 2007].

This Chapter reports the synthesis, aggregation and photophysical studies of two light-responsive amphiphilic glycopolymers, **PSP-b-PBG** and **PMAzo-b-PBG**. The structure of the glycopolymers is shown in Scheme 1. In this study, an isopropylidene-protected sugar-carrying acrylate, BipG, was selected as a comonomer for the synthesis of photo-responsive water-soluble highly branched glycopolymers. In this study we have made use of CuBr/ pentamethyldiethylenetriamine (PMDETA) catalyst system to obtain well-defined and monodisperse photoresponsive glycopolymers. Dissolution of the polymers in water compatible solvents followed by the addition of excess water and

subsequent removal of the organic solvents resulted in the formation of ordered aggregates. Exposing these self-assembled structures to UV radiation resulted in the photoisomerization of the light-responsive block, leading to an increase in overall hydrophilicity of the polymer, thereby rupturing the aggregates. Irradiation with visible light brings about reverse isomerization which restores the hydrophobic-hydrophilic balance of these block copolymers thereby regenerating the aggregates. Various hydrophobic fluorescent dyes could be encapsulated in the hydrophobic domain of these polymer aggregates and their UV induced release was investigated. Reverse isomerisation was also observed to bring about partial re-encapsulation of the released dyes.

PSP-b-PBG   **PMAzo-b-PBG**
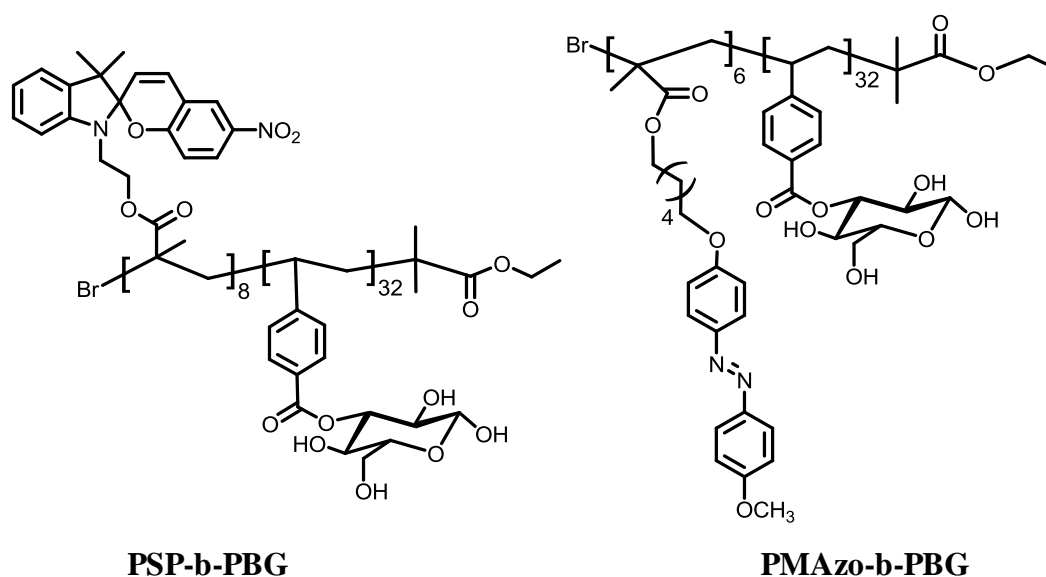
Chart 4.1.

4.3. Results and Discussion

4.3.1. Synthesis and Characterization

The synthesis of the diblock copolymer **PSP-b-PBG** is outlined in Scheme 4.1 and Scheme 4.2. Details regarding the synthetic procedure and characterization are provided in Section 4.5.3. BipG was polymerized under ATRP conditions using

CuBr/PMDETA with ethyl 2-bromoisobutyrate at 60 ^{0}C in THF for 24 hours. The number-average molecular weight of PBipG as determined by conventional GPC was 12,499 which correspond to 32 BipG units and the polydispersity index (PDI) was 1.23. Copolymerization of SPM was conducted using CuBr/PMDETA with PBipG as the macroinitiator at 60 ^{0}C in THF for 24 hours. The resultant polymer PSP-b-PBipG had a number-average molecular weight of 15,791 and a PDI value of 1.45. Figure 4.4 shows the GPC trace of PSP-b-PBipG together with that of the homopolymer PBipG. It can be seen that the molecular weight of PSP-b-PBipG shifts towards the high molecular weight region without any trace of the low molecular weight macroinitiator. This shows that PBipG is an efficient macroinitiator for the polymerization of SPM while maintaining low polydispersity. The polydispersity however increases slightly during the second polymerization stage. The diblock copolymer PSP-b-PBipG was purified by reprecipitating it three times from THF into methanol. The resulting polymer PSP-b-PBipG was composed of 8 units of SP and 32 units of BipG.
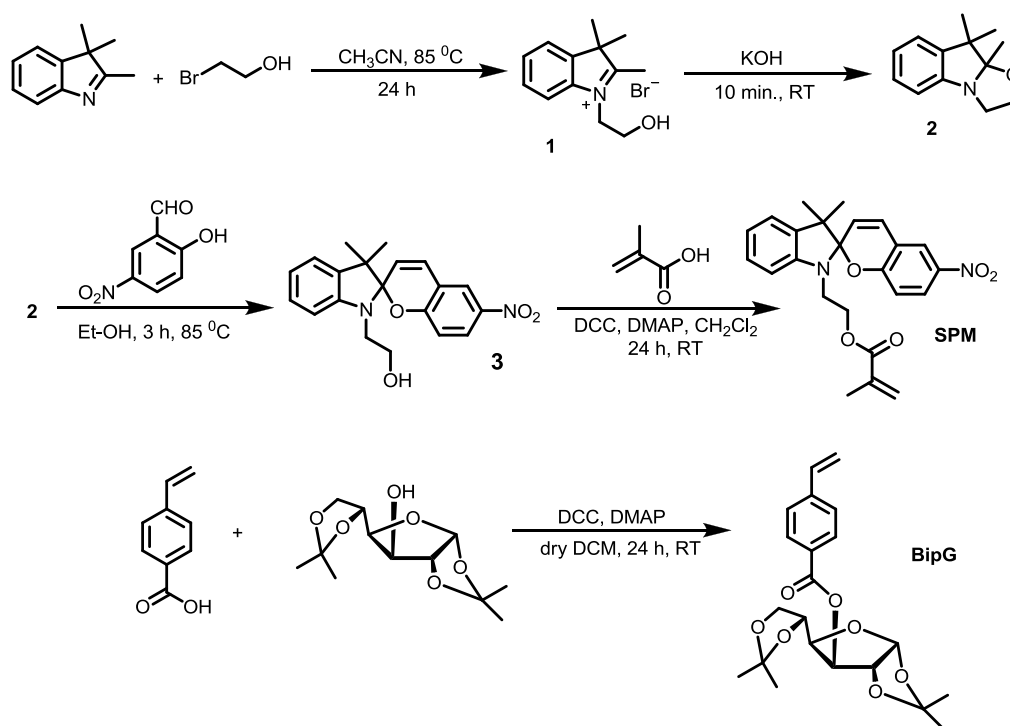
Scheme 4.1. Synthesis of the monomers SPM and BipG.
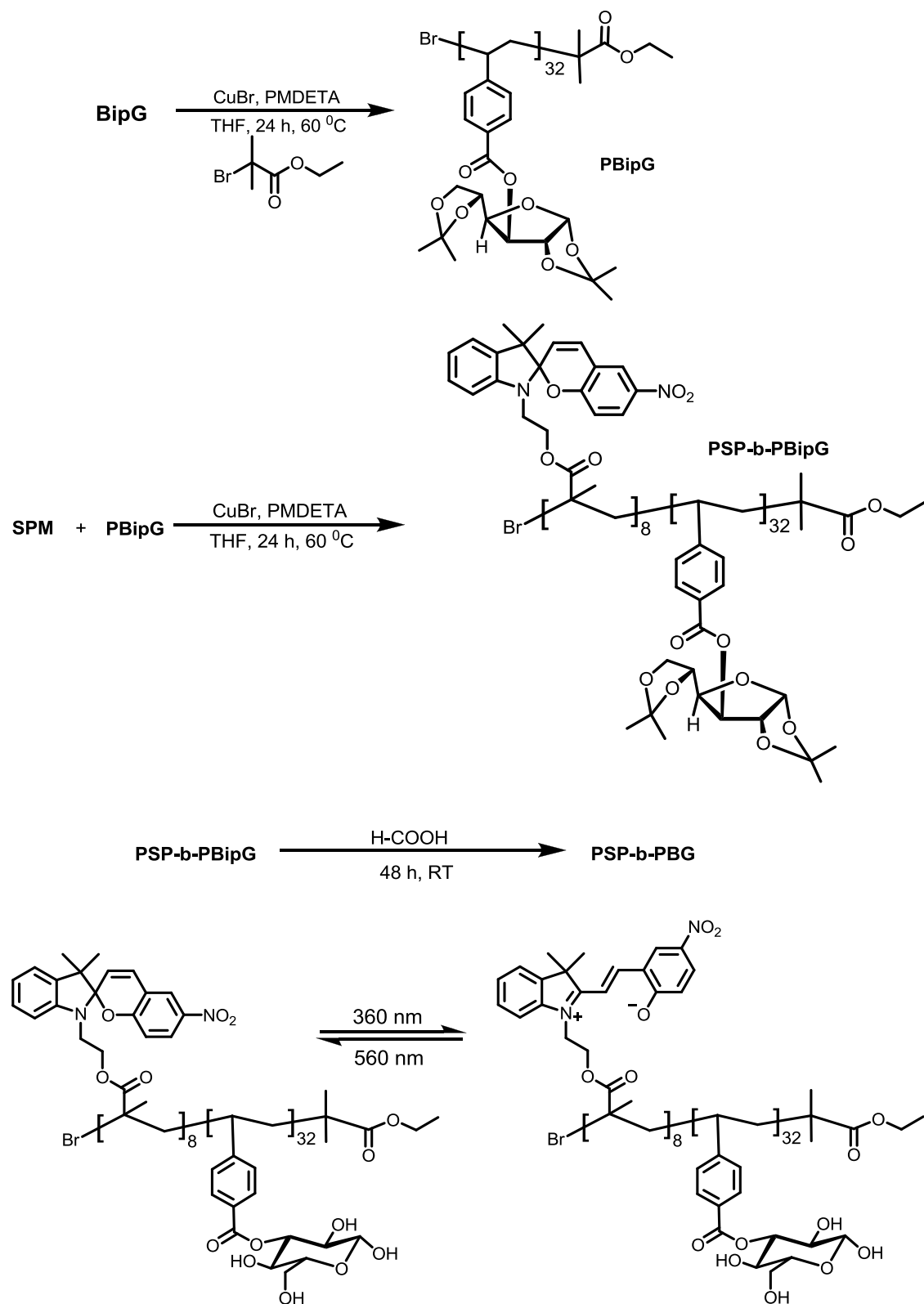
Scheme 4.2. Synthesis of **PSP-b-PBG** and its photoisomerization.
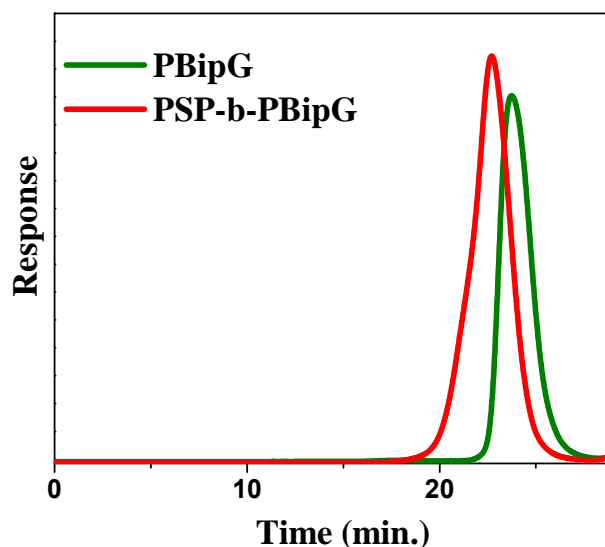
Figure 4.4. GPC curves of PSP-b-PBipG and the corresponding precursor PBipG.

Hydrolysis of the isopropylidene groups in PSP-b-PBipG was performed by treating the samples with formic acid. The final product **PSP-b-PBG** was obtained by freeze-drying after the deprotected polymer was dialyzed against water. The structure of the polymers PBipG, PSP-b-PBipG and **PSP-b-PBG** was confirmed by ^{1}H NMR. Figure 4.5 shows the ^{1}H NMR spectra of the respective polymers. The characteristic peaks at 1.2-1.4 (isopyledene protons), 6.3-6.5 (aromatic protons), 7.4-7.7 ppm (aromatic protons) are clearly seen in PBipG. In the case of the copolymer PSP-b-PBipG, besides the signals of the PBipG segment, the PSP signals appear at 5.77 and 6.80 ppm attributed to alkene protons and at 7.89 ppm corresponding to the spiropyran aromatic protons. This confirmed the presence of both PSP and PBipG block in the resultant copolymer. The structure of the deprotected polymer could be determined by ^{1}H NMR in DMSO-d$_6$. Figure 4.5c reveals that the signals of the isopropylidene protons (1.2-1.4 ppm) completely disappear after the hydrolysis of PSP-b-PBipG and a broad signal corresponding to the anomeric hydroxyl groups of the sugar moieties (6.5-7.0 ppm) appears. This indicates the quantitative deprotection of the isopropylidene protecting groups.
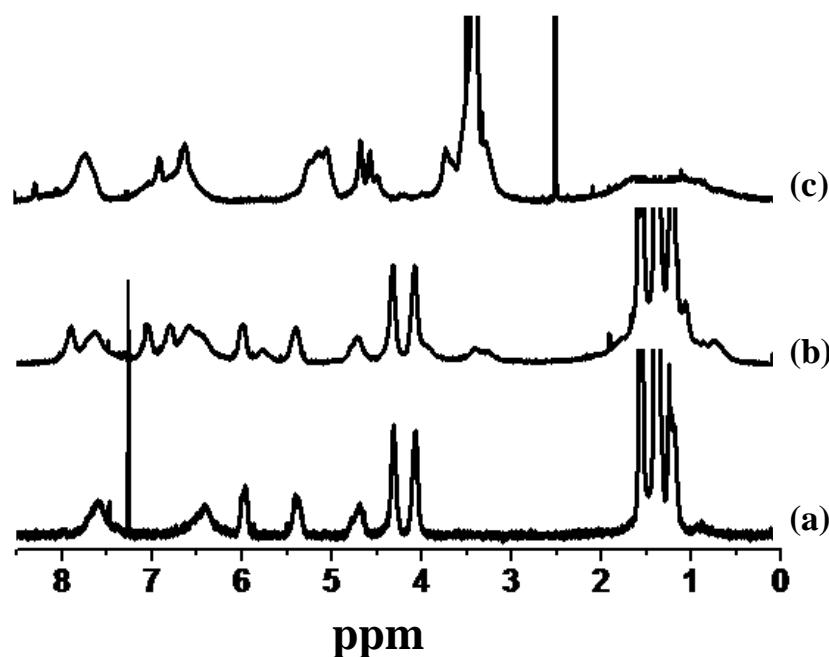
Figure 4.5. ^{1}H NMR spectra of (a) PBipG in CDCl$_3$ (b) PSP-b-PBipG in CDCl$_3$ and (c) **PSP-b-PBG** in DMSO-d$_6$ at room temperature.

The synthesis of the diblock copolymer **PMAzo-b-PBG** is outlined in Scheme 4.3 and Scheme 4.4. Copolymerization of MAzo was conducted using CuBr/PMDETA with PBipG as the macroinitiator at 60 ^{0}C in THF for 24 hours. The resultant polymer PMAzo-b-PBipG had a number-average molecular weight of 14,758 and a PDI value of 1.31. Figure 4.6 shows the GPC trace of PMAzo-b-PBipG together with that of the homopolymer PBipG. The diblock copolymer PMAzo-b-PBipG was purified by reprecipitating three times from THF into methanol. The resulting polymer PSP-b-PBipG was composed of 6 units of MAzo and 32 units of BipG.

Hydrolysis of the isopropylidene groups in PMAzo-b-PBipG was performed by treating the samples with formic acid. The final product **PMAzo-b-PBG** was obtained by freeze-drying after the deprotected polymer was dialyzed against water. The structure of the polymers PBipG, PMAzo-b-PBipG and **PMAzo-b-PBG** was confirmed by ^{1}H NMR. Figure 4.7 shows the ^{1}H NMR spectra of the respective polymers. The characteristic peaks at 1.2-1.4 (isopylidene protons), 6.3-6.5 (aromatic protons), 7.4-7.7 ppm (aromatic

protons) are clearly seen in PBipG. In the case of the copolymer PMAzo-b-PBipG, besides the signals of the PBipG segment, the PMAzo signals appear at 7.89 and 6.80 ppm corresponding to the azobenzene aromatic protons. This confirmed the presence of both PMAzo and PBipG block in the resultant copolymer. The structure of the deprotected polymer could be determined by ^{1}H NMR in DMSO-d$_6$. Figure 4.7 c reveals that the signals of the isopropylidene protons (1.2-1.4 ppm) completely disappear after the hydrolysis of PMAzo-b-PBipG and a broad signal corresponding to the anomeric hydroxyl groups of the sugar moieties (6.5-7.0 ppm) appears. This indicates the quantitative deprotection of the isopropylidene protecting groups.
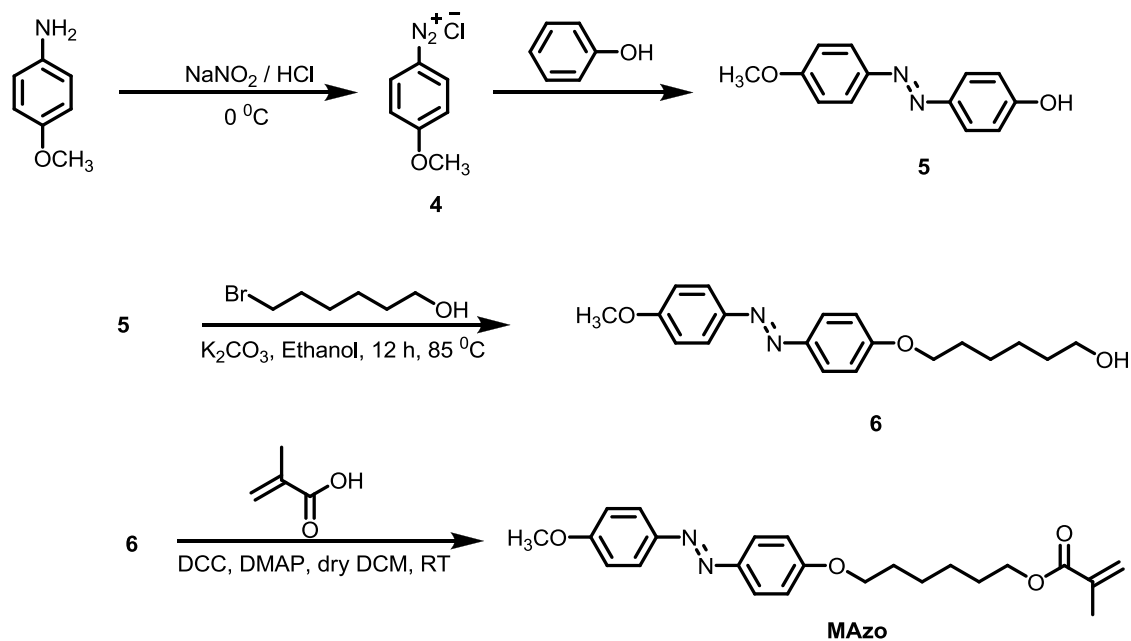
Scheme 4.3. Synthesis of azobenzene monomer MAzo.
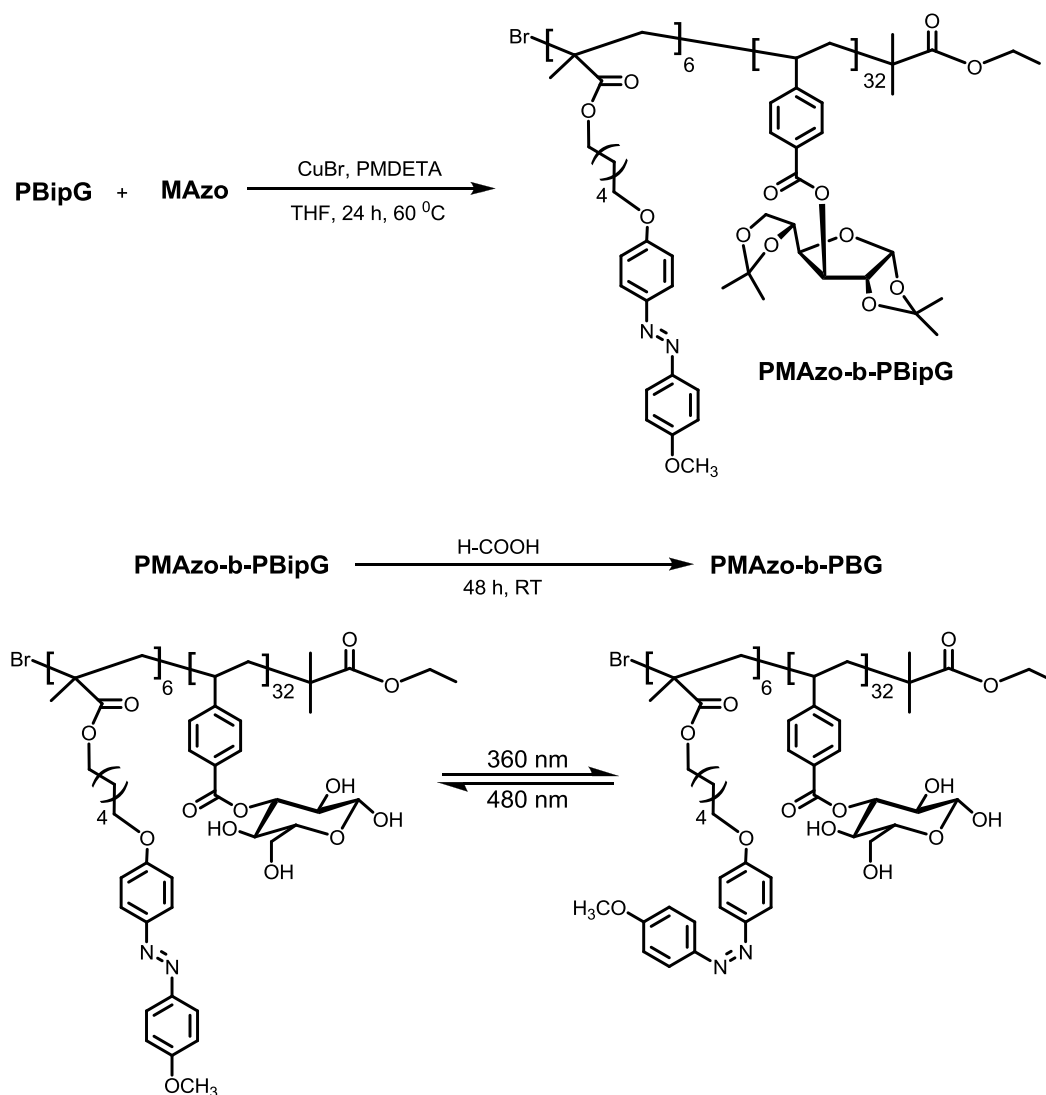
Scheme 4.4. Synthesis of **PMAzo-b-PBG** and its photoisomerization.
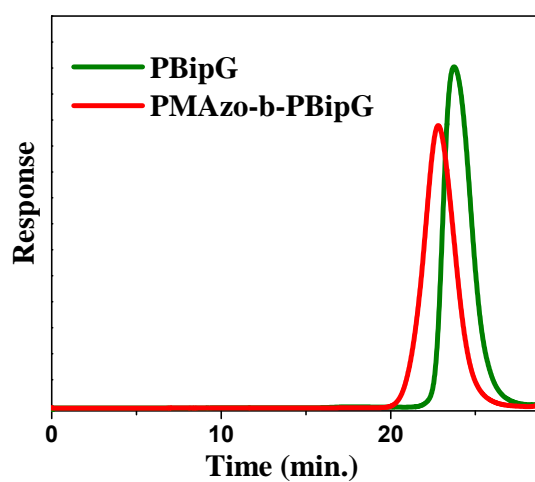
Figure 4.6. GPC curves of PMAzo-b-PBipG and the corresponding precursor PBipG.
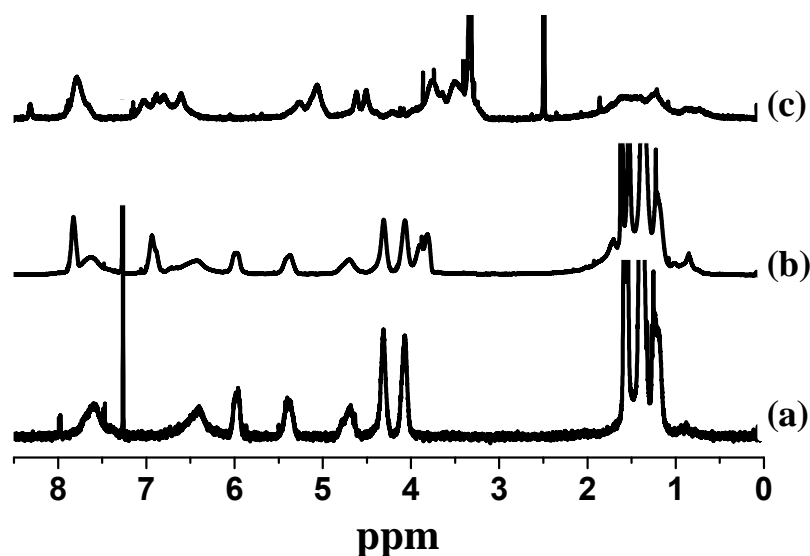
Figure 4.7. ^{1}H NMR spectra of (a) PBipG in CDCl$_3$ (b) PMAzo-b-PBipG in CDCl$_3$ and (c) **PMAzo-b-PBG** in DMSO-d$_6$ at room temperature.

4.3.2. Morphological Investigation of PSP-b-PBG Aggregates

In aqueous solutions **PSP-PBG** associate to form aggregates in which hydrophilic BG block forms the corona and hydrophobic SP block forms the core of the aggregates. Irradiation with UV light led to photoisomerization which results in the conversion of hydrophobic SP into hydrophilic zwitterionic MC. Thus photoisomerization converts the initial hydrophilic-hydrophobic block copolymer into a double hydrophilic block copolymer which results in almost complete disruption of the polymer aggregates on account of the loss in amphiphilicity. Irradiation with 560 nm visible light gives back the closed ring SP form which restores the amphiphilicity of the glycopolymer thereby regenerating the polymer aggregates.

Morphological investigations of the polymer aggregates were carried out using dynamic light scattering (DLS), atomic force microscopy (AFM) and transmission electron microscopy (TEM). To prepare an aqueous micellar solution of **PSP-b-PBG**, 1 mg of the polymer was first dissolved in spectroscopic grade DMF, and then 1 mL of

deionized water was added at a rate of 500 µL/h to form the aggregates. When water addition was complete 10 mL deionized water was added quickly to kinetically quench the aggregates. The resulting colloidal solution was then put into a dialysis bag (molecular weight cut: 3,000) and dialyzed against deionized water for two days to remove the organic solvent. The solution was then filtered through a 0.45 µm filter (Millipore Millex-HV) before use. DLS analysis of the solution thus prepared indicated the presence of spherical particles with an average diameter of 366 nm with a PDI value of 0.165 (Figure 4.8a). This solution was then exposed to 360 nm UV light for 1 hour. DLS investigation of the irradiated solution revealed that there was a drastic decrease in the size of the aggregates after irradiation. The solution now contained ill-defined aggregates with an average size of about 48 nm (Figure 4.8b). The same solution was then exposed to visible light of wavelength 560 nm for 1 hour. This solution now contained 280 nm sized particles (PDI = 0.226) as confirmed by DLS (Figure 4.8c).
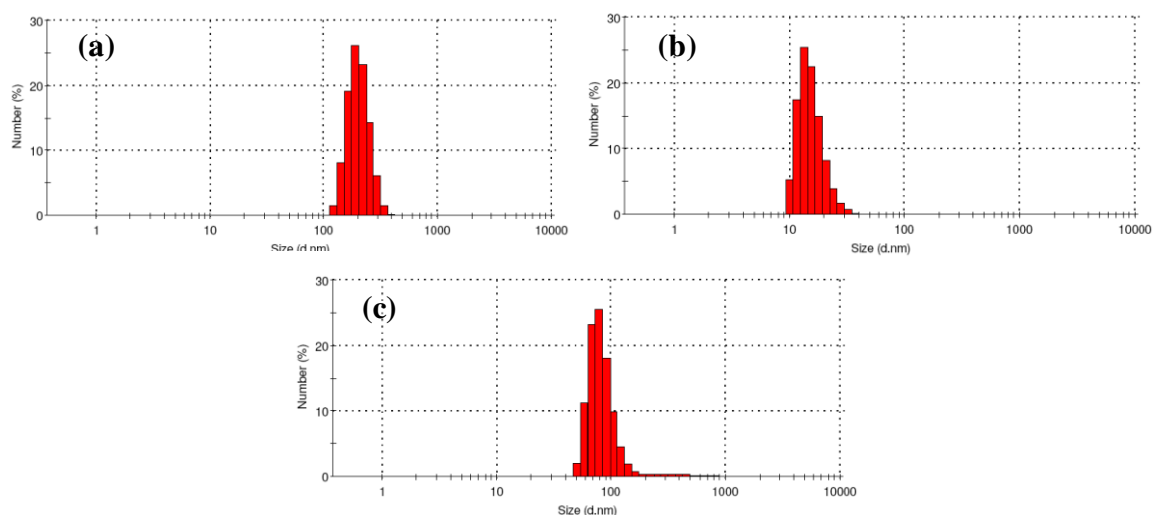
Figure 4.8. Size distribution of **PSP-b-PBG** aggregates in water during various stages of irradiation (a) before irradiation (b) UV irradiation for 1 h and (c) 1h UV irradiation followed by 1h visible light irradiation.

DLS analysis thus confirmed the formation, destruction and regeneration of the glycopolymer aggregates during various stages of irradiation. A further insight about the nature of these aggregates was obtained from microscopic analysis. A part of the initially

prepared non-irradiated aggregate solution was drop-cast on a mica sheet and dried at room temperature. AFM images of the resultant solution of the solution indicated the presence of uniform well-dispersed microsized nearly spherical aggregates with an average width of around 1.5 μm and an average height of 0.9 μm (Figure 4.9a). Another portion of the solution was exposed to UV light for 2 hours and was quickly drop-cast into another mica sheet. AFM images of the UV exposed solution showed almost complete absence of such aggregates and some small ill-defined smaller aggregates were observed which was consistent with disruption of polymer aggregates brought about by the conversion of closed SP form into open zwitterionic MC form upon UV irradiation (Figure 4.9b and Figure 4.9c). The UV irradiated solution was then exposed to 560 nm visible light for 2 hours. This time the microsized aggregates were absent but instead nanometer sized spherical particles with an average diameter of 250 nm were observed due to the regeneration of hydrophobic SP form (Figure 4.9d). TEM analysis was also carried out to find out the morphology of the aggregates. TEM images of the non-irradiated aggregates showed that there was a clear contrast difference between the core and the periphery of the aggregates indicating vesicular morphology (Figure 4.10a) while no such aggregates was observed after UV irradiation (Figure 4.10b). On the other hand TEM images of the visible light irradiated solution showed that the morphology now consisted of a mixture of vesicles and micelles (Figure 4.10c). The observed evolution of morphology of the aggregates after UV and visible light treatment can be attributed to the various equilibrating process occurring during visible light irradiation. During visible light irradiation the aggregates will not get sufficient time to arrange themselves in a bilayer fashion which results in the formation smaller micellar aggregates rather than vesicles.
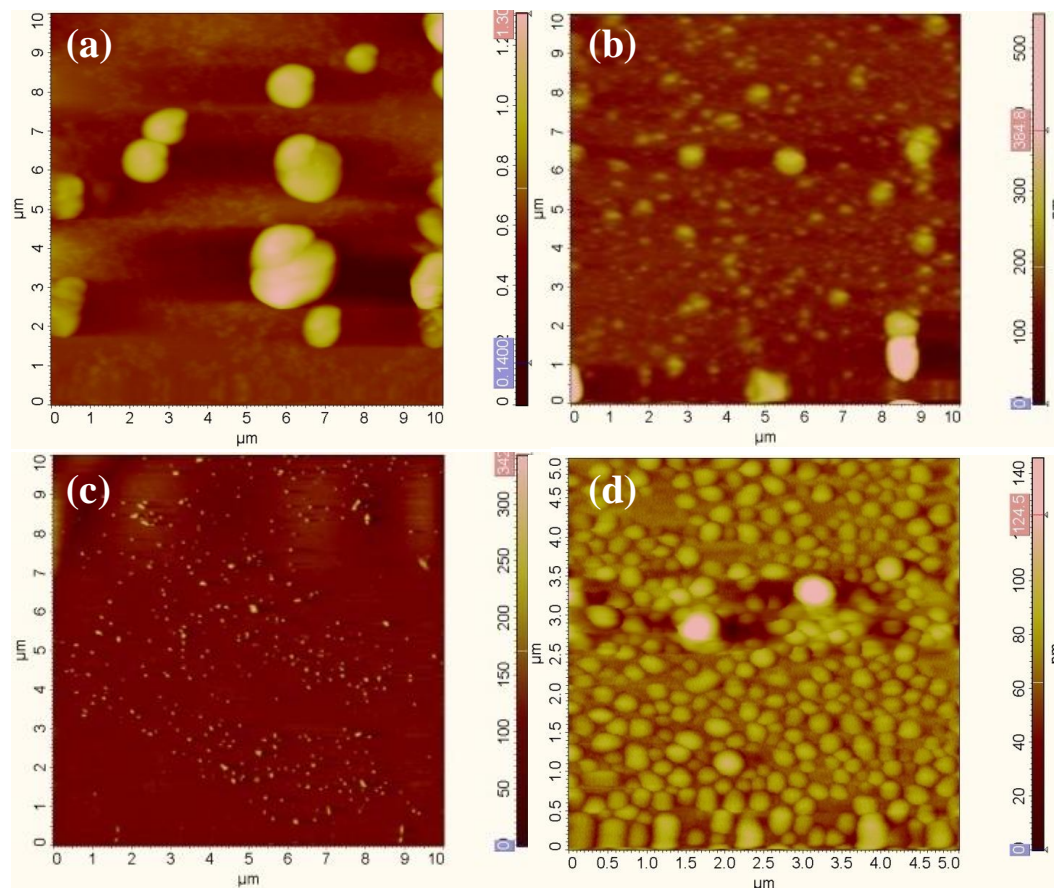
Figure 4.9. AFM images of **PSP-b-PBG** aqueous solutions drop-cast and dried on mica under various conditions (a) before exposure to 360 nm UV light (b) exposure to 360 nm UV light for 30 min. (c) exposure to 360 nm UV light for 2 h and (d) after exposure to 360 nm UV light for 2 h followed by exposure to 560 nm visible light for 2 h.
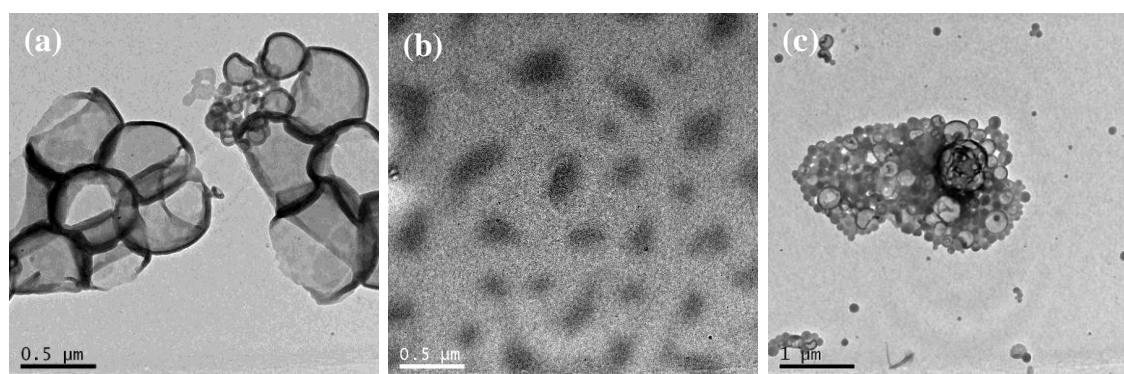
Figure 4.10. TEM images of **PSP-b-PBG** aqueous solutions drop-cast and dried on carbon coated copper grids under various conditions (a) before exposure to 360 nm UV light (b) exposure to 360 nm UV light for 2 h and (c) after exposure to 360 nm UV light for 2 h followed by exposure to 560 nm visible light for 2 h.

4.3.3. Irradiation and Coumarin 7 Encapsulation Studies of PSP-b-PBG Aggregates

UV-Vis absorption spectroscopy confirmed the photochemical isomerization of spiropyran moieties. A portion of the colloidal solution prepared as described earlier was irradiated alternatively with UV (360 nm) and visible light (560 nm). Before UV irradiation the aggregate solution did not show any absorption above 400 nm indicating almost complete absence of open MC form. Upon UV irradiation however a strong absorption band at 560 nm appeared, which is the characteristic π-π^* absorption band of the MC chromophore [Choi *et al.* 2003]. At the same time the colorless turbid solution became pink. Irradiation with visible light isomerizes the MC back to the SP form as indicated by the gradual decrease in absorption at 560 nm. Figure 4.11 shows the changes in the absorption spectra of an aqueous solution of **PSP-b-PBG** upon alternate UV (Figure 4.11a) and visible (Figure 4.11b) irradiation.
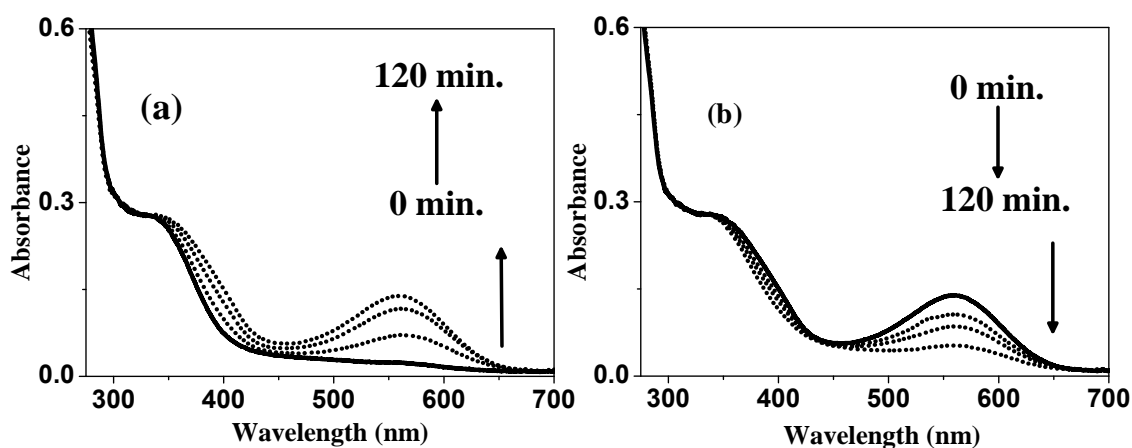
Figure 4.11. UV-Vis spectra of an aqueous solution **PSP-b-PBG** upon (a) UV irradiation and (b) visible irradiation.

The ability of these photoresponsive aggregates to encapsulate hydrophobic dyes in water was demonstrated using coumarin 7 as an example. Coumarin 7 is a hydrophobic fluorescent dye which is almost insoluble in water. To encapsulate the dye inside the block copolymer aggregates, 1 mg of the polymer and 0.1 mg of coumarin 7 were

dissolved in 1 mL of spectroscopic grade DMF. To this 1 mL deionized water was added dropwise from a syringe with stirring. Subsequently 9 mL of water was quickly added and the organic solvent was removed by dialyzes against distilled water for 2 days. The solution was finally filtered through a 0.45 μm filter before use. Figure 4.12a shows the absorption spectra of coumarin 7 encapsulated polymeric aggregates in water. Before UV irradiation the colloidal solution showed a band at 434 nm corresponding to the absorption band of the polymer encapsulated coumarin 7 dye. Upon irradiation with 360 nm light for 1 hour the absorption band corresponding to coumarin 7 at 434 nm decreased and the band corresponding to the merocyanine dye appeared at 560 nm. This can be attributed to the release of coumarin 7 into water due to the breakage of polymeric aggregates upon the formation of MC form. The reversible release and encapsulation of hydrophobic coumarin dye was confirmed by fluorescence resonance spectroscopy. Figure 4.12b shows the emission spectra of the dye encapsulated polymeric aggregates upon consequent UV and visible light irradiation. Upon excitation at 450 nm where spiropyran has no absorption the dye encapsulated solution showed a strong emission at 485 nm corresponding to the emission of coumarin 7. Upon 360 nm UV irradiation for 120 minutes however, the emission at 485 nm decreased to about 32% of its initial value with concomitant red shift in the emission maxima to 496 nm indicating release of coumarin 7 into water. Complete quenching in emission was not observed even after 120 minutes of irradiation due to the photostationary state reached between the hydrophobic SP form and hydrophilic colored MC form. As a result of the attainment of such a photostationary state complete disruption of the polymer aggregates was not possible. Consequent irradiation with 560 nm visible light for 120 minutes resulted in about 94% recovery in emission which was accompanied by re-encapsulation of released coumarin dye due to the regeneration of the polymer aggregates.
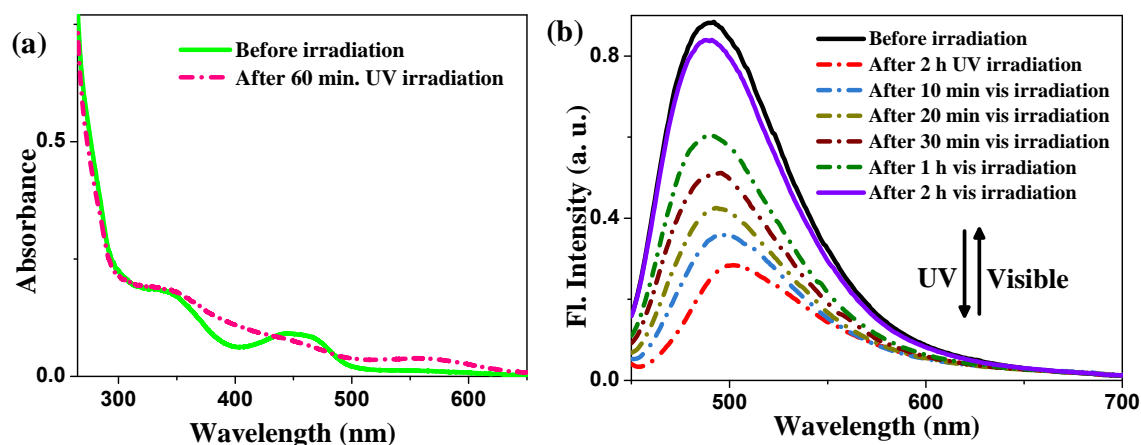
Figure 4.12. (a) Absorption spectra of coumarin 7 encapsulated **PSP-b-PBG** aggregates before and after UV irradiation (b) emission spectra of coumarin 7 encapsulated **PSP-b-PBG** aggregates upon alternate UV and visible irradiation.

4.3.4. *Morphological Investigation of PMAzo-b-PBG Aggregates*

In order to prepare light responsive aggregates of **PMAzo-b-PBG**, 1mg of the polymer was dissolved in 1 mL HPLC grade DMF which is a good solvent for both the blocks. To this 1 mL deionized water was added with gentle stirring at a rate of 0.5 mL/h. When water addition was complete 9 mL more water added quickly to quench the aggregates. The resultant turbid solution was put in dialyzes bag (molecular weight cut: 3,000) and dialyzed against deionized water for two days to remove the organic solvent. The solution was then filtered through a 0.45 µm filter (Millipore Millex-HV) before use. One portion of the resultant solution was used for DLS studies which revealed the presence of uniform aggregates with an average diameter of 352 nm and PDI value of 0.322. This solution was then exposed to 350 nm UV light for one hour. DLS data revealed that the solution now contained much smaller particles with an average diameter of 43 nm. Figure 4.13 shows the size distribution of the particles in the solution before and after UV irradiation.
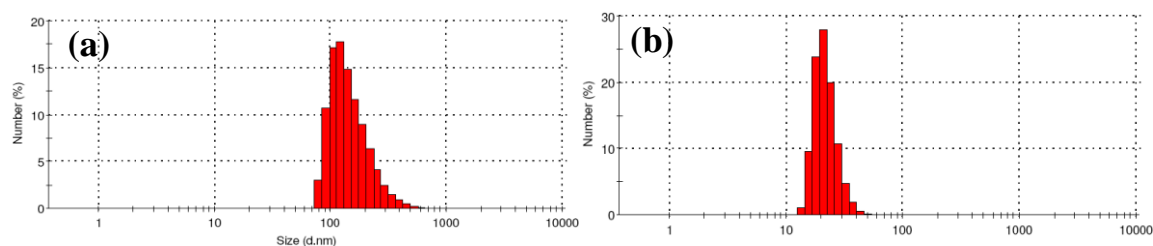
Figure 4.13. Size distribution of **PMAzo-b-PBG** aggregates in water (a) before and (b) after UV irradiation.

The morphology of the polymer aggregates before and after irradiation was investigated using AFM, SEM and TEM. For AFM and SEM one drop of the non-irradiated solution was drop-cast on a freshly cleaved mica sheet and dried at room temperature. AFM images of the resultant sample showed the presence of uniform, well-dispersed spherical aggregates with an average height of 440 nm (Figure 4.14a). Another part of the aggregate solution was exposed to 350 nm light for one hour and quickly drop-cast on another mica sheet. This time the uniform, well-dispersed aggregates were absent and some non-uniform smaller aggregates were observed indicative of the disruption of aggregates upon UV irradiation (Figure 4.14b). The same solution was then exposed to 450 nm visible light for one hour. The AFM images of the sample obtained after this step showed tubular or wire like morphology probably formed as a result of the association of the spherical aggregates (Figure 4.14c). Interestingly when the initial non-irradiated sample was allowed to age for two months the AFM images of the resultant aged solution indicated the presence of spiral or twisted fibers having the same dimensions as that of the spherical aggregates indicating that the twisted fibers are formed due to the association of the initially formed spherical aggregates (Figure 4.14d). It is presumed that the twists in these fibers could have been formed due to the presence of chiral glucose moieties in the polymer chain. AFM height profiles of the spherical aggregates obtained from freshly prepared aqueous solutions of **PMAzo-b-PBG** before

UV irradiation and the twisted fibers obtained from the aged solutions are shown in Figure 4.15.
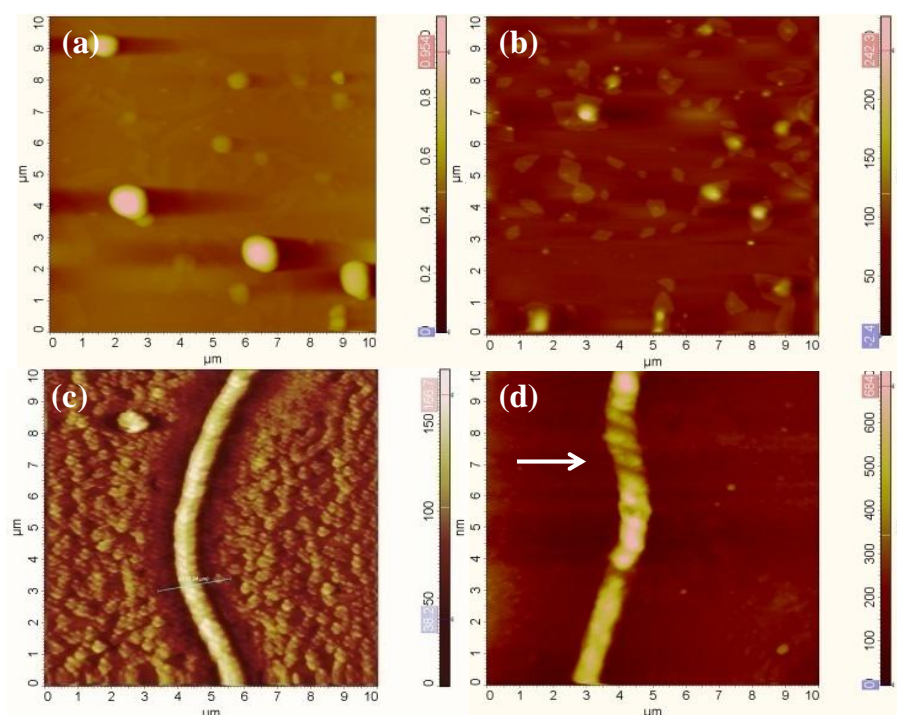
Figure 4.14. AFM images of **PMAzo-b-PBG** aqueous solutions drop-cast and dried on mica under various conditions (a) before irradiation (b) after exposure to 350 nm UV light for 1 h (c) after exposure to 450 nm visible light for 1 h (d) Non-irradiated solution aged for 2 months.

Figure 4.16 shows the SEM images of the morphology changes occurring when the 1 h UV irradiated solution of **PMAzo-b-PBG** were exposed to visible light. It was observed that after 30 minutes of visible light irradiation spherical aggregates were regenerated from the solution and the regenerated aggregates were connected by narrow bridges. After 1 h visible irradiation it can be seen that the interconnected aggregates completely fused to form long wires. TEM images of the initially prepared aggregates of the azo-glycopolymer revealed that these aggregates are hard spheres or micelles (Figure 4.17a). Rod shaped aggregates were observed after 1 h visible light irradiation following UV irradiation (Figure 4.17b). For the non-irradiated solution aged for 15 days, it was observed that the spherical micelles changed to ellipsoidal ones (Figure 4.17c) which

after about one month started to fuse together or arranged one-behind-other (Figure 4.17d).
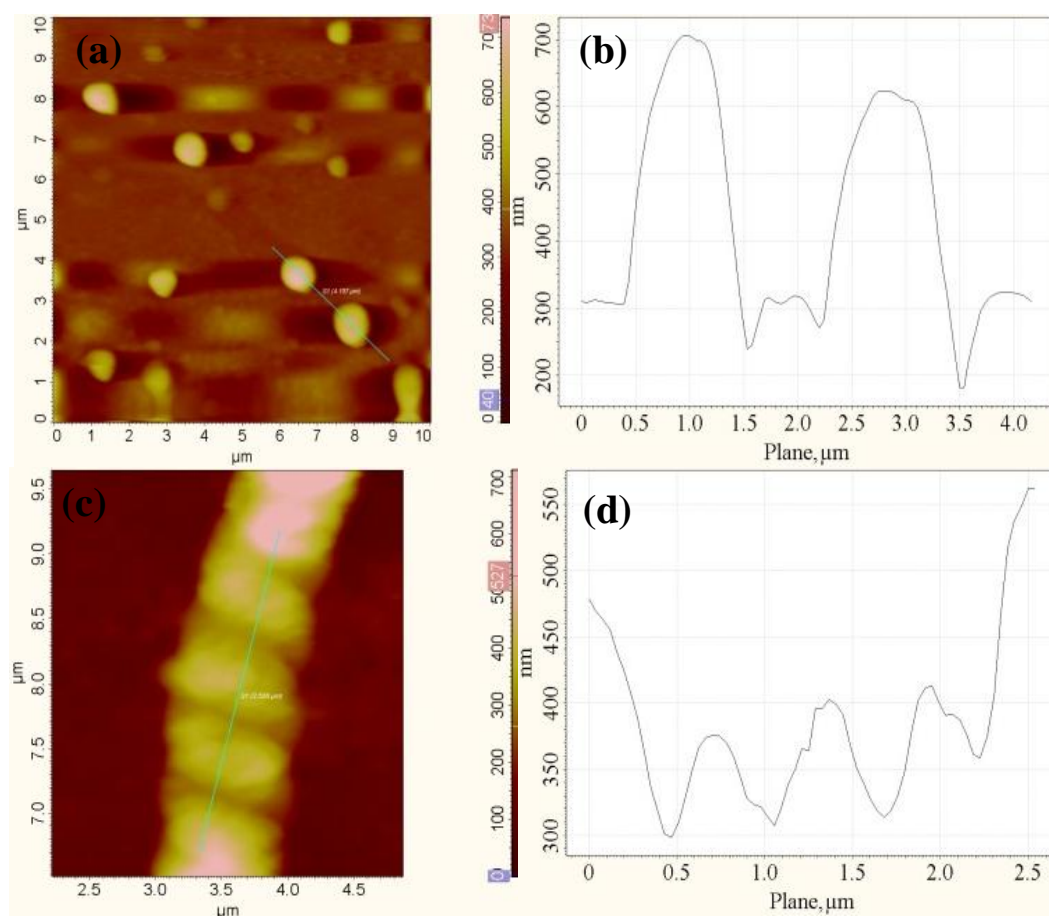
Figure 4.15. AFM images of **PMAzo-b-PBG** aqueous solutions drop-cast and dried on mica under various conditions (a) before exposure to 350 nm UV light (b) height profile of image (a) (c) Non-irradiated solution aged for 2 months and (d) height profile of image (c).
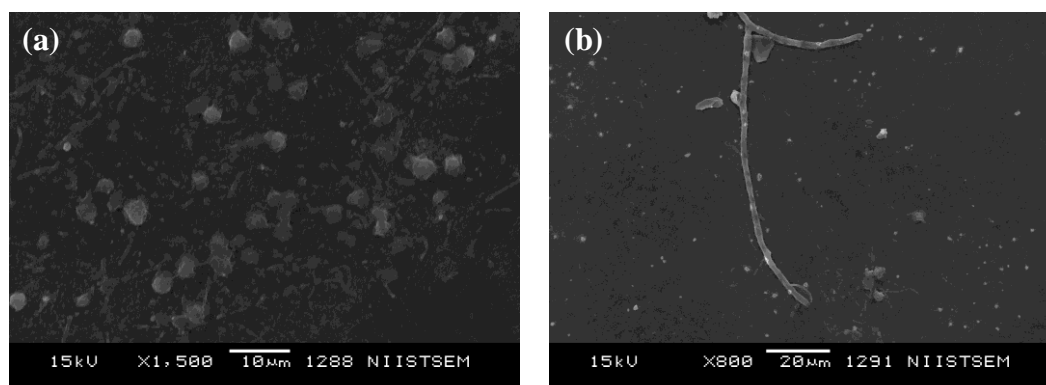
Figure 4.16. SEM images of **PMAzo-b-PBG** aqueous solutions drop-cast and dried on mica during various stages of visible irradiation following 60 minutes UV irradiation (a) after 30 minutes (b) after 60 minutes.
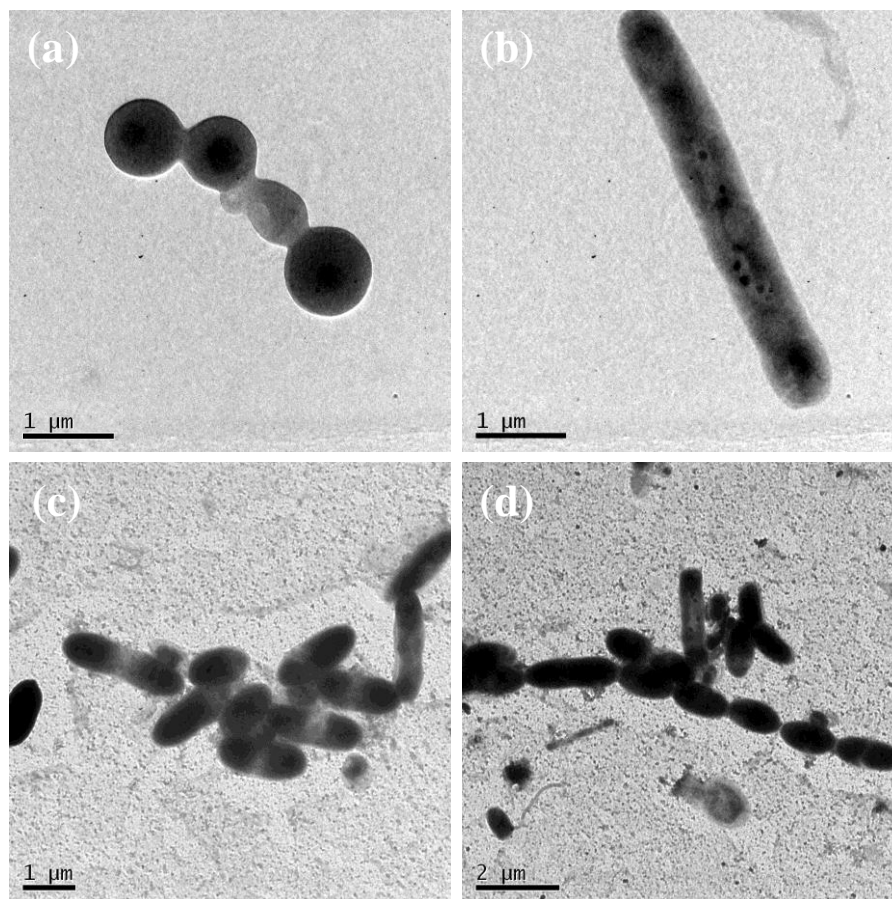
Figure 4.17. TEM images of **PMAzo-b-PBG** aqueous solutions drop-cast and dried on carbon coated copper grids under various conditions (a) before exposure to 350 nm UV light (b) after exposure to 350 nm UV light for 1 h followed by 450 nm irradiation for 1 h (c) non-irradiated solution aged for 15 days (d) non-irradiated solution aged for 1 month.

4.3.5. Irradiation and Nile Red Encapsulation Studies of PMAzo-b-PBG Aggregates

Photochemical isomerization of azobenezene units upon irradiation was confirmed by UV-Vis absorption spectroscopy. A colloidal suspension of the polymer prepared as described above was alternatively irradiated with UV (350 nm) and visible light (450 nm). A series of UV-Vis spectra of the colloidal solution varying with UV irradiation time is shown in Figure 4.18a. The occurrence of *trans-cis* isomerization upon UV light exposure is confirmed by the decrease in absorption maxima of the π-π^* transition band of *trans*-azobenzene chromophores at 340 nm, which is accompanied by increase in the

n-π* transition band of the *cis*-azobenzene at 450 nm. On vis-light irradiation, *cis*-azobenzene reverts back to *trans*-azobenzene as shown in Figure 4.18b. It was observed that the recovered absorbance of *trans*-azobenzene is slightly lower than that of the non-irradiated solution. Also the absorption maximum of the *trans*-azobenzene was red shifted from 340 nm to 360 nm. When the UV irradiated sample was kept in the dark the spectrum gradually reverted to the original form which indicates that *cis-trans* isomerization takes place even in dark in the absence of vis-light.
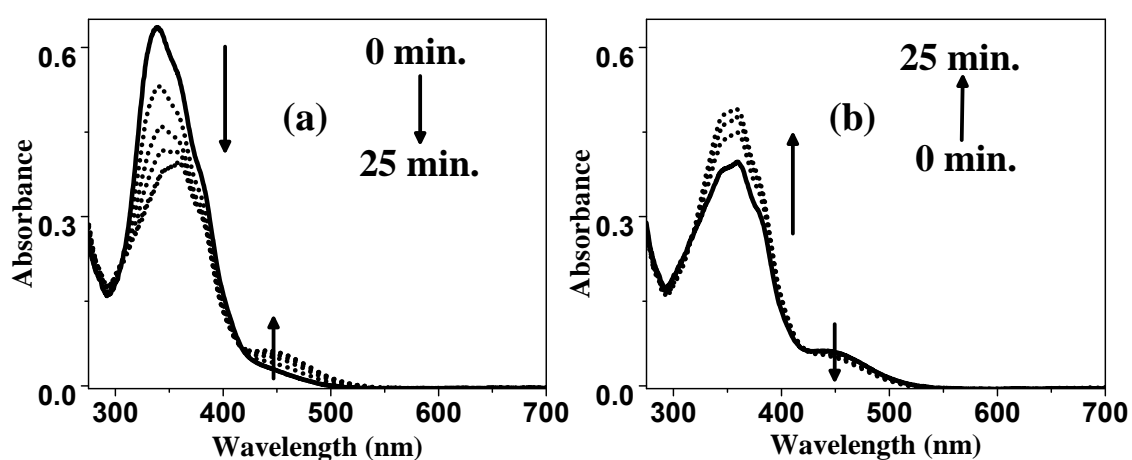
Figure 4.18. UV-Vis spectra of an aqueous solution **PMAzo-b-PBG** upon (a) UV irradiation and (b) visible irradiation.

To demonstrate the potential applications of these polymer aggregates in controlled release upon light irradiation, we prepared Nile Red loaded polymer aggregates in water. Nile red is a hydrophobic fluorescent polymer showing very good emission in organic solvents whereas it is practically insoluble in water. To encapsulate the dye inside the block copolymer aggregates, 1 mg of the polymer and 0.1 mg of Nile Red were dissolved in 1 mL of spectroscopic grade DMF. Then 1 mL deionized water was added dropwise with stirring. Afterwards 9 mL was added quickly and the organic solvent and the free dye were removed by dialyzes against distilled water for 2 days. The solution was finally filtered through a 0.45 μm filter before use. Figure 4.19a shows the emission spectra of Nile Red encapsulated polymeric aggregates in water. Before UV irradiation the Nile

Red encapsulated aggregates upon excitation at 530 nm shows a strong emission at 647 nm which arises as a result of the encapsulated Nile Red. This emission was quenched to almost half of its initial value upon 60 minutes UV irradiation. This decrease in emission is assumed to be caused due to the release of encapsulated Nile Red accompanied by the breakage of the polymer aggregates. Release of Nile Red into water will result in its precipitation since it is insoluble in water. Further decrease in emission was not observed even after 2 hours of UV irradiation indicative of incomplete aggregate dissociation. Irradiation with 450 nm light resulted in the partial encapsulation of the release Nile Red molecules resulting in almost 50% restoration in the emission intensity at 547 nm. It was also observed that when the UV irradiated solution was kept in the dark for 3 days, fluorescence emission of Nile Red was completely restored with a 14 nm blue shift (Figure 4.19b). This shows that the morphology of the aggregates formed by the *cis-trans* isomerization of azobenzene units under thermal conditions is slightly different from that formed under photochemical conditions as indicated by the AFM images.
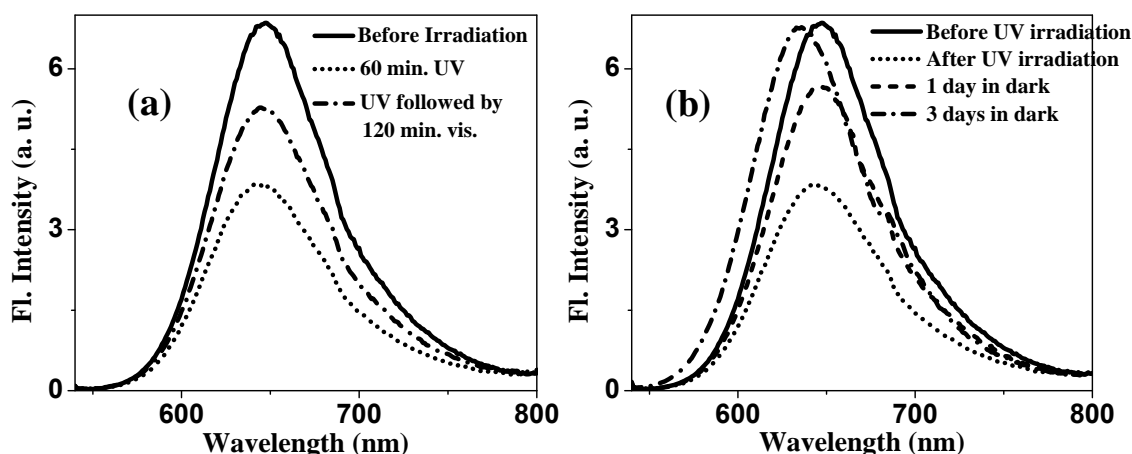
Figure 4.19. (a) Emission spectra of Nile Red encapsulated **PMAzo-b-PBG** aggregates upon alternate UV and visible irradiation (b) Thermal recovery of Nile Red emission after UV irradiation.

4.4. Conclusions

In conclusion we have synthesized photo dissociable glycopolymer aggregates from two light responsive glycopolymers **PSP-b-PBG** and **PMAzo-b-PBG**. Well-defined spherical aggregates formed from these amphiphilic polymers were reversibly dissociated upon UV irradiation. Vesicles were observed in the case of **PSP-b-PBG** and hard-core micelles in the case of the azo glycopolymer. Dissociated aggregates was regenerated upon visible irradiation or when kept in the dark for a few days. Morphology change from spheres to untwisted or twisted fibers was observed in the case of **PMAzo-b-PBG** depending on whether the isomerization of azobenzene units was brought about in the presence or absence of light respectively. These glycopolymer aggregates can act as a cage holding hydrophobic dyes in aqueous solution and can be partially released upon UV illumination. In the case of **PMAzo-b-PBG** slow thermal reverse isomerization caused the released molecules to be fully re-encapsulated inside the regenerated aggregates. It is expected that such light operated control release systems can find applications in the field of drug delivery, nanotechnology and catalysis.

4.5. Synthesis and Experimental Section

4.5.1. Materials

N,N,N',N',N''-Pentamethyldiethylenetriamine (PMDETA), ethyl-2-bromoisobutyrate, 1,2:5,6-Di-o-isopropylidene-α-D-glucofuranose, 2,3,3-trimethyl-3H-indole, 2-bromoethanol, 2-hydroxy-5-nitrobenzaldehyde, p-anisidine, 6-bromo-1-hexanol, methacrylic acid, 4-vinylbenzoic acid, dicyclohexylcarbodiimide (DCC), 4-(N,N-dimethylamino)pyridine (DMAP), coumarin 7 and Nile Red were purchased from Aldrich and used without further purification. CuBr (98%, Aldrich) was stirred in glacial acetic acid overnight, filtered, and then it was washed with ethanol and dried under

vacuum overnight. Solvents were purchased locally and purified using standard procedures before use.

4.5.2. Analysis and Measurements

^{1}H and ^{13}C NMR spectra were recorded on Bruker DPX 500 MHz Spectrometer using tetramethylsilane (TMS) as the internal standard and chloroform-d (CDCl$_3$) as solvent. The molecular weights of the polymers were determined by gel permeation chromatography (GPC) in tetrahydrofuran (THF) using polystyrene standards for the calibration. The GPC was calibrated with different polystyrene standards having molecular weights ranging from 2950 to 177,000 g/mol (Polymer Standards Service).Waters 515 pump connected through three series of Styragel HR columns (HR-3, HR-4E, and HR-5E) and Waters Model 2487 Dual wavelength UV-Vis Detector and a Waters 2414 Differential Refractometer were used for analyzing the samples. The flow rate of the THF was maintained as 1 mL/min throughout the experiments, and the sample solutions at very dilute concentration were filtered and injected for recording the GPC chromatograms at 30 ^{0}C. Mass spectral analyses were carried out using a JEOL JMS600 instrument in FAB ionization mode. Melting points are uncorrected and were determined on a Mel-Temp II melting point apparatus. Absorption spectra were recorded on a Shimadzu UV-3101PC UV-Vis-NIR spectrophotometer. The excitation and emission spectra were recorded on a SPEX Fluorolog F112X spectrofluorimeter. Steady-state photolysis was carried out using the output from a 200 W high-pressure mercury lamp filtered through a 350 nm, 450 nm or 560 nm Oriel band-pass filter. Dynamic light scattering (DLS) measurements were done by using a Nano ZS Malvern instrument employing a 4-mW He-Ne laser ($\lambda = 632.8$ nm) and equipped with a thermo stated sample chamber. Samples for scanning electron microscopy (SEM) were provided with a thin gold coating using JEOL JFC-1200 finecoater. SEM images were recorded using a

JEOL JSM-5600 LV instrument. Atomic force microscopy (AFM) images were recorded under ambient conditions using NTEGRA Prima - NT-MDT, Russia Scanning probe microscope operated in tapping mode. Micro-fabricated silicon cantilever tips (NSG 20) with a resonance frequency of 260-630 kHz and a force constant of 20-80 Nm^{-1} were used. The tip curvature radius was 10 nm. The scan rate was 1 Hz. To prepare samples for SEM and AFM measurements, a drop of the polymer colloidal solution was placed on a freshly cleaved mica sheet and the solution was allowed to evaporate at room temperature in air. Transmission electron microscopy (TEM) images were recorded using a JEOL JEM 1011 instrument with an accelerating voltage of 100 kV. Samples were prepared by drop-casting aqueous solutions of the polymers on a carbon coated copper grids under ambient conditions. The solvent was allowed to evaporate at room temperature. TEM images were obtained without staining.

4.5.3. Synthesis and Characterization Details

4.5.3.1. Synthesis of 1-(-2-hydroxyethyl)-2,3,3-trimethyl-3H-indolium bromide (1).

A solution of 2,3,3-trimethyl-3H-indole (2.83 g, 17.8 mmol) and 2-bromoethanol (3.31 g,26.5 mmol) in MeCN(20 mL) was heated for 24 hours under reflux and nitrogen. After cooling down to ambient temperatures, the solvent was distilled off under reduced pressure. The residue was suspended in hexane (25 mL) and the mixture was sonicated and filtered. The resulting solid was precipitated from chloroform by adding hexane to give a pink solid. Yield = 4.7 g (93.43%); mp = 191 ^{0}C; FAB MS : m/z = 204.35 [M-Br]$^{+}$; ^{1}H-NMR (500 MHz, CDCl$_3$, Me$_4$Si): δ (ppm) = 7.79 (m, 1H, aromatic), 7.58-7.27 (m, 3H, aromatic), 4.90 (t, 2H, =N-**CH$_2$**-CH$_2$-), 4.19 (t, 2H, N-CH$_2$-**CH$_2$**-), 2.18 (s, 3H, -N=C-**CH$_3$**), 1.65 (s, 6H, -C(**CH$_3$**)$_2$-); ^{13}C-NMR (125 MHz, CDCl$_3$, Me$_4$Si): δ (ppm) = 197.37, 141.27, 140.74, 129.77, 128.51, 122.99, 110.86, 58.06, 51.44, 50.72, 22.91, 15.78.
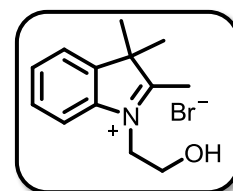
4.5.3.2. Synthesis of 9,9,9a-trimethyl-2,3,9,9a-tetrahydro-oxazolo[3,2-a] indole (2).

A solution of **1** (4.30 g, 15.9 mmol) and KOH (930 mg, 16.6 mmol) in water (50 mL) was stirred at ambient temperature for 10 min. and, then, it was extracted with ether (3 X 20 mL). The organic phase was concentrated under reduced pressure to afford **2** as yellow oil.
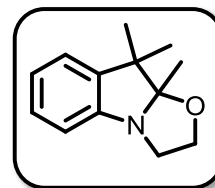
Yield = 3.11 g (96.23%); FAB MS : m/z = 204.39 [M+H]$^+$; ^{1}H-NMR (500 MHz, CDCl$_3$, Me$_4$Si): δ (ppm) = 7.14-7.03 (m, 2H, aromatic), 6.90 (t, 1H, aromatic), 6.74 (d, 1H, aromatic), 3.81-3.65 (m, 2H, -CH$_2$-**CH$_2$**-O-), 3.57-3.46 (m, 2H, -N-**CH$_2$**-CH$_2$-), 1.41 (s, 3H, -C-**CH$_3$**), 1.36 (s, 3H, -C-(**CH$_3$**)$_2$), 1.18 (s, 3H, -C-(**CH$_3$**)$_2$); ^{13}C-NMR (125 MHz, CDCl$_3$, Me$_4$Si): δ (ppm) = 150.33, 139.77, 127.31, 122.20, 121.51, 111.77, 108.75, 62.75, 49.84, 46.73, 27.90, 15.12.

4.5.3.3. Synthesis of 2-(3',3'-dimethyl-6-nitrospiro[chromene-2,2'-indoline]-1'-yl) ethanol (3).

A solution of 2-hydroxy-5- nitrobenzaldehyde (3.70 g, 22.2 mmol) and **2** (3.0 g, 14.8 mmol) in EtOH (35 mL) was maintained under N$_2$ and heated under reflux for 3 hours. After being cooled to ambient temperature, the mixture was filtered. The resulting purple solid was washed with EtOH (10 mL) and dried to afford **3** as shining purple crystals.
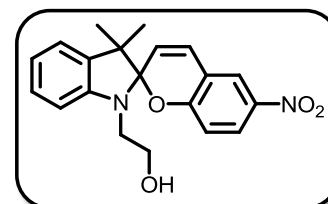
Yield = 3.73 g (71.72%); mp = 171 ^{0}C; FAB MS : m/z = 353.26 [M+H]$^+$; ^{1}H-NMR (500 MHz, CDCl$_3$, Me$_4$Si): δ (ppm) = 8.04 (d, 1H, aromatic), 7.99 (dd, 1H, aromatic), 7.14 (pt, 1H, aromatic), 7.10 (1H, d, aromatic), 6.92 (d, 1H, -O-C-CH=C**H**-), 6.78 (pt, 1H, aromatic), 6.68 (d, 1H, aromatic), 6.65 (d, 1H, aromatic), 5.90 (d, 1H, -O-C-C**H**=CH-), 3.81-3.70 (m, 2H, -N-CH$_2$-**CH$_2$**-OH), 3.45-3.31 (m, 2H, -N-**CH$_2$**-CH$_2$-OH), 1.24 (s, 3H, -C-(**CH$_3$**)$_2$), 1.19 (s, 3H, -C-(**CH$_3$**)$_2$); ^{13}C NMR (125 MHz, CDCl$_3$, Me$_4$Si): δ (ppm) =

166.09, 146.95, 141.00, 135.78, 129.76, 128.15, 127.77, 125.86, 122.70, 121.95, 119.85, 118.93, 115.45, 106.81, 106.31, 60.75, 52.76, 46.02, 25.82, 19.93.

4.5.3.4. Synthesis of 2-(3',3'-dimethyl-6-nitrospiro[chromene-2,2'-indoline]-1'-yl)ethyl methacrylate (SPM).

To a mixture of **3** (3.52 g, 10 mmol), methacrylic acid (1.03 g, 11.6 mmol) and 1,3-dicyclohexylcarbodiimide (2.5 g, 12 mmol) in dichloromethane (55 mL) was added dimethylaminopyridine (0.15 g, 1.2 mmol), and stirred at room temperature for 24 hours. After the reaction the solid was filtered off, washed several times with dichloromethane and the filtrate was concentrated and finally purified by column chromatography (basic alumina, 10% EtOAc-hexane as eluent).
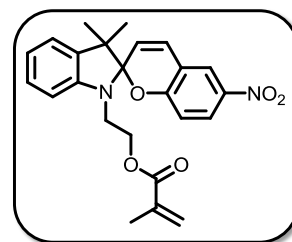
Yield = 3.43 g (81.70%); mp = 85 ^{0}C; FAB MS : m/z = 421.94 [M+H]$^+$; ^{1}H-NMR (500 MHz, CDCl$_3$, Me$_4$Si): δ (ppm) = 8.03 (d, 1H, aromatic), 8.00 (dd, 1H, aromatic), 7.21 (t, 1H, aromatic), 7.10 (d, 1H, aromatic), 6.92 (d, 1H, -O-C-CH=C**H**-), 6.88 (t, 1H, aromatic), 6.74 (d, 1H, aromatic), 6.70 (d, 1H, aromatic), 6.07 (s, 1H, -OCO-C(CH$_3$)=C**H$_2$**), 5.87 (d, 1H, -O-C-CH=C**H**-), 5.56 (s, 1H, -OCO-C(CH$_3$)=C**H$_2$**), 4.30 (t, 2H, -N-CH$_2$-C**H$_2$**-), 3.50 (m, 2H, N-C**H$_2$**-CH$_2$-), 1.92 (s, 3H, -OCO-C(C**H$_3$**)=CH$_2$), 1.28 (s, 3H, -C-(C**H$_3$**)$_2$), 1.17 (s, 3H, -C-(C**H$_3$**)$_2$); ^{13}C-NMR (125 MHz, CDCl$_3$, Me$_4$Si): δ (ppm) = 167.17, 159.36, 146.62, 141.04, 136.00, 135.66, 128.26, 127.81, 125.88, 122.74, 121.77, 119.89, 118.39, 115.53, 106.72, 106.49, 62.60, 52.77, 42.39, 29.66, 26.87, 25.80, 19.79, 18.32.

4.5.3.5. Synthesis of 3-O-4-vinylbenzoyl-1,2:5,6-di-O-isopropyliden-D-glucofuranose (BipG).

To a mixture of 4-vinylbenzoic acid (2.85 g, 19.3 mmol), 1,2:5,6-di-O-isopropyliden-D-glucofuranose (5.00 g, 19.2 mmol) and 1,3-dicyclohexylcarbodiimide (4.20 g, 20.4 mmol) in dichloromethane (100 mL) was added dimethylaminopyridine

(250 mg, 2.05 mmol), and stirred at room temperature for 24 hours. After the reaction the solid was filtered off, washed several times with dichloromethane and the filtrate was concentrated and finally purified by column chromatography (Silica gel, 10% EtOAc-hexane as eluent).
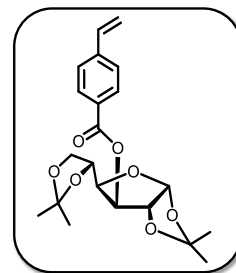
Yield = 6.17 g (81.9%); FAB MS : *m/z* = 413.38 [M+Na]$^{+}$; ^{1}H-NMR (500 MHz, CDCl$_3$, Me$_4$Si): δ (ppm) = 7.99 (d, 2H, aromatic), 7.47 (d, 2H, aromatic), 6.75 (m, 1H, -**CH**=CH$_2$), 6.00 (dd, 1H, -CH=**CH$_2$**), 5.89 (dd, 1H, -O-**CH**(O)-CH-), 5.52 (dd, 1H, -CH=**CH$_2$**), 4.71 (m, 1H, -CH(COOAr)-**CH**(O)-CH-), 4.34 (m, -CH-**CH**(COOAr)-CH-, -CH-**CH**(O)-CH(COOAr)-), 4.10 (m, 1H, -CH$_2$(O)-**CH**(O)-CH), 3.77 (m, 2H, -O-**CH$_2$**-CH(O)-), 1.32-1.42 (m, 12H, -O-C(**CH$_3$**)$_2$-O-) ; ^{13}C-NMR (125 MHz, CDCl$_3$, Me$_4$Si): δ (ppm) = 165, 142.50, 135.8, 130.29, 130.04, 126.26, 117, 112.50, 109.40, 105.50, 83.13, 76.81, 72.59, 68.27, 64.23, 26.82, 25.20.

4.5.3.6. Synthesis of poly(3-O-4-vinylbenzoyl-1,2:5,6-di-O-isopropyliden-D-glucofuranose) (PBipG).

CuBr (10 mg, 0.07 mmol) was added to a 10 mL round bottom flask containing BipG (1.0 g, 2.7 mmol), ethyl-2-bromoisobutyrate (10.6 mg, 0.06 mmol) and PMDETA (9.13 mg, 0.05 mmol) in THF (3.0 mL). The flask was sealed with rubber septum and was purged with argon for 20 minutes before adding the catalyst. The flask was placed in a preheated oil bath at 60 ^{0}C for 24 hours. The viscous liquid was dissolved in THF and was passed through a neutral alumina column to remove the catalyst and was then concentrated and precipitated in methanol twice.

Yield = 675 mg (67.5%); ^{1}H-NMR (500 MHz, CDCl$_3$, Me$_4$Si): δ (ppm) = 7.59 (m, 2H, aromatic), 6.40 (m, 2H, aromatic), 5.97 (m , 1H), 5.37 (m, 1H), 4.69 (m, 1H,), 4.31 (m,

2H), 4.06 (m, 2H), 1.55-1.60 (m, 3H, -**CH₂CH**-), 1.25-1.38 (m, 12H, -O-C(**CH₃**)₂-O-);

M_n = 12,499, M_w/M_n = 1.23.

4.5.3.7. Synthesis of poly(spiropyran)-b-poly(3-O-4-vinylbenzoyl-1,2:5,6-di-O-isopropyliden-D-glucofuranose) (PSP-b-PBipG).

CuBr (11 mg, 0.08 mmol) was added to a 10 mL round bottom flask containing SPM (500 mg, 1.19 mmol), PBipG (500 mg, 0.04 mmol) and PMDETA (12.5 mg, 0.07 mmol) in THF (3.0 mL). The flask was sealed with rubber septum and was purged with argon for 20 minutes before adding the catalyst. The flask was placed in a preheated oil bath at 60 ^{0}C for 24 hours. The viscous liquid was dissolved in THF and was passed through a neutral alumina column to remove the catalyst and was then concentrated and precipitated in methanol thrice.
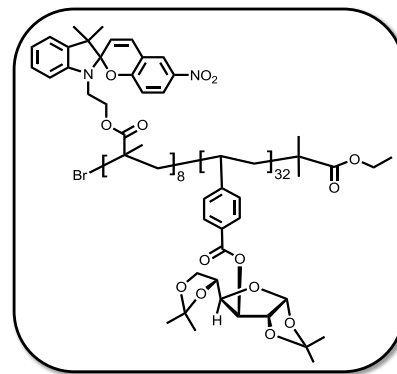
Yield = 612 mg (61.20%); ^{1}H-NMR (500 MHz, CDCl₃, Me₄Si): δ (ppm) = 7.89 (m, 2H, aromatic), 7.63 (m, 2H, aromatic), 7.03 (m, 2H, aromatic) , 6.80 (m, 2H, aromatic, -O-C-CH=**CH**-), 6.58 (m, 2H, aromatic), 6.41 (m, 2H, aromatic), 5.97 (m , 1H), 5.77 (m, 1H, -O-C-C**H**=CH-), 5.40 (m, 1H), 4.72 (m, 1H), 4.32 (m, 2H), 4.08 (m, 2H), 3.94 (m, 2H, -N-CH₂-**CH₂**-), 3.41 (m, 2H, -N-C**H₂**-CH₂-), 1.55-1.60 (m, 3H, -**CH₂CH**-), 1.25-1.38 (m, 12H, -O-C(**CH₃**)₂-O-), 0.77-1.08 (m, 5H, -(**CH₃**)C(COOSP)C**H₂**-); GPC (THF): M_n = 15,791, M_w/M_n = 1.45.

4.5.3.8. Synthesis of poly(spiropyran)-b-poly(3-O-4-vinylbenzoyl-D-glucopyranose) (PSP-b-PBG).

100 mg of the protected polymer **PSP-b-PBipG** was dissolved in 80% formic acid (10 mL) and stirred for 48 hours at room temperature. Additional 5 mL water was added and stirred for another 3 hours. The solution was dialyzed against distilled water for 2 days, concentrated in-vacuum and finally lyophilized to give **PSP-b-PBG** in quantitative yield.
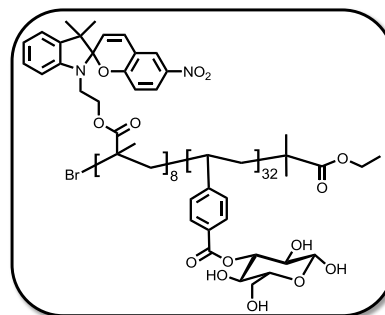
4.5.3.9. Synthesis of 4-(4-Methoxyphenylazo)phenol (5).

A solution of NaNO$_2$ (3.0 g, 43.5 mmol) in distilled water (15 mL) was added slowly with vigorous stirring to a solution of p-anisidine (5.0 g, 40.7 mmol) in 3 M HCl (50 mL) at 0 ^{0}C. To the resulting diazonium salt a stirred solution of phenol (3.82 g, 40.6 mmol) in 10% aq. NaOH (40 mL) was added at 0 ^{0}C. The dark brown suspension was acidified and the precipitate collected. The crude product was washed with copious amounts of water and finally purified by column chromatography. (Silica gel, 10% EtOAc-hexane as eluent).
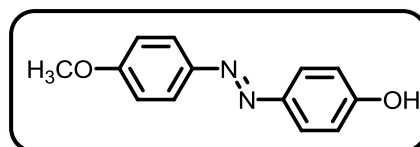
Yield = 5.13g (55.4%); m.p. = 137 ^{0}C; FAB MS : m/z = 229.44 [M+H]$^+$; ^{1}H-NMR (500 MHz, CDCl$_3$, Me$_4$Si): δ (ppm) = 7.88-7.81 (m, 4H, aromatic), 7.01-6.91 (m, 4H, aromatic), 3.88 (s, 3H, -O-C**H$_3$**); ^{13}C-NMR (CDCl$_3$): δ = 157.95, 157.64, 146.94, 125.14, 124.72, 123.54, 115.98, 114.07, 56.11.

4.5.3.10. Synthesis of 6-[4-(4-Methoxyphenylazo)phenoxy]hexanol (6).

4 (2.0 g, 8.8 mmol) was dissolved in ethanol (35 mL) and 3.0 g K$_2$CO$_3$ (21.7 mmol) was added. Then 6-
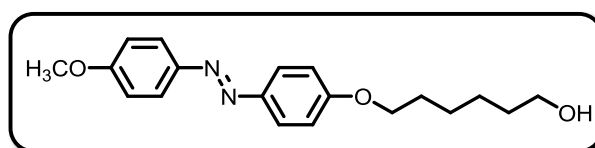
bromohexanol (2.05 g, 11.5 mmol) was added and the mixture refluxed for 24 hours. The solvent was removed under reduced pressure, and dil. HCl was added to acidify the mixture. The precipitate was filtered, washed several times with water and finally purified by column chromatography. (Silica gel, 10% EtOAc-hexane as eluent).

Yield = 2.6 g (90.7%); m.p. = 124 ^{0}C; FAB MS : m/z = 329.80 $[M+H]^+$; ^{1}H-NMR (500 MHz, CDCl$_3$, Me$_4$Si): δ (ppm) = 7.98-7.85 (m, 4H, aromatic), 7.01-6.96(m, 4H, aromatic), 4.03(t, 2H, -O-C**H$_2$**-CH$_2$-), 3.87 (s, 3H, -O-C**H$_3$**), 3.66 (t, 2H, -CH$_2$-C**H$_2$**-OH), 1.85-1.26(m, 8H, -CH$_2$-(C**H$_2$**)$_4$-CH$_2$-OH); ^{13}C-NMR (125 MHz, CDCl$_3$, Me$_4$Si): δ (ppm) = 161.48, 161.10, 147.04, 146.89, 124.30, 114.62, 114.13, 68.12, 62.82, 55.51, 32.61, 29.14, 25.82, 25.51.

4.5.3.11. Synthesis of 6-[4-(4-Methoxyphenylazo)phenoxy]hexayl methacrylate (MAzo).

To a mixture of **5** (1.0 g, 3.0 mmol), methacrylic acid (300 mg, 3.5 mmol) and 1,3-dicyclohexylcarbodiimide (720 mg, 3.50 mmol) in dichloromethane (40 mL) was added dimethylaminopyridine (40 mg, 0.35 mmol), an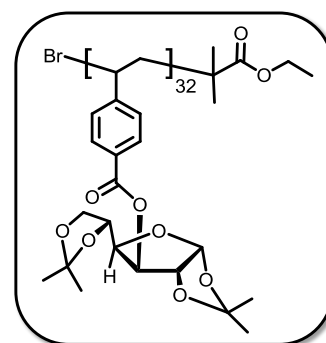d stirred at room temperature for 24 hours. After the reaction the solid was filtered off, washed several times with dichloromethane and the filtrate was concentrated and finally purified by column chromatography (Silica gel, 10% EtOAc-hexane as eluent).
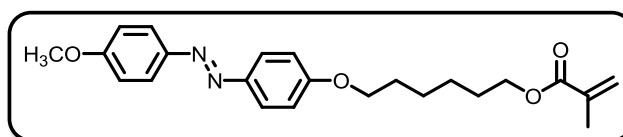
Yield = 730 mg (60.4%); m.p. = 82 ^{0}C; FAB MS : m/z = 397.71 $[M+H]^+$; ^{1}H-NMR (500 MHz, CDCl$_3$, Me$_4$Si): δ (ppm) = 7.88-7.85 (m, 4H, aromatic), 7.00-6.97 (m, 4H, aromatic), 6.10 (s, 1H, -OCO-C(CH$_3$)=C**H$_2$**), 5.55(s, 1H, -OCO-C(CH$_3$)=C**H$_2$**), 4.17 (t, 2H, -C**H$_2$**-OCO-), 4.03 (t, 2H, -O-C**H$_2$**-CH$_2$-), 3.87 (s, 3H, -O-C**H$_3$**), 1.94 (s, 3H, -OCO-C(C**H$_3$**)=CH$_2$), 1.83-1.26 (m, 8H, -CH$_2$-(C**H$_2$**)$_4$-CH$_2$) ; ^{13}C-NMR (125 MHz, CDCl$_3$, Me$_4$Si): δ (ppm) = 167.50, 161.49, 161.05, 147.01, 136.42, 125.31, 124.81, 123.72, 114.41, 113.96, 68.01, 64.59, 56.04, 29.05, 28.50, 26.38, 25.72, 18.34.

4.5.3.12. Synthesis of poly(6-[4-(4-Methoxyphenylazo)phenoxy]hexayl methacrylate)-b-poly(3-O-4-vinylbenzoyl-1,2:5,6-di-O-isopropyliden-D-glucofuranose) (PMAzo-b-PBipG).

CuBr (11.0 mg, 0.08 mmol) was added to a 10 mL round bottom flask containing MAzo (500 mg, 1.26 mmol), PBipG (500 mg, 0.04 mmol) and PMDETA (12.45 mg, 0.07 mmol) in THF (3.0 mL). The flask was sealed with rubber septum and was purged with argon for 20 minutes before adding the catalyst. The flask was placed in a preheated oil bath at 60 ^{0}C for 24 hours. The viscous liquid was dissolved in THF and was passed through a neutral alumina column to remove the catalyst and was then concentrated and precipitated in methanol thrice.
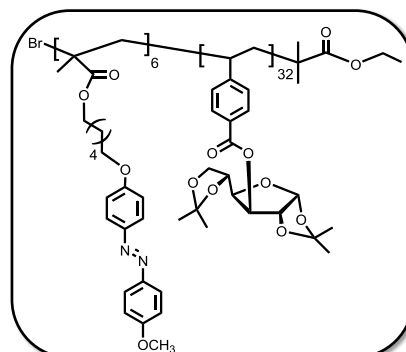
Yield = 475 mg (47.5%); ^{1}H-NMR (500 MHz, CDCl$_3$, Me$_4$Si): δ (ppm) = 7.81 (m, 4H, aromatic), 7.59 (m, 2H, aromatic), 6.93 (m, 4H, aromatic), 6.40 (m, 2H, aromatic), 5.97 (m , 1H), 5.37 (m, 1H), 4.69 (m, 1H,), 4.31 (m, 2H), 4.06 (m, 2H), 3.88 (m, 3H, -O-C**H$_3$**), 3.83 (m, 4H, -O-C**H$_2$**-(CH$_2$)$_4$-C**H$_2$**-), 1.55-1.60 (m, 3H, -C**H$_2$**CH-), 1.42 (m, 8H, -O-CH$_2$-(C**H$_2$**)$_4$-CH$_2$-), 1.25-1.38 (m, 12H, -O-C(C**H$_3$**)$_2$-O-), 0.83-1.00 (m, 5H, -(C**H$_3$**)C(COOAzo)C**H$_2$**-) ; GPC (THF): M$_n$ = 15,049, M$_w$/M$_n$ = 1.32.

4.5.3.13. Synthesis of poly(6-[4-(4-Methoxyphenylazo)phenoxy]hexayl methacrylate)-b-poly(3-O-4-vinylbenzoyl-D-glucopyranose) (PMAzo-b-PBG).

100 mg of the protected polymer **PMAzo-b-PBipG** was dissolved in 80% formic acid (10 mL) and stirred for 48 hours at room temperature. Additional 5 mL water was added and stirred for another 3 hours. The solution was dialyzed against distilled water for 2 days, concentrated in-vacuum and finally lyophilized to give **PMAzo-b-PBG** in quantitative yield.
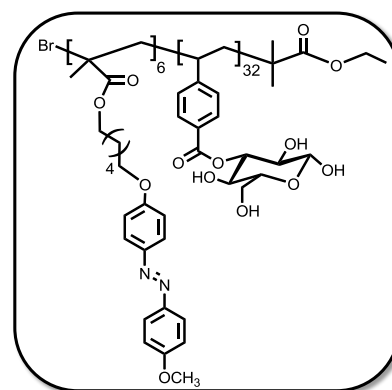
References

Aggarwal, B. B.; Shishodia, S. 'Molecular targets of dietary agents for prevention and therapy of cancer' *Biochemical Pharmacology* 71 (**2006**) 1397-1421.

Alarcón, C. I. H.; Pennadam, S.; Alexander, C. 'Stimuli responsive polymers for biomedical applications' *Chem. Soc. Rev.* 34 (**2005**) 276-285.

Alexandridis, P.; Lindman, B., Eds. 'Amphiphilic block copolymers - Self-assembly and applications' *Elsevier*: Amsterdam, **2000**.

Astafieva, I.; Zhong, X. F.; Eisenberg, A. 'Critical micellization phenomena in block polyelectrolyte solutions' *Macromolecules* 26 (**1993**) 7339-7352.

Babin, J.; Pelletier, M.; Lepage, M.; Allard, J.-F.; Morris, D.; Zhao, Y. 'A new two-photon-sensitive block copolymer nanocarrier' *Angew. Chem. Int. Ed.* 48 (**2009**) 3329-3332.

Bang, J.; Jain, S.; Li, Z; Lodge, T. P. 'Sphere, cylinder and vesicle nanoaggregates in poly(styrene-b-isoprene) diblock copolymer solutions' *Macromolecules* 39 (**2006**) 1199-1208.

Barker, S. L. R.; Ross, D.; Tarlov, M. J.; Gaitan, M.; Locascio, L. E. 'Control of flow direction in microfluidic devices with polyelectrolyte multilayers' *Anal. Chem.* 72 (**2000**) 5925–5929.

Bates, F. S. 'Polymer-polymer phase behaviour' *Science* 251 (**1991**) 898-905.

Bates, F. S.; Fredrickson, G. H. 'Block copolymers – designer soft materials' *Phys. Today* 52 (**1999**) 32-38.

Battaglia, G.; Ryan, A. J. 'The evolution of vesicles from bulk lamellar gels' *Nature Mater.* 4 (**2005**) 869-876.

Bawa, P.; Pillay, V.; Choonara, Y. E.; du Toit, L. C. 'Stimuli-responsive polymers and their applications in drug delivery' *Biomed. Mater.* 4 (**2009**) 1-15.

Bigot, J.; Charleux, B.; Cooke, G.; Delattre, F.; Fournier, D.; Lyskawa, J.; Sambe, L.; Stoffelbach, F.; Woisel, P. 'Tetrathiafulvalene end-functionalized poly(*N*-isopropylacrylamide): A new class of amphiphilic polymer for the creation of multistimuli responsive micelles' *J. Am. Chem. Soc.* 132 (**2010**) 10796-10801.

Bisht, S.; Feldmann, G.; Soni, S.; Ravi, R.; Karikar, C.; Maitra, A.; Maitra, A. 'Polymeric nanoparticle-encapsulated curcumin ("nanocurcumin"): A novel strategy for human cancer therapy' *J. Nanobio.* 5:3 (**2007**) 1-18.

Blanazs, A.; Armes, S. P.; Ryan, A. J. 'Self-assembled block copolymer aggregates: from micelles to vesicles and their biological applications' *Macromol. Rapid Commun.* 30 (**2009**) 267-277.

Boffa, L. S.; Novak, B. M., Eds. 'Transition metal catalysis in macromolecular design' *ACS Symposium Series 760*: Washington DC, **2000**.

Boyer, C.; Bulmus, V.; Davis, T. P.; Ladmiral, V.; Liu, J.; Perrer, S. 'Bioapplications of raft polymerization' *Chem. Rev.* 109 (**2009**) 5402-5436.

Braun, D. 'Initiation of free radical polymerization by thermal cleavage of carbon-carbon bonds' *Macromol. Symp.* 111 (**1996**) 63-71.

Braunecker, W. A.; Matyjaszewski, K., 'Controlled/living radical polymerization: Features, developments and perspectives' *Prog. Polym. Sci.* 32 (**2007**) 93-146.

Burattini, S.; Colquhoun, H. M.; Greenland, B. W.; Hayes, W.; Wade, M. 'Pyrene-functionalised, alternating copolyimide for sensing nitroaromatic compounds' *Macromol. Rapid Commun.* 30 (**2009**) 459-463.

Burke, S. E.; Eisenberg, A. 'Effect of sodium dodecyl sulfate on the morphology of polystyrene-b-poly(acylic acid) aggregates in dioxane-water mixtures' *Langmuir* 17 (**2001**) 8341–8347.

Burke, S. E.; Eisenberg, A. 'Kinetics and mechanisms of the sphere-to-rod and rod-to-sphere transitions in the ternary system PSt_{310}-b-PAA_{52}/dioxane/H_2O' *Langmuir* 17 (**2001**) 6705-6714.

Cameron, N. S.; Corbierre, M. K.; Eisenberg, A. 'Asymmetric amphiphilic block copolymers in solution: A morphological wonderland' *Can. J. Chem.* 77 (**1999**) 1311-1326.

Chen, J.; Zeng, F.; Wu, S.; Zhao, J.; Chen, Q.; Tong, Z. 'Reversible fluorescence modulation through energy transfer with ABC triblock copolymer micelles as scaffolds' *Chem. Commun.* 43 (**2008**) 5580-5582.

Chen, X. M.; Dordick, J. S.; Rethwisch, D. G. 'Chemoenzymic synthesis and characterization of poly(.alpha.-methyl galactoside 6-acrylate) hydrogels' *Macromolecules* 28 (**1995**) 6014-6019.

Chen, X. R.; Ding, X. B.; Zheng, Z. H.; Peng, Y. X. 'Thermosensitive cross-linked polymer vesicles for controlled release system' *New J. Chem.* 30 (**2006)** 577–582.

Chiefari, J.; Chong, Y. K. (Bill); Ercole, F.; Krstina, J.; Jeffery, J.; Le, T. P. T.; Mayadunne, R. T. A.; Meijs, G. F.; Moad, C. L.; Moad, G.; Rizzardo, E.; Thang, S. H. 'Living free-radical polymerization by reversible-addition fragmentation chain transfer: The RAFT process' *Macromolecules* 31 (**1998**) 5559-5562.

Choi, D. H.; Ban, S. Y.; Kim, J. H.; 'Stability of photochromism in new bifunctional copolymers containing spiropyran and chalcone moiety in the side chain' *Bull. Korean Chem. Soc.* 24 (**2003**) 441-445.

Chong, Y. K. (Bill); Le, T. P. T.; Moad, G.; Rizzardo, E.; Thang, S. H. 'A more versatile route to block copolymers and other polymers of complex architecture by living radical polymerization: The RAFT process' *Macromolecules* 32 (**1999**) 2071-2074.

Choucair, A.; Eisenberg, A. 'Control of amphiphilic block copolymer morphologies using solution conditions' Eur. *Phys. J.* 10 (**2003**) 37-44.

Das, M.; Zhang, H.; Kumacheva, E. 'Microgels - Old materials with new applications' *Ann. Rev. Mater. Res.* 36 (**2006**) 117-142.

Davis, M. E.; Chen, Z.; Shin, D. M. 'Nanoparticle therapeutics: An emerging treatment modality for cance*r*' *Nat. Rev. Drug Discovery 7* (**2008**) 771–782.

Deepak, V. D.; Asha, S. K. 'Photophysical investigation into the self-organization in pyrene-based urethane methacrylate comb polymer' *J. Phys. Chem. B* 113 (**2009**) 11887-11897.

Desjardins, A.; Eisenberg, A. 'Colloidal properties of block ionomers. 1. Characterization of reverse micelles of styrene-b-metal methacrylate diblocks by size exclusion chromatography' *Macromolecules* 24 (**1991**) 5779-5790.

Desjardins, A.; Van de Ven, T. G. M.; Eisenberg, A. 'Colloidal properties of block ionomers. 2. Characterization of reverse micelles of styrene-b-methacrylic acid and styrene-b-metal methacrylate diblocks by size exclusion chromatography' *Macromolecules* 25 (**1992**) 2412-2421.

Discher, D. E.; Eisenberg, A. 'Polymer vesicles' *Science* 287 (**2002**) 967-973.

Dordick, J. S.; Linhardt, R. J.; Rethwisch, D. G. 'Enzymatic and chemoenzymatic preparation of hydrophilic polymers and gels' *Chemtech* 24 (**1994**) 33-39.

Du, J.; Chen, Y.; Zhang, Y.; Han, C. C.; Fischer, K.; Schmidt, M. 'Organic/inorganic hybrid vesicles based on a reactive block copolymer' *J. Am. Chem. Soc.1*25 (**2003**) 14710-14711.

Duhamel, J. 'Polymer chain dynamics in solution probed with a fluorescence blob model' *Acc. Chem. Res.* 39 (**2006**) 953-960.

Edmondson, S.; Osborne, V. L.; Huck, W. T. S. 'Polymer brushes *via* surface-initiated polymerizations' *Chem. Soc. Rev. 33* (**2004**) 14-22.

Entezami, A. A.; Abbasian, M. 'Recent advances in synthesis of new polymers by living free radical polymerization' *Iran. Polym. J.* 15 (**2006**) 583-611.

Evans, D. F.; Wennerström, H. 'The colloidal domain: Where physics, chemistry, biology, and technology meet' *Wiley-VCH*: New York, **1994**.

Fredrickson, G. H.; Bates, F. S. 'Dynamics of block copolymers: Theory and experiment' *Annu. Rev. Mater. Sci.* 26 (**1996**) 501-550.

Froster, S.; Antonietti, M. 'Amphiphilic block copolymers in structure controlled nanomaterial hybrids' *Adv. Mater.* 10 (**1998**) 195-217.

Gädt, T.; Ieong, N. S.; Cambridge, G.; Manners, I.; Winnik, M. A. 'Complex and hierarchical micelle architectures from diblock copolymers using living, crystallization-driven polymerizations' *Nature Mater.* 8 (**2009**) 144-150.

Galaev, I. Y.; Mattiasson, B. 'Smart polymers and what they could do in biotechnology and medicine' *Trends Biotechnol.* 17 (**1999**) 335–340.

Gao, Z.; Desjardins, A.; Eisenberg, A. 'Solubilization equilibria of water in nonaqueous solutions of block ionomer reverse micelles: An NMR study' *Macromolecules* 25 (**1992**) 1300-1303.

Gil, E. S.; Hudson, S. M. 'Stimuli-reponsive polymers and their bioconjugates' *Prog. Polym. Sci.* 29 (**2004**) 1173-1222.

Gupta, P.; Vermani, K.; Garg, S. 'Hydrogels: From controlled release to pH-responsive drug delivery' *Drug Discov. Today* 7 (**2002**) 569–579.

Hales, M.; Barner-Kowollik, C.; Davis, T. P.; Stenzel, M. H. 'Shell-cross-linked vesicles synthesized from block copolymers of poly(d,l-lactide) and poly(*N*-isopropyl acrylamide) as thermoresponsive nanocontainers' *Langmuir* 20 (**2004**) 10809–10817.

Hamley, I. W. 'Introduction to soft matter' *Wiley*: Chichester, **2000**.

Hamley, I. W. 'The physics of block copolymers' *Oxford University Press*: Oxford, **1998**.

Han, D.; Tong, X.; Zhao, Y. 'Fast photodegradable block copolymer micelles for burst release' *Macromolecules* 44 (**2011**) 437-439.

Hawker, C. J.; Barclay, G. G.; Orellana, A.; Dao, J.; Devonport, W. 'Initiating systems for nitroxide mediated "living" free radical polymerizations: Synthesis and evaluation' *Macromolecules* 29 (**1996**) 5245-5254.

Hawker, C. J.; Bosman, A. W.; Harth, E. 'New polymer synthesis by nitroxide mediated living radical polymerization' *Chem. Rev.* 101 (**2001**) 3661-3688.

Huang, C.-K.; Lo, C.-L.; Chen, H.-H.; Hsiue, G.-H. 'Multifunctional micelles for cancer cell targeting, distribution imaging, and anticancer drug delivery' *Adv. Funct. Mater.* 17 (**2007**) 2291–2297.

Ichimura, K. 'Photoalignment of liquid-crystal systems' *Chem. Rev.* 100 (**2000**) 1847-1874.

Jeong, B.; Kim, S. W.; Bae, Y. H. 'Thermosensitive sol–gel reversible hydrogels' *Adv. Drug Delivery Rev.* 54 (**2002**) 37-51.

Jiang, J.; Qi, B.; Lepage, M.; Zhao, Y. 'Polymer micelles stabilization on demand through reversible photo-cross-linking' *Macromolecules* 40 (**2007**) 790-792.

Jiang, J.; Tong, X.; Morris, D.; Zhao, Y. 'Toward photocontrolled release using light-dissociable block copolymer micelles' *Macromolecules* 39 (**2006**) 4633-4640.

Jiang, J.; Tong, X.; Zhao, Y. 'A New Design for Light-Breakable Polymer Micelles' *J. Am. Chem. Soc.* 127 (**2005**) 8290-8291.

Jönsson, B.; Lindman, B.; Holmberg, K.; Kronberg, B. 'Surfactants and polymers in aqueous solution' *J. Wiley and Sons*: Chichester, **1998**.

Juodkazis, S.; Mukai, N.; Wakaki, R.; Yamaguchi, A.; Matsuo, S.; Misawa, H. 'Reversible phase transitions in polymer gels induced by radiation forces' *Nature* 408 (**2000**) 178-181.

Kamigaito, M.; Ando, T.; Sawamoto, M. 'Metal-catalyzed living radical polymerization' *Chem. Rev.* 101 (**2001**) 3689-3745.

Keerl, M.; Smirnovas, V.; Winter, R.; Richtering, W. 'Copolymer microgels from mono- and disubstituted acrylamides: Phase behavior and hydrogen bonds' *Macromolecules* 41 (**2008**) 6830-6836.

Khandpur, A. K.; Forster, S.; Bates, F. S.; Hamley, I. W.; Ryan, A. J.; Bras, W.; Almdal, K.; Mortensen, K. 'Polyisoprene-polystyrene diblock copolymer phase diagram near the order-disorder transition' *Macromolecules* 28 (**1995**) 8796-8806.

Khougaz, K.; Astafieva, I.; Eisenberg, A. 'Micellization in block polyelectrolyte solutions. 3. Static light scattering characterization' *Macromolecules* 28 (**1995**) 7135-7147.

Kikuchi, A.; Okano, T. 'Pulsatile drug release control using hydrogels' *Adv. Drug Delivery Rev.* 54 (**2002**) 53–77.

Kim, H.-C., Park, S.-M.; Hinsberg, W. D. 'Block copolymer based nanostructures: materials, processes, and applications to electronics' *Chem. Rev.* 110 (**2010**) 146-177.

Kim, S. J.; Park, S. J.; Lee, S. M.; Lee, Y. M.; Kim, H. C.; Kim, S. I. 'Electroactive characteristics of interpenetrating polymer network hydrogels composed of poly(vinyl alcohol) and poly(*n*-isopropylacrylamide)' *J. Appl. Polym. Sci.* 89 (**2003**) 890–894.

Klaikherd, A.; Nagamani; C.; Thayumanavan, S. 'Multi-stimuli sensitive amphiphilic block copolymer assemblies' *J. Am. Chem. Soc.* 131 (**2009**) 4830-4838.

Klein, J.; Kunz, M.; Kowalczyk, J. 'Poly(vinylsaccharide)s, 7 new surfactant polymers based on carbohydrates' *Makromol. Chem.* 191 (**1990**) 517-528.

Klok, H.-A.; Lecommandoux, S. 'Supramolecular materials via block copolymer self-assembly' *Adv. Mater.* 13 (**2001**) 1217-1229.

Kost, J.; Langer, R. 'Responsive polymeric delivery systems' *Adv. Drug. Deliv. Rev.* 46 (**2001**) 125–148.

Kumar, A.; Srivastava, A.; Galaev, I. Y.; Mattiasson, B. 'Smart Polymers: Physical Forms and Bioengineering Applications' *Prog. Polym. Sci.* 32 (**2007**) 1205–1237.

Kumar, G. S.; Neckers, D. C. 'Photochemistry of azobenzene-containing polymers' *Chem. Rev.* 89 (**1989**) 1915-1925.

Ladmiral, V.; Melia, E.; Haddleton, D. M. 'Synthetic glycopolymers: an overview' *Eur. Polym. J.* 40 (**2004**) 431-449.

Lakowicz, J. R. 'Principles of Fluorescence spectroscopy', *Springer*: New York, 3rd edition, **2006**.

Larsson, K. 'Lipids − Molecular organization, physical functions and technical applications' *The Oily Press Ltd.*: Scotland, **1994**.

Laughlin, R. G. 'The aqueous phase behaviour of surfactants' *Academic Press*: London, **1994**.

Lazzari, M.; Liu, G.; Lecommandoux, S., Eds. 'Block copolymers in nanoscience' *Wiley-VCH*: Weinheim, **2006**.

Lee, H.; Wu, W.; Oh, J. K.; Mueller, L.; Sherwood, G.; Peteanu, L.; Kowalewski, T.; Matyjaszewski, K. 'Light-induced reversible formation of polymeric micelles' *Angew. Chem. Int. Ed.* 46 (**2007**) 2453-2457.

Leibler, L. 'Theory of microphase separation in block copolymers' *Macromolecules* 13 (**1980**) 1602-1617.

Li, G.; Song, S.; Guo, L.; Ma, S. 'Self-assembly of thermo- and pH-responsive poly(acrylic acid)-b-poly(N-isopropylacrylamide) micelles for drug delivery' *J. Polym. Sci. Part A: Polym. Chem.* 46 (**2008**) 5028-5035.

Li, M.-H; Keller, P. 'Stimuli-responsive polymer vesicles' *Soft Matter* 5 (**2009**) 927-937.

Li, S. K.; D'Emanuele, A. 'On–off transport through a thermoresponsive hydrogel composite membrane' *J. Controlled Release* 75 (**2001**) 55–67.

Li, Y.; Lokitz, B. S.; McCormick, C. L. 'Thermally responsive vesicles and their structural "locking" through polyelectrolyte complex formation' *Angew. Chem. Int. Ed.* 45 (**2006**) 5792–5795.

Li, Z.-C.; Liang, Y.-Z.; Chen, G.-Q.; Li, F.-M. 'Synthesisnof amphiphilic block copolymers with well-defined glycopolymer segment by atom transfer radical polymerization' *Macromol. Rapid Commun.* 21 (**2000**) 375-380.

Li, Z.-C.; Liang, Y.-Z.; Li, F.-M. 'Additives induced morphological transition of molecular assemblies from PS-b-PGEA in aqueous solutions' *New J. Chem.* 26 (**2002**) 1805-1810.

Liang, Y.-Z.; Li, Z.-C.; Li, F.-M. 'Multiple morphologies of molecular assemblies formed by polystyrene-block-poly[2-(β-D-glucosyloxy)ethyl acrylate] in water' *New J. Chem.* 24 (**2000**) 323-328.

Liu, R.; Winnik, M. A.; Di Stefano, F.; Vanketessan, J. 'Polymerizable anthracene derivatives for labeling emulsion copolymers' *J. Polym. Sci. Part A*: *Polym. Chem.* 39 (**2001**) 1495-1504.

Lou, X.; Daussin, R.; Cuenot, S.; Duwez, A.-S.; Pagnoulle, C.; Detrembleur, C.; Bailly, C.; Jérôme, R. 'Synthesis of pyrene-containing polymers and noncovalent sidewall functionalization of multiwalled carbon nanotubes' *Chem. Mater.* 16 (**2004**) 4005-4011.

Lowe, A. B.; McCormick, C. L. 'Reversible addition–fragmentation chain transfer (raft) radical polymerization and the synthesis of water-soluble (co)polymers under homogeneous conditions in organic and aqueous media' *Prog. Polym. Sci.* 32 (**2007**) 283-351.

Lu, F.-Z; Meng, J.-Q.; Du, F.-S.; Li, Z.-C; Zhang, B.-Y. 'Pyrene end-labeled diblock glycopolymers: Synthesis and aggregation' *Macromol. Chem. Phys.* 206 (**2005**) 513-520.

Martin, R. E.; Diederich, F. 'Linear monodisperse π-conjugated oligomers: model compounds for polymers and more' *Angew. Chem. Int. Ed. Engl.* 38 (**1999**) 1350-1377.

Massey, J. A.; Power, K. N.; Manners, I.; Winnik, M. A. 'Self-assembly of a novel organometallic-inorganic block copolymer in solution and the solid state: Nonintrusive observation of novel wormlike poly(ferrocenyldimethylsilane)-b-poly(dimethylsiloxane) micelles' *J. Am. Chem. Soc.* 120 (**1998**) 9533-9540.

Massey, J. A.; Temple, K.; Cao, L.; Rharbi, Y.; Raez, J.; Winnik, M. A.; Manners, I. 'Self-assembly of organometallic block copolymers: The role of crystallinity of the core-forming polyferrocene block in the micellar morphologies formed by poly(ferrocenylsilane-*b*-dimethylsiloxane) in *n*-alkane solvents' *J. Am. Chem. Soc. 122* (**2000**) 11577-11584.

Matsumura, Y.; Maeda, H. 'A new concept for macromolecular therapeutics in cancer chemotherapy: Mechanism of tumoritropic accumulation of proteins and the antitumor agent smancs' *Cancer Res. 46* (**1986**) 6387–6392.

Matyjaszewski, K. 'Controlled polymer structures by atom transfer radical polymerization and other controlled/living radical polymerizations' *Macromol. Symp.* 195 (**2003**) 25-31.

Matyjaszewski, K. 'Lifetime of polystyrene chains in atom transfer radical polymerization' *Macromolecules* 32 (**1999**) 9051-9053.

Matyjaszewski, K. 'Mechanistic features and radical intermediates in atom transfer radical polymerization' *Macromol. Symp.* 183 (**2002**) 71-81.

Matyjaszewski, K. 'Transition Metal catalyses in controlled radical polymerization: Atom transfer radical polymerization' *Chem. Eur. J.* 5 (**1999**) 3095-3102.

Matyjaszewski, K., Ed. 'Controlled radical polymerization' *ACS Symposium Series 685:* Washington, **1998**.

Matyjaszewski, K., Ed. 'Controlled/living radical polymerization, progress in ATRP, NMP, and RAFT' *ACS Symposium Series 768*: Washington DC, **2000**.

Matyjaszewski, K.; Xia, J. 'Atom transfer radical polymerization' *Chem. Rev.* 101 (**2001**) 2921-2990.

Meier, H. 'The photochemistry of stilbenoid compounds and their role in materials technology' *Angew. Chem. Int. Ed. Engl.* 31 (**1992**) 1399-1540.

Meng, F.; Zhong, Z.; Feijen, J. 'Stimuli-responsive polymersomes for programmed drug delively' *Biomacromolecules* 10 (**2009**) 197–209.

Muthukrishnan, S.; Jutz, G.; André, X.; Mori, H.; Müller, A. H. E. 'Synthesis of hyperbranched glycopolymers via self-condensing atom transfer radical copolymerization of a sugar-carrying acrylate' *Macromolecules* 38 (**2005**) 9-18.

Namazi, H.; Sharifzadeh, R. 'Regioselective synthesis of vinylic derivatives of common monosccarides through their activated stannylene acetal intermediates' *Molecules* 10 (**2005**) 772-782.

Natansohn, A.; Rochon, P. 'Photoinduced motions in azo-containing polymers' *Chem. Rev.* 102 (**2002**) 4139-4176.

Ohm, C.; Brehmer, M.; Zentel, R. 'Liquid crystalline elastomers as actuators and sensors' *Adv. Mater.* 22 (**2010**) 3366-3387.

Ohno, K.; Tsuji, Y.; Yamamoto, S.; Miyamoto, T.; Fukuda, T. 'Nitroxide-controlled free radical polymerization of a sugar-carrying acryloyl monomer' *Macromol. Chem. Phys.* 200 (**1999**) 1619-1625.

Okada, M. 'Molecular design and synthesis of glycopolymers' *Prog. Polym. Sci.* 26 (**2001**) 67-104.

Otsu, T.; Yoshida, M. 'Role of initiator-transfer agent-terminator (iniferter) in radical polymerizations: Polymer design by organic disulfides as iniferters' *Makromol. Chem. Rapid Commun.* 3 (**1982**) 127-132.

Ouchi, M.; Terashima, T.; Sawamoto, M. 'Transition metal-catalyzed living radical polymerization: Towards perfection in catalysis and precision polymer synthesis' *Chem. Rev.* 109 (**2009**) 4963-5050.

Pasparakis, G.; Cockayne, A.; Alexander, C.; 'Control of bacterial aggregation by thermoresponsive glycopolymer' *J. Am. Chem. Soc.* 129 (**2007**) 11014-11015.

Patten, T. E.; Matyjaszewski, K., 'Atom transfer radical polymerization and synthesis of polymeric materials' *Adv. Mater.* 10 (**1998**) 901-915.

Patten, T. E.; Xia, J.; Abernathy, T.; Matyjaszewski, K. 'Polymers with very low polydispersities from atom transfer radical polymerization' *Science* 272 (**1996**) 866-868.

Patten, T. E.; Xia, J.; Matyjaszewski, K. 'Controlled / "living" radical polymerization. Kinetics of the homogeneous atom transfer radical polymerization of styrene' *J. Am. Chem. Soc.* 119 (**1997**) 674-680.

Petronio, M. G.; Mansi, A.; Gallinelli, C.; Pisani, S.; Seganti, L.; Chiarini, F. 'In vitro effect of natural and semi-synthetic carbohydrate polymers on chlamydia trachomatis infection' *Chemotherapy* 43 (**1997**) 211-217.

Pincock, J. 'Photochemistry of arylmethyl esters in nucleophilic solvents: Radical pair and ion pair intermediates' *Acc. Chem. Res.* 30 (**1997**) 43-49.

Pochan, D. J.; Chen, Z.; Cui, H.; Hales, K.; Qi, K.; Wooley, K. L. 'Toroidal triblock copolymer assemblies' *Science 306* (**2004**) 94-97.

Qiu, Y.; Park, K. 'Environment-sensitive hydrogels for drug delivery' *Adv. Drug. Deliv. Rev.* 53 (**2001**) 321–339.

Raula, J.; Shan, J.; Nuopponen, M.; Niskanen, A.; Jiang, H.; Kauppinen, E. I.; Tenhu, H. 'Synthesis of gold nanoparticles grafted with a thermoresponsive polymer by surface-induced reversible-addition-fragmentation chain-transfer polymerization' *Langmuir* 19 (**2003**) 3499–3504.

Riegel, I. C.; Samios, D.; Petzhold, C. L.; Eisenberg, A. 'Self-assembly of amphiphilic di and triblock copolymers of styrene and quaternized 5(n,n-diethylamino)isoprene in selective solvents' *Polymer* 44 (**2003**) 2117-2128.

Riehemann, K.; Schneider, S. W.; Luger, T. A.; Godin, B.; Ferrari, M.; Fuchs, H. 'Nanomedicine-challenge and perspectives' *Angew. Chem. Int. Ed. 48* (**2009**) 872–897.

Riess, G. 'Micellization of block copolymers' *Prog. Polym. Sci.* 28 (**2003**) 1107-1170.

Rofstad, E. K.; Mathiesen, B.; Kindem, K.; Galappathi, K. 'Acidic extracellular pH promotes experimental metastasis of human melanoma cells in athymic nude mice' *Cancer Res.* 66 (**2006**) 6699–6707.

Rowan, S. J. 'Micelles make a living' *Nature Mater.* 8 (**2009**) 89-91.

Ryu, J.-H.; Chacko, R. T.; Jiwpanich, S.; Bickerton, S.; Babu, R. P.; Thayumanavan, S. 'Self-cross-linked polymer nanogels: A versatile nanoscopic drug delivery platform' *J. Am. Chem. Soc.* 132 (**2010**) 17227-17235.

Schild, H. G. 'Poly(*N*-isopropylacrylamide): Experiment, theory and application' *Prog. Polym. Sci.* 17 (**1992**) 163–249.

Schmaljohann, D. 'Thermo and pH responsive polymers in drug delivery' *Adv. Drug. Delivery Rev.* 58 (**2006**) 1655–1670.

Schumers, J.-M.; Fustin, C.-A.; Gohy, J.-F. 'Light-responsive block copolymers' *Macromol. Rapid Commun.* 31 (**2010**) 1588-1607.

Seydack, M.; Bendig, J. 'Trans-stilbene photochemistry beyond 500 nm' *J. Fluoresc.* 10 (**2000**) 291-294.

Shen, H.; Eisenberg, A. 'Block length dependence of morphological phase diagram of the ternary system of PSt_{310}-b-PAA_{52}/dioxane/H_2O' *Macromolecules* 33 (**2000**) 2561-2572.

Shen, H.; Eisenberg, A. 'Morphological phase diagram for a ternary system of block copolymer PSt$_{310}$-b-PAA$_{52}$/dioxane/H$_2$O' *J. Phys. Chem. B* 103 (**1999**) 9473-9487.

Shen, Y.; Tang, H.; Ding, S. 'Catalyst seperation in atom transfer radical polymerization' *Prog. Polym. Sci.* 29 (**2004**) 1053-1078.

Shi, J.; Votruba, A. R.; Farokhzad, O. C.; Langer, R. 'Nanotechnology in drug delivery and tissue engineering: From discovery to applications' *Nano Lett.* 10 (**2010**) 3223-3230.

Shimizu, T.; Masuda, M.; Minamikawa, H. 'Supramolecular nanotube architecture based on amphiphilic molecules' *Chem. Rev.* 105 (**2005**) 1401-1444.

Slomkowski, S.; Winnik, M. A.; Furlog, P.; Reynolds, W. F. 'Synthesis of low-polydispersity poly(tetramethylene oxide) using benzil and pyrene derivatives as initiators' *Macromolecules* 22 (**1989**) 503-509.

Song, X.; Geiger, C.; Farahat, M.; Perlstein, J.; Whitten, D. G. 'Aggregation of stilbene derivatized fatty acids and phospholipids in monolayers and vesicles' *J. Am. Chem. Soc.* 119 (**1997**) 12481-12491.

Song, X.; Perlstein, J.; Whitten, D. G. 'Self-assembly of styrylthiophene amphiphiles in aqueous dispersions and interfacial films: aggregate structure, assembly properties, photochemistry, and photophysics' *J. Phys. Chem. A* 102 (**1998**) 5440-5450.

Soomro, S. A.; Schulz, A.; Meier, H. 'Dendrimers with peripheral stilbene chromophores' *Tetrahedron* 62 (**2006**) 8089-8094.

Spiliopoulos, I. K.; Mikroyannidis, J. A. 'Synthesis of methacrylic monomers bearing stilbenoid chromophore and their free-radical polymerization to give luminescent polymers' *Macromolecules* 35 (**2002**) 7254-7261.

Strukelj, M.; Martinho, J. M. G.; Winnik, M. A. 'Intermolecular excimer formation for pyrene-end-capped polystyrene: a model for the termination process in free-radical polymerization' *Macromolecules* 24 (**1991**) 2488-2492.

Szwarc, M. 'Living polymers. Their discovery, characterization, and properties' *J. Polym. Sci. Part A: Polym. Chem. 36* (**1998**) ix-xv.

Szwarc, M. 'Living polymers' *Nature* 178 (**1956**) 1168-1169.

Szwarc, M.; Levy, M.; Milkovich, R. 'Polymerization initiated by electron transfer to monomer. A new method of formation of block polymers' *J. Am. Chem. Soc.* 78 (**1956**) 2656-2657.

Timko, B. P.; Dvir, T.; Kohane, D. S. 'Remotely triggerable drug delivery systems' *Adv. Mater.* 22 (**2010**) 4925-4943.

Tong, J. D.; Ni, S.; Winnik, M. A. 'Synthesis of polyisoprene-*b*-polystyrene block copolymers bearing a fluorescent dye at the junction by the combination of living anionic polymerization and atom transfer radical polymerization' *Macromolecules* 33 (**2000**) 1482-1486.

Tong, X.; Wang, G.; Soldera, A.; Zhao, Y. 'How can azobenzene block copolymer vesicles be dissociated and reformed by light?' *J. Phys. Chem. B* 109 (**2005**) 20281-20287.

Tsarevsky, N. V.; Matyjaszewski, K. '"Green" atom transfer radical polymerization: From process design to preparation of well-defined environmentally friendly polymeric materials' *Chem. Rev.* 107 (**2007**) 2270-2299.

Tuzar, Z.; Kratochvil, P.; Matijievic, E., Eds. 'Surface and colloidal science' *Springer*: New York, **1993**.

Varghese, S.; Kumar, N. S. S.; Krishna, A.; Rao, D. S. S.; Prasad, S. K.; Das S. 'Formation of highly luminescent supramolecular architectures possessing columnar order from octupolar oxadiazole derivatives: hierarchical self-assembly from nanospheres to fibrous gels' *Adv. Funct. Mater.* 19 (**2009**) 2064-2073.

Vemula, P. K.; Li, J.; John, G. 'Enzyme catalysis: Tool to make and break amygdalin hydrogelators from renewable resources: A delivery model for hydrophobic drugs' *J. Am. Chem. Soc.* 128 (**2006**) 8932-8938.

Wagner, V.; Dullaart, A.; Bock, A. K.; Zweck, A. 'The emerging nanomedicine landscape' *Nat. Biotechnol. 24* (**2006**) 1211–1217.

Wang, G.; Tong, X.; Zhao, Y. 'Preparation of azobenzene-containing amphiphilic diblock copolymers for light-responsive micellar aggregates' *Macromolecules* 37 (**2004**) 8911-8917.

Wang, J.-S.; Matyjaszewski, K. 'Controlled / "living" radical polymerization. Atom Transfer radical polymerization in the presence of transition-metal complexes' *J. Am. Chem. Soc.* 117 (**1995**) 5614-5615.

Wang, J.-S.; Matyjaszewski, K. 'Controlled / "living" radical polymerization. Halogen atom transfer radical polymerization promoted by a Cu (I)/Cu (II) redox process' *Macromolecules* 28 (**1995**) 7901-7910.

Wang, Q.; Dordick, J. S.; Linhardt, R. J. 'Synthesis and application of carbohydrate-containing polymers' *Chem. Mater.* 14 (**2002**) 3232-3244.

Wang, Q.; Zhao, Y. B.; Yang, Y. J.; Xu, H. B.; Yang, X. L. 'Thermosensitive phase behaviour and drug release of in situ gelable poly(n-isopropylacrylamide-co-acrylamide) microgels' *Colloid Polym. Sci.* 285 (**2007**) 515-521.

Wang, R.; Geiger, C.; Chen, L.; Swanson, B.; Whitten D. G. 'Direct observation of sol-gel conversion: The role of the solvent in organogel formation' *J. Am. Chem. Soc.* 122 (**2000**) 2399-2400.

Wang, X.; Guerin, G.; Wang, H.; Wang, Y.; Manners, I.; Winnik, M. A. 'Cylindrical block copolymer micelles and co-micelles of controlled length and architecture' *Science 317* (**2007**) 644-647.

Wang, X.; Zhang, Y.; Zhu, Z.; Liu, S. 'Well-defined amphiphilic block copolymer incorporated with a single C_{60} moiety at the diblock junction point' *Macromol. Rapid Commun.* 29 (**2008**) 340-346.

Watson, P.; Jones, A. T.; Stephens, D. J. 'Intracellular trafficking pathways and drug delivery: Fluorescence imaging of living and fixed cells' *Adv. Drug. Delivery Rev.* 57 (**2005**) 43–61.

Weldeck, D. H. 'Photoisomerization dynamics of stilbenes' *Chem. Rev.* 91 (**1991**) 415-436.

Whitten, D. G.; Chen, L.; Geiger, H. C.; Perlstein, J.; Song, X. 'Self-assembly of aromatic-functionalized amphiphiles: the role and consequences of aromatic-aromatic noncovalent interactions in building supramolecular aggregates and novel assemblies' *J. Phys. Chem. B* 102 (**1998**) 10098-10111.

Winnik, F. M. 'Photophysics of preassociated pyrenes in aqueous polymer solutions and in other organized media' *Chem. Re*v. 93 (**1999**) 587-614.

Xu, R.; Winnik, M. A.; Hallett, F. R.; Riess, G.; Croucher, M. D. 'Light-scattering study of the associated behaviour of styrene-ethylene oxide block copolymers in aqueous solution' *Macromolecules* 24 (**1991**) 87-93.

Yamato, M.; Konno, C.; Utsumi, M.; Kikuchi, A.; Okano, T. 'Thermally responsive polymer-grafted surfaces facilitate patterned cell seeding and co-culture' *Biomaterials* 23 (**2002**) 561–567.

You, L.; Schlaad, H. ' An easy way to sugar-containing polymer vesicles or glycosomes' *J. Am. Chem. Soc.* 128 (**2006**) 13336-13337.

Yu, K.; Eisenberg, A. 'Bilayer morphologies of self-assembled crew-cut aggregates of amphiphilic PS-b-PEO diblock copolymers in solution' *Macromolecules* 31 (**1998**) 3509-3518.

Yu, Y.; Zhang, L; Eisenberg, A. 'Morphological effect of solvent on crew-cut aggregates of amphiphilic diblock copolymers' *Macromolecules* 31 (**1998**)1144–1154.

Zhang, H.; Klumperman, B.; Linde, R. 'Synthesis of anthracene end-capped poly(methyl methacrylate)s via atom transfer radical polymerization and its kinetic analysis' *Macromolecules* 35 (**2002**) 2261-2267.

Zhang, L.; Eisenberg, A. 'Formation of crew-cut aggregates of various morphologies from amphiphilic block copolymers in solution' *Polym. Adv. Technol.* 9 (**1998**) 677-699.

Zhang, L.; Eisenberg, A. 'Multiple morphologies and characteristics of "crew-cut micelle-like aggregates of polystyrene-b-poly(acrylic acid) diblock copolymers in aqueous solutions' *J. Am. Chem. Soc.* 118 (**1996**) 3168-3181.

Zhang, L.; Eisenberg, A. 'Multiple morphologies of "crew-cut" aggregates of polystyrene-b-poly(acrylic acid) block copolymers' *Science* 268 (**1995**) 1728-1731.

Zhang, L.; Eisenberg, A. 'Thermodynamic vs kinetic aspects in the formation and morphological transitions of crew-cut aggregates produced by self-assembly of polystyrene-b-poly(acrylic acid) block copolymers in dilute solution' *Macromolecules* 32 (**1999**) 2239-2249.

Zhang, L.; Gu, F. X.; Chan, J. M.; Wang, A. Z.; Langer, R. S.; Farokhzad, O. C. 'Nanoparticles in medicine: Therapeutic applications and developments' *Clin. Pharmacol. Ther. 83* (**2008**) 761–769.

Zhang, L.; Yu, Y.; Eisenberg, A. 'Ion-induced morphological changes in "crew-cut" aggregates of amphiphilic block copolymers' *Science* 272 (**1996**) 1777–1779.

Zhao, Y. 'Photocontrollable block copolymer micelles. What can we control?' *J. Mater. Chem.* 19 (**2009**) 4887-4895.

Zhao, Y. 'Rational Design of Light-Controllable Polymer Micelles' *Chem. Rec.* 7 (**2007**) 286-294.

Zhao, Y.; He, J. 'Azobenzene-containing block copolymers: The interplay of light and morphology enables new functions' *Soft Matter* 5 (**2009**) 2686-2693.

Zheng, W.; Wang, Z.-G. 'Morphology of abc triblock copolymers' *Macromolecules* 28 (**1995**) 7215-7223.

Curriculum Vitae

Sajith Menon was born on 11 August, 1981, in Kerala, India. He had his early education at Sri Cochin Gujarati Vidyalaya High School, Mattancherry and completed his schooling in 1997. He obtained his Bachelor of Science Degree in Chemistry from The Cochin College, Kochi, affiliated to the Mahatma Gandhi University, Kottayam in 2002 and degree of Master of Science from the Department of Chemistry, Sacred Heart College, Thevara, affiliated to the Mahatma Gandhi University, Kottayam in 2004. Later he worked as a guest Lecturer in the Department of Chemistry, Sacred Heart College, Thevara from 2005 to 2007. He qualified UGC-JRF in the year 2006 and joined for Ph.D. programme in the Photosciences and Photonics Section of the National Institute for Interdisciplinary Science and Technology (NIIST), CSIR under the guidance of Dr. Suresh Das in April 2007. His research interests include synthesis of photoresponsive amphiphilic block copolymers and investigation of their self-assembling and photophysical properties. The results of his work are described in this thesis.

List of Publications

1. Photoresponsive Self-Assembling Structures from a Pyrene-Based Triblock Copolymer, **Sajith Menon** and Suresh Das, *J. Polym. Sci. Part A: Polym. Chem.* **2011**, *49*, 4448 - 4457.

2. Photoresponsive Soft Materials: Synthesis and Photophysical Studies of a Stilbene-Based Diblock Copolymer, **Sajith Menon**, Remyamol Thekkayil, Shinto Varghese and Suresh Das, *J. Polym. Sci. Part A: Polym. Chem.* **2011**, *49*, 5063 – 5073.

3. Photocleavable Glycopolymer Aggregates, **Sajith Menon** and Suresh Das (To be submitted).

4. Photoresponsive Fluorescent Glycopolymer, **Sajith Menon** and Suresh Das (To be submitted).

5. Photoresponsive Glycopolymer Aggregates as Control Release Systems, **Sajith Menon** and Suresh Das (To be submitted).

6. Sphere-to-Rod Transition of a Triblock Copolymer Aggregates upon Irradiation, **Sajith Menon** and Suresh Das (To be submitted).

Oral Presentations/Posters in Academic Conferences

1. Photoresponsive Self-Assembling Structures from Block Copolymers. **Sajith Menon** and Suresh Das, 6th *Jawaharlal Nehru Centre for Advanced Scientific Research National Conference* in Chemistry held at Alleppy on September 27-30, **2009**. (Awarded best presentation).

2. Photoresponsive Polymersomes from Block Glycopolymers. **Sajith Menon** and Suresh Das, *Meeting on Chemistry and Physics of Advanced Materials* held at Vedic Village, Calcutta on October 28-30, **2011**.

3. Photoinduced Reversible Formation of Supramolecular Glycopolymer Aggregates. **Sajith Menon** and Suresh Das, *Research Council Meeting* held at National Institute for Interdisciplinary Science and Technology (NIIST), CSIR, Trivandrum on June 23-24, **2011**.

4. Controlling Block Copolymer Self-Assembly using Light. **Sajith Menon** and Suresh Das, 7th *Jawaharlal Nehru Centre for Advanced Scientific Research National Conference* in Chemistry held at Cochin on October 02-04, **2010**.

5. Self-Assembling Smart Materials from Diblock Copolymers. **Sajith Menon** and Suresh Das, 12th *National Symposium in Chemistry by Chemical Research Society of India* held at Indian Institute of Chemical Technology, Hyderabad on February 04-07, **2010**.

6. Photoresponsive Self-Assembling Structures from Block Copolymers. **Sajith Menon** and Suresh Das, 6th *Jawaharlal Nehru Centre for Advanced Scientific Research National Conference* in Chemistry held at Alleppy on September 27-30, **2009**.